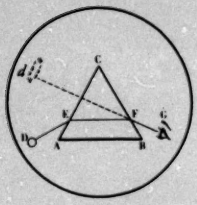

optics and spectroscopy

volume viii
number 5
may 1960

OPTICAL SOCIETY OF AMERICA

USSR ACADEMY OF SCIENCES

RUSSIAN EDITORIAL STAFF FOR
OPTIKA I SPEKTROSKOPIYA sponsored by
USSR ACADEMY OF SCIENCES

Editor: S. E. FRISH

Assistant Editor: P. P. FEOFILOV
Corresponding Secretary: L. S. SAZONOV

Associate Editors:

M. M. GUREVICH M. A. EL'IASHEVICH A. A. LEBEDEV V. P. LINNIK
S. L. MANDEL'SHTAM I. V. OBREIMOV V. K. PROKOF'EV
N. N. SOBOLEV A. N. TERENIN A. I. TUDOROVSKII

Translated from *OPTIKA I SPEKTROSKOPIYA* on the initiative of
THE OPTICAL SOCIETY OF AMERICA, INC.
with a grant-in-aid from
THE NATIONAL SCIENCE FOUNDATION

TRANSLATION EDITORIAL STAFF

Scientific Editors

CYRUS FELDMAN, *Oak Ridge National Laboratory*

CARL W. GARLAND, *Massachusetts Institute of Technology*

MATHEW G. GIBBONS, *Oakland, California*

Administrative Editor: PATRICIA R. WAKELING, *OSA*

Published monthly by the Optical Society of America, Inc. Executive office: 1155 Sixteenth Street, N.W., Washington, D.C. Subscriptions for one year to members of the Society: Associates $13.00; Regular members and Fellows $17.00. Subscriptions for non-members of the Society: One year U. S. and Possessions, $25.00; Foreign $28.00. Back numbers: $3.00 per copy. Subscriptions, changes of address and undeliverable copies should be referred to the Executive offices in Washington, D.C. The office of publication is 2500 South State Street, Ann Arbor, Michigan. Second class postage paid at Ann Arbor, Michigan.

Printed in the U.S.A. by Edwards Brothers, Inc., Ann Arbor, Michigan.

SPECTROSCOPIC INVESTIGATION OF THE STATE OF THE GAS BEHIND A SHOCK WAVE. II

F. S. Faizullov, N. N. Sobolev, and E. M. Kudryavtsev

Received 28 September 1959

A photoelectric method was developed for measuring the temperature of the gas behind a shock wave; the method is based on the measurement of emission and absorption intensities of spectral lines. The accuracy of the method is discussed. The distribution of the shock-wave velocity along the shock tube was investigated. Using the schlieren method, data on the length of the region of hot gas and on the lag of the sodium D line emission were obtained.

A previous communication[1] gave an exposition of the numerous difficulties associated with an attempt to apply a method based on the measurement of the relative intensities of spectral lines in the thermometric study of the state of the gas behind a shock wave. It was established that a reliable measurement of intensities of nonresonance lines of sodium and lithium (at a temperature of 4000°K) was possible only by introducing in the shock tube such large quantities of salts of these elements that the thermodynamic properties of the gas under study were greatly changed and an alteration of the spectral line intensities was produced because of reabsorption. It was further shown that a boundary layer consisting of a large quantity of cold sodium and lithium vapors produces a significant effect on the results.

In an attempt to measure the temperature by means of the bands of cyanogen, introduced into the tube as gaseous dicyanogen, we encountered another difficulty. Temperatures determined from different pairs of vibrational bands of cyanogen were not the same, and this cannot be explained as an effect of reabsorption. The effect is probably related either to a lag in the establishment of equilibrium in the vibrational degrees of freedom of cyanogen or to insufficient data on the vibrational transition probabilities.

The difficulties mentioned above led us to the conclusion that the method of spectrum-line reversal must be used for the thermometric study of the state of the gas behind a shock wave. This method has a number of advantages as compared with that based on the measurement of relative intensities. In particular, the measurements in this case are carried out on a single resonance line for which a high intensity can be obtained with extremely small amounts of contamination; thus, the thermodynamic properties of the gas being studied are not changed, and reabsorption of the spectral line (if it occurs) only increases the accuracy of the measurements. There are, however, certain difficulties associated with the adaptation of the method of spectrum-line reversal to the study of short-lived processes. It was therefore necessary to develop a photoelectric variant of the method which would permit the study of the time variation of the temperature cycle in a process which lasts a few tens of microseconds. In the development of such a technique we used as our starting point the results of a previous investigation,[2] in which a generalized method of spectrum-line reversal, based on the measurement of emission and absorption intensities of spectral lines, was proposed.

The method was applied to a thermometric study of the state of nitrogen and air behind a shock wave propagated in a shock tube; shock-wave velocities in the range from 1.8 to 4.3 km/sec were used. The results obtained and a discussion of these will be given in a future communication. A summary of the main part of the present work was given at the Ninth All-Union Conference on Spectroscopy in December, 1957.[3]

METHOD OF TEMPERATURE MEASUREMENT

As follows from reference 2, in determining the temperature by the generalized reversal method it is not essential to observe the moment of reversal; it suffices in the general case to measure three quantities: (1) the radiation flux Φ_x from the gas in the region corresponding to the spectral line, (2) the radiation flux Φ_{x+1} when the gas is irradiated by the comparison source, and (3) the flux Φ_1 from the comparison source emitting a continuous spectrum.

If $\delta\lambda$ is the effective width of the spectral line, these three quantities can be expressed by Kirchhoff's law and Wien's* formula in the following form:

*For $\lambda T < 0.3$ cm·deg Wien's formula gives an error not exceeding 1%. For higher temperatures it is necessary to use Planck's formula.

$$\Phi_x = aC_1\lambda^{-5}e^{-\frac{C_2}{\lambda T_x}}\delta\lambda\left(\frac{d_2}{f_2}\right)^2 s'h', \tag{1}$$

$$\Phi_{x+1} = C_1\lambda^{-5}e^{-\frac{C_2}{\lambda T_1}}D_2\left(\frac{d_2}{f_2}\right)^2 s'h' - aC_1\lambda^{-5}e^{-\frac{C_2}{\lambda T_{x+1}}}\delta\lambda\left(\frac{d_2}{f_2}\right)^2 s'h' + aC_1\lambda^{-5}e^{-\frac{C_2}{\lambda T_x}}\delta\lambda\left(\frac{d_2}{f_2}\right)^2 s'h', \tag{2}$$

$$\Phi_1 = C_1\lambda^{-5}e^{-\frac{C_2}{\lambda T_1}}D_2\left(\frac{d_2}{f_2}\right)^2 s'h', \tag{3}$$

where a is the absorptive power in the region of the line in question, D the linear dispersion in A/mm, d_2/f_2 the aperture ratio of the camera objective, s and s′ the widths of the entrance and exit slits, h′ the height of the exit slit of the monochromator, C_1 and C_2 radiation constants, T_x the true temperature of the gas, and T_1 the brightness temperature of the comparison source.

By simple transformations of the above equations it is easy to obtain the following expression for the temperature,

$$T_x = T\cdot\left[1+\frac{\lambda T_1}{C_2}\cdot\ln\left(1-\frac{\Phi_{x+1}-\Phi_1}{\Phi_x}\right)\right]^{-1} \tag{4}$$

and for the absorptive power

$$a\frac{\delta\lambda}{D\cdot s} = \frac{\Phi_x-(\Phi_{x+1}-\Phi_1)}{\Phi_1}. \tag{5}$$

In the present investigation the temperature was measured by the sodium D lines. Either the natural contamination of the tube and air was used, no sodium at

all being introduced into the tube, or the walls of the tube were lighly smeared with sodium chloride solution. As the comparison source a tungsten temperature lamp and a dc xenon arc lamp were used; the former had a brightness temperature of 2660°K and the latter an effective brightness temperature of 4750°K in the region of the sodium D lines. The calibration of the xenon lamp was carried out by means of a standard temperature lamp; the accuracy of the calibration was about ±50°. Auxiliary experiments showed that the emission of the xenon lamp in the visible region was continuous with a few lines in the 0.46—0.49 μ region, and that the emission intensity was sufficiently constant with time. We note incidentally that the photoelectric variant of the generalized reversal method does not demand a homogeneous temperature field at all levels of the comparison source, which is most essential in the photographic variant.

A diagram of the apparatus used for temperature measurements with the pulsed variant of the generalized reversal method developed by us is given in Fig. 1. In the same diagram is shown the arrangement used for the study of the flow by means of the schlieren method. The plane glass windows O_1 and O_2, 30 mm in diameter, are located opposite each other at a distance of 3.5 meters from the diaphragm of the shock tube. The comparison source C_1 is focused by the lens L_1 inside the shock tube. The lens L_2, which must be filled with light from each effective point of the comparison source, projects an image of the central part of the plug* and of the comparison source on the curved entrance slit of the monochromator. A diaphragm, mounted on the entrance slit of the monochromator, divides the length of the slit into two equal parts. It is arranged that the image of the comparison source falls only on the upper part of the entrance slit and the image of the plug on the whole slit. After emerging from the exit slit the light which has come through the upper part of the entrance slit falls by way of the mirror Z_1 onto the photomultiplier P_1, and the light which has come through the lower part of the entrance slit falls by way of the mirror Z_2 onto the photomultiplier P_2. FEU-17 photomultipliers with a very low dark current (10^{-10} amp at a sensitivity of 1 amp/lumen) were used.

*Translator's note: the word "plug" is used as the translation of a Russian word designating the region of hot gas between the shock-wave front and the beginning of the contact region.

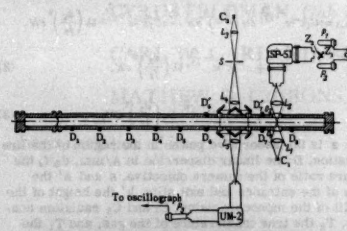

Fig. 1. Diagram of the arrangement for the spectroscopic study of the state of the gas behind a shock wave (D_1, ... D_6—ionization probes). Arrangement for investigating the shock-wave velocity with the schlieren shadow method: C_2—SVDSH-1000 mercury lamp; L_3—lens (f = 50 mm); S—slit; L_4—collimator lens (f = 800 mm); L_5—lens (f = 800 mm); P_3—FEU-19 photomultiplier. Arrangement for temperature measurements: C_1—DKSSH-1000 xenon lamp; L_1 and L_2—lenses (f = 90 mm); O_1 and O_2—windows; Z_1 and Z_2—mirrors; P_1 and P_2—FEU-17 photomultiplier.

If the flux Φ_1 from the comparison source is constant in time and the fluxes Φ_x and Φ_{x+1} are pulses, in recording the signals from P_1 and P_2 with a double-beam pulse oscilloscope, the first beam records a signal from the photomultiplier P_1 proportional to the flux difference, $\Phi_{x+1} - \Phi_1$, and the second beam records a signal from P_2 proportional to Φ_x.

A typical oscillogram obtained in the temperature measurement is shown in Fig. 2. The procedure for determining the temperature is reduced by this method to two measurements instead of three, the relative sensitivities of the channels being determined by calibration. The calibration is carried out under the same conditions (values of the lens apertures, heights of both parts of the slit, slit widths) as those in which the experiment itself was performed, using a source which produces identical illumination of both parts of the entrance slit (MgO screen illuminated by a pulse lamp or by the emission from the plug itself).

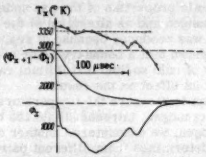

Fig. 2. A typical oscillogram obtained in the temperature measurement (air, p_1 = 10 mm Hg, U_s = 3.08 km/sec, $T_{calc.}$ = 3350°K). The upper curve is the experimentally observed variation of the temperature behind the shock wave.

In temperature measurements by the generalized reversel method it is necessary to take into account the light losses by reflection, absorption, and scattering at the lens L_1 and the window O_1. The losses at the window amount to about 10%, and those at the lens L_1, if a multicomponent lens is used, can reach 30%; this leads to a lowering of the effective temperature of the image of the comparison source inside the tube (by 250° if the temperature of the comparison source is 4500°K). Similarly, any decrease in the transparency of the window O_1 due to dirt can also lead to an increase in the measured temperature. It is therefore necessary to keep the window clean.

ACCURACY OF THE METHOD OF TEMPERATURE MEASUREMENT

The accuracy with which the temperature can be determined by the generalized reversal method depends on the accuracy of the measurement of the ratio of the two light fluxes,

$$\beta = \frac{\Phi_{x+1} - \Phi_1}{\Phi_x}. \qquad (5a)$$

Differentiation of (4) gives the relative error of the temperature determination,

$$\frac{\Delta T_x}{T_x} = \frac{\lambda T_x}{C_2} \cdot \frac{\Delta\beta}{1-\beta}. \tag{6}$$

The mean square error in the determination of β is equal to

$$\overline{\Delta\beta^2} = \frac{(\Phi_{x+1}-\Phi_1)^2}{\Phi_x^2} \cdot \frac{\overline{\Delta\Phi_x^2}}{\Phi_x^2} + \frac{\overline{\Delta(\Phi_{x+1}-\Phi_1)^2}}{\Phi_x^2}. \tag{7}$$

In photoelectric measurements the accuracy of the flux measurement is limited by fluctuations of the photocurrent. The rms value of the current fluctuation is proportional to the electron current i from the photocathode and to the width Δf of the pass band of the recording system, that is,

$$\overline{\Delta i^2} = 2ei\Delta f, \tag{8}$$

where e is the electronic charge.

From Eqs. (1)-(3) and (8), and taking into account the proportionality of the photocurrent and the light flux, $i = \gamma_\lambda \Phi$, expression (7) for the case of a monochromator with exit and entrance slits of equal widths can be written in the following form:

$$\overline{\Delta\beta^2} = \frac{2e\Delta f e^{\frac{2C_2}{\lambda T_x}}}{C_1 \lambda^{-5} \tau_\lambda \left(\frac{d_2}{f_2}\right)^2 h'} \left[\frac{(1+\beta^2)\, e^{-\frac{C_2}{\lambda T_x}} - e^{-\frac{C_2}{\lambda T_1}}}{a b i_3} + \frac{D e^{-\frac{C_2}{\lambda T_1}}}{a^2 b^2 i_3^2} \right]. \tag{9}$$

For the ratio of the fluxes we have from (4):

$$\beta = 1 - e^{-\frac{C_2}{\lambda}\left(\frac{1}{T_1} - \frac{1}{T_x}\right)}. \tag{9a}$$

Substituting this expression for β in (9) and (6), we obtain after some elementary manipulations the following formula for the rms value of the error in the temperature determination:

$$\sqrt{\frac{\overline{\Delta T_x^2}}{T_x^2}} = \frac{T_x}{C_2 a b \lambda \left(\frac{d_2}{f_2}\right)} \sqrt{\frac{2e\Delta f \lambda^7}{C_1 \tau_\lambda h'} \cdot e^{\frac{C_2}{\lambda T_1}}} \times \sqrt{\frac{a b \lambda}{i_3} \left(2 e^{\frac{C_2}{\lambda}\left(\frac{1}{T_1} - \frac{1}{T_x}\right)} + e^{-\frac{C_2}{\lambda}\left(\frac{1}{T_1} - \frac{1}{T_x}\right)} - 3 \right) + D}. \tag{10}$$

Analysis of formula (10) shows that the best accuracy can be obtained with an apparatus of large light power and dispersion and for large values of the total absorption ($a b \lambda$). At the reversal point, for which $T_x = T_1$, the error does not depend on the slit width and is equal to

$$\sqrt{\frac{\overline{\Delta T_x^2}}{T_x^2}} = \frac{T_1}{C_2 a b \lambda \left(\frac{d_2}{f_2}\right)} \sqrt{\frac{2e\Delta f \lambda^7}{C_1 \tau_\lambda h'} \cdot e^{\frac{C_2}{\lambda T_1}} D}. \tag{11}$$

Figure 3 shows how the magnitude of the error depends on the value of the temperature being measured; the curves for two values of T_1 are plotted according to formula (10) for our experimental conditions. As is evident from the graph, the lower limit of measurable temperatures is practically independent of the temperature of the comparison source, and is determined entirely by the sharp drop in the emission intensity and by the related decrease in the signal-to-noise ratio. In the region of high temperatures the signal-to-noise ratio becomes more favorable, and the determining factor limiting the accuracy of the measurement is not fluctuations but rather the width of the oscillograph beam. In our case the beam width was about 0.5 mm; for a maximum beam deflection of 25 mm, this gave an accuracy of about ±8% for the measurement of the flux ratio β. The corresponding error in the temperature being measured is shown by the dashed curve in Fig. 3. It is evident from the diagram that for temperature measurements by the generalized

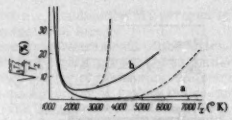

Fig. 3. Dependence of the magnitude of the error on the temperature being measured, plotted according to formula (10). Curve a—T_1 = 4500°K; curve b—T_1 = 2700°K. The dashed curve gives the value of the error calculated from the error in the determination of β (~8%) due to the thickness of the oscillograph beam.

reversal method the comparison source should have a brightness temperature higher than the temperature being measured.

We note that for the photoelectric variant of the generalized reversal method, in contrast to the photographic method,[2] it is advantageous to work with wide slits. By this means the light flux is increased, so that the accuracy of the measurements can be increased or the time resolution can be improved (at the expense of lowering the load resistance of the photomultiplier).

In our investigation an ISP-51 spectrometer with a dispersion of 85 A/mm in the region of the sodium D lines was used as the monochromator. For slit widths of 0.1 mm and temperatures of about 4000°K the signal-to-noise ratio was such that temperature measurements with an accuracy of ±60° were possible. A calculation using formula (10) gave the error as ±40° (cf. Fig. 3). The sensitivity to changes in the temperature was sufficiently great to show small temperature fluctuations occurring in the plug.

MEASUREMENT OF THE SHOCK-WAVE SPEED BY THE IONIZATION METHOD

To study the dependence of the temperature of the plug on the speed of the shock wave and to compare the experimental results with theory it was essential to measure reliably not only the temperature but also the speed of the wave. To study the distribution of temperature along the plug, it is necessary to know in addition the limits of the plug (that is, its beginning and end), and also the distribution of the speed of the shock wave along the shock tube. Moreover, it is necessary to determine the limits of the plug experimentally, since it is well known that the length of the region of hot gas is considerably less than that predicted by elementary theory.

In our experimental practice the ionization method of speed measurements is widely used. The signals from the ionization probes were applied directly to the input of an OK-17M cathode ray oscillograph. Time pips were obtained by using a sine-wave voltage generator with a frequency of 100 kc. An auxiliary probe activated the beam sweep of the oscillograph. In working out the results the deviation of the beam sweep from linearity was taken into account. A diagram of the connection of the probes is shown in Fig. 4, and a typical oscillogram obtained in the speed measurement in Fig. 5a. The normal oscillogram with an abrupt rise in the signal from the probes, as shown in Fig. 5a, allows the determination of the speed with sufficient accuracy. However, under some conditions the following effect was observed. On the oscillogram in Fig. 5b obtained for argon (p_1 = 2 mm Hg and U_s = 3.60 km/sec), it is seen that the signal rises gradually, not

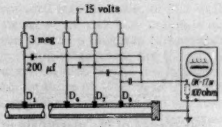

Fig. 4. Diagram of the connection of the ionization probes (D_1, ... D_8) for measurement of the shock-wave speed.

sharply, and it appears before the shock wave has arrived at the probe. Similar oscillograms were obtained under extreme conditions also in the case of nitrogen. The effect increases with increasing shock-wave speed and with decreasing initial pressure p_1 of the gas in the shock tube, and also with increasing voltage on the ionization probes.

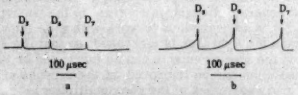

Fig. 5. Typical oscillograms obtained in measuring the shock-wave speed. a—a normal oscillogram; b—an anomalous oscillogram.

The effect can be explained by the fact that at high temperatures and low initial pressures the short wavelength emission of the hot gas is propagated far ahead of the shock wave and causes photoemission from the probes. This explanation is quite plausible when it is considered that there are always impurities with low photothresholds (salts of sodium, calcium, etc.) on the walls of the tube and on the probes, and that there is a potential of about 150 volts on the probes. To eliminate the effect in the speed measurements under extreme conditions (expecially for argon) it was necessary to use the lowest possible voltage on the probes. We note that triggering circuits (especially thyratron circuits as in the IV-13M time measuring device) for the measurement of shock-wave speeds can be used only with great care, since signals which are not sharp enough can lead to large errors.

MEASUREMENT OF SHOCK-WAVE SPEEDS BY THE SCHLIEREN METHOD

As a control of the ionization method a way of measuring speeds, based on an application of the schlieren method,[4] was developed; a diagram of the arrangement used is included in Fig. 1.

A light beam from the source C_2 falls on the slit S and is rendered parallel by passing through the lens L_4. The width of the parallel beams of light passing through the tube is 2 mm and the distance between the beams is 190 mm. The lens L_5 gives an image of the slit S in the plane of the entrance slit of the monochromator, the output of which falls on the photomultiplier P_2. As is evident from the diagram, it is possible with this arrangement to record the change of refractive index at two cross sections of the tube with a single photomultiplier. By feeding the signal from the photomultiplier to the cathode ray oscillograph, the time of travel of the shock wave between the two cross sections of the shock tube can be measured and the shock-wave speed can thus be found. The time constant of the electronic circuit was about 0.5 μsec. With the help of this same arrangement also the length of the plug was measured by recording the change in the refractive index at the first cross section of the tube at the moment of passage not only of the shock wave but also of the contact surface. A typical oscillogram from which the speed of the shock wave and the length of the plug could be determined is shown in Fig. 6. It is evident from the figure that the distance between the two cross sections, which is used in the measurement of the shock-wave speed, must be chosen so that the signal Φ′, corresponding to the passage of the shock wave through the second cross section, must be recorded by the oscillograph earlier than the signal K, corresponding to the passage of the beginning of the contact region through the first cross section.

Fig. 6. Form of the oscillogram from which the shock-wave speed and the length of the plug were obtained. Φ—shock-wave front at the first cross section; Φ′—shock-wave front at the second cross section; K—beginning of the contact region at the first cross section.

Tests showed that this method of measuring the speed and the length of the plug was suitable for work with nitrogen, air, and argon in the range of initial pressures from 50 to 11 mm Hg and for corresponding shock-wave speeds from 2 to 4 km/sec. The schlieren method of measuring speeds has an indisputable advantage over the ionization method; it is more reliable and permits moreover a simultaneous determination of the length of the plug. Its reliability is due to the fact that it is based on the recording of density changes of the principal gas and does not depend on the presence of impurities as does the ionization method. The schlieren method was used to show that reliable speed measurements using ionization probes are possible. For this purpose the speed was measured simultaneously by the schlieren method and by the ionization probes D_6 and D_7 (Fig. 1). A comparison of the results obtained is given in Fig. 7. As is evident from the graph the two methods gave results agreeing

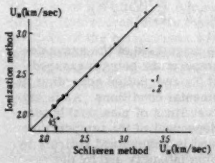

Fig. 7

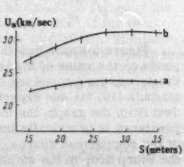

Fig. 8

Fig. 7. Comparison of the results of measurements of the shock-wave speed by the schlieren method and by ionization probes. 1—argon; 2—nitrogen.

Fig. 8. Distribution of the shock-wave speed along the tube. Each curve is the average of 8 experiments. a—nitrogen (p_1 = 50 mm Hg); b—nitrogen and air (p_1 = 10 mm Hg); S—distance from the diaphragm.

within the limits of the experimental error which amounted to about 2%.

Taking these facts into consideration we used the ionization method (since it was the simpler) for studying the variation in the shock-wave speed along the tube. The reduction of a large number of oscillograms allowed the distribution of the shock-wave speed along the shock tube to be found for air and nitrogen under various conditions. The results are given in Fig. 8, in which the curves a and b represent the normal distribution of the shock-wave velocity along the shock tube according to data given in the literature.[5] The speed of the shock wave increases monotonically with the distance from the diaphragm and reaches a maximum at a distance of approximately 2.5 meters from the diaphragm. This distance (the so-called formation distance of the shock wave) increases with the speed of the shock wave and depends in the last analysis on the opening speed of the diaphragm.

THE LENGTH OF THE PLUG AND THE LAG OF THE SODIUM EMISSION

The experimental data on the length of the plug as a function of the shock-wave speed, as obtained by the schlieren method, are given in Fig. 9 for air and nitrogen. The solid line on this diagram represents the theoretical length of the plug for air, calculated from the x–t diagram assuming a constant shock-wave speed; the dashed line refers to nitrogen.

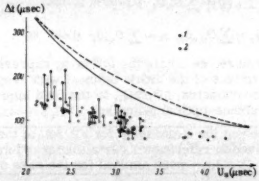

Fig. 9. Dependence of the length of the plug on the speed of the shock wave. The time of passage of the plug between the points of observation is plotted along the ordinate axis. The solid and dashed curves give the theoretical length of the plug for air and nitrogen, respectively. The points represent the experimental data on the length of the plug: 1—air; 2—nitrogen.

On oscillograms of the shadow signal, especially for air, a contact surfact with a sharp density gradient was not observed, but rather a contact region with a fairly smooth density variation. Portions of the contact region in which a smooth density gradient occurred are represented in Fig. 9 as line segments. In spite of the considerable scatter of the points it is evident from the data presented that the length of the plug found experimentally is approximately half as great as the theoretical length. This may be related to the final period of opening of the diaphragm which leads to the formation of a region of mixing of the driver gas and the gas under study. In experiments with air, combustion of hydrogen is usually observed in the region of mixing.

In addition to measurements of the shock-wave speed and the length of the plug, the schlieren method allowed us to study also the lag of the sodium emission. For this purpose a monochromator to isolate the sodium D lines was added to the usual shadow system (cf. Fig. 1). The system was arranged so that both the shadow signal and the sodium emission were recorded simultaneously. Typical oscillograms obtained in this way are shown in Fig. 10. These experiments showed that the process of sodium D line emission begins immediately behind the shock-wave front and already after a few microseconds has a value within 10% of the maximum. The maximum emission is reached after 10-20 μsec. This time is probably required mainly for the vaporization of the minute particles of sodium chloride found in the shock tube. The nature of the sodium D line luminescence in our experiments is very similar to that observed by Clouston, Gaydon, and Glass,[6] who introduced sodium into the tube by passing the gas to be studied over molten sodium chloride, but differs significantly from the results given in reference 7 where a lag of the beginning of the emission of 50 μsec was observed.

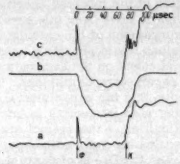

Fig. 10. Typical oscillograms of (a) the shadow signal, (b) the sodium D line emission, (c) the shadow signal and the sodium D line emission (nitrogen, p_1 = 10 mm Hg, U_s = 3.1 km/sec). Φ—shock-wave front; K—beginning of the contact region.

REFERENCES

1. N. N. Sobolev, A. V. Potapov, V. F. Kitaeva, F. S. Faizullov, V. H. Alyamovskii, E. T. Antropov, and I. L. Isaev. Opt. i Spektr. **6**, 284 (1959), Opt. i Spectr. **6**, 185 (1959).
2. A. G. Sviridov and N. N. Sobolev. Zhur. Exptl. i Teoret. Fiz. **24**, 93 (1953).
3. N. N. Sobolev, A. V. Potapov, V. F. Kitaeva, F. S. Faizullov, V. N. Alyamovskii, E. T. Antropov and I. L. Isaev. Izvest. Akad. Nauk SSSR, Ser. Fiz. **22**, 730 (1958).
4. "Fizicheskie izmereniya v gazovoi dinamike," p. 141. Physical Measurements in Gas Dynamics), Moscow, 1957.
5. D. R. White. J. Fluid Mech. **4**, 585 (1958).
6. J. G. Clouston, A. G. Gaydon, and I. I. Glass. Proc. Roy. Soc. (London) **A248**, 429 (1958).
7. J. G. Clouston and A. G. Gaydon. Spectrochim. Acta **14**, 56 (1959).

THEORY OF THE INFRARED SPECTRAL INTENSITIES OF DEUTEROETHYLENES. VII

L. M. Sverdlov

Received 22 August 1959

A calculation of the integrated intensities of the infrared spectra of the partially deuterated ethylenes C_2H_3D, as-$C_2H_2D_2$, cis-$C_2H_2D_2$, trans-$C_2H_2D_2$, and C_2HD_3 has been carried out to the first approximation of the valence-optical scheme, using the electro-optical parameters of ethylene. Sufficiently good agreement of the calculated and observed intensities has been obtained for the molecules trans-$C_2H_2D_2$ and cis-$C_2H_2D_2$. A calculation of the integrated intensities of the intensities of the infrared bands of a mixture of deuteroethylenes has also been carried out.

1. Previously[1] we carried out a calculation of the infrared spectral intensities and the electro-optical parameters of ethylene and tetradeuteroethylene to the first approximation of the valence-optical scheme.[2, 3] Using the set of electro-optical parameters obtained, we may turn to consideration of the intensities of the infrared bands of the partially deuterated ethylenes. Such a calculation is of interest for a number of reasons. The integrated intensities of the infrared spectra of cis- and trans-dideuteroethylene have been measured experimentally,[4] and a comparison of the calculated and observed intensity values would provide a possibility of making an additional check on the accuracy of the set of electro-optical parameters of ethylene. Furthermore, since it is well known that the experimental determination of absolute integrated intensities in infrared spectra presents great difficulties, a theoretical evaluation of the intensities of molecules not yet studied—particularly of C_2H_3D, as-$C_2H_2D_2$, and C_2HD_3—is of current significance.

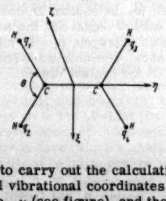

2. In order to carry out the calculations, we introduce the internal vibrational coordinates q_i, β_i (i = 1-4), Q_a, α_{12}, α_{34}, ρ_1, ρ_2, χ (see figure), and the angular valence-optical coordinates β_{ni}, φ_i, ψ_i. Taking into account the exact and approximate symmetry of the molecules, we introduce symmetry coordinates expressed by means of the normal coordinates Q_i.

The C_2H_3D molecule.

$$A': q_1,\ q_2,\ q_3,\ q^+ = \frac{1}{\sqrt{2}}(q_3+q_4);\ q^- = \frac{1}{\sqrt{2}}(q_3-q_4);\ Q_a,\ \beta_1,\ \beta_2,$$

$$\alpha_{12},\ \alpha_{34},\ \beta^+ = \frac{1}{\sqrt{2}}(\beta_3+\beta_4);\ \beta^- = \frac{1}{\sqrt{2}}(\beta_3-\beta_4);\ A'': \chi,\ \rho_1,\ \rho_2.$$

$$q_1 = \sum C^A_{qi}Q_i;\ q_2 = \sum C^H_{qi}Q_i;\ q^+ = \sum C^+_{qi}Q_i;\ q^- = \sum C^-_{qi}Q_i;$$

$$\beta_1 = \sum D^A_{\beta i}Q_i; \qquad \beta_2 = \sum D^H_{\beta i}Q_i;\ \beta^+ = \sum D^+_{\beta i}Q_i;\ \beta^- = \sum D^-_{\beta i}Q_i;$$

$$\alpha_{12} = \sum D_{\alpha i}Q_i \quad (i = 1-3;\ 5,\ 6;\ 9-12).$$

$$\chi = \sum D_{\pi i}Q_i;\ \rho_1 = \sum D_{\rho_1 i}Q_i;\ \rho_2 = \sum D_{\rho_2 i}Q_i \quad (i = 4;\ 7,\ 8).$$

The as-$C_2H_2D_2$ molecule.

$$A_1: q^A_a = \frac{1}{\sqrt{2}}(q_1+q_2);\ q^A_H = \frac{1}{\sqrt{2}}(q_3+q_4);\ Q^{A_1}_a,\ \alpha^{A_1}_{12},\ \alpha^{A_1}_{34},$$

$$\beta^{A_1}_a = \frac{1}{\sqrt{2}}(\beta_1+\beta_2);\ \beta^{A_1}_H = \frac{1}{\sqrt{2}}(\beta_3+\beta_4).$$

$$B_1: q^B_a = \frac{1}{\sqrt{2}}(q_1-q_2);\ q^B_H = \frac{1}{\sqrt{2}}(q_3-q_4);$$

$$\beta^{B_1}_a = \frac{1}{\sqrt{2}}(\beta_1-\beta_2);\ \beta^{B_1}_H = \frac{1}{\sqrt{2}}(\beta_3-\beta_4).\ B_2: \rho_1,\ \rho_2.$$

$$q^{A_1}_a = \sum C^A_{qi}Q_i;\ q^{A_1}_H = \sum C^H_{qi}Q_i;\ \beta^{A_1}_a = \sum D^A_{\beta i}Q_i;$$

$$\beta^{A_1}_H = \sum D^H_{\beta i}Q_i \quad (i = 1-3;\ 11,\ 12).$$

$$q^B_a = \sum C^A_{qi}Q_i;\ q^B_H = \sum C^H_{qi}Q_i;\ \beta^B_a = \sum D^A_{\beta i}Q_i;$$

$$\beta^B_H = \sum D^H_{\beta i}Q_i \quad (i = 5,\ 6;\ 9,\ 10).$$

$$\rho_1 = \sum D_{\rho_1 i}Q_i;\ \rho_2 = \sum D_{\rho_2 i}Q_i \quad (i = 7,\ 8).$$

Furthermore, we obtain the following expressions for the derivatives of the dipole moment with respect to the normal coordinates, $\partial P_i/\partial Q_i$, to the first approximation of the valence-optical scheme:*

*We also present the expression for $\partial P/\partial Q_i$ of the C_2H_4 molecule, since in reference 1 certain interactions—$\partial\sqrt{}/\partial q_j$, and $\partial\mu_i/\partial\varphi_j$—were omitted for the sake of brevity.

The C_2H_4 molecule.

$$\frac{\partial P_\xi}{\partial Q^{B_2}_i} = \frac{\partial P_\xi}{\partial q^{B_2}_m}C_{qi} + \frac{\partial P_\xi}{\partial\beta^{B_2}_m}D_{\beta i}$$

$$= \left\{-2\sin\frac{\theta}{2}\left[\left(\frac{\partial\mu_1}{\partial q_1}-\frac{\partial\mu_2}{\partial q_1}+\frac{\partial\mu_3}{\partial q_1}-\frac{\partial\mu_4}{\partial q_1}\right)\right.\right.$$

$$\left.+\mu_{CH}\cot\frac{\theta}{2}\left(\frac{\partial\mu_1}{\partial q_1}-\frac{\partial\mu_2}{\partial q_1}+\frac{\partial\mu_3}{\partial q_1}-\frac{\partial\mu_4}{\partial q_1}\right)\right]C_{qi} + \frac{2\cos\frac{\theta}{2}}{r_{CH}}$$

$$\left.+\left[\mu_{CH}+2\tan\frac{\theta}{2}\left(\frac{\partial\mu_1}{\partial r_1}-\frac{\partial\mu_2}{\partial r_1}+\frac{\partial\mu_3}{\partial r_1}-\frac{\partial\mu_4}{\partial r_1}\right)\right]D_{\beta i}\right\},\ (i = 9,\ 10);$$

$$\frac{\partial P_\eta}{\partial Q^{B_2}_i} = \frac{\partial P_\eta}{\partial q^{B_2}_m}C_{qi} + \frac{\partial P_\eta}{\partial\alpha^{B_2}_m}D_{\alpha i}$$

$$= \left\{-2\cos\frac{\theta}{2}\left[\left(\frac{\partial\mu_1}{\partial q_1}+\frac{\partial\mu_2}{\partial q_1}-\frac{\partial\mu_3}{\partial q_1}-\frac{\partial\mu_4}{\partial q_1}\right)\right.\right.$$

$$-\frac{1}{\cos\frac{\theta}{2}}\frac{\partial\mu_{CC}}{\partial q_1}-\tan\frac{\theta}{2}\left(\frac{\partial\mu_1}{\partial q_1}+\frac{\partial\mu_2}{\partial q_1}-\frac{\partial\mu_3}{\partial q_1}-\frac{\partial\mu_4}{\partial q_1}\right)\mu_{CH}\left.\right]C_{qi}$$

$$+\sqrt{2}\sin\frac{\theta}{2}\left[\mu_{CH}-2\cot\frac{\theta}{2}\left(\frac{\partial\mu_1}{\partial r_1}+\frac{\partial\mu_2}{\partial r_1}-\frac{\partial\mu_3}{\partial r_1}-\frac{\partial\mu_4}{\partial r_1}\right)\right.$$

$$\left.\left.+\frac{2}{\sin\frac{\theta}{2}}\frac{\partial\mu_{CC}}{\partial r_1}\right]D_{\alpha i}\right\},\ (i = 11,\ 12); \qquad (1)$$

$$\frac{\partial P_\zeta}{\partial Q^{B_2}_i} = \frac{\partial P_\zeta}{\partial\rho^{B_2}_m}D_{\rho i} = \sqrt{2}\,\frac{\mu_{CH}}{r_C}\,D_{\rho i}.$$

The C_2H_3D molecule.

$$\left.\begin{aligned}
\frac{\partial P_\xi}{\partial Q_i^A} &= \frac{1}{2}\left\{\frac{\partial P_\xi}{\partial q^{B_{1u}}}(C_{gl}^d - C_{gl} + \sqrt{2}\,C_{gl}^-)\right. \\
&\left. + \frac{\partial P}{\partial p^{B_{1u}}}(D_{al} + 2D_{gl}^d + \sqrt{2}\,D_{gl}^-)\right\}; \\
\frac{\partial P_\eta}{\partial Q_i^{A'}} &= \frac{1}{2}\left\{\frac{\partial P_\eta}{\partial q^{B_{2u}}}(C_{gl}^d - C_{gl}^H) + \sqrt{2}\,\frac{\partial P_\eta}{\partial a^{B_{2u}}}(D_{al} + \sqrt{2}\,D_{gl}^+)\right\}; \\
\frac{\partial P_\zeta}{\partial Q_i^{A''}} &= \frac{1}{\sqrt{2}}\,\frac{\partial P_\zeta}{\partial p^{B_{1u}}}(D_{t\gamma l} + D_{t\gamma' l}).
\end{aligned}\right\} \quad (2)$$

The as-$C_2H_2D_2$ molecule.

$$\left.\begin{aligned}
\frac{\partial P_\xi}{\partial Q_i^{B_1}} &= \frac{1}{\sqrt{2}}\left\{\frac{\partial P_\xi}{\partial q^{B_{1u}}}(C_{gl}^d + C_{gl}^H) + \frac{\partial P_\xi}{\partial p^{B_{1u}}}(D_{gl}^d + D_{gl}^H)\right\}; \\
\frac{\partial P_\eta}{\partial Q_i^{A_1}} &= \left\{\frac{1}{\sqrt{2}}\,\frac{\partial P_\eta}{\partial q^{B_{2u}}}(C_{gl}^d - C_{gl}^H) + \frac{\partial P_\eta}{\partial a^{B_{2u}}}(D_{gl}^H - D_{gl}^d)\right\}; \\
\frac{\partial P_\zeta}{\partial Q_i^{B_2}} &= \frac{1}{\sqrt{2}}\,\frac{\partial P_\zeta}{\partial q^{B_{1u}}}(D_{t\gamma l} + D_{t\gamma' l}).
\end{aligned}\right\} \quad (3)$$

The cis-$C_2H_2D_2$ molecule.

$$\left.\begin{aligned}
\frac{\partial P_\xi}{\partial Q_l^{A_1}} &= \frac{1}{\sqrt{2}}\left\{\frac{\partial P_\xi}{\partial q^{B_{1u}}}(C_{gl}^d - C_{gl}^H) + \frac{\partial P_\xi}{\partial p^{B_{1u}}}(D_{gl}^d - D_{gl}^H)\right\}, \\
&\qquad (l = 1\text{–}3;\ 9,\ 10); \\
\frac{\partial P_\eta}{\partial Q_l^{B_1}} &= \left\{\frac{1}{\sqrt{2}}\,\frac{\partial P_\eta}{\partial q^{B_{1u}}}(C_{gl}^d + C_{gl}^H) - \frac{\partial P_\eta}{\partial a^{B_{1u}}}(D_{gl}^d + D_{gl}^H)\right\}, \\
&\qquad (l = 5,\ 6;\ 11,\ 12); \\
\frac{\partial P_\zeta}{\partial Q_l^{B_2}} &= \frac{\partial P_\zeta}{\partial p^{B_{1u}}} D_{gl}.
\end{aligned}\right\} \quad (4)$$

The trans-$C_2H_2D_2$ molecule.

$$\left.\begin{aligned}
\frac{\partial P_\xi}{\partial Q_l^{B_u}} &= \frac{1}{\sqrt{2}}\left\{\frac{\partial P_\xi}{\partial q^{B_{1u}}}(C_{gl}^d - C_{gl}^H) + \frac{\partial P_\xi}{\partial p^{B_{1u}}}(D_{gl}^d - D_{gl}^H)\right\}; \\
\frac{\partial P_\eta}{\partial Q_l^{B_u}} &= \left\{\frac{1}{\sqrt{2}}\,\frac{\partial P_\eta}{\partial q^{B_{1u}}}(C_{gl}^d + C_{gl}^H) - \frac{\partial P_\zeta}{\partial a^{B_{1u}}}(D_{gl}^d + D_{gl}^H)\right\}, \quad (l = 9\text{–}12); \\
\frac{\partial P_\zeta}{\partial Q_l^{A_u}} &= \frac{\partial P_\zeta}{\partial p^{B_{1u}}} D_{gl} \quad (l = 4,\ 7).
\end{aligned}\right\} \quad (5)$$

3. The form of the normal vibrations of deuteroethylenes was considered by us previously.[5] In Tables 1-3 are presented the normalized coefficients C_{ql}, D_{gl}, D_{al}, and D_{gl} for the partially deuterated ethylenes. The derivatives of the dipole moments with respect to the normal coordinates, in numerical form, were evaluated with the help of formulas (2)-(5) by substituting the coefficients C_{ql}, D_l, and the electro-optical parameters of ethylene[1] into these formulas (Table 4). The values of $\partial P/\partial Q_l$ obtained are presented in Tables 5-7. The values of the integrated intensities I_l are also given in these tables.

The evaluation of the coefficients C_{ql}, D_l, the derivatives $\partial P/\partial Q_l$, and the intensity values I_l was carried out with high accuracy—as shown by the fulfillment of the intensity sum rules of both first[6] and second[7] order. As can be seen from Table 8, the discrepancy between the two sides of the equalities does not exceed 1.5% of the quantities entering into these formulas. Finally, let us compare the calculated and observed values for the derivatives of the dipole moment with respect to the normal coordinates, $\partial P/\partial Q_l$, of the trans-$C_2H_2D_2$ and cis-$C_2H_2D_2$ molecules. For the trans-$C_2H_2D_2$ molecule, the discrepancy for most of the vibrations (ν_4, ν_7, ν_9, ν_{11}, ν_{12}) is not large (2-5%). Only the vibration ν_{10} constitutes an exception. The large discrepancy in this case must be charged entirely to experimental error, which amounts to around 300%. For the cis-$C_2H_2D_2$ molecule, the agreement between theory and experiment is somewhat worse (1-15%). This may be explained by the face that a number of bands—for example, ν_1 and ν_{11}, ν_5 and ν_9—overlap and errors may creep in during their separation, as the authors of reference 4 point out. In addition, the discrepancy may be explained by the influence of mechanical and electrical anharmonicity. The large discrepancy in the case of vibration ν_6 is again to be explained by experimental error, amounting to about 70% of the value itself.

The electro-optical parameters used in this calculation correspond to one of the four possible combinations of signs of $\partial P_\xi/\partial Q_{b_u\,10}$ and $\partial P_\eta/\partial Q_{a_u\,12}$ for the C_2H_4 and and C_2D_4 molecules, namely $(\pm\pm)$. If one uses the electro-optical parameters corresponding to the other three combinations of signs $(\pm\mp;\ \mp\pm;\ \mp\mp)$ for ethylene, the agreement between the calculated and observed values of $\partial P/\partial Q_l$ in the case of the trans-$C_2H_2D_2$ and cis-$C_2H_2D_2$ molecules becomes worse. This fact again confirms the correctness of the calculation of the set of electro-optical parameters of ethylene in reference 1.

Table 1. Coefficients C_{ql} and D_l of the C_2H_3D and C_2HD_3 Molecules (in units of $10^{12} \cdot gm^{-1/2}$)
(Symmetry Type A′)

Coordinate	C_2H_3D								
	Q_1	Q_2	Q_3	Q_4	Q_5	Q_6	Q_{10}	Q_{11}	Q_{12}
q_1^+	0.7545	0.0201	−0.013	0.019	−0.0054	−0.0118	0.0007	−0.0125	0.0175
Q_{a_u}	−0.0546	0.2652	−0.0305	−0.0101	−0.018	0.0121	0.0045	−0.0791	0.1044
a	−0.0017	0.3895	0.0162	−0.0730	0.5404	0.0258	−0.1107	−0.0489	0.4935
q_2	−0.0852	0.0201	0.0017	0.722	−0.0149	−0.2629	0.0281	0.0281	0.0135
β^+	0.0002	0.0016	−0.3546	−0.086	0.7285	−0.0525	0.4043	0.0909	−0.0527
q_1^-	−0.0171	−0.0011	0.0186	0.2791	−0.0454	0.741	−0.0724	−0.0161	0.0018
β_1	−0.006	−0.1935	0.0287	0.0195	−0.9617	0.0229	0.4281	−0.0199	−0.1518
q_3^+	0.0124	0.0547	−0.0112	−0.0143	−0.0074	0.0281	−0.0252	0.5706	0.0184
β^+	0.0546	−0.4986	−0.1317	0.008	−0.0322	0.0018	0.0017	0.0183	0.0032

Coordinate	C_2HD_3								
	Q_1	Q_2	Q_3	Q_4	Q_5	Q_6	Q_{10}	Q_{11}	Q_{12}
q_2^+	0.4991	0.0502	0.0154	−0.1618	−0.0006	−0.0524	0.021	−0.229	−0.0283
Q_{a_u}	−0.1117	0.2717	0.023	0.0291	−0.041	−0.0386	−0.0025	0.0703	−0.0728
β^+	0.0602	−0.2226	0.4183	−0.0118	−0.3148	0.0057	−0.0018	0.0457	0.1714
q_1^-	0.1565	0.0034	0.0063	0.5711	0.0117	0.014	−0.0315	−0.0122	0.0027
β_1	0.1345	−0.3182	0.2071	0.0567	0.117	−0.0169	0.2152	−0.0314	−0.71
q_3^+	0.014	0.0219	−0.0144	−0.0251	−0.0183	0.7749	−0.0265	−0.0196	0.0108
β^+	−0.1124	0.0028	−0.3305	−0.1269	−0.3802	0.0571	0.4468	0.0555	0.1402
a	0.2175	0.0819	0.0031	−0.0343	−0.0165	0.0053	−0.0008	0.5652	−0.0246
	−0.1028	0.5267	0.1634	0.0207	0.2611	−0.0084	0.0092	0.0037	0.8025

Table 2. Coefficients C_{ql} and D_l of the as-$C_2H_2D_2$, cis-$C_2H_2D_2$, and trans-$C_2H_2D_2$ Molecules (in units of $10^{12} \cdot gm^{-1/2}$)

Coordinate	as-$C_2H_2D_2$ Symmetry type A_1					Coordinate	as-$C_2H_2D_2$ Symmetry type B_1			
	Q_1	Q_2	Q_3	Q_{11}	Q_{12}		Q_4	Q_5	Q_6	Q_{10}
q_H	0.7507	0.0181	0.0067	−0.0168	0.0216	q_d	0.5974	0.0058	0.0182	−0.0355
Q_a	−0.0596	0.2507	0.0442	0.1118	0.1414	β_H	0.1335	0.8089	−0.0765	0.364
β_a	0.0077	−0.1804	0.5345	0.113	−0.202	q_H	−0.0253	−0.0491	0.7903	−0.0246
q_d	0.0089	0.0704	0.01	0.5477	0.0459	β_d	−0.1577	−0.4697	0.0744	0.5315
β_H	0.0655	−0.5555	0.0281	0.0282	0.5799					

Coordinate	cis-$C_2H_2D_2$ Symmetry type A_1					Coordinate	cis-$C_2H_2D_2$ Symmetry type B_1			
	Q_1	Q_2	Q_3	Q_9	Q_{10}		Q_4	Q_5	Q_{11}	Q_{12}
q_d	0.5675	0.0722	0.0554	−0.0566	−0.0291	q_H	0.7755	0.03	0.0221	−0.0186
Q_a	−0.1102	0.2771	0.07	−0.053	0.0062	β_d	0.1239	0.7265	−0.0018	0.0806
β_H	0.0445	−0.3832	0.5766	0.03	−0.3597	q_d	−0.048	−0.0168	0.575	0.039
q_H	0.0308	0.0319	−0.0008	0.7748	0.0328	β_H	−0.0628	−0.3179	0.1716	0.8369
β_d	0.0505	−0.2908	0.1688	0.015	0.4751					

Coordinate	trans-$C_2H_2D_2$ Symmetry type B_2			
	Q_7	Q_8	Q_{13}	Q_{14}
q_H	0.7746	0.0035	0.046	−0.0124
β_d	0.0302	0.4963	0.025	0.3108
q_d	−0.0648	−0.0328	0.5726	0.0152
β_H	0.0252	−0.3838	0.0407	0.6904

Table 3. Coefficients $D_{\rho l}$ and $D_{\chi l}$ of Deuteroethylenes (in units of $10^{12} \cdot gm^{-1/2}$)

Molecule	Coordinate	Symmetry type	Q_1	Q_2	Q_3	Molecule	Coordinate	Symmetry type	Q_4	Q_5	Q_6
C_2H_2D	χ	A''	0.7499	−0.0122	−0.3288	as-$C_2H_2D_2$	ρ_1	B_2	—	0.9969	−0.1765
	ρ_2	A''	0.0156	1.2586	−0.0103		ρ_2	B_2	—	−0.0081	1.2587
	ρ_1	A''	0.0241	−0.1829	0.9389	cis-$C_2H_2D_2$	ρ	B_2	—	1.0965	—
C_2HD_3	χ	A''	0.3827	−0.3232	−0.4825	trans-$C_2H_2D_2$	χ	A_u	0.6477	−0.397	—
	ρ_2	A''	0.5213	0.9536	−0.1585		ρ	A_u	0.7747	0.6887	—
	ρ_1	A''	0.4744	−0.3709	0.9666						

Table 4. Electro-Optical Parameters of Deuteroethylenes (in D units/A)

$$\left\{\left(\frac{\partial a_1}{\partial q_1}-\frac{\partial a_4}{\partial q_1}\right)-\frac{1}{2\cos\frac{\theta}{2}}\frac{\partial r_{CC}}{\partial q_1}+p_{CH}\left[\cot\theta\left(\frac{\partial r_1}{\partial q_1}-\frac{\partial r_4}{\partial q_1}\right)-\frac{1}{\sin\theta}\left(\frac{\partial r_2}{\partial q_1}-\frac{\partial r_3}{\partial q_1}\right)\right]\right\} \quad -0.4982$$

$$\left\{\left(\frac{\partial a_2}{\partial q_1}-\frac{\partial a_3}{\partial q_1}\right)-\frac{1}{2\cos\frac{\theta}{2}}\frac{\partial r_{CC}}{\partial q_1}+p_{CH}\left[-\frac{1}{\sin\theta}\left(\frac{\partial r_1}{\partial q_1}-\frac{\partial r_4}{\partial q_1}\right)+\cot\theta\left(\frac{\partial r_2}{\partial q_1}-\frac{\partial r_3}{\partial q_1}\right)\right]\right\} \quad -0.0004$$

$$\left\{p_{CH}-2\left[\cot\theta\left(\frac{\partial a_1}{\partial r_1}-\frac{\partial a_4}{\partial r_1}\right)+\frac{1}{\sin\theta}\left(\frac{\partial a_2}{\partial r_1}-\frac{\partial a_3}{\partial r_1}\right)\right]+\frac{1}{\sin\frac{\theta}{2}}\frac{\partial r_{CC}}{\partial r_1}\right\}\frac{1}{r_{CH}} \quad -0.0644$$

$$\left\{\left[\left(\frac{\partial a_1}{\partial r_1}-\frac{\partial a_4}{\partial r_1}\right)+\cos\theta\left(\frac{\partial a_2}{\partial r_1}-\frac{\partial a_3}{\partial r_1}\right)\right]-\cos\frac{\theta}{2}\frac{\partial r_{CC}}{\partial r_1}\right\}\frac{1}{r_{CH}} \quad 0.0863$$

p_{CH} (in D units) 0.6858

Table 5. Infrared Band Intensities I_l (in $cm^{-1}/cm \cdot bar$) and Values of the Quantities $\partial P/\partial Q_l$ (in cgs units/$cm \cdot gm^{1/2}$) for the C_2H_2D and C_2HD_3 Molecules

Vibration No.	Symmetry	C_2H_2D Frequency (cm^{-1})	$\frac{\partial P_x}{\partial Q_l}$	$\frac{\partial P_y}{\partial Q_l}$	$\frac{\partial P_z}{\partial Q_l}$	$\frac{\partial P}{\partial Q_l}$	I_l	C_2HD_3 Frequency (cm^{-1})	$\frac{\partial P_x}{\partial Q_l}$	$\frac{\partial P_y}{\partial Q_l}$	$\frac{\partial P_z}{\partial Q_l}$	$\frac{\partial P}{\partial Q_l}$	I_l
ν_1	A'	3002	2.7043	−33.505	0	33.611	35.3264	2280	−0.7878	6.1418	0	11.5554	4.1746
ν_2	A'	1600	1.5748	8.4209	0	8.5669	2.2946	1596	−1.6059	−6.0614	0	6.2705	1.2293
ν_3	A'	1290	0.6108	−9.2645	0	9.2846	2.6052	1047	−0.0686	−17.377	0	17.3771	9.441
ν_4	A''	1001	0	0	40.2502	40.2502	50.6519	724	0	0	62.6899	62.6899	122.8725
ν_5	A'	3062	−14.0666	17.8262	0	22.5511	15.8099	2332	35.4918	−3.955	0	36.205	40.9823
ν_6	A'	1128	1.6504	−9.8861	0	10.0229	3.1409	995	−0.3304	4.0605	0	4.1039	0.5265
ν_7	A''	943	0	0	67.6864	67.6864	143.2394	765	0	0	29.8099	29.8099	27.7831
ν_8	A''	807	0	0	58.4255	58.4255	106.7246	919	0	0	50.8449	50.8449	80.8266
ν_9	A'	3103	50.8374	−6.6003	0	51.2641	82.1648	3045	21.9962	21.3827	0	38.4835	46.3029
ν_{10}	A'	730	5.1459	2.5248	0	5.7319	1.0272	610	4.7835	−1.3779	0	4.978	0.7748
ν_{11}	A'	2272	19.7076	18.8259	0	27.2545	23.2238	2222	7.2251	−30.0724	0	30.9282	29.9067
ν_{12}	A'	1403	1.0615	−30.5598	0	30.5782	29.2337	1290	−1.0153	−23.3862	0	23.4083	17.1316

Table 6. Infrared Band Intensities I_1 (in $cm^{-1}/cm \cdot bar$) and Values of the Quantities $\partial P/\partial Q_i$ (in cgs units/$cm \cdot gm^{1/2}$) for the as-$C_2H_2D_2$ and cis-$C_2H_2D_2$ Molecules

Vibration No.	as-$C_2H_2D_2$					cis-$C_2H_2D_2$					
	Symmetry	Frequency (cm^{-1})	$\frac{\partial P_i}{\partial Q_i}$	Calculated $\frac{\partial P_i}{\partial Q_i}$	I_1	Symmetry	Frequency (cm^{-1})	$\frac{\partial P_i}{\partial Q_i}$	Calculated $\frac{\partial P}{\partial Q_i}$	Experimental[a] $\frac{\partial P}{\partial Q_i}$	I_1
ν_1	A_1	3019	$\partial P_1/\partial Q_1$	31.1092	30.4331	A_1	2300	$\partial P_1/\partial Q_1$	28.6397	$\pm 27.5 \pm 1.0$	25.6446
ν_2	A_1	1585	$\partial P_2/\partial Q_2$	14.4198	6.501	A_1	1567	$\partial P_2/\partial Q_2$	3.2712	~ 0	0.3348
ν_3	A_1	1032	$\partial P_3/\partial Q_3$	16.4859	8.4974	A_1	1215	$\partial P_3/\partial Q_3$	$-$ 1.4208	~ 0	0.0631
ν_5	B_1	2333	$\partial P_5/\partial Q_5$	30.4367	28.9638	B_1	3055	$\partial P_5/\partial Q_5$	30.7108	± 32.4	29.4874
ν_6	B_1	1150	$\partial P_6/\partial Q_6$	0.9183	0.0264	B_1	1052	$\partial P_6/\partial Q_6$	13.7217	$\pm 7.5 \pm 5$	5.8868
ν_7	B_2	752	$\partial P_7/\partial Q_7$	62.2145	121.016	B_2	842	$\partial P_7/\partial Q_7$	92.2283	101.1 ± 2.0	265.9427
ν_8	B_2	943	$\partial P_8/\partial Q_8$	68.0978	144.9859	—	—	—	—	—	—
ν_9	B_1	3095	$\partial P_9/\partial Q_9$	43.3237	58.6828	A_1	3058	$\partial P_9/\partial Q_9$	-44.4256	± 44.7	61.7058
ν_{10}	B_1	676	$\partial P_{10}/\partial Q_{10}$	5.0623	0.8012	A_1	646	$\partial P_{10}/\partial Q_{10}$	4.6542	~ 0	0.6627
ν_{11}	A_1	2228	$\partial P_{11}/\partial Q_{11}$	25.0362	19.5973	B_1	2251	$\partial P_{11}/\partial Q_{11}$	26.1645	$\pm 30.0 \pm 1.0$	21.4035
ν_{12}	A_1	1384	$\partial P_{12}/\partial Q_{12}$	-24.2952	18.4544	B_1	1342	$\partial P_{12}/\partial Q_{12}$	29.2573	$\pm 31.3 \pm 0.2$	26.7626

Table 7. Infrared Band Intensities I_1 (in $cm^{-1}/cm \cdot bar$) and Values of the Quantities $\partial P/\partial Q_i$ (in cgs units/$cm \cdot gm^{1/2}$) for the trans-$C_2H_2D_2$, C_2H_4, and C_2D_4 Molecules*

Vibration No.	trans-$C_2H_2D_2$								C_2H_4		C_2D_4
	Symmetry	Frequency (cm^{-1})	$\frac{\partial P_1}{\partial Q_i}$	$\frac{\partial P_4}{\partial Q_i}$	$\frac{\partial P_6}{\partial Q_i}$	$\frac{\partial P}{\partial Q_i}$	Experimental[a] $\frac{\partial P}{\partial Q_i}$	I_1	Symmetry	I_1	I_1
ν_1	A_u	987	0	0	68.9336	68.9336	72.5 ± 1.0	148.5667	—	—	—
ν_7	A_u	725	0	0	61.2808	61.2808	59.4 ± 1.0	117.4109	B_{1u}	335.1829	196.702
ν_8	B_u	3064	-44.868	30.1141	0	54.037	55.4 ± 0.5	91.294	B_{2u}	112.4062	62.7556
ν_{10}	B_u	660	4.848	3.6027	0	6.0766	2.2 ± 6	1.1545	B_{2u}	1.1031	0.6388
ν_{11}	B_u	2270	28.0811	26.5555	0	38.649	37.7 ± 0.4	46.702	B_{1u}	62.6772	38.1408
ν_{12}	B_u	1300	-2.1437	32.4528	0	32.5235	33.2 ± 0.3	33.0716	B_{2u}	43.2808	23.2228

*Values of $\partial P/\partial Q_i$ for the C_2H_4 and C_2D_4 molecules are presented in reference 1.

Table 8. Fulfillment of the Intensity Sum Rules by the Infrared Bands of Deuteroethylenes

$\frac{3}{4}\sum I_1(C_2H_4) + \frac{1}{4}\sum I_1(C_2D_4) = \sum I_1(C_2H_2D)$			Δ
	B_{1u} 300.5627	A'' 300.6159	−0.0532
	B_{2u}, B_{3u} 195.7899	A' 195.0065	0.7834
$\frac{1}{4}\sum I_1(C_2H_4) + \frac{3}{4}\sum I_1(C_2D_4) = \sum I_1(C_2HD_2)$			Δ
	B_{1u} 234.3222	A'' 231.4823	−0.1601
	B_{2u}, B_{3u} 148.4353	A' 150.4693	−2.0343
$\frac{1}{2}\sum I_1(C_2H_4) + \frac{1}{2}\sum I_1(C_2D_4) = \sum I_1$ (as-$C_2H_2D_2$)			Δ
	B_{1u} 265.9424	B_2 266.002	−0.0596
	B_{2u} 88.4519	B_1 88.4741	−0.0222
	B_{3u} 83.6608	A_1 83.4832	0.1776
$\frac{1}{2}\sum I_1(C_2H_4) + \frac{1}{2}\sum I_1(C_2D_4) = \sum I_1$ (cis-$C_2H_2D_2$)			Δ
	B_{1u} 265.9424	B_2 265.9427	−0.0003
	B_{2u} 88.4519	A_1 88.4109	0.041
	B_{3u} 83.6608	B_1 83.5402	0.1206
$\frac{1}{2}\sum I_1(C_2H_4) + \frac{1}{2}\sum I_1(C_2D_4) = \sum I_1$ (trans-$C_2H_2D_2$)			Δ
	B_{1u} 265.9424	A_u 265.9777	−0.0353
	B_{2u}, B_{3u} 172.1126	B_u 172.222	−0.1094
$\frac{1}{3}[(\sum I_1)^2(C_2H_4) + (\sum I_1)^2$ (as-$C_2H_2D_2$) $+ (\sum I_1)^2$ (cis-$C_2H_2D_2$) $+ (\sum I_1)^2$ (trans-$C_2H_2D_2$)$] = (\sum I_1)^2(C_2H_2D) + \frac{1}{3}(\sum I_1)^2(C_2HD_3)$			Δ
	B_{1u}, B_{2}, B_{2}, A_u 108191.4324	A'' 108231.271	39.8386
	B_{2u}, B_{2u}, A_1, B_1, B_u 45654.2658	A' 45574.5685	79.6973
$\frac{1}{3}[(\sum I_1)^2(C_2D_4) + (\sum I_1)^2$ (as-$C_2H_2D_2$) $+ (\sum I_1)^2$ (cis-$C_2H_2D_2$) $+ (\sum I_1)^2$ (trans-$C_2H_2D_2$)$] = (\sum I_1)^2(C_2HD_3) + \frac{1}{3}(\sum I_1)^2(C_2H_2D)$			Δ
	B_{1u}, B_{2}, A_u 83639.4658	A'' 83707.2616	67.7958
	B_{2u}, B_{2u}, A_1, B_1, B_u 34787.168	A' 35316.9455	529.7775

Table 9. Comparison of the Calculated and Observed Intensity Values Γ_1 (in cm^2/mole) in the Infrared Spectra of a Mixture of Deuteroethylenes

ν(cm^{-1})	Molecule	Vibration No.	Experimental	Calculated*	Error (%)
3095	as-$C_2H_2D_2$	ν_8			
3019	as-$C_2H_2D_2$	ν_1			
3103	C_2H_3D	ν_9			
3092	C_2H_3D	ν_2	707±9.9	717.8049	1.5
3002	C_2H_3D	ν_1			
3105	C_2H_4	ν_9			
2989	C_2H_4	ν_{11}			
2333	as-$C_2H_2D_2$	ν_5			
2228	as-$C_2H_2D_2$	ν_{11}	765±9.8	427.4579	43.4
2272	C_2H_3D	ν_{11}			
1585	as-$C_2H_2D_2$	ν_6			
1384	as-$C_2H_2D_2$	ν_{12}	369±9.2	414.5003	12.3
1403	C_2H_3D	ν_{13}			
1444	C_2H_4	ν_{12}			
1150	as-$C_2H_2D_2$	ν_9			
1032	as-$C_2H_2D_2$	ν_3			
943	as-$C_2H_2D_2$	ν_8			
752	as-$C_2H_2D_2$	ν_7			
676	as-$C_2H_2D_2$	ν_{10}	6775±68	7331.0545	8.2
1001	C_2H_3D	ν_4			
943	C_2H_3D	ν_7			
807	C_2H_3D	ν_8			
949	C_2H_4	ν_7			

*a = $C_2H_2D_2$ (85%) + C_2H_3D (8.5%) + C_2H_4 (6.1%).

The results obtained in the present calculation permit us to carry out one more comparison of theory with experiment. In reference 4, data were given for the integrated intensities of the infrared bands of a mixture of isotopic molecules (the intensities themselves, $I = \int a_\nu d\nu$, were not measured, but rather the quantities $\Gamma = \int a_\nu d\ln\nu$, connected with the intensities by the relationship $\Gamma_1 = I_1/\nu_1$). Mass-spectrographic analysis permitted the composition of the mixture to be determined: 85.4% as-$C_2H_2D_2$, 8.5% C_2H_3D, and 6.1% C_2H_4. Evidently, using the theoretical values of I_1, one can calculate the intensities of the infrared bands of isotopic molecules in the given ratio. As can be seen from Table 9, the agreement obtained between theory and experiment is not bad for most of the band groups (in the regions 3100-2980; 1600-1350; 1150-650 cm^{-1}). The band group in the region 2250-2350 cm^{-1} constitutes an exception; for these bands, the discrepancy between the calculated and observed intensities is quite large.

Such calculations are of considerable interest in the interpretation of the infrared spectra of samples which represent a mixture of isotopic molecules.

REFERENCES

1. L. M. Sverdlov. Opt. i Spektr. 4, 697 (1958).
2. M. V. Vol'kenshtein, M. A. El'yashevich, and B. I. Stepanov. "Kolebaniya molekul." Vol. 2. (Molecular Vibrations), Gosudarst. Izd. Tekh.-Teoret. Lit., Moscow, 1949.
3. L. M. Sverdlov. Opt. i Spektr. 6, 729 (1959), Optics and Spectroscopy 6, 477 (1959); Ibid. 7, 21, 152 (1959), Ibid. 7, 11, 97 (1959).
4. R. Golike, I. Mills, W. Person, and C. Crawford. J. Chem. Phys. 25, 1266 (1956).
5. L. M. Sverdlov and N. L. Pakhomova. Zhur. Eksprl. i Teoret. Fiz. 26, 64 (1954).
6. J. Decius. J. Chem. Phys. 20, 1039 (1952).
7. L. M Sverdlov. Opt. i Spektr. 8, 253 (1960), Optics and Spectroscopy, 8, 129 (1960).

SPECTROSCOPIC INVESTIGATION OF THE HYDROGEN BOND IN ACID SILICATES AND PHOSPHATES

Ya. I. Ryskin and G. P. Stavitskaya

Received 29 August 1959

Infrared absorption spectra (in the range 420-3600 cm^{-1}) have been obtained for the acid silicates $Ca_4(SiO_3OH)OH$ and $Ca_4(SiO_3OD)OD$ and the acid phosphates K_2HPO_4, K_2DPO_4, $K_2HPO_4 \cdot 3H_2O$, $BaHPO_4$, and $BaDPO_4$. The bands observed have been assigned to normal vibrations of O_3XOH ions (X = Si, P), of water molecules, and of metal-oxygen polyhedra. The mutual influence of the interionic hydrogen bond and the intraionic X—O bonds is discussed. The frequencies of the planar deformation vibrations δOH of the O_3SiOH and O_3POH ions have been established.

INTRODUCTION

It is well known that, in order to form a hydrogen bond R'AH ... BR" between electronegative atoms A and B, a number of conditions must be fulfilled.** (a) The

**Aside from the condition R(A ... B) ≤ 2.71 A.

A—H bond must be partially ionic, or at least must possess the capability of becoming partially ionic under the influence of atom B, essentially so that the 1s orbital of the hydrogen atom will not be entirely occupied by its "own" electron and may be used to a corresponding extent for the formation of a donor-acceptor bond with atom B; (b) atom B must possess a pair of unshared electrons occupying an elongated orbital; (c) in order to attain maximum quantum-mechanical interaction between A and B, collinearity of the A—H bond with the axis of the orbital of the unshared electron pair of atom B is required.

In communication 2 we tried to link condition (a) with the electronic configuration of the molecule R'AH. In that work, the mutual influence of the X—O bonds in ions of the type O_3XOH (X = P, Si) and the interionic hydrogen bond XOH ... O was considered in more detail. The results obtained allow us to explain how strong hydrogen bonds can arise in acid phosphates and silicates. The reason why the range of variation of acid properties in hydroxyl-containing silicon compounds is significantly broader than in the analogous carbon compounds has also been clarified. The deformation vibrations δOH and the influence of a strong hydrogen bond on them have recently been considered in reference 3. Consequently, we shall here deal only cursorily with this question. The absorption spectra of the phosphates K_2HPO_4 and $BaHPO_4$ down to 700 cm^{-1} have been published in reference 4. We are apparently the first to carry out the extension of the spectral range to 420 cm^{-1}, to investigate the region of the

hydroxyl valence vibration with an apparatus of sufficiently high dispersion, and to obtain the spectra of the deuterated salts K_2DPO_4 and $BaDPO_4$.

An interpretation of the spectrum of dicalcium silicate α-hydrate was carried out in reference 2. An analysis of the spectra of monohydrogen orthophosphates, taking into account the effect of deuteration, has not been carried out up to the present time.

"SKELETAL" VIBRATIONS OF O_3XOH IONS (X = Si, P)

Among the compounds investigated in the present work, barium monohydrogen phosphate is characterized by the most complete structural data.[5] The crystal lattice of $BaHPO_4$ consists of discrete tetrahedral PO_4 ions, linked together by Ba^{2+} ions and by hydrogen bonds.* The P—O bond lengths are the same, within the limits of error of the measurements (±0.09 A), and equal to 1.56 A. The coordination sphere of the Ba atom consists of 10 oxygen atoms, of which 7 are more firmly bonded than the remaining 3.

*On the basis of the x-ray scattering data, it was possible to speak only of the probability of the presence of hydrogen bonds.

The structure of dicalcium silicate α-hydrate has been determined only to a first approximation.[6] The unit cell of the α-hydrate contains 8 $Ca_2(SiO_3OH)OH$ "molecules." The tetrahedral SiO_3OH groups are linked to the OH^- ions by short hydrogen bonds. The length of the hydrogen bridge R(OH ... O) is estimated as ~2.5 A. However, the precision with which inter-atomic distances were determined in the work referred to is only 0.2 A. Each Ca atom is surrounded by 6 O atoms, located at distances of 2.3-2.7 A.

In analyzing the skeletal vibrations of the O_3XOH group, one may consider the mass of the hydroxyl as concentrated at one point. With this assumption, the problem reduces to making the spectral transition $T_d(XO_4) - C_{3v}$ (O_3XOH). Such a transition is well known to be accompanied by a reduction in the degree of degeneracy of the F_2 vibrations and may be schematically represented in the following form:

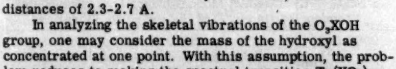

In the particular case where X = P, one may expect a significant lowering of the frequency of the vibration $\nu_1(A_1)$:

$$\nu_1(O_3POH) < \nu_1(PO_4). \quad (1)$$

Furthermore, the relationship

$$\frac{1}{2}(\nu_{3a} + \nu_{3s}) > \nu_3. \quad (2)$$

must be satisfied.

These conclusions arise from the following considerations. One of the unpaired electrons of the hydroxyl O atom is being used for the bond with hydrogen; hence the order of the bond between the hydroxyl O_1 atom (we shall designated it by the subscript $_1$) and the central X atom cannot exceed unity. At the same time, the order of the P—O bonds in the PO_4^{3-} ion amounts to 1.4, according to Siebert's estimate.[7] Assuming the valence of phosphorus in the phosphates to be constant, we must expect that when the order of one of the bonds ($P—O_1$) decreases, the order of the other three P—O bonds will increase.

Using the experimental dependence[8] between the order of the bond and its force constant f, we can approximately determine the quantities $f(P—O_1)$ and $f(P—O)$ relative to f(P—O) of the PO_4^{3-} ion, and then, with the help of the frequency formulas for the five-point model (C_{3v}),[9] convince ourselves of the truth of the inequalities (1) and (2).

In the range 420-1200 cm^{-1}, the experimental values for the frequencies of the strong absorption bands of the phosphates and the α-hydrate studied are in accord with the above scheme (see Fig. 1 and Table 1), and the intensities and widths of the absorption bands generally

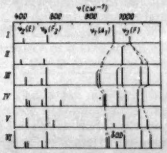

Fig. 1. Appearance of the transition $[PO_4]^{3-} \rightarrow [HOPO_3]^{2-}$ in Raman spectra (I, II) and in absorption spectra (III-VI) of solutions of various compounds. I—$[PO_4]^{3-}$; II—K_2HPO_4 (62% solution); III—K_2HPO_4; IV—$K_2HPO_4 \cdot 3H_2O$; V—$BaHPO_4$; VI—$BaDPO_4$.

correspond with the interpretation given (see Fig. 2). The presence of two components in the ν_{3bc} bands corresponds to the degree of degeneracy of this vibration in the isolated O_3PO_1 ion. The small splitting of the simple vibration $\nu_1(A_1)$ is also not unexpected and may be explained, for instance, by the resonance interaction of identical oscillators. It is possible that the presence of two components in the ν_{3a} band is brought about by the same cause. The latter are separated by a very large interval (~50 cm^{-1}), but the bond between the oscillators in this case is very strong. In crystalline and liquid silanols we have observed splittings of the ν(SiOH) frequency which reach 10-20 cm^{-1}, and in the silanols the energy of the hydrogen bond is several times weaker than in the phosphates under consideration. It is also possible that the splitting of the totally symmetric vibrations arises as a result of their interaction with lattice vibrations. For a more definite solution of the question discussed here, additional investigations are required, es-

Table 1. Infrared Absorption Spectra of Dicalcium Silicate α-Hydrate and of Monohydrogen Orthophosphates Frequencies (in cm^{-1}) of the "Skeletal" Vibrations of the O_3XOH Ions (X = Si, P)

Symmetry type	Symbol	Approximate interpretation	$Ca_2(SiO_3OH)OH$	$Ca_2(SiO_3OD)OD$	$BaHPO_4$	$BaDPO_4$	$K_2HPO_4 \cdot 3H_2O$	K_2HPO_4	K_2DPO_4
A_1	ν_{3a}	ν_aXO_3	863	862	948 (928)	986	998 950	978 949	975 940
	ν_{3s}	νXO_1	754	745	882	896	882	850	848
	ν_1	ν_sXO_3	747	732		884	871	835	836
	ν_{4s}	δ_sXO_3	428	428	?	514	517	517	517
E	ν_{3bc}	$\nu_{as}XO_3$	(990) (980)	(1007) (991)	1119 1073	1137 1085	1093 1068	1128 1085	1129 1083
			942	940					
	δ_{as}	$\delta_{as}XO_3$	472	464	540	542	541	544	540
	ν_2	ρXO_3	<400		428	430 442	416	426* 625	426	425
Other bands of significant intensity			679 513 (ν CaO)	655 497 (ν CaO)					

*Very weak.

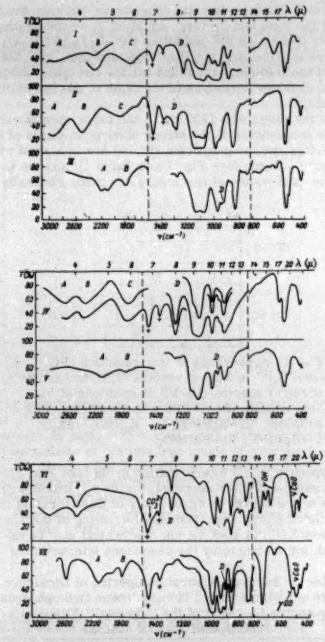

Fig. 2. Absorption spectra of powdered samples of potassium and barium monohydrogen phosphates, dicalcium silicate α-hydrate, and their deutero-analogs. I—$K_2HPO_4 \cdot 3H_2O$; II—K_2HPO_4; III—K_2DPO_4; IV—$BaHPO_4$; V—$BaDPO_4$; VI—$Ca_2[SiO_3OH]OH$; VII—$Ca_2[SiO_3OD]OD$. Bands of the immersion liquid are marked with the sign +.

pecially investigations of the polarization of the absorption bands in the spectra of monocrystalline samples.

The origin of the band at 625 cm^{-1} in the spectrum of $K_2HPO_4 \cdot 3H_2O$ remains unclear. This band appears too narrow for the rotational vibration of water.

In the region $\nu < 1100$ cm^{-1} (Fig. 2), in addition to the bands of the skeletal vibrations of the O_3SiOH ion, there are also observed in the spectrum of the α-hydrate bands which we assign to the valence vibration of the calcium-oxygen polyhedron (ν = 513 cm^{-1}) and to the "out-of-plane" deformation vibration of hydrogen γOH (ν = 712 cm^{-1}). The first assertion is based on the fact that a band $\nu \sim 500$ cm^{-1} is preserved in the spectra of calcium oxide (ν = 453 cm^{-1}, reflection spectrum), dicalcium orthosilicate β-Ca_2SiO_4 (ν = 524 cm^{-1}), and a number of other calcium silicates. The second assertion is demonstrated by the isotopic band shift: in the spectrum of the deutero-analog of the α-hydrate, the band at 712 cm^{-1} is absent, but there is a new band at 526 cm^{-1}. The frequency ratio of these bands amounts to 1.35. The assignment of the skeletal vibrations of the O_3SiOH ion is given in Table 1, and the scheme of the spectral transition $SiO_4 \rightarrow O_3SiOH$ has been published previously. The vibration $\nu_{3a}(A_1)$ of the α-hydrate is not split. The band at 942 cm^{-1} is evidently a component of the ν_{3bc} vibration of type E. It is possible that the difference just referred to in the shape of the ν_{3a} band of the α-hydrate and of the acid phosphates results from a structural peculiarity of the former: according to the opinion of Heller,[9] the short hydrogen bonds in the α-hydrate are localized not between identical $(O_3SiOH)^{3-}$ ions, but between an $(O_3SiOH)^{3-}$ ion and a hydroxyl OH^-.

The vibration $\nu_1(A_1)$ in the spectra of the α-hydrate and its deutero-analog is split. The average ν_1 frequency of the deuterated α-hydrate is somewhat lowered, which may be explained by the small increase in the mass of the oscillator ($m_{OH} < m_{OD}$).

VALENCE AND DEFORMATION VIBRATIONS OF THE HYDROXYLS

The absorption bands produced by hydrogen vibrations (νOH, δOH, and γOH) are easily recognized by the change in their frequencies on replacement of H by D. As is well known, the ratio k of the corresponding frequencies of these vibrations

$$k = \frac{\nu OH}{\nu OD}, \frac{\delta OH}{\delta OD}, \frac{\gamma OH}{\gamma OD},$$

in the absence of strong interactions with other normal vibrations of the molecule or ion, lies within the limits $1.30 \leq k \leq 1.41$. The frequencies presented in Table 2 have been picked out on the basis of this indication.

Table 2. Infrared Absorption Spectra of Dicalcium Silicate α-Hydrate and Monohydrogen Orthophosphates Frequencies (in cm^{-1}) of the Hydroxyl Vibrations

Assignment	Band symbol	$Ca_2[SiO_3OH]OH$	$Ca_2[SiO_3OD]OD$	$BaHPO_4$	$BaDPO_4$	$K_2HPO_4 \cdot 3H_2O$*	K_2HPO_4*	K_2DPO_4
ν(OH)—νOH(H_2O)		3532	2610			3300		
	A	2847	2120	(2882) (2755)	2115	2940	2940	(2210) (2105)
νOH, νOD (O_3XOH)	B	2594	1910					
	B	2450	1790	2420	1745	2285	2480	1825
	C			1730		1740	1910	
δOH, δOD	D	1282	910	1255	943	1214	(1280) (1275)	924
γOH, γOD		712	526					

*Potassium phosphate frequencies $\nu > 2500$ cm^{-1} are only approximate, since they were obtained on a spectrometer with an NaCl prism.

The spectra of the phosphates in the region 1200-3000 cm^{-1} each contain three characteristic very broad bands, designated by the letters A,* B, and C, and one narrow band D (see Figs. 2 and 3). The ranges of the positions of the maxima of these bands in the compounds studied are respectively 2850-2950, 2280-2450, 1700-1900, and 1200-1300 cm^{-1}. The isotopic coefficients of the A, B, and D bands vary within the limits 1.33-1.41, being usually nearer the upper limit for the D band.

*The A bands in some spectra are split.

The character of the spectrum of the α-hydrate in the region 1200-3000 cm^{-1} (see Figs. 2 and 3) is fundamentally the same as for the phosphates. In it there are bands of types A and B with halfwidths of 240 and 150 cm^{-1} respectively, and also a D band with a halfwidth of 20 cm^{-1}. In contrast to the phosphates, the α-hydrate does not have a band of type C; furthermore, a maximum at 2594 cm^{-1}, between the A and B bands, can be dis-

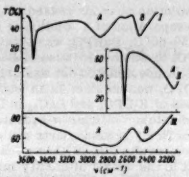

Fig. 3. Absorption spectra of acid silicates and phosphates in the region of the valence vibrations of the OH groups (LiF prism). I—$Ca_2[SiO_3OH]OH$; II—$Ca_2[SiO_3OD]OD$; III—$BaHPO_4$.

tinguished in its spectrum.

The ascription of the C band to a hydrogen vibration must be made with reservations, since this band has not yet been discovered in the spectra of the deuterated substances. It is possible that, when H is replaced by D, it becomes of low intensity and is masked by the absorption bands of the immersion liquids. The use of samples pressed into potassium bromide also gave no positive results, since, during the preparation of the samples, the highly hygroscopic phosphates exchange their deuterium for hydrogen too readily. The sensitivity of the position of the C band to hydrogen bonding and to the mass of the hydrogen impels one to think that this band corresponds to some vibration in which hydrogen takes part.

There can be no doubt that the A and B bands belong to the valence and the D band to the deformation vibrations of hydrogen in the XOH groups. Bands of types A and B are characteristic of a very wide circle of compounds with short (strong) hydrogen bonds.[4, 10]

The individual peculiarities of the spectra under discussion which appear in the frequency region 1200-3000 cm^{-1} are explained by the structural features of the corresponding compounds. The sharp peak around 3532 cm^{-1} in the spectrum of the α-hydrate may be ascribed to the OH^- ion. The band with a maximum around 3300 cm^{-1} in potassium monohydrogen phosphate trihydrate (not shown in the figure) is produced by the water of crystallization.

The new experimental data obtained allow us to reduce the number of possible explanations of the causes of the splitting of the valence vibration νOH when strong hydrogen bonds are present. Thus, for example, the supposition has been expressed that the bands of type A and B in the spectrum of potassium dihydrogen phosphate correspond to two normal vibrations of the $O_2P(OH)_2$ ion.[11] However, the almost complete similarity of the spectra of the secondary and tertiary phosphates makes this ascription of the A and B bands inadmissible. There is also no basis for introducing A, B, and C bands corresponding to hydrogen bonds of a different length, since in those cases where the crystal structure is known the OH ... O distances are identical within the limits of error of the measurement (for example, in the $BaHPO_4$ crystal all the R(OH ... O) = 2.52).

THE INTERIONIC HYDROGEN BOND AND THE ORDER OF THE INTRAIONIC BONDS

The conversion of the crystal K_2HPO_4 into $K_2HPO_4 \cdot 3H_2O$ is apparently accompanied by a strengthening of the hydrogen bonds, since the frequencies of the B and C bands are lowered by 200 and 170 cm^{-1} respectively during this transition. Simultaneously, a leveling of the P—O and P—O_I bonds takes place, manifesting itself in a closer approach of the bands ν_{3s} and ν_{3bc}. The influence of the hydrogen bond on the force constant and, evidently, on the order of the intraionic bonds manifests itself also in the spectrum of $BaHPO_4$, although here it is partially masked by the action of the doubly-charged cation. The phenomenon just described may be explained in the following way. In the system $O_3PO_IH \ldots O_{II}PO_3OH$,* the electrostatic influence of the O_{II} atom produces a displacement of a negative charge σ⁻ (σ < e) from the hydrogen atom of the O_3PO_IH ion in the direction of the oxygen O_I. If the 1s orbital of the hydrogen is hereby freed to any significant extent, then there arises a corresponding probability of a transition of one of the unshared electrons of the O_{II} atom into this orbital; i.e., in other words, an H ... O_{II} bond of donor-acceptor character is formed. The latter may attain a high strength only in the case when the shift of the charge σ⁻ within the O_3XO_I group is energetically favored. In the ion O_3PO_I, the charge σ⁻ is distributed over the three oxygen atoms of the O_3P group, lowering their valence and the order of their bonds with P. This manifests itself in a lowering of the frequencies of the components of the ν_{3bc} band as the hydrogen bond grows stronger. The displacement of the charge σ⁻ also brings about a partial freeing of one of the unpaired electrons of the O_I atom, which, if the valence of phosphorus is preserved, must lead to a strengthening of the P—O_I bond. Actually, the frequency $\nu_1(A_1)$ increases by 30 cm^{-1} upon even the relatively small strengthening of the hydrogen bond which takes place in the transition from the structure K_2HPO_4 to the structure $K_2HPO_4 \cdot 3H_2O$. Evidently the leveling of the bonds of the O_3PO_I ion to an average order of 1.25-1.41[7] and the formation of a strong $O_IH \ldots O_{II}$ hydrogen bond are energetically favored.

In contrast to the case considered here, the displacement of an electron from H to R in systems of the type $R_3CO_IH \ldots O_{II}R'$ (where the R's are aliphatic or aromatic radicals) would be linked with a weakening of the single C—R bonds and an increase in the order of the C—O_I bond. Such a process is energetically disfavored,* and R_3COH molecules (alcohols, phenols) do not form strong hydrogen bonds.

The ion $(O_3SiOH)^{3-}$, as was shown above, is capable of entering into strong hydrogen bonds. This fact is hardly compatible with the assumption of the quadrivalence of silicon. This can be explained by admitting that, beside the hybrid $3sp^3$ orbital, a 3d orbital of silicon is also made use of in the Si—O_I bond. Indeed, if in the formation of the Si—O bond only electrons lying in sp^3 orbitals could take part, the fixation of the negative charge σ⁻ of the hydrogen within the SiO_4 group would have entailed, as in the $R_2SOH \ldots OR'$ systems, a strengthening of the Si—O_I bond at the expense of a lowering of the covalent character (i.e., the order) of the single Si—O bonds of the SiO_3 group. But, as has already been noted, such a process is energetically disfavored. We must then assume that the probability of transition of an electron of the hydrogen atom to the 3d orbital of silicon is sufficiently large. Energetically, this process may be compensated for (and with something to spare, evidently) by the formation of a $d\pi-p\pi$ bond between Si and O_I and a strong $O_I \ldots O_{II}$ hydrogen bond. We must take into account here that in the $(O_3SiOH)^{3-}$ ion the central Si atom carries a normal positive charge and is surrounded by strongly electronegative atoms. The positive charge of the central

*O_I and O_{II} are the oxygen atoms joined by an H-bond.

*As is well known, the energy of a double bond is less than twice the energy of the corresponding single bond.

atom increases its electron affinity and at the same time lowers the energy of the 3d orbital.[12]

It is possible that the 3d orbital of silicon is used to some degree even in the ion $(SiO_4)^{4-}$ and, consequently, in the O_3Si group of the isolated O_3SiOH ion, since according to Siebert's estimate the order of the Si—O bond in $(SiO_4)^{4-}$ amounts to 1.19.[7] In this case, the leveling of the SiO_3 and SiO_T bonds would also play some part in the fixation of the charge σ^-. But the formation of several $d\pi-p\pi$ bonds with a tetrahedral atom with sp^3 hybridization is unlikely, since a d orbital which is oriented in such a way as to ensure maximum interaction with a π orbital of one of the O atoms will evidently not be favorably oriented for any other O atom.[13]

A great strengthening of the $Si-O_T$ bond may be observed on formation of a hydrogen bond between the molecules of any silanol and pyridine or dioxane (the latter, as is well known, is distinguished by its very pronounced electron-donating ability). Thus, for example, the "isolated" $(C_2H_5)_3SiOH$ molecule (a dilute solution of the silanol in carbon disulfide) has the frequency νSiO = 806 cm^{-1}, but when there is interaction with a dioxane molecule, νSiO = 864 cm^{-1}. The increase in frequency cannot be ascribed to a change in the ionic character of the bond, since the latter shows no significant influence on the force constant or the characteristic frequency.[14]

In the light of the data set forth, we may understand the cause of the great width of the range of variation of acid properties in the hydroxyl-containing compounds of silicon. It is known that the νOH frequencies of isolated silanol molecules are 80-90 cm^{-1} higher than the corresponding frequencies of carbinols. This is a reflection of the fact that the energy of the covalent fraction of the hydrogen-to-oxygen bond proves to be higher for the silanols. In other words, isolated silanol molecules are distinguished from the analogous carbinol molecules by their more basic character. The basic properties are still more pronounced in SiOH groups located on the dehydrated surface of silica gel or silicate glass: for them, $\nu OH = 3749 \pm 1$ cm^{-1},[15] while for carbinols νOH = 3600 cm^{-1}.

Thus one may draw the conclusion that the hydrogen bond lowers the covalent fraction of the energy of the O—H bond and correspondingly increases the acidity of the compound. The latter is also true for those hydroxyl-containing carbon compounds in which the central atom has no multiple bonds. However, in the analogous silicon compounds, which are distinguished by the possibility of the formation of $d\pi-p\pi$ bonds between Si and O, the process of diminution of the electronic screening of the hydrogen may operate within wider limits.

EXPERIMENTAL

Substances. K_2HPO_4 (anhydrous) was obtained from Chda (a trademark?) trihydrate by drying in vacuo at 50-60°C until the evolution of water ceased. K_2DPO_4 was obtained by the evaporation of a solution of K_2HPO_4 in D_2O in vacuo at 50-60°C. $BaHPO_4$ was obtained from a solution of K_2HPO_4 to which a solution of $BaCl_2$ was added. The $BaHPO_4$ which precipitated out was dried in vacuo at 50-60°C. $BaDPO_4$ was obtained in an analogous manner from solutions of K_2DPO_4 and $BaCl_2$ in D_2O.

Deuterated dicalcium silicate α-hydrate was obtained from a mixture of finely ground quartz and calcium oxide, suspended at a temperature of 70°C in a fourfold quantity (with respect to the weight of the dry mixture) of D_2O and kept for 4 days in a hydrothermal bomb at 170°C. The ordinary α-hydrate was similarly obtained from a suspension in distilled water.

The compounds obtained were checked by x-ray analysis. Small admixtures of $BaCl_2$ were found in the $BaHPO_4$ and $BaDPO_4$, and of calcite in the α-hydrate and the α-hydrate-d.

Samples. Freshly-dried paraffin and fluorinated oils were used as immersion liquids.

Apparatus. Spectra were obtained with the help of single-prism autocollimating apparatus: VIKS M-3 (700-3000 cm^{-1} region, NaCl prism), ISP-14 (420-700 cm^{-1} region, KBr prism), IKS-11 (3700-2000 cm^{-1} region, LiF prism).

REFERENCES

1. C. G Cannon. Spectrochim. Acta **10**, 341 (1958).
2. Ya. I. Ryskin. Opt. i Spektr. **7**, 278 (1959), Optics and Spectroscopy **7**, 177 (1959).
3. Ya. I. Ryskin, G. P. Stavitskaya. Opt. i Spektr. **7**, 834 (1959), Optics and Spectroscopy **7**, 488 (1959).
4. F. Miller and C. Wilkins. Anal. Chem. **24**, 1253 (1952).
5. G. Burley. J. Research Natl. Bur. Standards **60**, 23 (1958).
6. L. Heller. Acta Cryst. **5**, 724 (1952).
7. H. Siebert. Z. anorg. u. allgem. Chem. **275**, 225 (1954).
8. H. Siebert. Z. anorg. u. allgem. Chem. **273**, 170 (1953).
9. J. Wagner. Z. physik. Chem. **40**, 36 (1938).
10. J. T. Braunholtz, G. E. Hall, F. G. Mann, and N. Sheppard. J. Chem. Soc. 868 (1959).
11. P. S. Narayanan. Proc. Indian Acad. Sci. **A33**, 240 (1951).
12. W. Moffitt. Proc. Roy. Soc. **A200**, 409 (1950).
13. H. H. Jaffe. J. Phys. Chem. **58**, 185 (1954); Uspekhi Khim. **26**, 1060 (1957).
14. J. Goubeau. Angew. Chem. **69**, 77 (1957).
15. V. A. Nikitin, A. N. Sidorov, and A. V. Karyakin. Zhur. Fiz. Khim. **30**, 117 (1956); R. S. McDonald. J. Am. Chem. Soc. **79**, 850 (1957).

VIBRATIONAL SPECTRA OF ALKOXYSILANES AND SILOXANES. III. VIBRATIONS OF SILICON-OXYGEN CHAINS IN THE SPECTRA OF POLYALKOXYSILOXANES

A. N. Lazarev and M. G. Voronkov

Received 11 August 1959

The vibrational spectra of polymethoxy- and polyethoxysiloxanes with different numbers of SiO_4 tetrahedra in the chain have been investigated. The change in the vibrations of the silicon-oxygen skeleton of the molecules on polymerization has been studied. The analogies between the spectra of the polyalkoxysiloxanes and of the silicates are discussed.

INTRODUCTION

The structure of the polyalkoxysiloxane molecules which are the products of the hydrolytic condensation of esters of orthosilicic acid—the tetraalkoxysilanes—recalls in many ways the structure of the silicates. The framework of the polyalkoxysiloxane molecules is formed of chains, rings, and more complex combinations of silicon-oxygen tetrahedra, joined together by shared oxygen atoms:

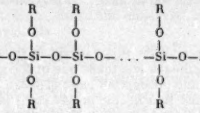

The complex anions in the silicates are constructed in a similar way. Therefore, a spectroscopic investigation of a series of polysilkoxysiloxanes with a gradually increasing number of "links" in the chain is of interest in two respects. On the one hand, the study of individual low-molecular polyalkoxysiloxanes facilitates the interpretation of the spectra of the high-molecular hydrolysis products of tetraalkoxysilanes. On the other hand, the analogies in structure and in spectra between the polyalkoxysiloxanes and the silicates may be used in the spectroscopic investigation of the structure of the latter.

In order to establish connections between the structure and the vibrational spectra of the polyalkoxysiloxanes and the silicates, it is necessary, in the first approximation, to solve two problems. First, the frequencies of the normal vibrations of the SiO_4 group must be identified, which has been accomplished through the investigation of the spectra of orthosilicates[1, 2] and the spectrum of the SiO_4 ion in solution.[3] The vibrations of the SiO_4 group in the spectra of the tetraalkoxysilane molecules $Si(OR)_4$ were discussed by us in a preceding communication.[4] The second problem is the study of the changes in the vibrations of the silicon-oxygen tetrahedra on polymerization. The present communication is devoted to this question.

EXPERIMENTAL PROCEDURE

The polyalkoxysiloxanes investigated were obtained by the hydrolysis of large quantities (1-1.5 kg) of $Si(OCH_3)_4$ and $Si(OC_2H_5)_4$ in a medium of the corresponding alcohol (HCl catalyst). The separation of the polyalkoxysiloxanes was accomplished by repeated fractional distillation in vacuo through a column with glass packing in the presence of traces of phosphoric acid—a disproportionation inhibitor. The physico-chemical constants and analytical data of the compounds studied are presented in Table 1.

Table 1. Physico-Chemical Constants and Analytical Data of the Investigated Compounds of Type $(RO)_3Si[OSi(OR)_2]_nOR$

R	n	T_b(p)**	d_4^{20}	n_D^{20}	Si content (%)	
					Found	Calculated
CH_3 . .	0	121.0(760)	1.035	1.3680	18.49; 18.50	18.45
CH_3 . .	1	58(1)	1.1222	1.3806	21.69; 21.62	21.72
CH_3 . .	2	107(1)	1.1655	1.3869	—	—
CH_3 . .	4*	163—164(5)	—	1.3905	23.99; 23.94	24.35
CH_3 . .	6*	170—172(1)	—	1.3944	—	—
C_2H_5 . .	0	168.3(760)	0.9334	1.3830	13.45; 13.47	13.48
C_2H_5 . .	1	98(1)	0.9879	1.3914	16.38; 16.44	16.40
C_2H_5 . .	2	132(1)	1.0300	1.3950	17.72; 17.79	17.67
C_2H_5 . .	4*	167(4)	—	1.3994	18.72; 18.68	18.85

*Formulas assumed on the basis of spectroscopic data.
**T_b – boiling point (°C); p – pressure (mm Hg).

The identification of the first three compounds in each series (the polymethoxy- and polyethoxysiloxanes) gives rise to no doubts. The matter is more complicated with the higher-boiling polyalkoxysiloxanes. The separation of the fractions is complicated by the small differences in boiling point. A reliable identification of the individual compounds is made more difficult by the insignificance of the differences in elementary composition (and molecular weight).

In Table 1, formulas corresponding to linear compounds with five or seven silicon-oxygen tetrahedra in the chain have been provisionally ascribed (on the basis of the spectroscopic data) to the high-boiling fractions. This is not in conflict with the physico-chemical constants of these fractions or the analytical results for Si content, inasmuch as, with regard to the latter, the assumed "pentamer" might be a "tetramer" as well as a "pentamer."

The apparatus and methods of the spectroscopic investigation did not differ from those used in previous works.[4, 5]

EXPERIMENTAL RESULTS

In Table 2 are presented the values of the frequencies in the vibrational spectra of the five polymethoxysiloxanes investigated by us. The corresponding infrared spectral curves are presented in Fig. 1.

As can be seen from the data presented, in the frequency region of "skeletal" vibrations the formation and lengthening of the chain lead to substantial changes in the spectrum. Thus the band of the valence vibrations of the C—O bonds, observed in the absorption spectrum of the "monomer"—tetramethoxysilane—at 1093 cm^{-1}, is split into three bands on going to the "dimer" $(CH_3O)_3SiOSi(OCH_3)_3$. The highest frequency of these three bands continues to shift toward higher frequencies on further lengthening of the chain. In the Raman spectrum of the "monomer," the two lines at 1082 and 1111 cm^{-1} correspond to C—O vi-

Table 2. Frequencies in the Vibrational Spectra of Polymethoxysiloxanes*

$Si(OCH_3)_4$				$OSi_2(OCH_3)_6$				$O_2Si_3(OCH_3)_8$			$O_3Si_4(OCH_3)_{10}$			$O_4Si_5(OCH_3)_{12}$
Ram.**			IR frequency (cm^{-1}) (intensity)	Ram.			IR frequency (cm^{-1}) (intensity)	Ram.		IR frequency (cm^{-1}) (intensity)	Ram.		IR frequency (cm^{-1}) (intensity)	IR frequency (cm^{-1}) (intensity)
Frequency (cm^{-1})	Intensity	Polarization ρ)		Frequency (cm^{-1})	Intensity	Polarization ρ)		Frequency (cm^{-1})	Intensity		Frequency (cm^{-1})	Intensity		
				168	0.5 d	—								
221	0.5 d	—		250—270	1 vd	—		254	1 d		210	0 vd		
312	1	—		325	0.5 vd	—		330	0 vd		311	1 d		
				386	1 vd	—		416	0 vd		403—440	0 vd		
412	1 vd	0.80	<418 s	445	1.5	—	442 s			450 s			424 s	453 s
458	?	—									488	?		
545	?	—												530 w
													557 vw	561 w
				577	10 sh	0.05	588 w	554	8 sh	560 w			589 w	597 w
640	10 sh	0.03	639 vw					639	0 d	629 m	638	8 sh	626 w	627 m
				692	0.5	—	681 m	702	3 sh	701 m	***		654 w	651 vw
													710 m	681 w
														712 w
				808	7 sh	0.50	—	817	5	804 w	827	2 d	797 w	797 w
844	3 d	0.80	825 s 838 s	838	4 d		841 s	840	5 vd (.)	843 s	842	3 d	844 s	843 s
1082	5	0.20	1093 vs	1000—1126	4 vd	0.40	1081 vs 1098 vs	~1024	3 vd (.)	1080 vs 1099 vs	1086—1126	2 d	1074 vs 1100 vs	1079 vs 1099 vs
1111	4						1133 m			1138 m			1140 m	1154 m
				1163	0.5 d	—		1164	0 d		1164	0 d		
1186	4 d	0.32	1190 s	1118	2	0.30	1157 s	1156	1 d	1196 s	1192	1 d	1158 s	1196 s
1463	6	0.80	1469 m	1461	9 d	0.80		1464	8 (o.vd)		1457	6 d		
1476	2			1471							1472			
2856	10	—		2853	9	—		2855	10 sh		2852	10 sh		
2953	4	—		2955	5	—		2957	6 sh		2956	6 sh		
								2962	2 d		2964	2 d		

*See first footnote in text.

**Symbols: Ram. – Raman spectrum (band character: vd – very diffuse, d – diffuse, sh – sharp); IR – infrared absorption spectrum (band intensity: vs – very strong, s – strong, m – medium, w – weak, vw – very weak).

***It is possible that there are 2 weak lines in the 680-720 cm^{-1} region.

brations;[4] in the spectra of the polymethoxysiloxanes, a band with a difficultly-resolvable structure is observed in this region.

For purposes of the present work, the changes in the valence vibrations of the Si–O bonds as the chain of silicon-oxygen tetrahedra lengthens are of the greatest interest. The double absorption band 838-825 cm^{-1} and the broad depolarized Raman line at 844 cm^{-1} in the spectrum of $Si(OCH_3)_4$ correspond to the trebly degenerate vibration of the $SiOH_4$ group (the small splitting of this vibration has been ascribed by us[4] to removal of the degeneracy in consequence of the lower symmetry (V_d) of the $Si(OCH_3)_4$ molecule as compared with the isolated SiO_4 group (T_d): $F_2 \rightarrow B_2 + E$). In the spectrum of hexamethoxydisiloxane, a single absorption band at 841 cm^{-1} is observed, to which corresponds a Raman line at 838 cm^{-1}. In addition, in the latter case there is a sharp line at 808 cm^{-1} which is absent from the absorption spectrum. In polarization measurements (with photoelectric recording), the lines 808 and 838 cm^{-1} are not resolved, but a lowering of the degree of depolarization ρ from 0.8 to 0.5 is noted on going from the "monomer" to the "dimer."* It may be supposed that one of the two lines of the "dimer," the one at 808 cm^{-1} judging from its intensity and small width, is polarized; i.e , that it is produced by a totally symmetric vibration. In the spectra of the "trimer" and of the polymethoxysiloxanes with a longer chain, two bands are observed in this region in both the absorption and the Raman spectrum.

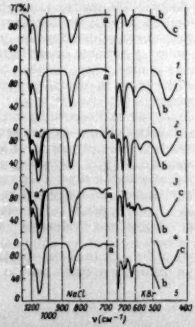

Fig. 1. Infrared absorption spectra of polymethoxysiloxanes. d—thickness of the absorbing layer (in mm); C—concentration of a solution in CS_2 (in %); C′—the same in CCl_4. 1—$Si(OCH_3)_4$ (curve a—d = 0.15, C = 6; curve b—d = 0.03, C = 100; curve c—d = 0.015, C′ = 20); 2—$OSi_2(OCH_3)_6$ (curve a—d = 0.015, C = 8; curve b—d = 0.03, C = 100; curve c—d = 0.015, C′ = 20); 3—$O_2Si_3(OCH_3)_8$ (curve a—d = 0.015, C = 10; curve a′—d = 0.015, C = 4; curve b—d = 0.03, C = 100; curve c—d = 0.015, C′ = 20); 4—$O_4Si_5(OCH_3)_{12}$ (curve a—d = 0.015, C = 10; curve a′—d = 0.015, C = 5; curve b—d = 0.03, C = 100; curve c—d = 0.015, C′ = 20); 5—$O_6Si_7(OCH_3)_{16}$ (curve a—d = 0.015, C = 10; curve b—d = 0.03, C = 100; curve c—d = 0.015, C′ = 20).

The frequency of the totally symmetric valence vibration of the SiO_4 group in the spectrum of liquid $Si(OCH_3)_4$ is observed in the form of an intense polarized Raman line at 640 cm^{-1} and a weak band in the absorption spectrum. In the absorption spectrum of the vapor this frequency is absent. In the spectrum of hexamethoxydisiloxane, the frequencies 577 and 692 cm^{-1} are observed, the first of which is more intense (and polarized) in the Raman spectrum while the second is much more intense in the absorption spectrum. In the spectrum of the "trimer" in the same region, three bands are observed, of which the lowest frequency one is the most intense in the Raman spectrum and weak in the absorption spectrum. In the absorption spectra of

*The measurements of the state of polarization of the Raman lines (the spectra being recorded photoelectrically) were carried out together with Ya. S. Bobovich and T. P. Tulub.[5]

Table 3. Frequencies in the Vibrational Spectra of Polyethoxysiloxanes*

$Si(OC_2H_5)_4$				$OSi_2(OC_2H_5)_6$				$O_2Si_3(OC_2H_5)_8$				$O_3Si_4(OC_2H_5)_{12}$
Raman.**			IR frequency (cm^{-1}) (intensity)	Raman.***			IR frequency (cm^{-1}) (intensity)	Raman.***			IR frequency (cm^{-1}) (intensity)	IR frequency (cm^{-1}) (intensity)
Frequency (cm^{-1})	Intensity	Polarization (ρ)		Frequency (cm^{-1})	Intensity	Polarization (ρ)		Frequency (cm^{-1})	Intensity	Polarization (ρ)		
232	0 d	—										
300												
328	1 d	—										
424	0 d	—										
498	—		478 m				482 m				484 m	483 s
												571 vw
				614	2	0.13	612 w	604	1.5	0.18	589 vw	614 w
650	6 sh	0.05	656 w					640	0	—	643 m	639 w
				685	0	—	687 m	703	0.5	—	706 m	664 w
												712 w
792	3 d	0.62	780 s	800	1.5	0.31	793 s	796	2	0.34	794 s	797 s
822			809 m				810 m				809 m	807 m
939	3	0.53	—	935	1	0.78	938 w	940	1	0.80	940 w	935 w
974	1	—	962 s	—			966 s	—			969 m	969 m
1086	8 d	0.27	1080 vs	1095	2.5	0.27	1084 vs	1076	2.5	0.22	1082 vs	1084 vs
			1102 vs				1105 vs				1105 vs	1105 vs
1173	4.5	0.15	1163 m	1170	0	—	1164 s	1170	0	—	1168 s	1166 s
1205	2	0.74	—									
1302	4.5 sh	0.77	1291 w	1296	1.5	0.70	1298 w	1295	2	0.48	1295 w	1297 w
1395	2 sh	—	1391 m									
1441	10	0.83	1441 w	1456	4	0.70		1456	4	0.55		
1456			1456 w									
1489	2 sh	—	1482 w									

*See first footnote in text.
**For symbols, see Table 2.
***Studied only with photoelectric recording. A large proportion of the weak lines escaped observation.

the two higher-boiling fractions in the spectral region under consideration, there are observed, respectively, five and seven bands.

In the region of deformation vibrations, a shift of the band near 400 cm^{-1} toward higher frequencies, according to the degree of "polymerization," may be noted. The experimental data in the lower-frequency region are apparently insufficient to judge the character of the frequency shift.

In the vibrations of the Si—O bonds of the polyethoxysiloxanes as the chain of silicon-oxygen tetrahedra is lengthened, changes are observed analogous to the changes in the polymethoxysiloxane spectra (Fig. 2, Table 3). In the spectrum of $Si(OC_2H_5)_4$, two absorption bands which change little on going over to the spectrum of the "dimer" correspond to the antisymmetric valence vibration of the SiO_4 group. However, in the Raman spectrum of the "dimer," which was studied only by the photoelectric method which did not permit resolution of the broad 800 cm^{-1} band into its components, a lowering of ρ from 0.6 to 0.3 may be noted, as in the case of hexamethoxydisiloxane. In the region of the symmetric valence vibration, the spectra of the polyethoxysiloxanes differ from the corresponding polymethoxysiloxanes only by a somewhat lesser splitting of this vibration.

The bands in the $Si(OC_2H_5)_4$ spectrum around 940 cm^{-1} (active in the Raman spectrum) and 970 cm^{-1} (active in both absorption and Raman spectra) correspond to the C—C valence vibrations. The change in symmetry of the molecules on "polymerization" results in the observation of both frequencies in the absorption spectra of the polyethoxysiloxanes.

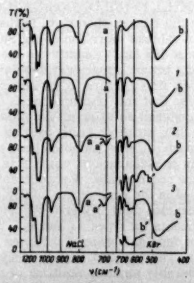

Fig. 2. Infrared absorption spectra of polyethoxysiloxanes. d—thickness of the absorbing layer (in mm), C—concentration of a solution in CS_2 (in %). 1—$Si(OC_2H_5)_4$ (curve a—d = 0.015, C = 8; curve b—d = 0.015, C = 100); 2—$OSi_2(OC_2H_5)_6$ (curve a—d = 0.015, C = 10; curve b—d = 0.02, C = 100); 3—$O_2Si_3(OC_2H_5)_8$ (curve a—d = 0.015, C = 12; curve a′—d = 0.015, C = 30; curve b—d = 0.02, C = 100; curve b′—d = 0.015, C = 100); 4—$O_3Si_4(OC_2H_5)_{12}$ (curve a—d = 0.015, C = 12; curve a′—d = 0.015, C = 25; curve b—d = 0.02, C = 100; curve b′—d = 0.015, C = 100).

DISCUSSION OF RESULTS

As was previously shown,[4] the shift in the SiO_4 group frequencies in the spectrum of the $Si(OCH_3)_4$ molecule in consequence of the interaction of the Si—O and C—O bonds is quite large. However, the splitting of the vibrations of the SiO_4 group brought about by the symmetry (lower than T_d) of the tetramethoxysilane molecule proved to be insignificant. This allows us to consider qualitatively the changes in the valence vibrations of the Si—O bonds in the spectra of the polymethoxysiloxanes as a result of joining a large number of silicon-oxygen tetrahedra into a chain, neglecting the influence of the CH_3 groups in the first approximation.

First of all, let us consider the transition from the $Si(OCH_3)_4$ molecule to $(CH_3O)_3SiOSi(OCH_3)_3$. Here, as already noted, we shall consider the changes in the spectrum brought about by the transition from a single SiO_4 tetrahedron to the "doubled" Si_2O_7 tetrahedra.

The Si_2O_7 group has a symmetry no higher than D_{3d} if the SiOSi angle equals 180°, and no higher than C_{3v} if ∠SiOSi ≠ 180°. If we neglect the deformation vibrations of SiOSi and the twisting ones of SiO_3, then we can carry out a comparison of the normal vibrations of the SiO_4 and Si_2O_7 groups:

The selection rules for the normal vibrations of these groups are presented in Table 4. From the scheme presented, it follows that the joining of silicon-oxygen tetrahedra into an Si_2O_7 group must lead to a splitting of the normal vibrations of the SiO_4 group: four ($2F_2$, E, A_1) vibrations of the SiO_4 group break down into 12 (D_{3d}) or 18 (C_{2v}) vibrations in the Si_2O_7 group. Polarized Raman lines (of symmetry types A_1 or A_{1g}) must then be observed in the regions of both the symmetrical and the antisymmetrical valence vibrations of the SiO_4 group.

Table 4. Selection Rules for the Vibrations of the SiO_4 and Si_2O_7 Groups

"Molecules"	Symmetry types of the vibrations, and selection rules			
SiO_4 (T_d)	A_1	E	F_2	
IR	inact.	inact.	act.	
Ram.	act., P	act., DP	act., DP	
Si_2O_7 (D_{3d}) ($\angle SiOSi = 180°$)	A_{1g}	A_{2u}	F_g	E_u
IR	inact.	act. ($\parallel C_3$)	inact.	act. ($\perp C_3$)
Ram.	act., P	inact.	act., DP	inact.
Si_2O_7 (C_{2v}) ($\angle SiOSi \neq 180°$)	A_1	A_2	B_1	B_2
IR	act.	inact	act.	act.
Ram.	act., P	act., DP	act., DP	act., DP

Symbols: Ram. – Raman spectrum; IR – infrared absorption spectrum; act. – active; inact. – inactive; P – polarized; DP – depolarized.

In Table 5 are presented the frequencies of the valence vibrations of the Si_2O_7 group, calculated for two different values of the SiOSi angle.

Table 5. Valence Vibrations of the Si_2O_7 Groups (Calculated Frequencies in cm^{-1})

SiO_4 according to ref. 2		Si_2O_7 (D_{3d}) $\angle SiOSi = 120°$ according to ref. 2		Splitting Δ* (%)	Si_2O_7 (C_{2v}) $\angle SiOSi = 180°$ according to ref. 7		Splitting Δ* (%)
A_1	775	A_1	736	10	A_{1g}	550	43
		B_1	812		A_{2u}	878	
F_2	935	A_1	862		A_{1g}	770	
		A_2	931				
		B_1	934		E_u	880	
		A_1	936				
		B_2	941		E_g	886	
		B_1	1029		A_{2u}	985	
		$f = 4.44$; $d = 0.62$; $d' = 0.19 \cdot 10^5$ dyne/cm			$f = 4.0$; $d = 0.3 \cdot 10^5$ dyne/cm		

*$\Delta = 2(\nu_{B_1} - \nu_{A_1})/(\nu_{B_1} + \nu_{A_1})$ (the relative magnitude of the splitting of the totally symmetric vibration of the SiO_4 tetrahedron).

Translator's Note: The headings (D_{3d}) and (C_{2v}) of Table 5 appear to be reversed in the Russian original.

For the case $\angle SiOSi = 120°$, the calculation of the frequencies of the Si_2O_7 group has been performed by Siebert.[2] For an approximate estimate of the frequencies of the Si_2O_7 groups when $\angle SiOSi = 180°$, we used the formulas introduced by Matossi[7] for a very primitive model with two force constants (one valence and one deformation). In applying these formulas, there was no point in using the force constants for the Si–O bond from Siebert's work, since in his calculations a larger number of constants was used. The force constant of the SiOSi angle and the difference in strength of the Si–O and Si–O(–Si) bonds were not taken into account in these calculations; this, however, is not essential for a rough estimate of the frequencies.

Two essential points must be noted. First, the splitting (the distance between the components) of the totally symmetric vibration of the SiO_4 tetrahedron is significantly larger than the splitting of the trebly degenerate vibration. Secondly, the splitting of the valence vibrations (particularly the totally symmetric one) increases as the SiOSi angle approaches 180°.*

*The calculated frequency values and the magnitude of the splitting depend, finally, not only on the SiOSi angle but also on the choice of force constants. Thus, for $\angle SiOSi = 180°$, $f = 4.5 \cdot 10^5$, and $d = 0.5 \cdot 10^5$ dyne/cm, the vibrations of types A_{1g} and A_{2u}, arising from the splitting of the totally symmetric vibration of the SiO_4 group, have the frequencies 577 and 746 cm^{-1} respectively, i.e., the relative splitting Δ amounts to 26% altogether, in contrast to $\Delta = 43\%$ in Table 5.

As can be seen from Table 5, at an SiOSi angle of 180° it is even possible to have an "overlapping" of the spectral regions in which lie the frequencies arising from the splitting of the symmetric and trebly degenerate vibrations of the SiO_4 tetrahedron.

These conclusions are not unexpected: the totally symmetric vibration, in which the amplitude of the vibrations of the O atoms is greater, is more sensitive to interactions.[4] An increase in the SiOSi angle must also lead to a strengthening of the interaction of the vibrations of the two tetrahedra which are linked by a common oxygen atom.

Let us now attempt to use the preliminary considerations just stated for the analysis of the spectrum of hexamethoxydisiloxane. As was mentioned above, the transition from $Si(OCH_3)_4$ to $(CH_3O)_3SiOSi(OCH_3)_3$ leads to the appearance in the Raman spectrum, in the region of the antisymmetric valence vibration of the SiO_4 group, of a polarized line at 808 cm^{-1} (inactive in the absorption spectrum) and a broad, apparently depolarized line at 838 cm^{-1}, which also appears in the absorption spectrum. We may suppose that this phenomenon is connected with the above-considered splitting of the antisymmetric vibration of the SiO_4 group on going over to the spectrum of the Si_2O_7 group. It must be noted here that the splitting is not large, in consequence of which it is not possible to separate all the components. A significantly larger splitting is observed in the case of the totally symmetric vibration—frequencies near 580 and 690 cm^{-1} correspond to the two components (of types A_1 and B_1). The intensities and degrees of depolarization of the lines agree with such an assignment. The fact that no frequency is forbidden and the considerably smaller splitting of the totally symmetric vibration than would be expected for $\angle SiOSi = 180°$ enable us to ascribe the symmetry C_{3v} to the molecule. The magnitude of the splitting, $\Delta = 15\%$, permits us to suppose that the SiOSi angle lies in the interval 130–140°; i.e., near the usual value for siloxanes.

The transition to the "trimer" spectra leads to the appearance of three frequencies in the region of the symmetric vibration of the tetrahedron. We may suppose that the observed splitting of the symmetric vibration of the SiO_4 group is brought about by the formation of a chain of equivalent coupled oscillators—the silicon-oxygen tetrahedra. It is well known that the formation of a chain of coupled oscillators must lead to a splitting of the characteristic vibration of the isolated oscillator into com-

ponents, the number of which is equal to the number of oscillators in the chain. This has been well studied experimentally in the investigation of the spectra of saturated linear hydrocarbons with chains of C—C bonds. Therefore we may expect that the high-boiling fractions of the polymethoxysiloxanes, in whose spectra are observed five and seven frequencies, correspond in their composition to a "penta-" and a "heptamer." The absence from the products studied of a "tetra-" and a "hexamer" may be explained in the following way: the central, nonshifted band must be observable only in the spectra of chains with an odd number of tetrahedra. The number (and position) of the other bands in the spectra of the "tetra-" and "pentamer" or "hexa-" and "heptamer" should not differ. Therefore a mixture of "tetra-" and "pentamer" (or "hexa-" and "heptamer") must give a spectrum corresponding to the compound with an odd number of links. Another hypothesis may, however, be expressed—beginning with the "tetramer," the formation of branched isomers is possible; the abrupt complication of the spectrum in the fractions which follow the "trimer" may be connected with an admixture of these isomers.

The investigation of the change in spectrum on formation of a closed chain—i.e., a ring of tetrahedra—is of interest. The only compound of this type which we have studied is hexa-tert-butoxycyclotrisiloxane $\{OSi[OC(CH_3)_3]_2\}_3$, the spectrum of which, in the region of the symmetric vibration of the SiO_4 group, proved to be similar to the spectra of the linear "trimers" described in the present article.

Thus the changes in the spectra of the polyalkoxysiloxanes may be interpreted as the result of a change in the vibrations of the SiO_4 groups when they are joined into a chain. This enables us to use the polyalkoxysiloxanes as organic "models" of the silicates.

REFERENCES

1. C. Schaefer, F. Matossi, and K. Wirtz. Z. Physik 89, 210 (1934).
2. H. Siebert. Z. anorg. u. allgem. Chem. 275, 225 (1954).
3. D. Fortnum and J. O. Edwards. J. Inorg. & Nuclear Chem. 2, 264 (1956).
4. A. N. Lazarev. Opt. i Spektr. 8, 511 (1960), Optics and Spectroscopy 8, 270 (1960).
5. A. N. Lazarev and M. G. Voronkov. Opt. i Spektr. 4, 180 (1958).
6. A. N. Lazarev, T. P. Tulub, and Ya. S. Bobovich. Opt. i Spektr. 4, 417 (1958).
7. F. Matossi. J. Chem. Phys. 17, 679 (1949).

THE TEMPERATURE DEPENDENCE OF THE DISPERSION AND ABSORPTION OF LIGHT IN MOLECULAR CRYSTALS. I. THEORY

V. L. Strizhevskii

Received 25 September 1959

We consider the temperature dependence of the dispersion and exciton absorption of light in molecular crystals with weak exciton-phonon coupling. We obtain equations describing the temperature dependence of the refractive index and the absorption coefficient. We give several qualitative results derived from these equations.

References 1 and 2 gave a general method for calculating the dispersion and absorption of light in crystals in the exciton absorption region at a temperature close to absolute zero. Then, in reference 3 this method was generalized (at the cost of certain limitations on the form of the Hamiltonian) to cover temperatures different from zero. The purpose of the present paper is to apply these results to an actual case of a molecular crystal with weak exciton-phonon coupling, with attention being paid chiefly to the temperature dependence of dispersion and absorption of light.

It is shown in reference 3 that in many cases, including the case under consideration, the complex polarizability β of a crystal at a nonzero temperature T is determined, for sufficiently low absorption, by the equation:

$$\beta = \beta' + \frac{E_f(\mathbf{k})\, V |P_f(0)|^2 \mathbf{P}_f^*(0)}{\hbar\omega\,(E_f(\mathbf{k}) - \hbar\omega - i\hbar\Gamma(2)}. \qquad (1)$$

where ω is the frequency of a monochromatic electromagnetic wave reaching the region of exciton absorption, $E_f(\mathbf{k})$ is the excitation energy of the exciton with quasimomentum $\mathbf{k}$ equal to the wave vector of the electromagnetic wave, $V = Nv_0$ is the volume of the basic periodic structure of the crystal, $\mathbf{P}_f(0)$ is the matrix element of the dipole moment of unit volume of the crystal, responsible for the phototransition, (it is assumed that only one exciton state makes a significant contribution to the expression for β), and β' defines the contribution from other states apart from the exciton state under consideration, the numerator in Eq. (1) must be treated as a dyad. The quantity γ is determined from Eqs. (5) to (8) of reference 3. The tensor β, which has been studied by several authors (for example, see references 1, 2, 4-7, etc.) has the property that β depends on $\mathbf{k}$ ("space dispersion"[4]). In these papers, however, the effect of temperature has not been investigated completely.

In our case, the complete Hamiltonian of the crystal $\hat{H}$ can be broken down into components $\hat{H}'$, $\hat{H}''$, and U[3] as follows:

$$\left.\begin{aligned} \hat{H}' &= \hat{H}_0 + V(r, R_0),\ \hat{H}'' = \hat{T}_R + \bar{V}(R) - \bar{V}(R_0), \\ U &= V(r, R) - V(r, R_0) - \bar{V}(R) + \bar{V}(R_0). \end{aligned}\right\} \qquad (2)$$

Here $\hat{H}_0$ and $\hat{T}_R$ are operators of the energy of internal motion of the molecules and their kinetic energy of motion as a whole, r and R are coordinates of the internal motion and of the motion of the molecules as a whole, respectively, R_0 is the equilibrium value of R, $V(r, R)$ is the interaction energy of the molecules and $\bar{V}(R)$ is the interaction energy averaged over r by using the ground state functions of the exciton subsystem described by the operator $\hat{H}'$ ($\hat{H}''$ and U are responsible for the phonon subsystem and the exciton-phonon interaction). We restrict ourselves below to the case of a cubic crystal, the molecules of which we will number by the index n,[8] while the different degrees of freedom of the molecule

will be numbered by the index σ. We will expand U as a power series in $R_n^\alpha - R_{n0}^\alpha$ and restrict ourselves to linear terms. We will then go over to real normal coordinates b_{qj} according to the equations

$$\left.\begin{aligned} R_n^\alpha - R_{n0}^\alpha &= N^{-\frac{1}{2}} \sum_{qj} e_{qj}^\alpha a_{qj} e^{iqn}, \\ a_{qj} &= \frac{1}{\sqrt{2}} (a'_{qj} + a''_{qj}), \\ b_{qj} &= \begin{cases} a'_{qj}, & q_z \geqslant 0, \\ a''_{qj}, & q_z < 0. \end{cases} \end{aligned}\right\} \tag{3}$$

(the coefficients e_{qj}^α, and also the frequencies of the normal vibrations ω_{qj} which occur below are determined by solving the problem of the dynamics of the molecular vibrations in the absence of intramolecular perturbations[5]); we then obtain U in the form:

$$\left.\begin{aligned} U &= \sum_{qj} V_{qj} b_{qj}, \quad V_{qj} = \sum_\alpha e_{qj}^\alpha e_{qj}^\alpha, \\ e_{qj}^\alpha &= \sum_n \frac{\partial V(r, R_0)}{\partial R_n^\alpha} \chi_{qj}(n), \\ \chi_{qj}(n) &= \sqrt{\frac{2}{N}} \begin{cases} \cos qn, & q_z \geqslant 0, \\ -\sin qn, & q_z < 0. \end{cases} \end{aligned}\right\} \tag{4}$$

The eigenfunctions of the operator $\hat{H}'$ have the form[6]

$$\psi_{fk} = N^{-\frac{1}{2}} \sum_n e^{ikn} \varphi_n^f(r), \tag{5}$$

where $\varphi_n^f(r)$ is the (antisymmetric) wave function of the crystal, when the electronic-vibrational excitation of index f is localized at the molecule with number n. The eigenfunctions of the operator $\hat{H}''$ are the oscillatory functions from the coordinates b_{qj}.

Next we need to calculate

$$(c_{qj}^\alpha)_{fk, f'k'} = \int \psi_{fk}^* C_\alpha' \psi_{f'k'} dr.$$

The result of the calculation has the form

$$(c_{qj}^\alpha)_{fk, f'k'} = (2N)^{-\frac{1}{2}} \varphi_\alpha^{f, f'}(k', k) \begin{cases} \delta_{k'-k, -q} + \delta_{k'-k, q}, & q_z \geqslant 0, \\ i(\delta_{k'-k, -q} - \delta_{k'-k, q}), & q_z < 0, \end{cases} \tag{6}$$

$$\varphi_\alpha^{f, f'}(k', k) = \varphi_\alpha^{f_0, f'}(k') + \varphi_\alpha^{f, f_0}(-k) + \varphi_\alpha^{00, ff'}(k' - k) - \varphi_\alpha^{00, 00}(k' - k) + \varphi_\alpha^{ff', 00}(0), \tag{7}$$

$$\varphi_\alpha^{f_0, 0f}(k) = \sum_{m \neq 0}' e^{-ikm} \varkappa_{0m}^{f_0, 0f} \tag{8}$$

and similarly for other combinations of the upper indices.

$$\varkappa_{0m}^{f_0, 0f} = \int \chi_m^{f*}(I) \chi_0^{0*}(I) \frac{\partial V_{m0}(R_0)}{\partial R_m^\alpha} \chi_m^0(I) \chi_0^f(I) \, dr - \sum_\mu (-1)^\mu \int \chi_m^{f*}(II_\mu) \chi_0^{0*}(II_\mu) \frac{\partial V_{m0}(R_0)}{\partial R_m^\alpha} \chi_m^0(I) \chi_0^f(I) \, dr, \tag{9}$$

where V_{m0} is the potential energy of the interaction of molecules m and 0, χ are the wavefunctions for an isolated molecule, I and II_μ designate symbolically certain distributions of electrons between molecules m and 0 where summation takes place over all the distributions except I, which are numbered in such a way that each distribution will be obtained from the previous one by the permutation of only one pair of electrons.

Knowing the value of $(c_q^\alpha)_{fk, f'k'}$ enables us to use Eq. (8) from reference 3 and find γ. Going over from summation over q to integration, we obtain

$$\gamma(\omega, k) = \frac{v_0}{8\pi^3} \sum_j \left\{ \int_{\tau_{fj}^+ = \hbar\omega} \frac{ds_{fj}^+}{|\nabla_q \tau_{fj}^+|} \frac{n_{qj} + 1}{\omega_{qj}} L_{fj}(q, k) + \int_{\tau_{fj}^- = \hbar\omega} \frac{ds_{fj}^-}{|\nabla_q \tau_{fj}^-|} \frac{n_{qj}}{\omega_{qj}} L_{fj}(q, k) \right\}; \tag{10}$$

$$L_{fj}(q, k) = \left| \sum_\alpha b_\alpha^* (k + q, k) e_{qj}^\alpha \right|^2. \tag{11}$$

Here

$$\tau_{fj}^\pm = E_f(k + q) \pm \hbar\omega_{qj}, \tag{12}$$

$ds_{fj}^\pm$ is an element of surface $\tau_{fj}^\pm = \hbar\omega$ in the three dimensional q-space,

$$n_{qj} = \left(e^{\frac{\hbar\omega_{qj}}{kT}} - 1 \right)^{-1}. \tag{13}$$

The quantity corresponding to γ in (10) was also calculated (by a different method) in reference 9. It should be remarked that in contrast to reference 9, γ as determined by Eq. (10) is a function of k. If we expand $\gamma(\omega, k)$ as a power series in k and confine ourselves to the zero power term of the expansion, we obtain a result identical with the conclusions of reference 9. The variation of γ with k can be important in some cases, however. For example, it must be taken into account in the frequency range where $\gamma(\omega, k = 0)$ is low, that is, at the edges of the absorption band. For this reason space dispersion*

*As is shown in reference 9, for one- and two-dimensional crystal structures cases are possible in which $\gamma(\omega, 0)$ has singularities. Near these points, γ cannot be expanded as a power series in k and Eq. (10) must be used, taking account of the dependence of γ on k. Thus space dispersion is also important in the neighborhood of these points.

must always be borne in mind in this region (especially in studying the absorption of light). We exclude this case from consideration in what follows.

For a practical calculation of the value of γ it is necessary to know several parameters which are characteristic for each individual crystal. Since these are not known to us in most cases, we can at present only speak of an order of magnitude estimate of γ. With only this estimate in mind, we will make several simplifying assumptions in order to avoid calculating unnecessary details. Let the exciton subsystem energy have the form

$$E_f(k) = \hbar\omega_0 - \frac{\hbar\gamma_1}{2} (\cos ka - 1) \tag{14}$$

(we assume the effective exciton mass M to be positive), and suppose that it interacts only with two branches of the lattice vibrations: the acoustical (translational molecular vibrations) with a dispersion law

$$\omega_q = 2 \frac{c'}{a} \sin \frac{(aq)}{2},$$

where c' is the velocity of sound, and the optical (rotational vibrations) with the law

$$\Omega_q = \Omega_0 + \left(\frac{\Delta\Omega}{2} \right) (\cos qa - 1)$$

(we neglect any interaction of translational and rotational vibrations). We will restrict ourselves to the interaction of closest neighbors, and we will take for the potential energy the dipole-dipole interaction energy, neglecting the contribution of exchange forces. In order to simplify (10) further, we will consider a linear chain of molecules; however, we will increase the final result correspondingly

to the value of the number of closest neighbors (~10) for real three-dimensional crystals. We will use the following values for the parameters, in cgs units, corresponding to the case of electron-vibrational excitation: the absolute value of the matrix element of the dipole moment for a transition within the molecule $p \sim 10^{-18}$, which corresponds to an oscillator strength of about 0.1, a molecular mass $m \sim 10^{-22}$, mean moment of inertia $I \sim 10^{-37}$, lattice constant $a \sim 10^{-7}$, and $\Omega_0 \sim \eta \sim 10^{13}$, we find that at $T \approx 0$ the value of γ within the absorption band is of the order 10^{10} sec^{-1}, and with increase in T, γ should grow rapidly. For the case of a pure vibrational excitation (assuming $p \sim 10^{-19}$, which corresponds to integral absorption in the gas phase of ~10^5 cm^{-2}, $\eta \sim 10^{11}$, and the same values for the other parameters as in the previous case) we get $\gamma \sim 10^8$ sec^{-1}.

If we expand $E_f(\mathbf{k})$ as a power series in $\mathbf{k}$

$$\mathbf{k}\left(E_f(\mathbf{k}) = \hbar\omega_0 + \frac{\hbar^2k^2}{2M}\right),$$

then for the values $\omega = 2\pi 10^4$ cm^{-1} (electron-vibrational excitation) and $2\pi \times 10^3$ cm^{-1} (pure vibrational excitation) we get $\hbar^2k^2/2M \sim 10^8\mu^2$ and $10^4\mu^2$ respectively ($\mathbf{k} = (\omega/c)\mu\mathbf{s}$, $|\mathbf{s}| = 1$). Therefore, the inequality $\hbar\gamma > \hbar^2k^2/2M$ is very frequently valid indicating, in agreement with (1), that space dispersion is unimportant.* Since the estimate made above is rough, it is possible that in some cases (especially for electron-vibrational excitations) the inequality $\hbar\gamma < \hbar^2k^2/2M$ will not be valid and space dispersion will be significant.

*The authors of reference 8 also made a similar assertion, but they did not estimate γ.

We will confine ourselves here to the consideration of cases where space dispersion may be neglected, or where the frequency range in which it is important is insignificant (our conclusions will be valid outside this frequency range). For these cases, by induction we take the electrical and magnetic fields to be proportional to

$$\exp\left(-\frac{\omega}{c}\varkappa\mathbf{rs} + i(\mathbf{kr} - \omega t)\right),$$

and from the system of Maxwell's equations, solutions of which we seek, we obtain $(\mu + i\chi)^2 = 1 + 4\pi\beta = \varepsilon_1 + i\varepsilon_2$ where

$$\varepsilon_1 = 1 + 4\pi\gamma' + \frac{\alpha(\omega_0 - \omega)}{\omega\left[(\omega_0 - \omega)^2 + \frac{\gamma^2}{4}\right]}, \quad \varepsilon_2 = \frac{\frac{\alpha\gamma}{2}}{\omega\left[(\omega_0 - \omega)^2 + \frac{\gamma^2}{4}\right]},$$

$$\alpha = 4\pi V\,|P_f(0)|^2\,\frac{\omega_0}{\hbar}. \tag{15}$$

In these equations μ and χ are expressed in terms of ε_1 ε_2 by using the relations

$$\mu = \frac{1}{\sqrt{2}}\left(\varepsilon_1 + \sqrt{\varepsilon_1^2 + \varepsilon_2^2}\right)^{\frac{1}{2}}, \quad \varkappa = \frac{1}{\sqrt{2}}\left(-\varepsilon_1 + \sqrt{\varepsilon_1^2 + \varepsilon_2^2}\right)^{\frac{1}{2}}. \tag{16}$$

In most cases, the inequality $\varepsilon_2 < \varepsilon_1$ is valid, and for μ and χ from (16) we obtain:

$$\mu \approx \varepsilon_1, \quad \varkappa = \frac{\varepsilon_2}{2\sqrt{\varepsilon_1}}, \tag{17}$$

the inequality $\varepsilon_2 < \varepsilon_1$ then becoming equivalent to the inequality $\chi < \mu$.

The temperature dependence of the refractive index μ and the absorption coefficient χ amounts to dependence of the value of T on γ. With increasing T, the value of γ increases monotonically, and for sufficiently high temperatures it has the form $\gamma = gT$ (the corresponding temperature region is limited ordinarily to $T > 50$-$100°$K). For μ and χ we then obtain (bearing in mind that in the region where χ is important usually $\mu \approx \mu' = 1 + 4\pi\beta'$):

$$\mu = \mu' + \frac{\alpha(\omega_0 - \omega)}{\omega\left[(\omega_0 - \omega)^2 + \frac{g^2T^2}{4}\right]}, \quad \varkappa = \frac{\frac{\alpha gT}{4\omega\sqrt{\mu'}}}{(\omega_0 - \omega)^2 + \frac{g^2T^2}{4}}. \tag{18}$$

From an analysis of these equations we can make several general deductions concerning the temperature and frequency dependence of the dispersion and absorption of light. These deductions may serve as a guide in the experimental verification of the theory.

1. It follows from (15) and (17) that the refractive index μ decreases with increasing temperature for all T.

2. Equations (15), (17), and (18) show that for values of ω close to ω_0 (the point at which $\mu = \mu'$ changes sign), χ decreases with increasing T (at high temperatures it ~1/T). At the point ω_0 itself, within the limits of validity of (18), this decrease should be identical for all substances and all absorption bands. Equation (18) shows that at a sufficient distance away from the frequency ω_0, $\chi \sim T$, so that in the neighborhood of the wings of the absorption band, absorption should increase with increasing temperature. As the temperature increases the rate of this growth decreases. We also notice that the dependence of χ on T is noticeably less marked than the dependence of μ.

3. If we neglect the dependence of g on ω, we obtain the dispersion (Lorentz) form of the absorption curve. In fact, g depends on ω in a complex way, so in the general case the form of the band does not coincide with the Lorentz, Gauss, or any other well-known form. In addition, it depends on temperature—the band widens with increasing T.

4. Since $g = g(\omega)$, the point ω_0 and the maximum of the absorption curve will not coincide in general, except for cases where g does not vary rapidly with ω. The absorption and dispersion curves are asymmetrical in the general case, relative to the frequency ω_0 or any other point.

5. The complex nature of the dependence of γ on ω can lead in many cases to more than one maximum of χ as a function of ω. Thus, in the temperature range in which the effect of the second term in (10) begins to be felt, a maximum can also appear at $\omega < \omega_0$ (for the case $M > 0$) as well as in the region $\omega > \omega_0$. From this, in certain cases it is evidently possible to explain the appearance of isolated split components in the transition from gas to crystal (besides Davydov's splitting[8]).

6. Making the same assumptions as used above in estimating the magnitude of γ, we can transform Eq. (10) to a form which leads us to expect that γ will be greater, the greater p (that is, the greater the oscillator strength of the given band). Therefore, the value of χ at the points of the contour of different bands which are equidistant from the corresponding frequencies ω_0 will fall rapidly with increasing T for values of ω close to ω_0; in the range of ω values sufficiently far from ω_0 it will grow more slowly—for bands with greater oscillator strength.

7. For the case of the purely vibrational excitation, in which the width of the zone is usually less than Ω_0 and c'/a, the range of values of ω, where $\gamma(\omega) \neq 0$, is basically determined by the values of the quantities Ω_0 and c'/a. Therefore, the halfwidths of the absorption bands should be of the same order of magnitude (the order of magnitude of the frequency of the lattice optical vibrations).

8. Using Eqs. (15) and (17) we can show that for absorption bands close in form to the Lorentz band, the value of the integral absorption determined by the value $(2/c)\int \omega\chi(\omega)\mathrm{d}\omega$ varies relatively slowly with T. If there are considerable departures from the Lorentz form we

may expect that the variation of the integral absorption with temperature will be more marked. To find the form of this variation the function $\gamma = \gamma(\omega)$ must be studied for each particular case.

A detailed comparison between theory and experiment will be made subsequently.

In conclusion, the author thanks A. S. Davydov, S. I. Pekar, and M. P. Lisitsa for their interest in the work, evaluation of the results, and critical comments.

REFERENCES

1. S. I. Pekar. Zhur. Eksptl. i Teoret. Fiz. **33**, 1022 (1957).
2. S. I. Pekar. Zhur. Eksptl. i Teoret. Fiz. **36**, 451 (1959).
3. S. I. Pekar and V. L. Strizhevskii. Fiz. Tverkogo Tel **2**, No. 5 (1960).
4. V. L. Ginzburg. Zhur. Eksptl. i Teoret. Fiz. **34**, 1593 (1958).
5. V. M. Agranovich and A. A. Rukhadze. Zhur. Eksptl. i Teoret Fiz. **35**, 982 (1958).
6. A. S. Davydov and A. F. Lubchenko. Zhur. Eksptl. i Teoret Fiz. **35**, 1499 (1958).
7. A. F. Lubchenko. Fiz. Tverkogo Tel **1**, 709 (1959).
8. A. S. Davydov. Trudy Inst. Akad. Nauk Ukr.SSR **1** (1951).
9. A. S. Davydov and E. I. Rashba. Ukrain Fiz. Zhur. **2**, 226 (1957).

ABSORPTION SPECTRA OF BENZENE HOMOLOGUES. IV. PECULIARITIES OF CRYSTAL SPECTRA

V. L. Broude and M. I. Onoprienko

Received 15 September 1959

This article presents an analysis of the experimental data obtained up to now with regard to exciton splitting in crystal spectra, the shape and width of absorption bands, and the sensitivity of the spectrum of a crystal to a small change in its structure.

Detailed studies of the absorption spectra of a large group of benzene homologues at low temperatures, the results of which have already been published in part,[1-4] enable us to draw some conclusions concerning a number of general questions about the structure of the crystal spectra of this class of compounds.

The present article contains an analysis of the observed experimental facts with regard to exciton splitting of crystal bands, the shape and width of absorption bands, and the sensitivity of the spectrum of a crystal to a small change in its structure.

EXCITON SPLITTING AND STRONG POLARIZATION OF CRYSTAL ABSORPTION BANDS

The purely electronic absorption bands of a benzene crystal provide a characteristic example of absorption bands of molecular crystals exhibiting exciton splitting, which has acquired in the literature the name of Davydov splitting.[5,6] In these works it was established that the transition $A_{1g} \rightarrow B_{2u}$, forbidden in the free molecule, is allowed in the crystal spectrum and appears as a doublet of bands strongly polarized along the a- and c-axes of the crystal. With a band halfwidth of about 3 cm^{-1} (20°K), the magnitude of the splitting amounts to approximately 40 cm^{-1}.

Bands corresponding to combinations of the purely electronic transition with the fundamental totally symmetric vibration at 925 cm^{-1} are also subject to splitting, the magnitude of the splitting diminishing practically in proportion to the intensity of the corresponding overtones in the crystal spectrum. Bands produced by combination of the purely electronic transition with the non-totally symmetric vibration E_{2g} do not undergo exciton splitting. In this case, one finds only a removal of the degeneracy in the corresponding transition ($A_{1g} \rightarrow E_{1u}$), as a result of which a doublet with an interval of 9 cm^{-1} between its components is observed in the spectrum. The absence of exciton splitting in these bands is usually connected with a deformation of the molecule during the corresponding electronic-vibrational transition, which favors localization of the excitation in the crystal.

The absorption of light by benzene homologues, as well as by benzene itself, is due to the excitation of the cloud of six π-electrons. The difference consists only in the influence of the various alkyl radicals on this cloud, which may lead to a change in its symmetry. Correspondingly, in such molecules as mesitylene, hexamethylbenzene, and hexaethylbenzene, the purely eletronic transition remains forbidden by the symmetry rules, while in the unsymmetrical benzene substitution products it is allowed.

We have investigated the absorption spectra of crystals of all these compounds, paying particular attention to the structure of the spectrum in the region of the purely electronic transition.

Figure 1 shows schematically the structure and polarization of the absorption bands in the region of the purely electronic transition in the crystal spectra of benzene and methyl-substituted benzenes. The upper and lower bands refer to the two component spectra of the crystal in polarized light. One's attention is drawn to the fact that, while the clearly-marked strong polarization of the relatively weak bands in the spectra of benzene, mesitylene, and hexamethylbenzene may serve as a direct indication of the connection of this absorption with the excitation of free excitons, the intense bands in the spectra of the other methyl-substituted benzenes are either split slightly (the magnitude of the splitting does not exceed the halfwidth of the bands) or do not undergo splitting at all. From this it follows that the most clearly marked exciton effects are observed in the absorption spectra of those crystals in whose molecules the purely electronic transition is forbidden in the free state. On the other hand, according to Davydov's theory, the exciton splitting for transitions which are forbidden in the free molecule should be significantly less than for allowed transitions (under otherwise equal conditions).[6] The absence of data on the crystal structure of most of

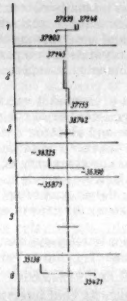

Fig 1. Structure and polarization of absorption bands in the region of the purely electronic transition in the crystal spectra of benzene and methyl-substituted benzenes. Substance (in parentheses, the halfwidth of the band in cm^{-1}): 1—benzene (~3); 2—toluene, high temperature form (~10); 3—m-xylene (~10); 4—mesitylene, low temperature form (~20); 5—durene (~100); 6—hexamethylbenzene, low temperature form (~10).

the compounds studied and on the position of the molecules within it does not permit us to make exact quantitative comparisons, but the experimental information already at hand indicates the necessity for further theoretical developments. As E. I. Rashba has kindly informed us, it is not impossible that agreement with experiment may be attained if, in particular, one takes into account the influence of the interaction of the electronic excitation with the lattice vibrations on the magnitude of the exciton splitting.[7] It should also be noted that the absence of marked exciton splitting in those electronic-vibrational transitions which are connected with non-totally symmetric vibrations may also prove to be closely linked with the effect under discussion.

As investigations of the absorption spectra of a series of crystals of benzene homologues have shown, in some cases there is observed strong polarization of a line which is not associated with the production of free excitons. It has been established[2] that in the spectra of most of these compounds two transitions take place—an electronic one and an electronic-vibrational one in combination with a non-totally symmetric vibration, these transitions being oriented in the plane of the molecule along two mutually perpendicular directions. The observed diversity in the polarization of some bands in the spectra of a series of crystals is associated with a pecularity in in the orientation of the molecules and of the corresponding transitions relative to the crystal cross section which was studied.

We discovered yet another class of cases of strong polarization of the absorption bands of a crystal[8] during a study of the spectra of samples subjected to thermal deformation. The deformation of the crystal took place on cooling a thin sample placed in optical contact with a quartz plate, as a result of the difference in the coefficients of thermal contraction of the crystals and of the support. Under these conditions, absorption bands which are unpolarized in the spectrum of the free crystal are noticeably broadened, and their maxima in polarized light prove to be displaced in the different component

Fig. 2. Spectra of free and thermally deformed crystals of benzene. Experimental conditions (in parentheses, crystal thickness in microns): 1—crystal free from deformation (2); 2—deformed (1); 3—considerably deformed (< 1).

spectra of the sample. Portions of the spectra of free and strained benzene crystals are presented in Fig. 2, as an example. It can be seen that, in the unpolarized doublet of the spectrum of the free crystal, there takes place on deformation a sharp increase in the distance between its components (from 9 to 29 cm^{-1}), and at the same time the short wavelength band of the doublet gradually weakens and fades out in one of the component spectra. The origin of the changes found in the spectra of deformed crystals is not yet clear, and the hypothesis which we expressed[8] about delocalization of the exciton needs additional experimental substantiation.

The complexity of treating the experimental results with regard to absorption spectra of molecular crystals consists, in particular, in the establishment of the actual causes of the splitting and polarization of the bands. As we see it, strong polarization of the absorption bands cannot by itself be an unequivocal criterion of the exciton origin of the corresponding excitations. On the other hand, those cases of splitting of molecular terms which we most confidently connect with the generation of free excitons (for example, in the spectrum of a benzene crystal) need further grounding in theory.

SENSITIVITY OF THE CRYSTAL SPECTRUM TO SMALL CHANGES IN MOLECULAR STRUCTURE

Analysis of the absorption spectra of benzene crystals and vapor has shown[3] that the purely electronic transition is forbidden in the free molecule in consequence of its high symmetry. The absorption band corresponding to this transition is absent in the vapor spectrum. As a result of the action of the anisotropic crystal field, which has a relatively low symmetry, this transition becomes allowed. The absorption bands which appear in the crystal spectrum are less intense than the bands corresponding to a combination of the purely electronic transition with a non-totally symmetric vibration, which are already allowed in the spectrum of benzene vapor. A rough estimate shows that the intensity ratio of these two groups of bands (group M_1 and group K_1, see reference 3) equals 3-5. The character of the polarization in absorption bands of group K_1—the presence of a doublet of a- and c-bands and the absence of absorption (or its very low

intensity) when the light is polarized along the b-axis of the crystal—is evidence that the local symmetry of the crystal in the region where the molecule is located is very close to C_{2h}.[8]

The symmetry of a free benzene molecule is close to D_{6h}, but in the crystal, according to x-ray studies, there are small deviations from this high symmetry.[9] The differences in the magnitudes of the interatomic distances and the angles at the vertices of the hexagonal framework lower the symmetry of the molecule in the crystal to C_{2h}. A certain noncoplanarity of the carbon atoms leads to the vanishing of a few more symmetry elements. As a result, the symmetry of the benzene molecule in the crystal corresponds to the point group C_i. The difference in the magnitude of the interatomic distances amounts to 0.005 A, or 4%, and in the angles, 1°14′ of 0.8%. The noncoplanarity of the atoms is caused by their shift out of the plane by 0.0013 A (Fig. 3).

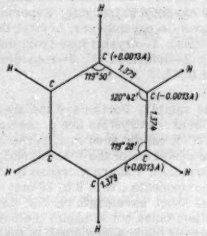

Fig. 3. Structure and dimensions of the benzene molecule in the crystal.[9]

In order to remove the symmetry prohibition from a transition within a molecule belonging to group D_{6h}, it is sufficient to transfer to the symmetry C_{2h}. Changes of 0.4-0.8% in lengths and angles are sufficient, as experiment shows, for previously forbidden transitions to appear in the spectrum with noticeable intensity. The significantly weaker distortions which lower the symmetry to C_i will influence the structure and the intensity of an already allowed transition.

Apparently the influence of the noncoplanarity of the carbon atoms is not great. Therefore, the spectrum fundamentally reflects the symmetry C_{2h} (the b-absorption is absent or very weak). It is possible, however, that the fine structure of the polarized absorption bands which is observed in spectra at 20°K [3] is partially connected with the reduction of the molecule from the symmetry C_{2h} to C_i.

Thus, from the absorption spectrum of the crystal (when concerned with allowing a transition forbidden by symmetry) one may judge distortions of the symmetry of the molecule produced by changes of 0.4% in the bond lengths. This manifests itself in the appearance of new bands with an intensity only one-third to one-fifth that of those already allowed in the vapor spectrum. Such a sensitivity of the absorption spectrum to changes in the structure of the molecule is not surprising, inasmuch as the allowing of a forbidden transition on account of non-totally symmetric vibrations (in benzene vapor) is also ultimately brought about by mutual atomic shifts in which the interatomic distances change by approximately 0.015 A,[9] disrupting the high symmetry of the molecule. This quantity is three times as large as the changes in bond lengths which allow the purely electronic transition (0.005 A). Apparently, the observed value (equalling 3-5) of the ratio between the intensity of a transition allowed on account of a vibration and the intensity of a transition allowed in consequence of the lowering of the symmetry of the molecule in the crystal, in comparison with the symmetry of a free molecule, is explained by just this difference.

From the analysis presented it can be seen that, on the basis of the relative intensity of the absorption bands of the purely electronic and electronic-vibrational transitions in the spectra of benzene homologues, one may judge the divergence of the symmetry of the cloud of six π-electrons from regularity.

On the other hand, the amount of splitting of the doubly degenerate benzene vibration of symmetry E_{2g}* may also serve as a quantity characterizing the divergence of the symmetry of the six π-electrons from regularity. On comparison of the absorption spectra of a large group of crystals of benzene homologues, it was established that the magnitude of the splitting of this vibration increases together with an increase in the relative strength of the purely electronic transition (see Table).

*The presence of the non-totally symmetric vibration in the spectrum is established by the relative polarization of the absorption bands in the crystal.[2]

Substance	Totally symmetric vibration	Non-totally symmetric vibration	Quantitative splitting Δ	$\frac{\varepsilon_{max}^{*}}{\varepsilon_{n-t.s.}}$
Benzene	520 (E_{2g})		0	~0.2
Toluene, high temperature form	454	526	72	~3
o-Xylene	506	443	65	~3
m-Xylene	470	450	20	~1
p-Xylene	388	450	62	~3
Mesitylene, high temperature form	360 (E')		—	~0.1
Ethylbenzene, high temperature form	473	558	85	~3
Hexylbenzene, high temperature form	458	538	80	~3

*The estimate of the intensity ratio was made visually from photographs of the spectra of crystals of various thicknesses and with variously developed planes.

SHAPE OF CRYSTAL ABSORPTION BANDS

We have not carried out quantitative measurements of the absorption curves of crystals. Therefore, in discussing the question of the shape of the absorption bands, we are in fact limited to analysis of the width and sharpness of the bands.

In the study of the absorption spectra of molecular crystals, it has been established that for certain compounds the absorption bands are broad, while in the spectra of others they are extremely narrow and sharp (so that they are often called lines). The spectra of anthracene, naphthacene, etc., the band widths in which reach 200-300 cm^{-1}, may serve as examples of spectra of the first type. Spectra consisting of narrow bands are observed in the cases of naphthalene, phenanthrene, and benzene, some bands of which do not exceed 2-3 cm^{-1} in width.

Among the absorption spectra of benzene homologues, there is also observed some diversity in the width of the absorption bands. Thus, the absorption bands of amorphous samples are always broad and diffuse, their shape changing little as the temperature is lowered to 20°K. The absorption bands of a number of low temperature forms of the crystals are also usually washed out and very broad—their width reaches 100 cm^{-1} and more. On the other hand, the bands in the spectra of crystals of the high temperature forms or of those compounds in which phase transitions are not observed are almost always equally sharp, their widths lying between 5 and 20 cm^{-1}. If we make a classification of the absorption spec-

tra of aromatic compounds, broad bands are observed in these spectra in the following basic cases: (1) in the spectra of some crystals which have intense absorption (anthracene, naphthacene, stilbene, etc.); (2) in the spectra of amorphous samples even at very low temperatures; (3) in the spectra of the majority of aromatic crystals at elevated temperatures (usually a substantial narrowing of the spectral bands is attained only at liquid hydrogen temperature); (4) in the low temperature (20°K) spectra of crystals subjected to mechanical deformation (this may be illustrated by the naphthalene spectra[9]). Those cases of washed-out absorption spectra whose appearance is connected with crystal imperfections in consequence of the presence of impurities apparently belong here also (as an example, we refer to the spectra of some deuterated compounds[4]). As analysis of the spectra of the crystalline modifications of toluene[10] has shown, the spectra of some low temperature forms of crystals of benzene homologues are to be assigned to the same group; the band broadening in these is also brought about by imperfections in the samples and the resulting deformations which arise.

In the first and third cases, the large band width is usually explained by very intense coupling of the electronic transition with lattice vibrations. Bands corresponding to these combinations are usually called satellites. In the first case of our classification, the intensity of the satellites increases because of an increase in the strength of the coupling between the electronic excitation and the phonons, and in the third it increases in conjunction with the rise in temperature and consequently with the increase in the exponential factor in the expression for the intensity of the satellite.

In the second case, the band width is usually explained by the nonequivalence of the positions of the molecules in the amorphous sample, as a result of which the position of the electronic transitions of the energy scale is slightly different for different molecules. Consequently, the absorption band represents the superposition of slightly shifted electronic transitions in a large number of light-absorbing molecules. The band broadening may also be partially explained in this case by dispersion in the values for the strength of the coupling between the electronic excitations and the phonons for different molecules.

At the present time there is no exact interpretation of the band broadening in the case of mechanical deformation of the crystals (fourth case). However, the most probable explanation is apparently associated with the nonuniformity of the strains set up within the crystal, as a result of which the absorption band represents the superposition of electronic transitions in molecules subjected to slightly different distortions.

In the spectra of crystals of benzene homologues, there is observed a stepwise increase in the absorption band width on going from benzene and toluene to the more highly substituted molecules (durene, pentamethylbenzene). This band broadening usually runs parallel to the general intensification of the absorption and is apparently due to an increase in the coupling between the electronic excitations and the phonons. The spectra of crystals in whose molecules the electronic transition is forbidden depart from this regularity, and their spectra usually contain narrower and sharper bands.

In many cases, anomalous broadening and diffuseness of the spectral bands of crystals may also be brought about by imperfections in the crystals or by mechanical deformations set up in them.

The conclusions obtained above concerning the nature and character of the individual features of the spectra of crystals of benzene homologues may be carried over, it seems to us, in large measure to the absorption spectra of other groups of molecular crystals.

The authors express their gratitude to A. F. Prikhot'ko and E. I. Rashba, who have taken part in discussion of this work.

REFERENCES

1. V. L. Broude. Zhur. Eksptl. i Teoret. Fiz. **22**, 600 (1952).
2. V. L. Broude. Opt. i Spektr. **1**, 387 (1956); **2**, 454 (1957).
3. V. L. Broude, V. S. Medvedev, and A. F. Prikhot'ko. Zhur. Eksptl. i Teoret. Fiz. **21**, 665 (1951); Ibid. **22**, 605 (1952); Opt. i Spektr. **2**, 317 (1957).
4. V. L. Broude, E. A. Izrailevich, A. L. Liberman, M. I. Onoprienko, O. S. Pakhomova, A. F. Prikhot'ko, and A. I. Shatenshtein. Opt. i Spektr. **5**, 113 (1958).
5. A. S. Davydov. Zhur. Eksptl. i Teoret. Fiz. **21**, 671 (1951).
6. A. S. Davydov. Trudy Inst. Fiz. Akad. Nauk SSSR, No. 1, 85 (1951).
7. E. I. Rashba. Opt. i Spektr. **3**, 568 (1957).
8. V. L. Broude, O. S. Pakhomova, and A. F. Prikhot'ko. Opt. i Spektr. **2**, 323 (1957); Ukrain. Fiz. Zhur. **2**, 96 (1957).
9. E. G. Cox, D. W. J. Cruickshank, and J. A. S. Smith. Proc. Roy. Soc. **A247**, 1 (1958).
10. V. L. Broude and M. I. Onoprienko. Opt. i Spektr. (in press).

SPECTROSCOPIC STUDY OF THE PROCESSES OF VIBRATIONAL ENERGY TRANSFORMATION OF COMPLEX MOLECULES IN COLLISIONS
I. ON THE DETERMINATION OF THE AMOUNT OF ENERGY TRANSFERRED AND THE EFFICIENCY OF COLLISIONS

B. S. Neporent and S.O. Mirumyants

Received 22 June 1959

The results of previous investigations of the authors and others on the stabilization of excited complex molecules by collisions are considered. It is shown that in studying the process of vibrational energy transformation in complex molecules in collisions with foreign gas molecules it is necessary to take into account the exchange of energy not only with the foreign particles but also with the translational and rotational degrees of freedom of the complex molecules themselves. A more precise expression for the accommodation coefficient is proposed and applied to data obtained in previous investigations. The results obtained are discussed briefly.

Stabilization of excited complex molecules, that is, a decrease in the probability of radiationless transitions when the molecules give up a part of their excess vibrational energy by collisions with foreign particles, was postulated by Neporent to explain an effect observed by him in 1939;[1] this effect was an enhancement of the fluorescence of vapors of aromatic compounds when foreign gases which did not quench the fluorescence were added. In a later paper[2] the same author proposed using the results of investigations of the fluorescence enhancement by foreign gases for studying the process of energy transfer in molecular collisions. The first investigation[1] was carried out with aniline vapor, the second[2] with β-naphthylamine vapor; as foreign gases various gases and vapors (He, H_2, N_2, CO, CO_2, NH_3, C_2H_4, $CHCl_3$, C_6H_6, C_6H_{12}) were used. Necessary data on the duration and yield of the fluorescence were obtained by studying the quenching of the fluorescence by oxygen.[2]

Later, Curme, and Rollefson[4] confirmed the interpretation which had been proposed[1] for the effect by studying the simultaneous action of stabilizing gases (C_6H_6 and C_6H_{12}) and a quenching gas (CCl_4) on the fluorescence of β-napthylamine vapor. The same substance was investigated by Boudart and Dubois[3] who used the fluorescence enhancement to study the processes of energy transfer in collisions of the molecule with D_2 and SF_6 molecules. Bowen and Veljkovic[5] studied the fluorescence enhancement of perylene vapor on adding nitrogen, and the vapors of p-cymene, naphthalene, and hexamethylbenzene, and drew certain conclusions concerning the efficiencies of the molecules of these compounds. Borisevich and Neporent,[7] from a study of the effects of a series of foreign gases on the fluorescence of the vapors of derivatives of phthalimide, observed that if, as a result of the excitation by small quanta, the average supply of vibrational energy of the excited molecule decreases, the effect of the foreign gases is not an enhancement but a weakening of the fluorescence; the collisions produce not a stabilization but rather a labilization of the excited molecule, as a consequence of the compensation of the vibrational energy deficit of the excited molecule at the expense of the energy of the molecules of the foreign gas. Okabe and Steacie[6] and Giacometti et al.[8] obtained a direct confirmation of the stabilizing action of foreign gases by studying their effect on the photolysis and fluorescence of hexafluoroacetone.

In reference 2 a method was developed for using the effect of foreign gases on the fluorescence of a vapor to determine the average amount of energy ΔE transferred in a collision of the excited molecule with a foreign particle. It was purposed[2] that the efficiency of collisions with respect to energy transfer should be described by means of an accommodation coefficient α which characterizes the degree of approach of the system of colliding particles to temperature equilibrium with respect to the distribution of the excess (or deficit) of vibrational energy among the particles. In analyzing the results of the determination of values of the accommodation coefficient for various gases, authors of papers[2, 5–7] and also of reviews[10–13] do not always arrive at the same results as regards the estimation of the participation of the various degrees of freedom (translational, vibrational, and rotational) of the acceptor molecule in the process of vibrational energy transfer from the donor molecule. We will return to the content of the above-mentioned papers in the second part of the present investigation; here we will consider some general questions pertaining to an improvement of the precision of the concept of the quantities ΔE and α, and of methods of determining their values. For this purpose we will use the typical experimental results given in Figs. 1 and 2.

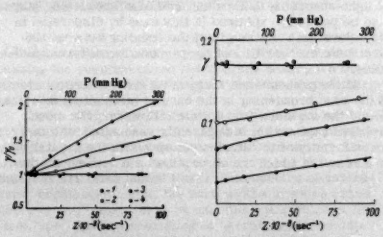

Fig. 1

Fig. 2

Fig. 1. Effect of deuterium on the magnitude of the relative fluorescence yield (γ/γ_0) of 3-dimethylamino-6-aminophthalimide vapor for excitation by various wavelengths λ_e. λ_e(mμ): 1—492; 2—436; 3—405; 4—365. P—pressure of the foreign gas; Z—number of collisions per second of the excited molecule with D_2 molecules. The effect of deuterium on the absorption coefficients of the gases studied[13] is included.

Fig. 2. Variation of quantum yield γ of the fluorescence of 3-dimethylamino-6-aminophthalimide vapor with the pressure of D_2. Designations are the same as for Fig. 1.

The following method of determining ΔE was proposed in reference 2. Having measured for each wavelength of the exciting light the duration τ of the excited state of the molecules under study, one chooses a pressure ΔP of the foreign gas such that the excited molecule experiences on the average one collision with a molecule of the foreign gas (that is, $\Delta Z = 1/\tau$). The changes of the emission yield $\Delta\gamma$ corresponding to these values of ΔZ are found from graphs of the type given in Fig. 2; these are then used in the determination of the required energy change ΔE by means of the yield curve (Fig. 3).

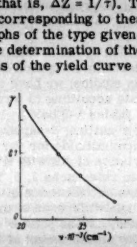

Fig. 3. Variation of the quantum yield of the fluorescence of 3-dimethylamino-6-aminophthalimide vapor with the frequency of the exciting light. Interpolation of the data of Borisevich[14] for the temperature 528°K.

Boudart and Dubois[5] proposed determining the value of the energy ΔE from the slope at the point Z = 0 of the curves for the fluorescence enhancement, the connection between the slope and ΔE being obtained from kinetic equations derived by them for the process. It must be emphasized here that in essence the two methods are equivalent, inasmuch as the magnitude of $\Delta Z = 1/\tau$ is usually so small that in measuring $\Delta\gamma$ it is necessary to use the value of the tangent of the angle φ of the slope of the curves $\gamma = f(Z)$(Fig. 2) close to Z = 0, that is, $\Delta\gamma = \Delta Z \cdot \tan\varphi$. Practically the value of tanφ is determined in the same way in both cases,[2, 5] although it is doubtful whether it was advisable in reference 5 to introduce the variation of τ with $T_{vibr.}$ in place of the variation with E,* and afterwards to make the reverse calculation to values of ΔE.

Actually, recognizing the fact that even for the case of $\Delta Z = 1/\tau$ the determination of ΔE involves measurements of small increments in the experimental curves, a graphical procedure was proposed,[2] although one of us had already obtained in 1939* an expression describing the kinetics of the stepwise enhancement and quenching of the fluorescence in a more general form than that derived in reference 5. The formulas proposed,[1] in the nomenclature adopted here have the form*

*After correction of obvious typographical errors in reference 1. It should be noted here that the fluorescence intensities F_0 in the absence of, and F_z in the presence of the foreign gas will give the quantum yields γ_0 and γ_z only for the case in which the introduction of the foreign gas has no effect on the absorption coefficient of the vapor of the fluorescing substance being studied.

$$\left.\begin{aligned} F_0 &= \frac{f}{f+d_1}, \\ F_z &= \frac{f}{f+d_1+(\varepsilon_{a_1}+\varepsilon_{q_1})z}\left[1+\sum_1^{k-1} z^k a_k\right], \end{aligned}\right\} \quad (1)$$

where

$$a_k = \frac{(\varepsilon_{a_1}+\varepsilon_{q_1})(\varepsilon_{a_2}+\varepsilon_{q_2})\cdots(\varepsilon_{a_k}+\varepsilon_{q_k})}{[f+d_2+(\varepsilon_{a_1}+\varepsilon_{q_1})z]\cdots[f+d_{k+1}+(\varepsilon_{a_{k+1}}+\varepsilon_{q_{k+1}})z]}. \quad (2)$$

Here f is the probability of emission assumed for the complex molecule; in conformity with experiment, f is independent of the supply of vibrational energy (otherwise quantities f_k must be introduced); d_k is the probability of a radiationless transition taking place after k – 1 collisions with foreign gas molecules, and ε_{a_k} and ε_{q_k} are the efficiencies of stabilizing and quenching collisions, respectively. The preliminary results of our investigations show that in certain cases (O_2, NO) both efficiencies ε_a and ε_q can be different from zero.

Assuming as a particular case that $\varepsilon_a = 1$ and $\varepsilon_q = 0$ (absence of quenching) and remembering that $1/(f_k + d_k) = \tau_k$, one can easily obtain from the formulas given above the expression deduced in reference 5,

$$S = \frac{F_z}{F_0} = \frac{1}{1+\tau_1 z}\left[1+\sum_1^{k-1} z^k \frac{\tau_2\tau_3\cdots\tau_{k+1}}{(1+\tau_2 z)\cdots(1+\tau_{k+1}z)}\right]. \quad (3)$$

We note that in determining the energy ΔE there are possible errors; these are related firstly to some arbitrariness in drawing the initial portion of the $\gamma = f(z)$ curves (Fig. 2) and, secondly, to the fact that the elimination of the effect of the foreign gases on the absorption of the vapor (cf. reference 15) has a very large effect on precisely these initial portions, since the effect varies particularly rapidly for small values of Z. There is also an error in the determination of ΔE due to the relative scarcity of points on the curves giving γ (or τ) as a function of the available vibrational energy of the molecules $E^* = (\nu_a - \nu_0)/h$. Estimates made by us show that the divergences in the determinations of ΔE in references 2 and 5 are due to just these sources of errors which have been mentioned.

In connection with the question of the participation of the various degrees of freedom in the processes of conversion of vibrational energy by collisions it must be noted particularly that in all previous investigations (in our own[1, 2, 7] as well as those of other authors[4-6]) it has been assumed that all the vibrational energy lost by the excited molecule is converted into energy of the various degrees of freedom (vibrational, rotational, and translational) of the molecules of the foreign gas. In reality one must consider that in the absorption of a quantum only the vibrational energy of the excited molecule essentially changes, whereas its external degrees of freedom—translational and rotational—probably preserve the average amount of energy corresponding to the temperature of the experiment. An exchange of energy between the internal and external degrees of freedom of the molecule in question is possible only during a collision with a foreign particle in which the conservation of the angular momentum of the system can be fulfilled. Thus, in processes in which energy is transformed by collision one must include not only the degrees of freedom of the foreign particle but also the external degrees of freedom of the molecule in question; this fact naturally complicates the analysis of the phenomenon.

Strictly speaking it would be necessary to determine the value of the energy transferred ΔE and the accommodation coefficient α separately for each of the possible modes of energy transfer and, furthermore, in each of these cases separately for the different degrees of freedom of the molecules taking up the energy excess. However, the experimental conditions do not permit separate determinations of the amounts of vibrational energy transferred to the foreign particle and to the external degrees of freedom of the molecule under study, or, even less so, the distribution of these amounts among the various degrees of freedom. Consequently we are forced to introduce the concept of an average value of the accommodation coefficient α which refers to the whole amount

of energy ΔE lost (or gained) by the vibrational degrees of freedom of the excited molecule; however, from the consideration below of the values obtained for α certain conclusions can be drawn concerning the predominance of one or other of the possible modes of energy transformation.

We will define the accommodation coefficient α as the degree of approach of the system of colliding particles to temperature equilibrium. We note that, in the form proposed in reference 2 and assumed in reference 5, the coefficient α is defined essentially as the effective part of the heat capacity of the foreign gas, that is, $\alpha = C''_{eff.}/C''$. In reference 7 we found it more expedient to define α as the ratio of the actual value of transferred energy, ΔE, and the value calculated assuming that thermal equilibrium is established during the collision of the molecules in question, that is, $\alpha = \Delta E_{expt.}/\Delta E_{calc.}$. In the further discussion we will adhere to the latter variant of the definition of the accommodation coefficient α, which represents essentially the efficiency of the first stabilizing collision ε_{z_1}, in expression (1).

Let us consider the expression for the accommodation coefficient taking into account the considerations introduced above, and arrange to calculate the thermal energy of the particles in question from the average values corresponding to the temperature T_0 of the experiment. Then the average excess vibrational energy of the excited molecule is equal to

$$E^* = h(\nu_0 - \nu_1), \tag{4}$$

where ν_0 is the frequency of the exciting light and ν_1 is the frequency corresponding to the distance between the electronic levels. The average energy of the foreign gas particle and the average energy of the external degrees of freedom of the excited molecule in the system in question are taken as equal to zero. We will designate the vibrational specific heat of the gas under study as $C'_{vibr.}$, the specific heat due to the external degrees of freedom of its molecules as $C'_{ext.} = C'_{trans.} + C'_{rot.}$, and the total specific heat of the foreign gas as $C'' = C''_{vibr.} + C''_{rot.} + C''_{trans.}$. The quantity of vibrational energy lost (or gained) by the excited molecule will be designated as ΔE.

The condition for equilibrium can obviously be written in the form

$$\frac{\Delta E'}{C'_{ext.}} = \frac{\Delta E''}{C''} = \frac{E^*}{C'_{vibr.} + C'_{ext.} + C''}$$

$$= \frac{E^* - \Delta E}{C'_{vibr.}} = \frac{\Delta E}{C'_{ext.} + C''} = \theta - T_0. \tag{5}$$

Here θ is the calculated equilibrium "temperature" of the complex formed by the colliding molecules,* $\Delta E'$ is the part of the energy E^* which is transformed into energy of the external degrees of freedom of the molecule under study, and $\Delta E''$ is the part transformed into energy of the foreign gas molecule. Obviously, $\Delta E' + \Delta E'' = \Delta E$.

*Equation (5) is based on the assumption of a uniform distribution of energy among the degrees of freedom at equilibrium. The temperature θ is introduced only for the calculation of the temperature trend of the specific heat.

The average value of the accommodation coefficient is defined by the expression

$$\alpha = \frac{\Delta E_{expt.}}{\Delta E_{calc.}}. \tag{6}$$

From (5) and (6) we obtain

$$\alpha = \frac{C'_{vibr.} + C'_{ext.} + C''}{C'_{ext.} + C''} \cdot \frac{\Delta E_{expt.}}{E^*}. \tag{7}$$

It is easy to show that in the case of the reverse energy transfer, that is, the vibrational degrees of freedom of the complex molecule when it is excited by low frequencies, $\nu_0 < \nu_1$, the expression for α has just the same form, but the values of ΔE and E^* (deficit of vibrational energy) are negative.

Since the definition of the accommodation coefficient assumed in the present investigation differs from that used in the previous studies, we have considered it expedient to recalculate according to formula (7) the data published earlier. Tables 1-3 below give the results of this recalculation for aniline, β-naphthylamine, and 3,6-tetramethyldiaminophthalimide for various foreign gases. The data on the variation of ΔE with E^* for these molecules are taken from references 2, 5, 7, and 16. For β-naphthylamine we assume the value of ΔE given in reference 2, since the slight difference of the data given in reference 5 is related, as was pointed out above, with inaccuracies due to the measurement of the increments of the curves rather than with a difference in the methods of calculation. We had at our disposal the original graphs with a much larger scale. In the calculations values of the specific heat corresponding to the computed equilibrium temperature θ were used (cf. Table 4).

Table 1. Values of the Accommodation Coefficient α for Energy Transfer by Collision of an Excited Aniline Molecule with Foreign Gas Molecules

Foreign gas (at 70° C) \ λ_0 (A)	2791	2870	2588	2529
ν_0 (cm^{-1})	35820	27440	38630	39540
E^* (cm^{-1})	1785	2405	4445	5505
H_2	—	—	0.07	0.15
N_2	—	—	0.07	0.15
CO	—	—	0.03	0.09
NH_3	0.10	0.10	0.19	0.25
C_2H_4	—	—	0.06	0.12

Table 2. Values of the Accommodation Coefficient α for Energy Transfer by Collision of an Excited β-Naphthylamine Molecule with Foreign Gas Molecules

Foreign gas or vapor** \ λ_0 (A)	3129	3022	2904	2853	2537
ν_0 (cm^{-1})	31930	33080	34440	35040	39400
E^* (cm^{-1})	2730	3880	5240	5840	10200
He (150)	—	—	—	0.04	0.04
H_2 (150)	—	—	—	0.03	0.05
D_2 (186)	—	—	—	0.06	—
N_2 (150)	—	—	0.07	0.10	0.16
CO_2 (150)	—	—	0.12	0.35	0.43
NH_3 (150)	0.05	0.09	0.20	0.63	0.8
NH_3 (190)	0.05	0.09	0.18	0.77	0.90
$CHCl_3$ (150)	0.16	0.17	0.22	0.55	0.80
C_5H_{12} (150)	0.06	0.08	0.13	0.37	0.52
C_5H_{12} (190)	0.05	0.07	0.14	0.44	0.47
C_6H_6 (150)	—	—	0.17	0.52	1.15
SF_6 (186)	—	—	—	0.24	—

**Temperature in °C given in the brackets.

Table 3. Values of the Accommodation Coefficient α for Energy Transfer by Collision of an Excited 3,6-Tetramethyldiaminophthalimide with Foreign Gas Molecules

Gas or vapor	λ_a (A)	5200	4920	4650	3650
	ν_a (cm^{-1})	19230	20330	21890	27400
	E* (cm^{-1})	−3710	−2810	1750	4480
N_2 (243)		0.01	0.02	0.20	0.2
NH_3 (243)		0.07	0.07	0.32	0.58
C_5H_{12} (243)		0.03	0.04	0.56	0.62
C_6H_{12} (335)		0.02	0.07	0.62	0.57

**Temperature in °C in the brackets.

The values of α given in Tables 1-3 are of course smaller than those computed in references 2 and 5. In all cases except one α is less than unity, although it sometimes approaches this value. This result indicates that the use of gas kinetic molecular radii for the energy exchange processes in question is not too rough an approximation. The value $\alpha > 1$ for benzene for λ_a = 2537 A is due, as was already pointed out in reference 3, to the presence in this case of a fluorescence of β-naphthylamine sensitized by benzene. It is evident that the value of α increases with increasing supply of vibrational energy in the excited molecules of the substance under study; this is clearly due to the inclusion of the additional degrees of freedom of the acceptor molecule in the process of energy transfer. Moreover, an increase in α associated with the degree of complexity of the foreign gas molecules is evidently due to the closer contact of the colliding molecules under the influence of the Van der Waals forces. Also light foreign gases apparently have a low efficiency with respect to creating the conditions for transfer of vibrational energy of the excited molecule to its own internal degrees of freedom.

The data given in Tables 1-3 are not sufficient for an estimate of the role of the various degrees of freedom in the processes which transform vibrational energy in molecular collisions. It is precisely for this reason that we have undertaken a study of the effect of a large group of different foreign gases on the fluorescence of the vapor of 3-dimethylamino-6-aminophthalimide; this is the subject of the second part of the present investigation, in which the questions touched on here will be discussed in more detail.

Table 4. Values of the Specific Heat C_v and of the Temperature Coefficient of the Specific Heat β of Various Gases and Vapors

Foreign gas**	C_v (cal mol^{-1} °C^{-1})**	β (cal mol^{-1} °C^{-1})
He	3	0
H_2	4.84 (15) [17]	0.0008 [18]
D_2	4.98 (25) [18]	0.0005 (a)
N_2	4.94 (15) [17]	0.001 [18]
CO	4.94 (15) [17]	0.001 [18]
CO_2	8.1 (150) [18]	0.006 (a)
NH_3	6.8 (15) [17]	0.006 [18]
$CHCl_3$	16.3 (150) [18]	0.002 (a)
C_5H_{12}	8.1 (150) [18]	0.02 (b)
SF_6	27 (186) (c)	0.04 (c)
iso-C_5H_{12}	32.3 (58) [20]	0.04 (c)
C_6H_6	23 (150) [18]	0.01 [18]
Aniline ($C_6H_5NH_2$)	30 (70) (c)	0.07 (c)
β-naphthylamine ($C_{10}H_7NH_2$)	87 (150) (c)	0.1 (c)
3,6-tetramethyldiaminophthalimide	83 (243) (c)	0.04 (b)

**Temperature in °C in the brackets.

Comments. (a) Interpolation of data in reference 18; (b) extrapolation of data in reference 18; (c) interpolation of data in reference 19; (d) extrapolation of data in reference 20; (e) assumed value, near the liquid; (f) vibrational specific heat determined in references 3 and 7; (g) by analogy with the liquid; (h) found from experimental data given in reference 7.

REFERENCES

1. B. S. Neporent. Zhur. Fiz. Khim. **13**, 965 (1939).
2. B. S. Neporent. Zhur. Fiz. Khim. **24**, 1219 (1950).
3. B. S. Neporent. Zhur. Fiz. Khim. **21**, 1111 (1947).
4. H. G. Curme and G. K. Rollefson. J. Am. Chem. Soc. **74**, 28 (1952).
5. M. Boudart and J. T. Dubois. J. Chem. Phys., **23**, 223 (1955).
6. E. J. Bowen and S. Veljkovic. Proc. Roy. Soc. (London) **A236**, 1 (1956).
7. N. A. Borisevich and B. S. Neporent. Opt. i Spektr. **1**, 536 (1956).
8. H. Okabe and E. W. R. Steacie. Can. J. Chem. **36**, 137 (1958).
9. G. Giacometti, H. Okabe, and E. W. R. Steacie. Proc. Roy. Soc. (London) **A250**, 287 (1959).
10. G. Porter. Ann. Rev. Phys. Chem. **7**, 207 (1956).
11. B. Stevens and M. Boudart. Proc. Natl. Acad. Sci. U.S. **67**, 570 (1957).
12. B. Stevens. Chem. Rev. **57**, 439 (1957).
13. J. C. McCoubrey and W. D. McGrath. Quart. Revs. (London), **11**, 87 (1957).
14. N. A. Borisevich. Kand. diss., Leningrad, 1954.
15. B. S. Neporent. Doklady Akad. Nauk SSSR **72**, 35 (1950); B. S. Neporent and A. A. Solodovnikov. Opt. i Spektr. **1**, 951 (1956); B. S. Neporent and V. P. Klochkov. Opt. i Spektr. **3**, 529 (1957); S. O. Mirumyants. Opt. i Spektr. **7**, 275 (1959), Optics and Spectroscopy **7**, 175 (1959).
16. B. S. Neporent. Dokt. diss., Moscow, 1945.
17. Landolt-Bornstein. "Tabellen," 2 Erg. Vol. II, p. 1227, 1931.
18. Landolt-Bornstein. "Tabellen," 3 Erg. Vol. III, pp. 1227, 2316, 2324, 1936.
19. E. G. Meyer and C. E. Buell. J. Chem. Phys. **16**, 744 (1948).
20. "Technicheskaya entsiklopediya. Spravochnik fizicheskikh, khimicheskikh i technologicheskikh velichin," Vol. 7, p. 269. (Technical Encyclopedia. Handbook of Physical, Chemical, and Technological Quantities), OGIZ RSFSR, Moscow, 1931.

ON THE THEORY OF LUMINESCENCE QUENCHING IN LIQUID SOLUTIONS

Yu. A. Kurskii and A. S. Selivanenko

Received 18 July 1959

Equations are formulated describing luminescence quenching of solutions. Expressions are obtained for the laws of damping taking account of the Brownian motion of the molecules and of resonance quenching.

The theoretical derivation of the law of luminescence damping for resonance quenching is generally carried out with the assumption of immobility of the radiating and quenching molecules in the solution during the lifetime of the excited state.[1-5] Therefore, it is of interest to introduce into the calculations the Brownian motion of the molecules, after having first examined the particular case of "immobile" molecules. In view of the discussion on this question,[2-4] it is evident that such an examination is expedient.

1. THE EQUATIONS OF THE TRANSFER KINETICS OF THE EXCITATION. THE CASE OF "IMMOBILE" MOLECULES

We introduce the distribution functions of the excited and quenching molecules $\rho_1(\mathbf{r}, t)$ and $\rho_2(\mathbf{r}', t)$ respectively, where $\mathbf{r}$ and $\mathbf{r}'$ are the radius vectors of the excited and quenching molecules. The kinetic equations are then written in the form,

$$\frac{\partial \rho_1}{\partial t} - D_1 \Delta \rho_1 = -\frac{\rho_1}{\tau_0} - \rho_1 \int \rho_2(\mathbf{r}', t) f(\mathbf{r} - \mathbf{r}')\, d\mathbf{r}', \qquad (1.1a)$$

$$\frac{\partial \rho_2}{\partial t} - D_2 \Delta \rho_2 = 0. \qquad (1.1b)$$

Here, τ_0 is the lifetime of the excited molecule in the absence of quenching, D_1 and D_2 are diffusion coefficients, and

$$f(\mathbf{r} - \mathbf{r}') = \frac{1}{\tau_0}\left(\frac{R_0}{|\mathbf{r} - \mathbf{r}'|}\right)^6$$

is the probability of resonance quenching,[5] where R_0 is a characteristic length of the resonance transfer, being expressed through the optical characteristics of the interacting molecules. Writing the initial and boundary conditions in a general form is exceedingly complex; therefore, we will formulate limited problems separately for the cases of large and small diffusion coefficients.

The conditions $D_1 = D_2 = 0$ in Eqs. (1.1) correspond to the case of "immobile" molecules. We will consider the initial distributions of n_0 excited molecules and of N quenching molecules in some sufficiently large volume.

$$\rho_1(\mathbf{r}, 0) = \sum_{i=1}^{n_0} \delta(\mathbf{r} - \mathbf{r}_i), \quad \rho_2(\mathbf{r}', 0) = \sum_{k=1}^{N} \delta(\mathbf{r}' - \mathbf{R}_k), \qquad (1.2)$$

where $\mathbf{r}_i$ (i = 1, 2, ..., n_0) and $\mathbf{R}_k$ (k = 1, 2, ..., N) are the coordinates of the excited and quenching molecules at the time t = 0, and $\delta(x)$ is the Dirac delta function. On using (1.1) with $D_1 = D_2 = 0$, and one of the conditions (1.2), we obtain

$$\frac{\partial \rho_1}{\partial t} = -\frac{\rho_1}{\tau_0} - \sum_{k=1}^{N} f(\mathbf{r} - \mathbf{R}_k)\, \rho_1. \qquad (1.3)$$

The integral of this equation, taking account of the initial conditions, has the form

$$\rho_1(\mathbf{r}, t) = \sum_{i=1}^{n_0} \delta(\mathbf{r} - \mathbf{r}_i) \exp\left\{-\frac{t}{\tau_0} - \sum_{k=1}^{N} f(\mathbf{r} - \mathbf{R}_k)\, t\right\}. \qquad (1.4)$$

From this the total number of excited molecules in a given volume equals

$$n(t) = \int \rho_1(\mathbf{r}, t)\, d\mathbf{r} = \sum_{i=1}^{n_0} \exp\left\{-\frac{t}{\tau_0} - \sum_{k=1}^{N} f(\mathbf{r}_i - \mathbf{R}_k)\, t\right\}. \qquad (1.5)$$

The probability of finding a given molecule excited at a given moment of time is obviously determined by dividing (1.5) by n_0, i.e.,

$$p^* = \frac{n(t)}{n_0} = n_0^{-1} \sum_{i=1}^{n_0} \exp\left\{-\frac{t}{\tau_0} - \sum_{k=1}^{N} f(\mathbf{r}_i - \mathbf{R}_k)\, t\right\}. \qquad (1.6)$$

Law (1.6) was obtained with the assumption of a completely determined, but arbitrary, location of the excited molecules and of the damping molecules at the initial moment of time.

In order to take account of the probability character of the assignment of the initial conditions, it is necessary to average the distribution function (1.5) over the corresponding distributions for $\mathbf{r}_i$ and $\mathbf{R}_k$. It is possible to carry out the average over all molecules independently of one another, i.e.,

$$\overline{n(t)} = \prod_{i=1}^{n_0} \int w(\mathbf{r}_i)\, d\mathbf{r}_i \prod_{k=1}^{N} \int w(\mathbf{R}_k)\, d\mathbf{R}_k\, n(t), \qquad (1.7)$$

where $w(\mathbf{r}_i)$ and $w(\mathbf{R}_k)$ are respectively the normalized distribution functions of the excited and quenching molecules at the time t = 0. For a first approximation it is natural to assume a uniform distribution for $w(\mathbf{r}_i)$ and $w(\mathbf{R}_k)$. Taking this into consideration, (1.7) is rewritten in the form

$$\overline{n(t)} = \prod_{i=1}^{n_0} \int \frac{d\mathbf{r}_i}{V} \prod_{k=1}^{N} \int \frac{d\mathbf{R}_k}{V} \sum_{i=1}^{n_0} \exp\left\{-\frac{t}{\tau_0} - \sum_{k=1}^{N} f(\mathbf{r}_i - \mathbf{R}_k)\, t\right\}, \qquad (1.8)$$

where V is the volume of solution, which is considered to be sufficiently large. We make a substitution of variables in the integrals over $\mathbf{R}_k$ ($\mathbf{R}_k - \mathbf{r}_i = \mathbf{R}_{ki}$), then all integrals over $\mathbf{R}_{ki}$ become identical. We obtain

$$\overline{n(t)} = \prod_{i=1}^{n_0} \int \frac{d\mathbf{r}_i}{V} \sum_{i=1}^{n_0} e^{-\frac{t}{\tau_0}} [I(t)]^N, \qquad (1.9)$$

where

$$I(t) = \int \frac{1}{V} e^{-f(\mathbf{R})t}\, d\mathbf{R}. \qquad (1.10)$$

The average over $\mathbf{r}_i$ simply leads to a multiplication by unity. Thus (1.9) can be rewritten in the form

$$\overline{n(t)} = n_0 e^{-\frac{t}{\tau_0}} [I(t)]^N. \qquad (1.11)$$

Dividing by n_0 we obtain the law of damping in the form proposed by Förster.[5]

We will now show that the equations used by Galanin[1, 2] follow from our formulation of the problem. We integrate Eq. (1.1a), with D_1 and D_2 equal to zero, over $\mathbf{r}$ and make a substitution of variables

$$\frac{dn(t)}{dt} = -\frac{n(t)}{\tau_0} - \int f(\mathbf{R})\, d\mathbf{R} \int \rho_2(\mathbf{r}-\mathbf{R})\, \rho_1(\mathbf{r}t)\, d\mathbf{r}. \quad (1.12)$$

We introduce the symbol

$$\int \rho_2(\mathbf{r}-\mathbf{R})\, \rho_1(\mathbf{r}, t)\, d\mathbf{r} = M(\mathbf{R}, t). \quad (1.13)$$

We carry out the average over $\mathbf{r}_1$ and $\mathbf{R}_k$ in Eq. (1.12)

$$\frac{d\overline{n(t)}}{dt} = -\frac{\overline{n(t)}}{\tau_0} - \int \overline{M(\mathbf{R}, t)}\, f(\mathbf{R})\, d\mathbf{R} \quad (1.14)$$

and introduce (still formally) the symbol

$$\overline{M(\mathbf{R}, t)} = N(\mathbf{R}, t)\, \overline{n(t)}. \quad (1.15)$$

Equation (1.14) then is transformed into the form

$$\frac{d\overline{n(t)}}{dt} = -\frac{\overline{n(t)}}{\tau_0} - \int N(\mathbf{R}, t)\, f(\mathbf{R})\, d\mathbf{R}\, \overline{n(t)}. \quad (1.16)$$

In order to obtain an expression for M(R, t), we must introduce into (1.13) the value of $\rho_2(\mathbf{r} - \mathbf{R})$ from (1.2b), of $\rho_1(\mathbf{r}, t)$ from (1.4), and then average over $\mathbf{r}_1$ and $\mathbf{R}_k$, that is,

$$\overline{M(\mathbf{R}, t)} = e^{-\frac{t}{\tau_0}} \prod_{i=1}^{n_0} \int w(\mathbf{r}_i)\, d\mathbf{r}_i \prod_{k=1}^{N} \int w(\mathbf{R}_k)\, d\mathbf{R}_k \times \sum_{k=1}^{N} \sum_{i=1}^{n_0} \delta(\mathbf{r}_i - \mathbf{R} - \mathbf{R}_k) \exp\left\{ -\sum_{k=1}^{N} f(\mathbf{r}_i - \mathbf{R}_k)\, t \right\}. \quad (1.17)$$

Using, as before, the substitution of variables ($\mathbf{R}_k - \mathbf{r}_i = \mathbf{R}_{ki}$) and considering the distributions to be uniform, it is easy to show that the products of the N − 1 integrals, the sum of which occurs in (1.17), are all equal to $[I(t)]^{N-1}$.

Taking this into consideration (1.17) acquires the form

$$\overline{M(\mathbf{R}, t)} = e^{-\frac{t}{\tau_0}} \sum_{i=1}^{n_0} \prod_{j=1}^{n_0} \int \frac{d\mathbf{r}'_j}{V} e^{-f(\mathbf{R})t} \frac{N}{V} [I(t)]^{N-1} = n_0 \frac{N}{V} e^{-\frac{t}{\tau_0} - f(\mathbf{R})t} [I(t)]^{N-1}. \quad (1.18)$$

For N(R, t) we obtain

$$N(\mathbf{R}, t) = \frac{N}{V} e^{-f(\mathbf{R})t} [I(t)]^{-1}. \quad (1.19)$$

Since I(t) approaches unity for $V \to \infty$ (cf. for example, reference 4), we have, finally,

$$N(\mathbf{R}, t) = \frac{N}{V} e^{-f(\mathbf{R})t}. \quad (1.20)$$

As is evident, Eqs. (1.16) and 1.20) were taken as the starting point in reference 2.

2. VISCOUS SOLUTIONS

For small diffusion coefficients, when diffusion mixing during the existence of the excited state is small in comparison with the mean distance between molecules, it is possible to neglect the boundary conditions at the surfaces of the colliding molecules. In this case the molecules can be considered as points, and the boundary and initial conditions are given by Eqs. (1.2) The solution of Eq. (1.1b) together with the conditions (1.2) gives

$$\rho_2(\mathbf{r}', t) = \sum_{k=1}^{N} (4\pi D_2 t)^{-\frac{3}{2}} e^{-\frac{(\mathbf{r}'-\mathbf{R}_k)^2}{4D_2 t}}. \quad (2.1)$$

We introduce (2.1) into Eq. (1.1a) and make a substitution of variables $\mathbf{r}' - \mathbf{R}_k = \mathbf{R}'_k$. Then

$$\frac{\partial \rho_1}{\partial t} - D_1 \Delta \rho_1 = -\frac{\rho_1}{\tau_0} - \sum_{k=1}^{N} (4\pi D_2 t)^{-\frac{3}{2}} \int e^{-\frac{\mathbf{R}_k'^2}{4D_2 t}} f(\mathbf{r} - \mathbf{R}'_k - \mathbf{R}_k)\, d\mathbf{R}'_k \rho_1. \quad (2.2)$$

The function f $(\mathbf{r} - \mathbf{R}_k' - \mathbf{R}_k)$ has a pole of the sixth order at the point $\mathbf{R}'_k = \mathbf{r} - \mathbf{R}_k$ and appears as a scalar. We introduce a new function $\tilde{f}$, which is defined by the following expression:

$$\tilde{f}(\mathbf{r} - \mathbf{R}'_k - \mathbf{R}_k) = f(|\mathbf{r} - \mathbf{R}'_k - \mathbf{R}_k| + a),$$

where $a > 0$. If $a = 0$, then $\tilde{f} \equiv f$. We substitute f for $\tilde{f}$ in formula (2.2)* and expand the latter in a series about the point $\mathbf{r} - \mathbf{R}_k$ to terms of second order. We have, finally,

$$\frac{\partial \rho_1}{\partial t} - D_1 \Delta \rho_1 = -\frac{\rho_1}{\tau_0} - \sum_{k=1}^{N} [\tilde{f}(\mathbf{r} - \mathbf{R}_k) + D_2 t \Delta \tilde{f}(\mathbf{r} - \mathbf{R}_k)]\, \rho_1. \quad (2.3)$$

We look for a solution of (2.3) in the form

$$\rho_1(\mathbf{r}, t) = X(\mathbf{r}, t) \exp \times \left\{ -\frac{t}{\tau_0} - \sum_{k=1}^{N} \int_0^t [\tilde{f}(\mathbf{r} - \mathbf{R}_k) + D_2 t' \Delta \tilde{f}(\mathbf{r} - \mathbf{R}_k)]\, dt' \right\}. \quad (2.4)$$

Putting (2.4) into (2.3) and introducing the symbol $w_k(\mathbf{r}, t') = \tilde{f}(\mathbf{r} - \mathbf{R}_k) + D_2 t' \Delta \tilde{f}(\mathbf{r} - \mathbf{R}_k)$, we have

$$\frac{\partial X(\mathbf{r}, t)}{\partial t} - D_1 \Delta X(\mathbf{r}, t) = D_1 \left[-2\nabla X(\mathbf{r}, t)\, \nabla \sum_{k=1}^{N} \int_0^t w_k(\mathbf{r}, t')\, dt' + X(\mathbf{r}, t) \left(\nabla \sum_{k=1}^{N} \int_0^t w_k(\mathbf{r}, t')\, dt' \right)^2 - X(\mathbf{r}, t) \Delta \sum_{k=1}^{N} \int_0^t w_k(\mathbf{r}, t')\, dt' \right]. \quad (2.5)$$

The right-hand part of Eq. (2.5) is a small correction. As a result of perturbation theory $X(\mathbf{r}, t) = X^{(0)}(\mathbf{r}, t) + X^{(1)}(\mathbf{r}, t)$. For the principal term, the initial conditions are

$$X^{(0)}(\mathbf{r}, 0) = \sum_{i=1}^{n_0} \delta(\mathbf{r} - \mathbf{r}_i),$$

and the solutions $X^{(0)}(\mathbf{r}, t)$ are given by Green functions of the diffusion equation. For $X^{(1)}(\mathbf{r}, t)$ we obtain the equation

$$\frac{\partial X^{(1)}}{\partial t} - D_1 \Delta X^{(1)} = D_1 S,$$

where

*In the following it will be possible to let a approach zero and obtain the desired result.

$$S(r, t) = -2\nabla X^{(0)}\nabla \sum_{k=1}^{N}\left[f(r-R_k)t + \frac{D_2 t^2}{2}\Delta f(r-R_k)\right]$$

$$+X^{(0)}\left\{\nabla \sum_{k=1}^{N}\left[f(r-R_k)t + \frac{D_2 t^2}{2}\Delta f(r-R_k)\right]\right\}^2$$

$$-X^{(0)}\Delta \sum_{k=1}^{N}\left[f(r-R_k)t + \frac{D_2 t^2}{2}\Delta f(r-R_k)\right].$$

The initial condition is $X^{(1)}(r, 0) = 0$

According to the general rules, we construct the solution

$$X^{(1)}(r, t) = D_1 \int_0^t dt' \int dr' S(r', t')[4\pi D_1 (t-t')]^{-\frac{3}{2}} e^{-\frac{(r-r')^2}{4D_1(t-t')}}.$$

In the calculation of these integrals we keep only the terms linear in D,

$$X^{(1)}(r, t) = D_1 \sum_{k=1}^{n_0}\left\{\Delta \sum_{k=1}^{N} f(r-R_k)\frac{t^2}{2}\right.$$

$$\left.+\left[\nabla \sum_{k=1}^{N} f(r-R_k)\right]^2 \frac{t^3}{3}\right\} b(r-r_i). \qquad (2.6)$$

Finally, the distribution function of the excited molecules is given by the expression

$$p_1(r, t) = (X^{(0)} + X^{(1)}) \exp$$

$$\times\left\{-\frac{t}{\tau_0} - \sum_{k=1}^{N}\left[f(r-R_k)t + \frac{D_2 t^2}{2}\Delta f(r-R_k)\right]\right\}, \qquad (2.7)$$

where $X^{(0)}(r, t)$ and $X^{(1)}(r, t)$ are defined above. To obtain the law of damping it is necessary to find the total number of excited molecules in the volume

$$n(t) = (n_0 + \overline{X^{(1)}}) \exp$$

$$\times\left\{-\frac{t}{\tau_0} - \sum_{k=1}^{N}\left[f(r_i-R_k)t + \frac{D_2 t^2}{2}\Delta f(r_i-R_k)\right]\right\}, \qquad (2.8)$$

where

$$\overline{X^{(1)}} = D_1 \sum_{i=1}^{n_0}\left\{-\Delta_{r_i}\sum_{k=1}^{N} f(r_i-R_k)\frac{t^2}{2} + \left[\nabla_{r_i}\sum_{k=1}^{N} f(r_i-R_k)\right]^2 \frac{t^3}{3}\right\}.$$

We average (2.8) over uniform distributions of the excited and quenching molecules (1.8).

$$\overline{n(t)} = \overline{n_1(t)} + \overline{n_2(t)},$$

$$\overline{n_1(t)} = n_0 e^{-\frac{t}{\tau_0}[K(t)]^N},$$

$$\overline{n_2(t)} = n_0 e^{-\frac{t}{\tau_0}} D_1\{-NL(t)[K(t)]^{N-1} + NM(t)[K(t)]^{N-1}$$

$$+N(N-1)[Q(t)]^2[K(t)]^{N-2}\}.$$

The letters denote the following integrals

$$K(t) = \int \frac{dR}{V} e^{-f(R)t - \frac{D_2 t^2}{2}\Delta f(R)},$$

$$L(t) = \int \frac{dR}{V}\Delta f(R)\frac{t^2}{2} e^{-f(R)t - \frac{D_2 t^2}{2}\Delta f(R)},$$

$$M(t) = \int \frac{dR}{V}[\nabla f(R)]^2 \frac{t^3}{3} e^{-f(R)t - \frac{D_2 t^2}{2}\Delta f(R)},$$

$$Q(t) = \int \frac{dR}{V}\nabla f(R)\sqrt{\frac{t^3}{3}} e^{-f(R)t - \frac{D_2 t^2}{2}\Delta f(R)}.$$

In these expressions it is already possible to substitute $\tilde{f}$ for f, i.e., to put a = 0. All of the integrals can be calculated approximately, if the small magnitude of the diffusion coefficient is taken into consideration. We will omit these calculations and write the final result

$$\overline{n(t)} = n_0 \exp$$

$$\left\{-\frac{t}{\tau_0} - 2q\sqrt{\frac{t}{\tau_0}} - 8.4\frac{\left(\frac{2}{3}D_1 + D_2\right)\tau_0}{R_0^2} q\left(\frac{t}{\tau_0}\right)^{\frac{7}{6}}\right\}. \qquad (2.9)$$

Here $q = (\sqrt{\pi}/2)((R_0/R_x)^3 N$, R_x is the radius of the volume of solution V ($V = \frac{4}{3}\pi R_x^3$), and N is the number of quenching molecules in the volume.

3. SOLUTIONS OF LOW VISCOSITY

For large diffusion coefficients it is necessary to consider the collision process of the excited and quenching molecules. This leads to a rejection of the assumption of "the point nature" of the particles; then it becomes necessary to formulate limiting conditions on the surfaces of the particles. The quenching action on the luminescence of dyes by substances such as KI is well known.[8] The spectrum of KI does not overlap the spectrum of the luminescing dye molecules (i.e., $R_0 - 0$). In this case quenching exists as a result of collisions of the "second kind."[6, 7] We take as probable the hypothesis that, together with the resonance quenching, during collisions of the quenching and excited molecules the latter undergo a radiationless transfer to the unexcited state (the concentration of the excited molecules at the surface of the quenching ones equals zero).

The kinetic equations for this case also have the form (1.1a, b). Since the strong Brownian motion must smooth out the fluctuations of the density of the molecules, the initial conditions will be given for averages of the molecular concentrations

$$p_1(r, 0) = \frac{n_0}{V}, \quad p_2(r', 0) = \frac{N}{V}. \qquad (3.1)$$

The problem can be solved if the resonance quenching is considered as a correction to the quenching resulting from collisions. We integrate Eq. (1.1a) over the volume and utilize Green's formula. We obtain

$$\frac{d\overline{n}(t)}{dt} - \sum_{k=1}^{N}\int (D_1 \nabla p_1 \cdot ds) =$$

$$-\frac{\overline{n}(t)}{\tau_0} - \int dr \int dR f(R) p_2(r-R) p_1(r, t). \qquad (3.2)$$

The second term on the left-hand side determines the sum of the fluxes going toward the quenching molecules. In reference 8 it was shown that, for Brownian motion of particles, their probability of not colliding with one another obeys the following equations

$$\frac{\partial W(R, t)}{\partial t} - D_{12}\Delta W(R, t) = 0,$$

$$W(R, t)|_{|R|=R_0} = 0, \quad W(R, 0)|_{|R|>R_0} = 1.$$

Here $D_{12} = D_1 + D_2$, $|R|$ is the distance between mole-

cules, $R_1 + R_2 = R_{12}$ is the sum of the molecular radii, and

$$W(R, t) = 1 - \frac{R_{12}}{|R|} + \frac{R_{12}}{|R|}\frac{2}{\sqrt{\pi}} \int_0^{\frac{|R|-R_{12}}{2\sqrt{D_{12}t}}} e^{-x^2} dx.$$

Thus, in the zero approximation for resonance interaction the number of excited molecules at time t at the distance | R | from the quenching molecules will equal

$$\frac{n(t)}{V} W(R, t). \tag{3.3}$$

From (3.2) and (3.3) we obtain

$$\frac{dn(t)}{dt} + 4\pi D_{12} R_{12} \frac{N}{V}\left[1 + \frac{R_{12}}{\sqrt{\pi D_{12} t}}\right] n(t) =$$

$$= -\frac{n(t)}{\tau_0} - \frac{N}{V}\int dR f(R) W(R, t) n(t). \tag{3.4}$$

For the conditions $R_{12}/R_0 \ll 1$ and $R_0^3 \ll D_{12}\tau_0$ this equation simplifies and assumes the form

$$\frac{dn(t)}{dt} + \frac{n(t)}{\tau_0} = -4\pi \frac{N}{V}\left[1 + \frac{R_{12}}{\sqrt{\pi D_{12} t}}\right]\left[D_{12} R_{12} + \frac{R_0^6}{12\tau_0 R_{12}^3}\right] n(t).$$

It is easy to verify by substitution that its solution is

$$n(t) = n_0 e^{-At - B\sqrt{t}}, \tag{3.5}$$

where

$$A = \frac{1}{\tau_0} + 4\pi D_{12} R_{12}\frac{N}{V} + \frac{4\pi R_0^6}{12\tau_0 R_{12}^3}\frac{N}{V}$$

and

$$B = 4\pi D_{12}\frac{N}{V}\frac{2R_{12}^2}{\sqrt{\pi D_{12}}} + \frac{4\pi R_0^6}{12\tau_0 R_{12}^3}\frac{N}{V}\frac{2}{\sqrt{\pi D_{12}}}.$$

In conclusion, we will cite the conditions for which the results (2.9) and (3.5) obtained by us are valid. The case of viscous solutions corresponds to the condition

$$D_{12}\tau_0 \ll 8R_0^2. \tag{3.6}$$

If we take $R_0/R_{12} \simeq 10$, then for solutions of low viscosity

$$\sqrt{D_{12}\tau_0} > 30R_0. \tag{3.7}$$

We note that both laws of damping (2.9) and (3.5) are valid for times $t \ll \tau_0$. Regrettably, by far the most frequently encountered case experimentally, $R_0 \simeq D_{12}\tau_0$, can be evaluated with the help of our equations only by numerical methods. Nonetheless, it is now possible to confirm that in this case the collisions between the excited and quenching molecules certainly will play a role. The question of the influence of these collisions on resonance damping of luminescence can serve as a subject for experimental investigation. We note that case (3.6) is encountered for many coloring materials in glycerine solutions,[4] and case (3.7) can occur for vapors of coloring materials and for alcohol or water solutions of uranyl compounds.

The authors express their thanks to V. L. Levshin for his interest in the work and to M. D. Galanin for critical remarks.

REFERENCES

1. M. D. Galanin. Zhur. Eksptl. i Teoret. Fiz. 28, 485 (1955).
2. V. V. Antonov-Romanovskii and M. D. Galanin. Opt. i Spektr. 3, 389 (1957).
3. B. Ya. Sveshnikov. Doklady Akad. Nauk SSSR 111, 78 (1956).
4. I. M. Rozman. Opt. i Spektr. 4, 536 (1958).
5. T. Förster. Z. Naturforsch. 4a, 321 (1949).
6. B. Ya. Sveshnikov. Trudy Gosudarst. Opt. Inst., Leningrad 12, 108 (1937).
7. S. I. Vavilov. Sobr. soch. (Complete Works) 1, 436, Moscow (1954).
8. A. Kolmogorov and M. Leontovich. Soviet Phys. 4, 1 (1933).

ON THE CONCENTRATION DEPOLARIZATION OF THE PHOSPHORESCENCE OF ORGANOLUMINOPHORS

P. I. Kudryashov and B. Ya. Sveshnikov

Received 5 August, 1959

The concentration depolarization of the total luminescence and phosphorescence of boroglycerine luminophors activated by fluorescein was studied at 20 and −186 C. It is shown, firstly, that the degree of polarization of a narrow spectral region of the phosphorescence does not change during the process of afterglow attenuation; secondly, that at room temperature the concentration depolarization of the total luminescence is smaller than the concentration depolarization of phosphorescence, and, thirdly, that at low temperatures the concentration depolarization of the phosphorescence is smaller than the concentration depolarization of fluorescence.

It is concluded that it is impossible to transfer excitation energy from a molecule in a metastable state to a molecule in the normal state over distances for which a concentration depolarization of fluorescence is observed. The results of the low temperature experiments contradict present day hypotheses about the mechanism for the transition of molecules into the phosphorescent state and about the concentration depolarization of fluorescence, whereas the room temperature experiments are in agreement with these hypotheses.

According to Vavilov's theory,[1] the concentration depolarization of fluorescence is caused by the transfer of electron excitation energy from one molecule in the fluorescent material to another. One consequence of this theory was the requirement that the degree of luminescence polarization should decrease in proportion to the attenuation of luminescence, which was in fact shown to be true for liquid dye solutions by means of the fluorometric measurements of Galanin, and for uranium glasses by means of the phosphoroscopic observations of Sevchenko.[2]

It is well known that along with the concentration depolarization of fluorescence there also occurs a concentration depolarization of phosphorescence. Feofilov[3] undertook an investigation for the purpose of determining whether there is a transfer of excitation energy from a molecule in the metastable state to a molecule in the normal state. If such a transfer were possible (by analogy with the rules found applicable for fluorescence), it would follow that one could expect a decrease in the degree of polarization in the process of phosphorescence quenching.

Feofilov tried to give an answer to the problem under discussion by comparing the degree of polarization of the total luminescence and the short wavelength phosphorescence which was observed with the help of a rapidly rotating Becquerel phosphoroscope. Feofilov assumed that if an energy transfer occurred only while the molecule was in the fluorescent state, then the degree of polarization of luminescence ought to be the same for both kinds of light, whereas the degrees of polarization would differ if the inverse were true. From the diagrams given in Feofilov's paper, it follows that for sugar ice activated with eosine there is observed a satisfactory agreement between the concentration depolarization curves for both kinds of luminescence, while in the case of sugar ice activated by tripaflavine the agreement is poorer. In view of the crudeness of the measurements, however, Feofilov assumed that the experiments had demonstrated that the curves coincided with each other, and he therefore concluded that energy transfer between molecules occurs only after the molecule makes a transition from the metastable state to the fluorescent state.

Sveshnikov[4] turned his attention to certain contradictions between these results and generally accepted hypotheses, namely, the following: that the energy transfer depends on the time the molecule spends in the excited state, which in this case is the fluorescent state, and that the molecule gets into the metastable state from the fluorescent state, i.e., molecules which are responsible for the short wavelength phosphorescence are in the fluorescent state twice—once before the transition to the metastable state and a second time after returning from the metastable state. From this it follows that the concentration depolarization of the short wavelength phosphorescence ought to be larger than the depolarization of the fluorescence.

We present a brief proof of this conclusion published in Sveshnikov's paper on the kinetics of phosphorescence.[5]

Under conditions of equilibrium excitation and in the absence of light saturation, when the number of unexcited molecules $n_2 = n_0$, the populations of molecules in the fluorescent and metastable levels will be determined by the expressions:

$$n_1 = \frac{wn_0}{p + q_1 + r}, \tag{1}$$

$$n_3 = \frac{rwn_0}{(p + q_1 + r)(\pi + \rho)}, \tag{2}$$

where n_1 and n_3 are the numbers of molecules in the fluorescent and metastable states, respectively, w is the probability of exciting a molecule with light, p, q_1, and r are the probabilities of deactivation of the molecule in the fluorescent level by radiation, by quenching, and by transition to the metastable state, respectively, and π and ρ are the probabilities of deactivation of molecules in the metastable state by radiation and as a result of returning to the fluorescent state.

From Eq. (1) it follows that the intensity of the total radiation in the short wavelength part of the spectrum, i.e., in the absence of long wavelength phosphorescence, is given by

$$I_\beta = pn_1 = \frac{pwn_0}{p + q_1 + r}. \tag{3}$$

We now find the intensities α and β of the phosphorescence bands at the instant after the excitation is interrupted:

$$\frac{dn_1}{dt} = -(p + q_1 + r)n_1 + \rho n_3$$

and

$$\frac{dn_3}{dt} = rn_1 - (\varkappa + \rho)\, n_3. \tag{4}$$

The following expressions are solutions of this system of equations:

$$\left.\begin{aligned} n_1 &= C_1 e^{\lambda_1 t} + C_2 e^{\lambda_2 t}, \\ n_3 &= p^{-1} C_1 (\lambda_1 + p + q_1 + r)\, e^{\lambda_1 t} + p^{-1} C_2 (\varkappa + \rho + p + q_1 + r)\, e^{\lambda_2 t}, \end{aligned}\right\} \tag{5}$$

where λ_1 and λ_2 are roots of the corresponding characteristic equations, and to a high degree of accuracy, are equal to

$$\left.\begin{aligned} \lambda_1 &= -(p + q_1 + r), \\ \lambda_2 &= -(\varkappa + \rho) + \frac{pr}{p + q_1 + r}. \end{aligned}\right\} \tag{6}$$

By determining C_1 and C_2 from the initial conditions (1) and (2) and bearing in mind that when the light is switched off mechanically, $e^{\lambda_1 t}$ can be considered equal to zero and $\lambda_1 + p + q_1 + r$ is very small, we have the following

$$\left.\begin{aligned} n_1 &= prwn_0 (p + q_1 + r)^{-2} (\varkappa + \rho)^{-1} e^{\lambda_2 t} \\ \text{and} \quad n_3 &= rwn_0 (p + q_1 + r)^{-1} (\varkappa + \rho)^{-1} e^{\lambda_2 t}. \end{aligned}\right\} \tag{7}$$

Hence

$$\left.\begin{aligned} I_\alpha &= pprwn_0 (p + q_1 + r)^{-2} (\varkappa + \rho)^{-1}, \\ I_\beta &= rwn_0 (p + q_1 + r)^{-1} (\varkappa + \rho)^{-1}, \end{aligned}\right\} \tag{8}$$

where I_α and I_β are the initial intensities of the phosphorescence bands after the light is mechanically interrupted.

The correctness of the conclusion given in the paper follows directly from Eqs. (3) and (8).

Experiments performed by Sveshnikov using a simple photoelectric polarimeter seemingly confirmed this conclusion, although the difference between the concentration depolarization curves of the total luminescence and the phosphorescence was not very large. As regards the basic assertions of Feofilov that it is impossible to transfer excitation energy from a molecule residing in a metastable state to a molecule in the normal state, this assertion was confirmed by Ermolayev and Sveshnikov[8] by means of measurements of the degree of polarization of the phosphorescence of frozen alcoholic solutions of tripaflavine at various stages of afterglow attenuation.*

*More accurately, these experiments demonstrated the absence of a transfer of excitation energy between molecules in the indicated states for those concentrations of the luminescing material for which a concentration depolarization of fluorescence is observed. From the work of Terenin and Ermolayev[7] on the sensitized phosphorescence of organic compounds, it follows that for very large concentrations of the luminescing material, a transfer of energy from a molecule in a metastable state in one material to an unexcited molecule in the other material can occur.

Although the results of these two papers confirmed the views stated above with respect to the mechanism of the phenomenon, we decided to repeat the experiments described in these papers for the following reasons. First of all, the objects of investigation in the experiments of Ermolaev and Sveshnikov were alcoholic solutions of tripaflavine at −186°C. It was subsequently observed that in these solutions an association of the dye molecules takes place. In Sveshnikov's experiments, boro-phosphors, activated by fluorescein, were used. Laminas made by fusing boric acid are not of high optical quality and they cannot be made very thin, which is important in order to eliminate the possibility of reabsorption of the luminescence. Besides, boro-glycerin phosphors had been successfully prepared only recently; these were of high optical quality and were easily prepared in the form of layers whose thickness was a few hundredths of a millimeter.[8]

In the second place, in the work of Sveshnikov, measurements of the degree of polarization of the phosphorescence and the total luminescence were made through a light filter, in crossed position with respect to the exciting radiation, which transmitted a rather wide spectral region; it could transmit that portion of the long wavelength phosphorescence which had a negative polarization, and the contribution of long wavelength phosphorescence to the afterglow, according to the data of Levshina and Vinokurov,[9] can increase as concentration increases. In this work, a monochromator was used to separate the short wavelength parts of the total radiation and phosphorescence spectra.

The apparatus of Ermolaev and Sveshnikov was substantially different. In their experiments the degree of polarization of the long wavelength phosphorescence was determined by successive measurements of the phosphorescence intensity for two orientations of the analyzer at definite times after the excitation was cut off, the excitation being always carried out for one and the same time interval. In our experiments the apparatus was constructed so that by means of a rapid rotation of a Polaroid plate from one orientation to the other the attenuation curves of the phosphorescence for the vertical and horizontal components of the electric vector were recorded directly on a film by a loop oscillograph. We also investigated the effect of activator concentration on the "polarized spectra"* of the total luminescence and phosphorescence. The spectral studies were made in the apparatus shown in Fig. 1.

*By "polarized spectrum" we mean the dependence of the degree of polarization on the wavelength in the luminescence spectrum.

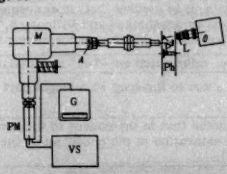

Fig. 1. Arrangement of apparatus for studying polarized phosphorescence spectra. M—monochromator; G—galvanometer; VS—high voltage stabilizer; PM—photomultiplier; O—excitation source; Ph—phosphoroscope; P—polarizer; A—analyzer; L—luminophor.

The degree of polarization was calculated from two successive readings of the galvonometer obtained for similar orientations of the analyzer. In this method of measurement one should take into account corrections to the polarization, introduced by the monochromator. In order to arrive at the magnitude of this correction, the sample cell in the dewar was filled with an aqueous solution of fluorescein.* To check the accuracy of the determination of the correction to the polarization introduced by the apparatus, the arrangement shown in Fig. 1

*The fluorescence of an aqueous solution of fluorescein is virtually unpolarized.

was modified so that the excitation and observation were made with a stationary analyzer and movable polarizer "in the opening." In such a case, as was shown by Vavilov,[10] all corrections to the polarization introduced by the spectral apparatus are excluded. As can be seen in Fig. 2, the polarized spectra of the total luminescence obtained at room temperature for boro-glycerine phosphors containing a small concentration of activator by the first method and by the second method are practically indistinguishable from each other. The polarized spectra of the long wavelength phosphorescence of boro-glycerin luminophors activated by fluorescein which we observed for different activator concentrations are shown in Fig. 3.

Fig. 2

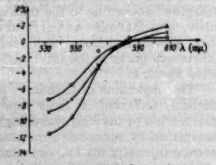

Fig. 3

Fig. 2. Polarized total-luminescence spectra of boro-glycerine luminophors activated by fluorescein at 20°C, obtained by rotating the polarizer (1) and the analyzer while taking into account corrections to the polarization introduced by the monochromator (2).

Fig. 3. Polarization of the long-wavelength phosphorescence spectra of boro-glycerine luminophors activated by fluorescein at −186°C for different activator concentrations. Activator concentration (in gm/gm): 1− 2×10^{-4}; 2−2×10^{-3}; 3−5×10^{-3}.

From these data, it is evident that, in agreement with the results obtained by Sveshnikov and Pilipovich,[11] the degree of polarization at −186°* changes during the transition from the short to the long wavelength part of the spectrum.*

*Editor's note: misprinted as −180° in Russian original.

*It should be noted that in the course of this work we tried to avoid saturation of the phosphor by the exciting light (436 mμ).

From Fig. 3, it follows also that there is a significant concentration depolarization of the long wavelength phosphorescence. It should, however, be pointed out that this depolarization is not caused by a migration of excitation energy from molecules in the metastable state to molecules in the normal state. Attempts to observe a decrease in the degree of polarization in proportion to quenching in the region of concentration depolarization in boro-glycerin luminophors activated by fluorescein were just as unsuccessful as the previously cited attempts by Sveshnikov and Ermolaev to observe this effect in a solution of tripaflavine. For example, with an initial value of the degree of polarization of boro-glycerine phosphors of 8 ± 0.5% (in the 510 and 550 mμ region), the value of the degree of polarization was 7.5 ± 0.5% when the initial intensity had fallen by a factor of ten.

Since no depolarization is observed in the process of the quenching of phosphorescence, then, from the assumptions about the mechanism of concentration depolarization of fluorescence and the transition of molecules into the phosphorescent state, it follows that all the depolarization of the long wavelength phosphorescence depends on the concentration depolarization during the time when the molecule resides in the fluorescent state. Hence, if the concentration depolarization of fluorescence at −186° and the limiting value (for the given spectral region) of the phosphorescence polarization are known, it is obviously possible to calculate the polarized spectrum of long wavelength phosphorescence for any activator concentration. In order to verify this conclusion, we studied the polarized spectrum of the total luminescence of boro-glycerine luminophors at −186° for a series of activator concentrations. In this regard it must be kept in mind that the concentration depolarization of fluorescence at −186° corresponds obviously to a change with concentration in the degree of polarization of the short wavelength part of the total luminescence spectrum in which the negatively polarized phosphorescence has not yet been superimposed onto the phosphorescence. The experimental results are shown in Fig. 4.

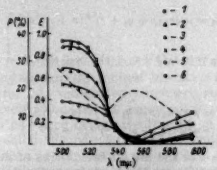

Fig. 4. Concentration depolarization of the total luminescence at −186°C of boro-glycerine luminophors, activated by fluorescein, for various activator concentrations. Activator concentration (in gm/gm): 1−5×10^{-5}; 2−10^{-4}; 3−5×10^{-4}; 4−10^{-3}; 5−2.5×10^{-3}; 6−10^{-2}.

A comparison of Figs. 3 and 4 shows that the concentration depolarization of the long wavelength phosphorescence occurs considerably more slowly than the concentration depolarization of the fluorescence. This result does not agree completely with the results of Sveshnikov cited above and it requires some explanation. Data on the concentration depolarization of the short wavelength phosphorescence which are shown in the Table are in considerably better agreement with theory. From the Table, it can be seen that, in agreement with the previous data of Sveshnikov, the short wavelength phosphorescence is considerably more depolarized than the total luminescence. Experiments were performed in the short wavelength parts of both spectra, and judging from the satisfactory agreement of the values of polarization for small dye concentrations, a superposition of the long wavelength phosphorescence did not occur.

Change in Degree of Polarization of the Total Luminescence (P_l) and Phosphorescence (P_{ph}) of Boro-Glycerine Luminophors as a Function of the Activator Concentration (P in %)

λ (mμ) \ C (gm/gm)		$1 \cdot 10^{-5}$	$5 \cdot 10^{-5}$	$1 \cdot 10^{-4}$	$5 \cdot 10^{-4}$	$1 \cdot 10^{-3}$	$2 \cdot 10^{-3}$	$5 \cdot 10^{-3}$
470	P_l	—	38.7	40.1	27.6	23.7	16.3	7.30
	P_{ph}	—	35.3	35.3	21.3	17.7	9.0	—
480	P_l	38.9	37.3	38.9	26.3	23.0	15.8	6.8
	P_{ph}	38.9	34.7	35.3	20.8	16.7	8.7	2.7
490	P_l	39.2	36.8	38.6	25.6	22.3	15.8	6.1
	P_{ph}	37.5	34.8	34.4	20.5	16.7	8.7	2.7
500	P_l	39.2	36.3	38.2	24.7	21.7	15.3	5.7
	P_{ph}	37.5	34.0	35.3	19.7	16.2	8.4	2.5

REFERENCES

1. S. I. Vavilov. Sobr. soch. 11, 1952.
2. M. D. Galanin. Doklady Akad. Nauk SSSR 57, 683 (1947).
3. A. N. Sevchenko. Doklady Akad. Nauk SSSR 42, 349 (1944).
4. P. P. Feofilov. Doklady Akad. Nauk SSSR 44, 159 (1944).
5. B. Ya. Sveshnikov. Doklady Akad. Nauk SSSR 58, 49 (1947); Zhur. Eksptl. i Teoret. Fiz. 18, 878 (1948).
6. B. Ya. Sveshnikov and V. L. Ermolaev. Doklady Akad. Nauk SSSR 71, 647 (1956).
7. A. N. Terenin and V. L. Ermolaev. Trans. Faraday Soc. 52, 1042 (1956); V. L. Ermolaev. Opt. i Spekt. 6, 642 (1959), Optics and Spectroscopy 6, 417 (1959).
8. P. I. Kudryashov, B. Ya. Sveshnikov, G. A. Tishchenko, and A. S. Cherkasov. Inzh.-Fiz. Zhur. 2, 62 (1959).
9. V. L. Levshin and L. A. Vinokurov. Physik. Z. Sowjetunion 10, 10 (1936).
10. S. I. Vavilov. Z. Physik 32, 721 (1925); Sobr. soch. 1, (1954).
11. B. Ya. Sveshnikov and V. A. Pipilovich. Doklady Akad. Nauk SSSR 119, 59 (1957).

PECULIARITIES OF THE LUMINESCENCE OF ORTHO-DISUBSTITUTED AROMATIC HYDROCARBONS. III. THE FLUORESCENCE AND ABSORPTION SPECTRA OF SOME CARBOXYLIC ACIDS

Yu. V. Naboikin, B. A. Zadorozhny, and E. N. Pavlova

Received 12 August 1959

The influence of ionization, intramolecular hydrogen bonds, and the formation of dimers on the electronic absorption spectra and fluorescence of some substituted carboxylic acids has been investigated. Differences in the luminescence of 2,3- and 1,4-derivatives of naphthalene are noted. It is shown that the variability of the fluorescence bands is connected with the structural peculiarities of the investigated substances.

Earlier, we studied the fluorescence of substances with intramolecular hydrogen bonds formed by a hydroxyl group directly connected to an aromatic ring.[1, 2] It is obvious that with ortho-disubstituted aromatic carboxylic acids specific peculiarities in the luminescence should be apparent which are connected with the presence of this carboxyl group. Such functional groups complicate the picture of the influence of the structure of molecules on their luminescence.

Hence, in the present paper we examine for the purposes of comparison, not only the spectra of the 2,3-derivatives of naphthalene, but also those of the corresponding 1,4-substituted compounds:

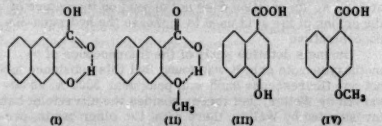

(I) (II) (III) (IV)

The fluorescence of salicylic (V) and o-methoxybenzoic (VI) acids,

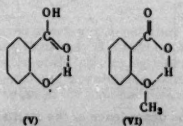

(V) (VI)

was described earlier by Weller,[3] and also by Izmailov and Kremer.[4] However, since certain peculiarities in the luminescence of the acids (V) and (VI) were not recorded by those authors, we also investigated the luminescence of these substances.

The experimental part of the work was carried out with the aid of the apparatus and arrangements described in the first communication.[1] A great deal of attention was given to the purity of the substances.

In Fig. 1a are shown absorption spectra of solutions 2,3-hydroxynaphthoic acid (I). As can be seen from the figure, in the spectrum of the methanolalkali solution there is an additional long wavelength absorption edge, which is apparently connected with the formation of anions of the completely ionized acid. The displacement of the absorption bands to the short wavelength region of the

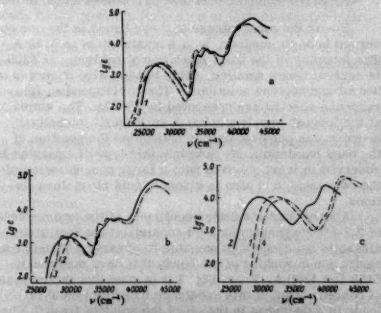

Fig. 1. Absorption spectra of 2,3-hydroxynaphthoic (a), 2,3-methoxynaphthoic (b), and 1,4-hydroxynaphthoic (c) acids in various solvents. Solvents: curve 1—methanol; curve 2—concentrated methanolic solution of KOH; curve 3—heptane; curve—absorption spectrum of 1,4-methoxynaphthoic acid in methanol.

spectrum upon replacement of heptane by methanol can be attributed to the formation of intermolecular bonds with the solvent.[5]

As can be seen in Fig 1b, the absorption spectrum of 2,3-methoxynaphthoic acid (II) in alkaline solutions is displaced toward short wavelengths relative to the spectra in heptane and methanol. It is apparently possible to explain this fact by the destruction of dimers and salt formation by the carboxyl. (An analogous picture is observed also in the case of o-methoxybenzoic acid.)

The absorption spectrum of 1,4-methoxynaphthoic acid (IV) (Fig. 1c) is very weakly affected by the solvent. In basic solutions only an insignificant shift of the absorption band to the short wavelength region is produced. In toluol or heptane the maximum of the absorption spectrum is in the vicinity of 3150 A, whereupon the character of the spectrum does not differ from the spectrum in alcoholic solution. In the same figure are drawn the absorption curves of 1,4-hydroxynaphthoic acid (III). As is seen from the data presented, the absorption spectrum of the hydroxy-acid undergoes a significant change in basic solutions: there occurs a bathochromic displacement of all the bands, which is obviously connected with the ionization of both the hydroxy group and the carboxyl group.

An important circumstance is that the absorption spectra of all the compounds considered do not change upon the acidification of the methanol solutions with sulfuric, hydrochloric, or acetic acids. From this point of view, the fluorescence spectra show a significantly greater sensitivity to the influence of the solvent than the absorption spectra.

Depending on the pH of the alcoholic solutions, it is possible to observe three bands of emission in the fluorescence spectra of 2,3-oxynaphthoic acid (see Table).

The Wavelengths λ_m (in A) of the Fluorescence Band Maxima of Methanol Solutions of 2,3-Hydroxynaphthoic Acid for Different Values of Solution pH

pH. . . .	3	3–5	6–8	>8
λ_m	~6500	~6500 and 4200	4200 and 5150	5150

By far the most intense of these bands is the one observed in basic medium, with a maximum near 5150 A. The intensity of the band which has a maximum at 4200 A is several times smaller. (This band is also observed in benzol and heptane solutions.) The corresponding fluorescence spectra are presented in Fig. 2a. The emission at the longest wavelength has a very small intensity; hence it was possible only to determine the position of the band maximum. We note that this type of emission is observed in inert solvents with a large concentration of the compound, and also in strongly acid alcoholic solutions.

A very characteristic peculiarity of the luminescence of 2,3-hydroxynaphthoic acid consists of the fact that in alcoholic solutions it is possible to observe a strong concentration quenching of the bands that have maxima at 5150 and 4200 A. From Fig. 3 it is seen that the increase of concentration of this substance in ethanol solution leads to a decrease in the pH of the solution from 7.5 to almost 3.0 units. Thereby, the concentration quenching of the yellow band of fluorescence begins when the solution becomes sufficiently acid. Parallel with the quenching of this band as the acidity increases is the growth in intensity of the band with maximum at 4200 A. At a pH near 3.5 the output of the blue glow attains a maximum, and then the concentration quenching begins, accompanied by the appearance of the red glow.

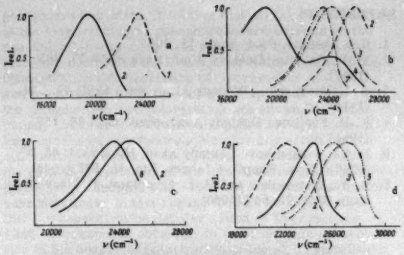

Fig. 2. Fluorescence spectra of 2,3-hydroxynaphthoic (a), 2,3-methoxynaphthoic (b), orthomethoxybenzoic (c), and 1,4-hydroxynaphthoic (d) acids in various solvents. Solvents: curve 1—benzene; curve 2—methanolic solution of KOH; curve 3—methanol; curve 4—methanolic solution of H_2SO_4; curve 5—toluene; curve 6—concentrated methanolic solution; curve 7—crystalline state.

From these data it follows that the concentration quenching of the bands with maxima at 4200 and 5150 A occurs when there is created in the solution the necessary concentration of hydrogen ions on account of the ionization of the 2,3 hydroxynaphthoic acid itself.

Thus, this substance, just like the salicylic acid, has three bands of fluorescence, one of which is strongly displaced toward the long wavelength region of the spectrum.

The study of the fluorescence spectra of 2,3-methoxynaphthoic acid has shown that this substance has at least three emission bands, which are presented in Fig 2b. The short wavelength band is observed in methanol-alkali solutions, whereas in toluene, polystrene, and alcohols a displacement of the maximum of this band from 3900 to 4300 A takes place as the concentration is increased. In acid alcoholic solutions, the short wavelength luminescence becomes extinguished; however, at the same time, a fluorescence band appears with a peak at 5180 A. Its position does not depend on the nature of the anions of the acid used to increase the hydrogen-ion concentration.

During a detailed study of the fluorescence of o-methoxybenzoic acid it was found that this substance has not one fluorescence band with peak near 3600 A, as observed by Weller,[3] but three: besides the ultraviolet band investigated by Weller, there exist two other bands, presented in Fig. 2c. The behavior of the luminescence bands

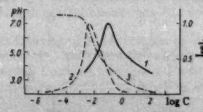

Fig. 3. The dependence of the intensity of various fluorescence bands of a solution of 2,3-hydroxynaphthoic acid in ethyl alcohol on the concentration. Wavelength of the band maxima (in A): curve 1—4200; curve 2—5150; curve 3—dependence of the pH of an alcoholic solution of 2,3-hydroxynaphthoic acid on the concentration.

of this substance is observed to be somewhat analogous to that of the 2,3-methoxynaphthoic acid. At high concentrations, it is possible to observe still another band in the spectrum of solutions of o-methoxybenzoic acid (along with the short wavelength luminescence), which belongs to a dimerized molecule; this coincides in position with the fluorescence band corresponding to the crystalline state of the investigated substance. Upon acidification of the alcoholic solutions it is possible to find a very weak glow analogous to that observed under the very same conditions in 2,3-methoxynaphthoic acid. In basic alcoholic solutions o-methoxybenzoic acid has a very strong luminescence with a maximum near 4050 A. It is also an extremely interesting fact that crystalline o-methoxybenzoic acid is characterized by the presence of a rather a rather intense yellow phosphorescence with a duration of about 1 sec.

The fluorescence spectra of 1,4-hydroxynaphthoic acid obtained under various conditions are shown in Fig. 2d. As can be seen from the figure, the bathochromic displacement of the absorption band in basic solutions (Fig. 1c) corresponds to the appearance of this long wavelength fluorescence band. Replacing toluene or benzene by methanol only leads to a small long wavelength shift of the fluorescence band. In the crystalline state the fluorescence peak of 1,4-hydroxynaphthoic acid is located near 4100 A. Thus, this substance lacks an emission band analogous to the same long wavelength bands of ortho-disubstituted acids.

It should be noted that 1,4-methoxynaphthoic acid lumineses only in the crystalline state (even in very concentrated solutions the intensity of the light is not great). In alkaline and acidic solutions this luminescence is completely extinguished.

As is known, carboxylic acids are dimerized on account of the presence of hydrogen bonds between the molecules.[6] Upon dimerization, the characteristic band of the hydroxy-group disappears from the infrared spectra of these substances, and instead of it there appears a wide band, strongly displaced to the long wavelength region of the spectrum, near 3220-2740 cm^{-1}. We have observed this phenomenon in all the ortho-derivatives studied. In the case of the hydroxy-acids (salicylic and 2,3-hydroxynaphthoic), there occurs in the spectra, besides the band belonging to the dimers, a narrow band characteristic of the OH-group bound to an aromatic ring. (In 2,3-hydroxynaphthoic acid it is located near 3230 cm^{-1}.) The molecules of this substance are evidently dimerized according to the scheme

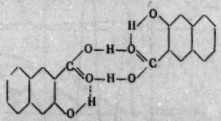

In the infrared spectra of crystalline methoxy-substituted acids one finds only the wide bands of the dimers, spanning the region of the stretching vibrations of the C–H– and CH_3-groups. In solutions, of course, there is an equilibrium between the monomeric and dimeric forms,

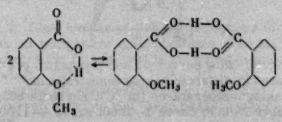

as a result of which there appear in the vibration spectra of solutions of these acids narrow bands which belong to the hydroxy-group and which are displaced to the long wavelength region because of intramolecular interactions. In o-methoxybenzoic acid the indicated band has a frequency of 3380 cm^{-1}, and in 2,3-methoxynaphthoic acid, 3395 cm^{-1}. The wide band characteristic of the dimers survives in solution.

The experimental data presented in the present paper indicate a complicated picture of the luminescence of substituted hydroxy- and methoxy-acids. On the one hand, this is connected with the formation in solutions of the ions

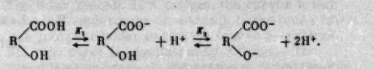

Because of this a strong dependence of the spectra and the fluorescence output on the pH of the medium is observed. In the example of 2,3-hydroxynaphthoic acid it can be seen that an insignificant change in the pH of the solution leads to a very marked increase in the fluorescence output, whereas the absorption spectrum remains completely unchanged during this. This allows one to draw the conclusion that the ionization constants K_1 and K_2 of the molecules in an excited state differ strongly from the corresponding constants of unexcited molecules. It also explains the high sensitivity of the luminescence spectra to the influence of the medium, as compared with the absorption spectra.

On the other hand, the molecules of the investigated acids are able to form hydrogen bonds of various types: intramolecular, intermolecular with the solvent, and intermolecular dimers. Naturally, in the excited state the properties of these bonds differ from the properties of the bonds of unexcited molecules. An analysis of the experimental results allows one to make a series of conclusions on the nature of the several bands in the fluorescence spectra. First of all, it is evident that the luminescence of the crystalline substances pertains to the dimerized molecules. In alkaline solutions one should observe only the luminescence of organic anions. In acid solutions the ionization of OH-groups is almost completely suppressed. The last circumstance evidently leads to the possible formation of intramolecular hydrogen bonds, even in o-methoxysubstituted acids. Thus, the appearance in 2,3-methoxynaphthoic acid of a fluorescence band with a large Stokes' shift can be explained on the basis of the scheme presented in the previous communication.[1]

The same intrinsic difference between 2,3-substituted naphthalenes and the corresponding 1,4-derivatives results in the absence in the latter of a strong displacement of the fluorescence bands to the long wavelength region of the spectrum. The data presented in this paper show that such bands arise as a result of the ortho-location of the substituents.

Undoubtedly the general picture of the luminescence of the substances considered is complex, and for a complete elucidation of the observed changes in the fluorescence spectra a more detailed study of them is required. However, at the present time one can already make the following conclusions: (1) fluorescence bands with a large Stokes' shift are observed in acids that can form intramolecular hydrogen bonds; (2) the dimerization of the acids on account of the hydrogen bridges leads to a long wavelength displacement of the fluorescence bands.

REFERENCES

1. Yu. V. Naboikin, B. A. Zadorozhny, and E. N. Pavlova. Opt. i Spektr. 6, 366 (1959), Optics and Spectroscopy 6, 231 (1959).

2. Yu. V. Naboikin, B. A. Zadorozhny, and E. N. Pavlova. Opt. i Spektr. 6, 492 (1959), Optics and Spectroscopy 6, 312 (1959).
3. A. Weller. Z. Elektrochem. 60, 1144 (1956).
4. N. A. Izmailov and V. A. Kremer. Izvest. Akad. Nauk SSSR, Ser. Fiz. 15, 565 (1951).
5. G. C. Pimentel. J. Am. Chem. Soc. 79, 3323 (1957).
6. L. J. Belamy. "Infrakrasnye spektry molekul." Inostrannoi Lit., Moscow, 1957. "The Infrared Spectra of Complex Molecules." Methuen, London, 1954; Wiley New York, 1954.

THERMOLUMINESCENCE AND THE LOCALIZED LEVELS OF ZnS:Mn PHOSPHORS

V. L. Levshin and V. F. Tunitskaya

Received 25 July 1959

We studied the structure, filling, and thermal emptying of capture levels of the cubic form of ZnS:Mn phosphors. We investigated the changes in the spectrum of the levels with increase in manganese concentration and the dependence of level filling on the wavelength of the exciting light.

INTRODUCTION

Most crystalline phosphors have several interacting activators. The study of activator interaction, which results in different processes of energy transfer and transformation, is one of the most interesting and important problems in the investigation of crystalline phosphors.

ZnS:Mn phosphors are very convenient for an investigation of this kind since the interactions between the centers of blue luminescence and the manganese centers are very intense and cause sharp changes in the majority of phosphor characteristics. In particular they cause a redistribution of luminescence energy between the blue and the orange radiation. The nonlinear luminescence effects of the ZnS:Mn phosphors have therefore drawn the attention of investigators more than once and have already been considered in a series of papers.[1-5]

However, the investigations in these papers were usually carried out on only a few samples and considered only isolated phenomena. Since the effects studied depend strongly on phosphor composition and experimental conditions, it is difficult to compare the results of different authors. Therefore, the study of luminescence kinetics and the transformation of the excitation energy absolutely requires complex investigations of all the properties of a single series of phosphors under different conditions of excitation. The present investigation was carried out for the solution of this problem. A large series of ZnS:Mn phosphors was studied in a wide temperature range under excitation by light of different wavelengths and different intensities. The results given below constitute the first part of this work.

PHOSPHOR COMPOSITION AND SCREENS

The series of phosphors studied was prepared by baking a batch in a current of nitrogen for 30 min at a temperature of 850°C. Manganese was introduced into the batch as $MnCl_2$. Its concentration (with reference to the metal) varied from 10^{-6} to 3×10^{-2} gm/gm. (The actual concentrations are given below when the samples are described.) An analysis showed that the amount of manganese in the finished products constituted about 60% of that introduced into the batch.* The amount of NaCl flux introduced was 2%. The finished phosphors apparently contained a certain amount of oxygen from ZnO and $ZnSO_4$ impurities in the starting ZnS material and also O_2 from the nitrogen flowing during baking.

*The phosphors were prepared by A. V. Lavrov, who also analyzed the activated luminophors for Mn content and prepared the screens.

X-ray studies showed that all the samples had a zinc blende structure. This does not exclude, however, the possibility that a small amount of wurtzite was present. As was to be expected, the lattice constant did not change (with an accuracy to the third decimal place) when Mn was introduced. (Also, no new lines were observed on the Debye powder patterns.)

We chose to study cubic structure phosphors for two reasons:

1. The nonlinear effects are more pronounced for them.[3]

2. Preliminary experiments have shown that the oxygen* peak of the thermoluminescence of zinc blende occurs at a lower temperature (−85°C) than for wurtzite (−60°C). (See the curves corresponding to 800 and 1100° C in Fig. 1.) It is also well separated from the manganese peak. The glow curves show that at the selected baking

*With regard to the origin of the individual peaks in the glow curves of the ZnS phosphors, cf., for example, references 10 and 11.

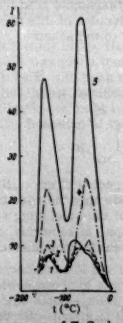

Fig. 1. Glow curves of ZnS phosphors prepared at different baking temperatures. Baking temperatures (in °C): curve 1—800; curve 2—900; curve 3—1000; curve 4—1100; curve 5—1300.

temperature of 850°C the amount of the zinc blende form present is several times that of the wurtzite form. The position of the oxygen peak at −80° permitted separate study of the development of each peak and greatly simplified the interpretation of the experiments.

The luminophors were carefully washed free of NaCl and were quite stable with regard to the action of ultraviolet light. The investigation was performed with phosphor samples deposited as thin layers by settling on a polished base of an aluminum-base alloy. The phosphors weighed 1.5 gm/cm^2, the layer thickness was ~4μ. During photoexcitation the layer was excited uniformly throughout its whole depth. The base was screwed into a copper holder, which could be heated or cooled.

GENERAL DESCRIPTION OF THE GLOW CURVES

Our purpose was to investigate the storage capability and the development of different systems of localized levels as a function of manganese concentration. To do this, we studied the glow curves of ZnS:Mn phosphors for $C_{Mn} = 0 - 3 \times 10^{-2}$ gm/gm. The luminescent screens were placed in a Dewar flask and excited at the boiling temperature of liquid nitrogen. At the end of excitation, the phosphor was kept for 1 min at −196°C. Then its deexcitation by heating was begun. (The heating rate was 15°/min.) Figure 2 shows glow curves of nine phosphors differing in manganese concentration. The curves correspond to the maximum excitation of the phosphors throughout their depth. This was shown by experiments with increasing duration and intensity of excitation and also by the proportionality of brightness and layer thickness when the latter is decreased from 3.7 to 0.67 μ. The excitation was performed with the 312 and 366 mμ Hg lines. The experimental points corresponding to excitation by 366 mμ are marked by circles, those corresponding to 312 mμ by crosses. It is easily seen that within the limits of experimental error the points represented by circles and crosses, respectively, fall on the same curves.

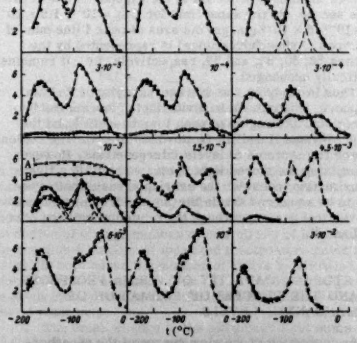

Fig. 2. Glow curves of ZnS:Mn phosphors for different manganese concentrations. The Mn concentration (in gm/gm) is indicated in the drawings. For $C_{Mn} = 3 \times 10^{-5} - 10^{-3}$, blue and orange phosphorescence correspond to the curves with two and three peaks, respectively.

The luminescence spectrum for thermal de-excitation consists of two bands, a blue and an orange one, the latter belonging to manganese. In Fig. 2 the phosphorescence of manganese and blue centers is represented by dashed and solid lines respectively. The figure shows that for manganese concentrations up to 10^{-5} only blue radiation is observed and only orange radiation for concentrations beyond 6×10^{-3}. Both radiations arise for intermediate values of manganese concentration.

In Fig. 2 for ZnS:Mn 10^{-3} gm/gm, the curves A and B represent the temperature dependence of the blue radiation of the phosphor under excitation (curve A—excitation by 312 mμ; curve B—excitation by 366 mμ). The curves A and B extend far into the region of temperatures for which blue radiation is absent under thermal de-excitation. This indicates a basic difference in the behavior of the two processes. A separate article will be devoted to a more detailed consideration of the kinetics and energetics of phosphor luminescence under excitation. Here we restrict ourselves to a description of the glow curves.

THE SHAPE OF THE THERMOLUMINESCENCE PEAKS AND THE NUMBER OF REPEATED ELECTRON LOCALIZATIONS

The peaks of the glow curves are in general asymmetrical in shape. For a small number of successive steps in the direction of higher temperatures the peak grows slowly and falls off rapidly.[12] Our experimental curves consisted of peaks of different shapes. The first (−160°) and the second (−80°) peaks fall gradually in the direction of higher temperatures. This shape is explained, however, by the presence in our phosphors of a certain amount of the wurtzite modification. (See next Section.) The high temperature slope of the third peak is very steep in all cases. In order to exhibit it, a phosphor with a high (3×10^{-2} gm/gm) concentration of manganese was de-excited at different temperatures in the range of −120° to −85°C up to the complete disappearance of the second peak (t°_{max} of peak II ≈ −90°). After this, thermal de-excitation was carried out. Figure 3 shows the shape of the peak obtained for de-excitation starting at −88°C. It is characterized by a noticeably steeper fall in the direction of higher temperatures. This proves that in this case the number of repeated electron localizations is insignificant. A small number of repeated localizations is also indicated by the fact that the positions of the maxima and the half-width of the thermoluminescence peaks are independent of the degree of filling of the localized levels.

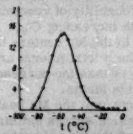

Fig. 3. Shape of the II + III peak in the glow curve of the phosphor ZnS:Mn (3×10^{-2} gm/gm).

THE ORIGIN AND THE POSITION OF LOCALIZED LEVELS AND THEIR VARIATION AS THE Mn CONCENTRATION IS INCREASED

The glow curves shown in Fig. 2 were taken separately for blue and for manganese luminescence. They

have three basic peaks, I, II, and III, at approximately −160, −90, and −30°C. The occurrence of peaks I, II, and III is connected with the presence in the lattice of centers of blue luminescence, oxygen,[10] and manganese, respectively. In addition to the basic peaks two weak peaks should be noted. These are IIa (−60°) which occurs in the slow descent of peak II towards higher temperatures for samples with $C_{Mn} = 3 \times 10^{-4}$, and Ia (~−120°), which manifests itself in the slow descent of peak I in the blue and the manganese phosphorescence and also in the sharp increase (by approximately 1.5 times) in the share of manganese phosphorescence in this temperature range as compared with the phosphorescence in the maxima of thermoluminescence peaks I and II. Peaks Ia and IIa are caused by the presence of an appreciable amount of the wurtzite modification of the phosphor. The shift of the glow curve towards higher temperatures[9] and the marked prevalence of the manganese phosphorescence (observed under excitation in reference 8) correspond to this phosphor modification. The small peak Ia was not taken into account in the analysis of the glow curves (Fig. 2, $C_{Mn} = 10^{-5}$ and 10^{-3}).

When we compare the blue and the manganese phosphorescence peaks in Fig 2, we see clearly the difference in the behavior of the glow curves of these two types of phosphorescence. The blue phosphorescence peaks are very distinct while those of the manganese phosphorescence (up to $C_{Mn} = 1.5 \times 10^{-2}$) are greatly washed out. This circumstance alone shows already that the levels which supply the electrons for blue and orange phosphorescence, respectively, are not quite identical. In other words there is a certain connection between the spots where electrons are localized and the luminescence centers at which they recombine. The same circumstance is confirmed by the difference in the ratio of intensities of blue and orange phosphorescence in the regions of the maxima of the thermoluminescence peaks. This ratio is characterized by the data in Table 1.

Table 1. The Share of Mn Phosphorescence in Thermoluminescence

No. of peak \ $C_{Mn} \cdot 10^{-3}$	0.1	0.3	1.0	1.5	4.5	6	10	30
I	0.1	0.26	0.4	0.68	0.9	1.0	1.0	1.0
Ia	0.15	0.37	0.6	0.88	1.0	1.0	1.0	1.0
II	0.11	0.3	0.5	0.8	1.0	1.0	1.0	—
IIa	0.23	0.6	0.65	0.96	1.0	1.0	1.0	—
III	0.67	1.0	1.0	1.0	1.0	1.0	1.0	1.0

Table 1 shows that practically all electrons from levels III recombine with the manganese centers. The electrons from other levels can recombine with centers of both types. The probability of recombination with Mn increases rapidly with increasing C_{Mn}. Levels II are more strongly bound to the Mn centers than levels I. Levels Ia and IIa of the wurtzite form are more strongly bound to the Mn centers than the corresponding levels I and II of the zinc blende form.

For $C_{Mn} > 10^{-3}$ gm/gm, the Mn peaks stand out clearly, and their position agrees satisfactorily with the position of the peaks of the blue phosphorescence. The shift of Mn peak II for $C_{Mn} = 10^{-3}$ (see Fig. 2) can be explained by the strong action of levels Ia on the development of Mn phosphorescence, giving rise to a stronger development of this phosphorescence for the wurtzite form.

The positions of the peaks of both types of phosphorescence as a function of C_{Mn} is shown in Fig. 4. The positions of the peaks of the blue and the Mn phosphorescence are denoted by circles and crosses, respectively.

In spite of the appreciable accidental fluctuations (of as much as 10°) in the peak positions, caused by experimental inaccuracies, the curves of Fig. 4 allow us to draw the following reliable conclusions:

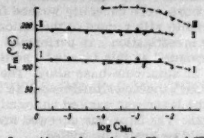

Fig. 4. Location of peaks I, II, and III in the glow curves of ZnS:Mn phosphors. Solid lines—blue phosphorescence; dashed lines—manganese (orange) phosphorescence.

The position of peak I of both the blue and the orange phosphorescence is practically unchanged up to a concentration of 4.5×10^{-3}. Starting with this concentration there is a systematic shift of the maximum of the orange phosphorescence towards lower temperatures, i.e., there is a decrease in the distance of the corresponding levels from the conduction band. Peak III exhibits the same tendency even more consistently starting with $C_{Mn} = 10^{-3}$ gm/gm. At $C_{Mn} = 2 \times 10^{-2}$ it is displaced by 30° toward lower temperatures. Peak II disappears for $C_{Mn} > 10^{-2}$ gm/gm.

Finally we should consider the change in the ratio of different peak heights as the manganese concentration increases. It is easily seen that at large concentrations ($1.5 \times 10^{-3} - 3 \times 10^{-2}$ gm/gm) the development of the manganese peak III proceeds at the expense of a decrease in II. An exact division of these maxima is difficult; however, the process may be characterized qualitatively by the ratio R of the intensities of the maxima of peaks II and III. (See Table 2.) (For $C_{Mn} = 1.5 \times 10^{-2}$ we used for R the ratio of the sums of orange and blue phosphorescence.)

It follows from the data given that the increase of the third maximum proceeds at the expense of a decrease in the second. At the same time for $C_{Mn} = 10^{-3}$, 1.5×10^{-3}, 4.5×10^{-3}, 6×10^{-3} gm/gm the area of peak I (the sum of both types of phosphorescence) is represented by the numbers 56, 60, 63, and 59, respectively, i.e., it remains practically unchanged.

Thus in studying the storage capacity of ZnS:Mn phosphors, it is natural to divide their glow curves into two regions: the region of peak I (up to −120°) and the region of peaks II and III, from −120° to 0°C. The regions of these two systems of levels interpenetrate. However, in computing the stored light sums, we may, to a first approximation, consider the overlap areas of both systems to be equal and divide the area under the glow curve by a vertical passing through the minimum between maxima I and II.

THE STORAGE CAPACITY OF ZnS:Mn PHOSPHORS AND THE PROCESS OF FORMATION OF MANGANESE LEVELS

An inspection of the glow curves of the phosphors (Fig. 2) shows that the total energy of the blue and orange afterglow does not vary significantly over a wide range of values of C_{Mn}. Fig. 5 gives the de-excitation light sums as a function of the logarithm of the concentration. (The sums were determined relatively, as the number of quanta emitted.) Curves 1 and 2 of Fig. 5 represent the

Table 2

C_{Mn}	$1.5 \cdot 10^{-4}$	$4.5 \cdot 10^{-4}$	$6 \cdot 10^{-4}$	10^{-3}	$3 \cdot 10^{-3}$
$R = \frac{I_{II}}{I_{III}}$	1.46	0.84	0.73	0.63	0.00

number of quanta of blue and orange phosphorescence, respectively, while curve 3 represents the sum. Figures 6a and 6b show the same quantities separately for peaks I and (II + III). Several important conclusions may be drawn from Figs. 5 and 6.

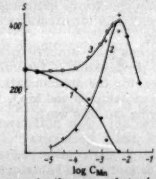

Fig. 5. Change in the complete (quantum) light sum of (curve 1) blue, (curve 2) manganese, and (curve 3) total phosphorescence of all localization levels as a function of manganese concentration.

1. Up to $C_{Mn} = 6 \times 10^{-3}$ gm/gm, the total number of electrons which may become localized on all the levels and subsequently recombine with the emission of radiation, as well as their distribution between the levels I and (II + III), depends but slightly on Mn concentration. This

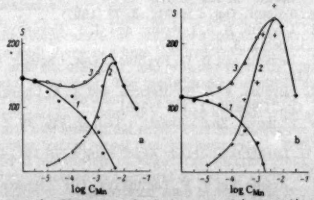

Fig. 6. Change in the light sum of (curve 1) blue, (curve 2) manganese, and (curve 3) total phosphorescence. a—when levels I are emptied; b—when levels II + III are emptied.

is possible if the Mn introduced does not form additional places of localization or if the localized electron blocks a definite volume of the crystal and does not permit further localizations to occur in it. Then, in spite of the formation of a large number of new places of localization, the maximum number of localized electrons remains the same. In both cases the number of active localization places remains constant. (For $C_{Mn} = 6 \times 10^{-3}$ gm/gm it is about four orders of magnitude smaller than the number of manganese ions.)

2. The small change in the integrated light sums up to $C_{Mn} = 6 \times 10^{-3}$ gm/gm indicates the following: the recombination effectiveness of electrons liberated from localized levels remains the same even though recombination occurs at a different place (manganese ions instead of blue luminescence centers); the position of the levels is changed; correspondingly, the electron path is changed as C_{Mn} is increased.

3. The Mn introduced into the phosphor occupies different positions. It is obvious from the glow curves that the major portion of Mn ions does not form new localization levels corresponding to thermal de-excitation in the region from −200° and above. Apparently, these Mn^{++} ions become regularly placed at lattice points and thus create extremely shallow localization levels. A much smaller portion of Mn ions becomes placed near oxygen ions, forming a specific manganese capture center, which is emptied at −40°. The number of purely oxygen traps ($t_{max} = -90°$) decreases correspondingly. However, the properties of the remaining oxygen traps and of the traps connected with blue phosphorescence centers ($t_{max} = -170°$) do not change with increased Mn concentration. (This follows from the conservation of the relative positions of the peaks corresponding to them.) The electrons localized on them can recombine with centers of both kinds. An increase in Mn concentration naturally increases the number of transitions to Mn centers.

The number of traps formed by the blue phosphorescence centers does not decrease with an increase in Mn concentration, as opposed to the case of the oxygen traps, i.e., the Mn ions do not unite with these centers.

4. Starting with $C_{Mn} = 6 \times 10^{-3}$ gm/gm, the storage capacity of the phosphors for levels lying above −200° decreases rapidly. This fall is caused by an appreciable decrease in the depth of all localization levels and the development of nonradiative transitions.

THE INFLUENCE OF THE WAVELENGTH OF THE EXCITING LIGHT ON THE FILLING OF SEPARATE SYSTEMS OF ELECTRON LOCALIZATION LEVELS

Figure 2 shows glow curves corresponding to excitation by light of 366 and 312 mμ lines. The drawing indicates that, within the limits of experimental error, the maximum number of localized electrons is the same in both cases. The same effect is also observed for the ZnS:Cu phosphor. (This is one of the phosphors investigated in reference 13, which has three peaks in the glow curve, at −150, −60, and +20°C.) The conclusion which we reached in reference 13 about obtaining a larger light sum for excitation by the 366 mμ line is apparently in error and is connected with insufficient thinness of the phosphor layers investigated.

The fact that the thermoluminescence light sum is the same for excitation by 366 and 312 mμ indicates one of the following: either light of these wavelengths has no

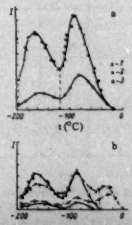

Fig. 7. Glow curves of (a) ZnS and (b) ZnS:Mn 10^{-3} gm/gm phosphors excited by the following Hg lines: (1)—312, (2)—366, and (3)—436 mμ. The vertical dashed lines bound the areas under peaks I, II, and III. (See Table 3.) The dashed curves represent orange luminescence.

de-exciting action on localized electrons at −196°C, or this de-exciting action is independent of the wavelength of the exciting light (which is not likely). On the other hand, excitation by 436 mμ (Fig. 7) results in a lesser filling of the levels. The results of evaluating the data of Fig. 7 are listed in Table 3.

Table 3 leads to the following results: for excitation by light of 436 mμ, the light sums stored by the inactivated ZnS phosphor and by ZnS:Mn (10^{-3}) are about 3 and 3.5 times, respectively, smaller than for excitation by light of 366 and 312 mμ. The decrease in the low temperature peak I is hereby more pronounced than in peak II, while the decrease in II is more pronounced than in III. Thus light at 436 mμ acts more strongly on electrons localized on shallow levels. We noted a similar effect earlier[12] in studying the effect of infrared radiation on ZnS:Cu, Co phosphors. Table 3 shows besides that the decrease in blue and orange phosphorescence is markedly different when excitation is due to light at 436 mμ, the blue phosphorescence decreasing more strongly.

Table 3. Decrease in the Light Sums of Thermoluminescence for Excitation by Light of 436 mμ Wavelength

Sample	Inactivated		$C_{Mn} = 10^{-4}$ gm/gm				
$\lambda_{exc.}$ (mμ)	I_B	II_B	I_B	II_B	I_o	II_o	III_o
312, 366	220	240	90	70	80	75	40
436	50	95	16	12	25	30	16
$\frac{S_{436}}{S_{366}}$	0.23	0.40	0.18	0.17	0.31	0.40	0.40

Note: The subscripts "B" and "O" refer to blue and orange luminescence, respectively.

CONCLUSIONS

1. The Mn activator introduced into ZnS does not by itself create the new localization levels which manifest themselves in the peaks of the glow curves above 80°K. Only a small portion of the Mn ions is arranged near the electron localization places formed by oxygen and greatly deepens the corresponding levels. As a result, a new peak at −30° appears on the glow curve. Its formation occurs at the expense of the oxygen peak at −90°.

2. The quantum light sums of the ZnS:Mn phosphor depend only slightly on Mn concentration up to $C_{Mn} = 6 \times 10^{-3}$ gm/gm. In this range of concentrations there are apparently no radiationless transitions of electrons from localization places during thermal de-excitation.

3. Light with 312 and 366 mμ wavelength does not affect localized electrons and leads to equal light sums for thermoluminescence. Light with λ = 436 mμ decreases the light sums to about 1/3, the decrease being much more pronounced for blue than for orange phosphorescence. Phosphorescence connected with shallow levels decreases much more than that connected with deep levels.

4. An increase in Mn content decreases the depth of electron localization levels.

5. The shape of the high temperature peak of the glow curve for ZnS:Mn phosphors indicates that no large number of repeated electron localizations occurs during thermal de-excitation.

The authors express their sincere appreciation to A. V. Lavrov for the preparation of the series of phosphors investigated and for the determination of the Mn content in the prepared samples and to O. M. Agafonova for her help in carrying out this work.

REFERENCES

1. J. H. Gisolf and F. A. Kröger. Physica **6**, 1101 (1939).
2. Riehl. Z. tech. Physik **20**, 152 (1939).
3. V. L. Levshin. Zhur. Eksptl. i Teoret. Fiz. **17**, 675 (1947).
4. N. A. Tolstoi and P. P. Feofilov. Doklady Akad. Nauk SSSR **68**, 285 (1949).
5. N. A. Tolstoi, N. N. Tkachuk, M. D. Tsenter, Z. S. Mansurov, and A. V. Burlakov. Opt. i Spektr. **1**, 719 (1956).
6. N. A. Tolstoi, A. M. Tkachuk, and N. N. Tkachuk. Opt. i Spektr. **2**, 759 (1957).
7. N. A. Tolstoi. Opt. i Spektr. **3**, 73 (1957).
8. V. L. Levshin, N. S. Borodin, and G. P. Neronova. Opt. i Spektr. **3**, 258 (1957).
9. V. L. Levshin and B. D. Ryzhikov. Opt. i Spektr. **4**, 358 (1958).
10. V. L. Levshin, V. F. Tunitskaya, and A. A. Cherepnev. Opt. i Spektr. **1**, 255 (1956).
11. N. V. Zhukova. Zhur. Eksptl. i Teoret. Fiz. **29**, 5 (1955).
12. Ch. B. Lushchik. Doklady Akad. Nauk SSSR **101**, 4 (1955).
13. V. L. Levshin and V. F. Tunitskaya. Opt. i Spektr. **2**, 350 (1957).

LUMINESCENCE OF UNACTIVATED CsI CRYSTALS. II*

*Presented at the Conference on the Physics of Alkali Halide Crystals at Tartu, June, 1959.

Z. L. Morgenshtern

Received 4 September 1959

The luminescence of unactivated and activated CsI crystals excited by γ-irradiation is investigated at room temperature and at the boiling point of liquid nitrogen. It is shown that three kinds of emission are observed in the luminescence spectra—ultraviolet, blue, and long wavelength (due to the activator)—corresponding to different luminescence centers. The spectral characteristics of the luminescence of the crystals and, in particular, the temperature dependence of the luminescence are studied for all of these wavelength intervals. The question of the origin of these various bands in the luminescence spectra of the crystals is considered.

1. In recent years a number of works have been devoted to the investigation of the luminescence of unactivated alkali halide crystals,[1-4] and, in particular, of CsI crystals.[5,6] Interest in the study of the luminescence of CsI crystals is explained by the fact that they are of great technical importance, being among the best scintillators, especially at low temperatures. Published works have investigated mainly the scintillation properties of CsI, but the results obtained by individual authors are in disagreement with respect to some questions. At present there exists no general picture of the luminescence nor any clear explanation of the nature of its individual luminescence bands. Hence, further investigations in this direction are needed. We propose to investigate principally the spectral properties of the luminescence of unactivated CsI and also the temperature dependence of the luminescence.

2. In an earlier work[7] we carried out investigations at room temperature. It was shown that in CsI grown from a melt there is a blue luminescence distinct from that due to the activator, and of lower intensity when an activator is present. The luminescence is easily excited by γ-rays and has a narrow range of wavelengths for photoexcitation, peaking at $\lambda_m \sim 240$ mμ and lying at the crystal's own absorption edge. This luminescence thus resembles the universal blue luminescence in ZnS, also excited at the absorption edge. The quantum yield of the blue luminescence in a crystal of CsI for excitation at the wavelength of its absorption edge is high, averaging from 0.4 to 0.7, depending on the crystalline specimen. The duration of the blue luminescence is ~0.55 μsec for photoexcitation, while the duration of the activator luminescence for photoexcitation in the same crystal is ~0.7 μsec.

In the present work the luminescence of CsI crystals at low temperatures has been investigated. The investigation was carried out on crystals of four types: (1) a crystal grown from a solution, using a twice-recrystallized raw material which had been previously purified of heavy metals with the aid of rubeanic acid (crystal no. 1); (2) a crystal grown by L. M. Soifer and kindly placed by him at our disposal (crystal no. 2). The original substance was twice recrystallized and was then purified with the aid of zonal melting Eight zonal passes were used, and the crystal was then found to have reached a high state of purity. The lower part of the crystal was used in the investigations; (3) crystals grown by the usual Stockbarger method in sealed quartz ampoules in the laboratory of L. M. Shamovskii (crystals nos. 3, 4, 5); (4) crystals also grown in the laboratory of L. M. Shamovskii and containing small additions of Tl(10^{-4}) or In(10^{-5})* (crystals nos. 6, 7).

Thus we had at our disposal at least three types of crystals, distinguished by the means of preparation.

3. The luminescence spectra of the crystals investigated were obtained by means of a quartz spectrograph, using excitation by Co^{60} γ-rays. During photographing of the spectra the crystal was placed between two quartz windows in a vacuum chamber which terminated in a special metallic dewar. Figure 1 gives curves showing the spectral distribution of the intensity of luminescence (corrected for the spectral sensitivity of the photographic film). Since the differences in exposure times and in thicknesses of the crystals have been taken into account, the areas under the curves are approximately proportional to the effectiveness x_i of the individual luminescence bands. (The effectiveness of the ultraviolet luminescence band of crystal no. 2 at liquid nitrogen temper-

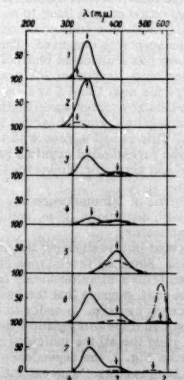

Fig 1. Luminescence spectra of various specimens of crystalline CsI at room temperature (dashed curves) and at the boiling point of liquid nitrogen (continuous curves). The numbers adjacent to the curves correspond to the numbers of the crystalline specimens. The dash-dotted curve gives the luminescence of CsI(Tl) (high concentration) at room temperature.

*I take this opportunity to thank L. M. Shamovskii and L. M. Soifer for the use of these crystals.

Luminescence Bands of CsI Crystals

CsI crystal no.	Temperature	Ultraviolet λ_m mμ	Ultraviolet λ_m ev	Ultraviolet $\varkappa_{uv.}$	Blue λ_m mμ	Blue λ_m ev	Blue $\varkappa_{bl.}$	Activator λ_m mμ	Activator λ_m ev	Activator $\varkappa_{act.}$	$\varkappa=\Sigma\varkappa_i$
1	r. t.	319	3.87	7	—	—	—	—	—	—	7
	l. n.	337	3.67	78	—	—	—	—	—	—	78
2	r. t.	319	3.87	10.5	—	—	—	—	—	—	10.5
	l. n.	336	3.68	100	—	—	—	—	—	—	100
3	r. t.	—	—	—	412	3.0	3.5	—	—	—	3.5
	l. n.	336	3.68	40.5	407	3.04	8.7	—	—	—	49.2
4	r. t.	—	—	—	408	3.02	9.3	—	—	—	9.3
	l. n.	343	3.60	12.7	405	3.05	8.0	—	—	—	20.7
5	r. t.	—	—	—	406	3.05	25	—	—	—	25
	l. n.	—	—	—	404	3.06	45	—	—	—	45
6	r. t.	—	—	—	405	3.05	5.5	577	2.14	2.9	8.4
	l. n.	339	3.64	~58	404	3.06	~16	580	2.13	~2	76
7	r. t.	—	—	—	405	3.05	~2	535	2.31	4	6.0
	l. n.	338	3.66	~48.5	403	3.07	~7	—	—	0	55.5

Notation: r. t. – room temperature; l. n. – liquid nitrogen temperature.

ature is taken as 100%.) The Table gives the results for the individual luminescence bands.

In agreement with the results of Enz and Rossel[8] we observed the ultraviolet luminescence band at low temperatures in crystals grown from a solution. Its maximum is situated at about 340 mμ, and its halfwidth is 0.4 ev.

The second component of the luminescence, the blue wavelength band, occurs with various intensities in the majority of the crystals investigated. We had observed it earlier at room temperature in both activated and unactivated crystals. Its maximum at low temperatures is located at about 405 mμ, and its halfwidth is 0.45 ev. In the case of crystals grown from a solution this wavelength band was not observed; nor was it observed in the spectrum of crystal no. 2. The introduction of an activator in small concentrations did not lower either the ultraviolet or the blue luminescence bands. However, an increase in concentration caused them to weaken considerably. At very high activator concentrations (~10^{-3}) only the activator luminescence is observed. The luminescence at room temperature has a different character. The ultraviolet luminescence band disappears for practically all crystals. Only crystals nos. 1 and 2 are exceptions, and weak ultraviolet bands at shorter wavelengths than for liquid nitrogen temperature were observed in their spectra (λ_m ~ 320 mμ). This result agrees with the results of Enz and Rossel, who investigated crystals grown from a solution. The blue and activator luminesces persist at room temperature.

Thus, three forms of luminescence are observed in CsI crystals, namely, ultraviolet, blue, and longer wavelength (due to an activator).

We are interested in investigating the nature of these luminescence bands. Since all three types of luminescence are observed (either simultaneously or separately) in our crystals, we may suppose that the bands belong to different luminescence centers. In order to clarify this question, we investigated the temperature dependence of the luminescence yield for all the indicated bands (Fig. 2).

As is clear from Fig. 2, the dependence of the luminescence yield on temperature for γ-excitation has a different form for the various bands. The ultraviolet luminescence yield increases strongly with decreasing temperature and saturates at about 100°K (curve 1). For the blue luminescence the curve slopes much less steeply (curve 2). For the activator luminescence the opposite dependence is observed, that is, the intensity of the activator luminescence falls with decreasing temperature (curve 3). This unusual dependence of the activator luminescence yield is observed only when the crystal also possesses blue and ultra violet luminescence. In a crystal

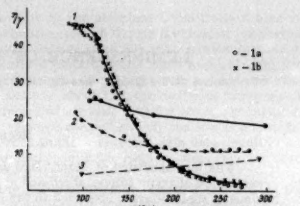

Fig. 2. Temperature dependence of the total luminescence yield in various bands for CsI crystals under γ-excitation. Curve 1—ultraviolet bands of crystals no. 1 (1a) and no. 2 (1b); curve 2—blue band of crystal no. 5; curve 3—activator band of a CsI(Tl) crystal (low concentration); curve 4—activator band of a CsI(Tl) crystal (high concentration).

with a high concentration of activator (~10^{-3}), where there is neither a blue nor an ultraviolet band, the usual temperature dependence, that is, an increase in activator luminescence yield with decreasing temperature, is observed (curve 4).

4. Other characteristics of the ultraviolet, blue, and activator centers of luminescence are also different. Thus the photoexcitation spectra of the activator bands correspond to absorption bands of the activator—and are different for crystals activated with Tl[8] than for crystals activated with In.[9] As was remarked above, the excitation spectrum of the blue luminescence is a narrow band located at the crystal's own absorption edge. With decreasing temperature this band moves into the short wavelength region, following the absorption edge. Photoexcitation of the ultraviolet luminescence band in the region of wavelengths longer than 200 mμ was not observed. Excitation by a shorter wavelength, in particular, the mercury line at λ185 mμ (with the aid of a vacuum monochromator) gave a small positive effect at liquid nitrogen temperature. Thus we may conclude that the ultraviolet luminescence is not excited in the first two absorption bands proper to CsI (λ_m 225 and 206 mμ[10]). The excitation evidently takes place only in the region of shorter wavelengths.

The damping time and its temperature dependence for the ultraviolet, blue, and activator bands are also different, as follows from references 6 and 7.

At low temperatures, after γ-excitation a certain amount of radiation is stored in all of the crystals. It is interesting to note that a greater amount of radiation is stored in those crystals whose spectra contain the blue luminescence than in crystals in which only the ultraviolet luminescence is observed. Curves of thermal de-excitation after γ-excitation, measured for three crystals (Fig. 3), showed that the difference in the stored amount of radiation was especially great in the region of the low temperature maximum (130°K).

5. The results given above support the proposition that the three luminescence bands of CsI are connected with three different types of centers. Under γ-excitation the reservoir from whence the energy for luminescence in all of these bands is derived appears to be a common one, inasmuch as the crystalline lattice becomes excited and the energy of excitation is transferred with more or less effectiveness to all of the centers. In unactivated crystals, in which there are no centers of blue luminescence, the effectiveness of the ultraviolet band is greatest.

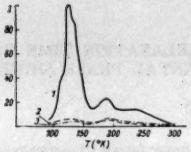

Fig. 3. Curves of thermal de-excitation in various bands for CsI crystals after γ-excitation. Curve 1—blue band of crystal no. 5; curve 2—ultraviolet band of crystal no. 2; curve 3—ultraviolet band of crystal no. 1;

In crystals where both types of luminescence occur, a definite relationship between them is observed: the more intense is the blue luminescence, the weaker is the ultraviolet (crystals nos. 3 and 4). In those cases where the effectiveness of the blue luminescence is greatest, the ultraviolet band disappears completely (crystal no. 5). Analogous effects are also observed in the activator bands. Of course, as we have seen, in crystals with a large concentration of Tl the other luminescence bands are not observed at all.

At the present time the question of the nature of the luminescence of CsI is not completely clear. On the basis of existing experimental evidence, only more or less reasonable statements may be made concerning the origin of the individual luminescence bands. Thus, Enz and Rossel[6] consider that the ultraviolet luminescence of CsI crystals grown from a solution is connected with the luminescence of a degenerate exciton, that is, is not connected with fixed structural lattice defects. This proposition is stated on the basis of the fact that, according to the same reference 6, the damping of the luminescence in the indicated bands is exponential. However, the absence of photoexcitation of the ultraviolet luminescence in the first two of the crystal's own absorption bands, which are usually considered to be due to excitons, makes us treat this conclusion with caution. It does not seem possible to us to say anything definite regarding a model for the ultraviolet luminescence center. We may, however, consider that in any case this center is not connected with defects of the vacancy type, since the ultraviolet luminescence is observed with great effectiveness in crystals grown from a solution at room temperature. (One hardly expects to find defects of the vacancy type in such crystals.)

The blue luminescence, analogous to the blue band of ZnS[11] may be connected with structural lattice defects (of the vacancy type). It is usually considered that the absorption due to structural defects is situated at the edge of the crystal's own absorption. The excitation band of the blue luminescence centers is located in this region. Knoepfel, Loepfe, and Stoll investigated the so-called "warm" component of the CsI luminescence. On the basis of their experiments on thermal treatment of the crystals, and on various methods of preparing them, these authors came to the conclusion that the luminescence centers of the "warm" component were frozen iodine vacancies. According to the results of these authors, the maximum in the luminescence spectrum of the "warm" component will be located somewhere in the interval from 410 to ~590 mμ, the exact location depending on the conditions under which the crystal was prepared. For Tl-activated crystals grown from a superheated melt these authors discovered that the duration of the luminescence and the intensity of the scintillation had the same temperature dependence. On the basis of this they came to the conclusion that Tl does not play the role of an activator, that is, does not directly create luminescence centers, but, owing to its ability to adapt itself to complexes, it stabilizes the iodine vacancies. This conclusion seems to us to be insufficiently well-founded, since the results of these authors apparently deal with the sum of two spectral components. It has been shown in many works that the activator introduces its own individuality into the luminescence of alkali halide crystals, and our investigation of crystals activated with Tl or In confirm that in this respect CsI is no exception.

In conclusion we wish to mention a qualitative observation of the luminescence of unactivated CsI under plastic deformation. If the crystal is compressed, then along with the blue luminescence there appears in it a yellowish luminescence similar in color to the Tl luminescence. The effect is well seen under excitation by a low pressure mercury lamp and observation through optical filters. This luminescence has not yet been studied, but it is evident that it is connected with structural defects which arise under plastic deformation. At the same time, this shows that the centers of the blue luminescence are not of the same nature as these defects, since the blue luminescence does not become stronger during compression.

We thank M. D. Galanin for his interest in the problem and N. V. Kostina and N. N. Vasil'eva for their assistance in carrying out the work.

REFERENCES

1. J. Bonanomi and J. Rossel. Helv. Phys. Acta **25**, 725 (1952);
B. Hahn and J. Rossel. Helv. Phys. Acta **26**, 803 (1953).
2. W. Van Sciver and R. Hofstadter. Phys. Rev. **97**, 1181 (1955).
3. K. J. Teegarden. Phys. Rev. **105**, 1222 (1957).
4. L. M. Belyaev, M. D. Galanin, Z. L. Morgenshtern, and Z. A. Chizhikova. Doklady Akad. Nauk SSSR **99**, 691 (1954); Ibid. **105**, 57 (1955); Izvest. Akad. Nauk SSSR, Ser. Fiz. **21**, 548 (1957).
5. H. Knoepfel, F. Loepfe, and P. Stoll. Helv. Phys. Acta **29**, 241 (1956); Ibid **30**, 521 (1957); Z. Naturforsch. **12a**, 348 (1957).
6. H. Enz and J. Rossel. Helv. Phys. Acta **31**, 25 (1958).
7. Z. L. Morgenshtern. Opt. i Spektr. **7**, 231 (1959).
8. Z. L. Morgenshtern. Doklady Akad. Nauk SSSR **105**, 250 (1955).
9. A. A. Dunina, Z. L. Morgenshtern, and L. M. Mamovskii. Opt. i Spektr. **4**, 105 (1958).
10. R. Hilsch and R. Pohl. Z. Physik **59**, 812 (1930);
E. C. Schneider and H. M. O'Bryan. Phys. Rev. **51**, 293 (1937);
W. Martienssen. Phys. and Chem. Solids **2**, 257 (1957).
11. Z. A. Trapeznikova. Mater. V Soveshchaniyu po Luminestsentsii (Proceedings of the Fifth Conference on Luminescence), Tartu, 1957;
F. A. Kröger and H. J. Vink, J. Chem. Phys. **22**, 250 (1954).

DEVELOPMENT OF A METHOD FOR DETERMINING RELAXATION TIME USING A SPECTROPHONE. II. ELIMINATING THE INSTRUMENTAL PHASE SHIFTS

P. V. Slobodskaya and E. S. Gasilevich

Received 25 July 1959

We consider the sources of systematic errors arising in the determination of relaxation times using a spectrophone. Different methods of eliminating the errors are described; these permit absolute values of the relaxation time to be obtained.

The spectrophone may be used to measure the phase shift of the signal of an optical-acoustic receiver, relative to the reference voltage; it may be found that for different concentrations of the gas under study and for different absorption bands the phase shift is not uniform. In order to use these measurements to determine absolute values of the relaxation time, the effect of the instrumental phase shifts introduced by the apparatus must be considered.

In part I[1] we showed that the phase shift φ measured with the apparatus was related to the relaxation time τ and the instrumental phase shift φ_0 (which we will now call the temporal instrumental shift in contrast with the spatial instrumental shift which will be discussed below), by the relation:

$$\varphi = \arctan \omega\tau + \varphi_0, \qquad (1)$$

where ω is the modulation angular frequency.

Previously,[1, 2] it has been assumed that φ_0 remains constant for all concentrations of the mixtures under study. However, strictly speaking, this quantity is not constant. Measurements made by us showed that the observed variations of phase shift with concentration are distorted by a variable temporal instrumental shift. These distortions are particularly noticeable when using resonance microphones, that is, in cases where the frequency characteristic of the optical-acoustic receiver may change with change in concentration. The observed variation of φ_0 with concentration makes it necessary to seek a better method of eliminating it than has been used up till now.*

*Measurements published by us earlier[1, 2] were not distorted by the variable instrumental shift φ_0 because they were made at modulation frequencies in the vicinity of which the frequency characteristic of the optical-acoustic receiver had a sufficiently gentle slope.

Another source of error is that any movement of the receiver relative to the photoelement or any change in the energy distribution in the beams of radiation directed to the receiver and photoelement can be mistaken for changes in the measured phase shift φ. In what follows we will call the error arising from this source the spatial instrumental phase shift. Usually the spatial instrumental shift is considerably less than the temporal one.

SOURCES OF SYSTEMATIC ERRORS

The spatial instrumental phase shift arises from the following cause.

The beams issuing from the monochromator cover a definite wavelength interval corresponding to the absorption band under study. For different bands, the energy which will be absorbed in the cell will have different distributions in the plane of the slit.

This difference can arise from several causes: from a difference in the contours of different absorption bands, nonuniform dispersion of the prism, inexact centering of the slit opposite the center of the band, etc. In consequence, for one band the rays more strongly absorbed in the cell may pass through points in the slit lying close to one of its edges, and for another band, these points may lie close to the opposite edge; that is, the energy center of gravity of the slit may not coincide with the geometrical one, and for different bands this deviation may be different.

Therefore, rays of the radiation corresponding to different absorption bands appear modulated with a slight difference in phase.

It will be shown in the next section that eliminating the spatial instrumental shift is simpler than eliminating the temporal instrument shift φ_0. The latter is defined as follows, using the notation introduced in reference 1.

$$\varphi_0 = \varphi_{\text{therm.}} + \varphi_{\text{acoust.}} + \varphi_{\text{el.}}.$$

The chief source of systematic errors is the change in φ_0 with change in concentration, due to the dependence of $\varphi_{\text{therm.}}$ and $\varphi_{\text{acoust.}}$ on concentration. We will consider the effect of these quantities more closely.

The dependence of $\varphi_{\text{therm.}}$ on concentration is explained by the variation of the receiver thermal inertia $1/\beta_1$ with the heat capacity and thermal conductivity of the mixture under study; the thermal inertia determines $\varphi_{\text{therm.}}$ ($\varphi_{\text{therm.}} = \arctan \omega/\beta_1$). Since usually $\omega \gg \beta_1$, the phase shift $\varphi_{\text{therm.}}$ should be close to 90° and consequently varies slowly with change in β_1. Therefore the variation of $\varphi_{\text{therm.}}$ with concentration should be small. The effect of concentration on the component $\varphi_{\text{acoust.}}$ is greater. This may be judged from the fact that, as mentioned above, change in the frequency characteristic of the optical-acoustic receiver corresponds to variability of φ_0 (with change in resonance frequency the phase of the vibrations of the microphone membrane changes also).

Finally, we can assume that systematic errors can arise because φ_0 may not have a uniform value for the different bands. This should be observed in cases when the energy corresponding to different bands is absorbed at different parts of the interior of the cell* (farther from or nearer to the input window). However, the dependence of φ_0 on the absorption band apparently lies inside the limits of error of the measurements, since with increase in concentration (when the difference in the absorption zones for different bands should be more marked) the observed difference in phase shifts φ_0 for different bands approaches zero.

*When the bands differ greatly in intensity.

ELIMINATING THE SPATIAL INSTRUMENTAL PHASE SHIFT

We will assume that the modulator of the shape shown in Fig. 1a chops the radiation entering the window of the optical-acoustic receiver and the light beam falling on the photoelement. The center of the receiver window is lo-

Fig. 1. Eliminating the spatial instrumental phase shift by rotating the modulator in opposite directions.

cated at the point O and the photoelement can be placed at any point of the arc of a circle of radius R.*

*Part I[1] describes the technique for measuring phase shifts with an apparatus based on the use of the spectrophone.

Suppose that the inertia of the photoelement is negligibly small and that the phase shifts introduced by the receiver and photoelement amplifiers differ by 90°. Then the galvanometer connected to the phase-sensitive detector output will show zero deflection if the radiation incident on the receiver and the light beam incident on the photoelement are modulated in opposite phases. We will call the position of the photoelement which corresponds to a zero galvanometer reading the photoelement zero position. Evidently, if the receiver inertia is also negligibly small, the photoelement zero position coincides with the point Φ (on the diameter OCΦ).

We will consider the case where the optical-acoustic receiver has inertia, that is, where a certain delay (in magnitude $\varphi = \arctan \omega\tau + \varphi_0$) occurs in the phase of the signal which it develops, relative to the reference signal taken from the photoelement. In this case the photoelement zero position depends on the direction of rotation of the disc. If the disc rotates clockwise, the photoelement should be placed at position Φ′, while if the rotation is anticlockwise, it should be at Φ″, symmetrical with Φ′ relative to the point Φ.* The zero positions of the photoelement are measured off along the circular arc with center C by using a scale (not shown in the figure), the zero division of which is located at an arbitrary point. If the scale readings corresponding to points Φ′ and Φ″ are α' and α'', the angle $\varphi = (\alpha' - \alpha'')/2$ determines the required phase delay of the receiver signal relative to the photoelement signal.

*Since the movement of the photoelement necessary to compensate the signal delay of the receiver should take place in the direction of rotation of the disc, in measuring phase shifts we always know which divisions of the scale of the micrometer moving the photoelement correspond to the greater value of relaxation time, and which to the lesser.

We will now consider another case, where the phase shift associated with receiver inertia is absent, but a spatial instrumental shift γ occurs (fig. 1b). This case is equivalent to radiation in the spectral range corresponding to the absorption band λ_1 being emitted by a source effectively located in front of the modulator opposite point O_1, while for the absorption band λ_2 the source is effectively located opposite point O_2. In this case the photoelement zero corresponds to point A for absorption band λ_1, and to point B for λ_2. It is important to emphasize that the position of points A and B does not depend on the direction of rotation of the modulator (clockwise or anticlockwise).

Evidently, in actual conditions both cases will arise simultaneously (Fig. 1c). Suppose that a phase shift φ_1 corresponds to the band λ_1, and φ_2 to the band λ_2, and suppose that the spatial shift is γ. Then for the band λ_1 the photoelement zero position falls at point Φ_1' for clockwise rotation, and at point Φ_1'' for anticlockwise rotation. The zeros for band λ_2 will be Φ_2' and Φ_2'', respectively. If we measure the angles α with the disc rotating in the clockwise direction, for example, the readings corresponding to the zero positions Φ_1' and Φ_2' will not differ by $\varphi_1 - \varphi_2$ as would be the case for $\gamma = 0$ but by $\gamma - (\varphi_1 - \varphi_2)$ while for anticlockwise rotation the difference would be $\gamma + (\varphi_1 - \varphi_2)$. The phase shift γ is evidently eliminated if we determine the angle φ_1 by half the difference of the angles α corresponding to points Φ_1' and Φ_1'', and the angle φ_2 by half the difference of the angles α corresponding to the points Φ_2' and Φ_2''.

Therefore, to eliminate the spatial phase shift for arbitrary concentration we must find the photoelement zero positions with one modulator rotation direction, for all the absorption bands under study, and then rotate the modulator in the opposite direction and repeat the measurements of the null positions.

ELIMINATING THE TEMPORAL INSTRUMENTAL PHASE SHIFT

(A) Eliminating φ_0 by Adding Moisture to the Mixture Under Study

To find the variation of the temporal instrumental phase shift φ_0 with concentration, it should be measured with the same ratio of the components of the mixture as is used for determining the relaxation time. A good approximation to these conditions can be obtained by making use of the fact that collisions of water vapor molecules with the molecules under study are effective in reducing the relaxation time of the latter to a value lower than the measurement error. When 1-2% water vapor is added, the thermal conductivity, heat capacity, and density of the mixture change negligibly. Therefore we can assume that the value of φ_0 remains the same for the dry and the moist mixtures.

We will now introduce experimental results showing the possibility of eliminating the temporal instrumental phase shift by a method based on these considerations. The measurements were made on mixtures of CO_2 and N_2 with three concentrations of the CO_2—10, 34, and 100% and at modulation frequencies 700, 850, 1000, 1100, 1200, 1500, and 2000 cps. Figures 2a and b show graphs for three of these frequencies (analysis of the measurements made at the other frequencies leads to the same results). The graphs of Fig. 2a show the variation of the micrometer reading l (in mm) with the concentration of dry mixtures of carbon dioxide with nitrogen at modulation frequencies 700, 1000, and 1500 cps; the graphs of Fig. 2b represent similar relationships for the case where the mixtures were moistened by passing them through water.*

*The curves of Fig. 2a, b are the results of measurements corrected by eliminating the spatial phase shift. This shift is revealed at 100% concentration (for the dry and the moist mixtures) by the fact that, with both clockwise and anticlockwise rotation of the modulator, the ordinates of the curve corresponding to the 4.3μ band are less than those of the 2.7μ band curve by 0.2 and 0.3 mm on the micrometer scale; consequently, the relationships observed with the two rotation directions are of the nature of the curves shown in Fig. 3. The line LL′ is the axis of symmetry of curves 2 and 3 and the line NN′ that of curves 1 and 4. The distance between these straight lines is equal to the spatial instrumental shift. When φ_{a1} changes, curves 3 and 4 undergo a parallel shift relative to curves 1 and 2.

The measurements were made with a receiver equipped

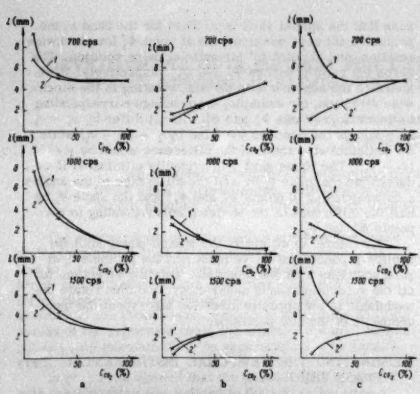

Fig. 2. Eliminating the temporal instrumental phase shift by moistening the mixture of gases under study. a, b—Dependence of the micrometer readings on concentration of CO_2 mixed with N_2 for dry and moist mixtures respectively; c—effect of the variation of the temporal instrumental shift with CO_2 concentration on the micrometer readings (explanation in the text). Curves 1, 1′—4.3μ CO_2 band; curves 2, 2′—2.7μ CO_2 band.

with an electromagnetic microphone (in the apparatus described in reference 1). Comparison of the curves of Fig. 2a and Fig. 2b corresponding to the same modulation frequency shows that they have a very different shape for the dry and the moist mixtures; in the moist mixtures the curves for both bands are shifted in the direction of lower relaxation times and agree with each other better at lower CO_2 concentrations than in the dry mixtures. In addition we see that in Fig. 2b the shapes of curves 1′ and 2′ at different frequencies are different; for frequencies 700 and 1500 cps there is even an increase in ordinate with increase in concentration, and not a decrease as occurs with the dry mixtures. These facts, especially the last, lead us to the conclusion that the curves of Fig. 2b correspond to a case where the relaxation time is close to zero. If we assume that curve 2′, with ordinates less than those of curve 1′, gives the temporal instrumental phase shift in the concentration range 10 to 100%, and if we determine the phase shift corresponding to the relaxation time of the 4.3μ band, using the difference in the ordinates of curves 1 and 2′, then for all modulation frequencies we obtain very similar results. Fig. 2c illustrates this; curves 1 of Fig. 2a and 2′ of Fig. 2b are redrawn here (at 100% concentration the points coincide within the limits of the measurement error). In this range of concentrations (that is, at concentrations over 10%) the phase shifts corresponding to the differences of the ordinates of curves 1 and 2′ are small. Due to this, the tangential dependence of phase shift on relaxation time can be approximated by a linear dependence, so that the difference between the ordinates of curves 1 and 2′ is proportional to $\tau_{4.3\mu}$, the coefficient of proportionality being independent of frequency.* For all three cases the differences of ordinate have approximately the same value, which shows that the elimination of the temporal instrumental error was correct. Figure 4 gives the mean relaxation times $\tau_{4.3\mu}$ for the three modulation frequencies.

*The frequency was changed by changing discs; then $\varphi = k\omega l$ and $\tau \approx \varphi/\omega = kl$ (k depends on the radius of the disc and the rotation speed, $k = 1.5 \times 10^{-5}$ sec/mm).

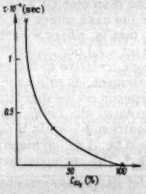

Fig. 4. Approximate curve for the variation of relaxation time $\tau_{4.3\mu}$ with CO_2 concentration.

Therefore, by measuring the phase shift in dry and moist mixtures at any one modulation frequency, we can determine the absolute values of τ, eliminating the temporal instrumental shift. It should be noted that this method is suitable for high concentrations only.

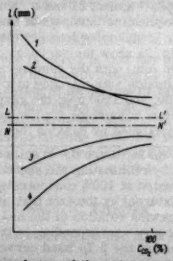

Fig. 3. Dependence of the micrometer readings on the carbon dioxide concentration in a mixture in the presence of spatial instrumental shift. Curves 1, 2—modulator rotated in one direction; curves 3, 4—modulator rotated in the opposite direction (explanation in the text). Curves 1, 4—4.3μ CO_2 absorption band; curves 2, 3—2.7μ CO_2 absorption band.

(B) ELIMINATING φ_0 BY USING THE BELL EFFECT

If wideband microphones are used in the optical-acoustic receiver, it can be assumed that the variation of φ_0 with concentration is negligible. However, even under these conditions it is best to verify that in measurements over a wide range of concentrations φ_0 remains constant. This information can be obtained by using the Bell effect, that is, by subjecting the gas to periodic radiation of a plate which absorbs nonselectively (the optical-acoustic effect is not selective in this case). If such a plate is placed in an optical-acoustic cell filled with the gas mixture under study, the sound radiation in the cell will arise from the effect in the plate and the effect in the gas. In the first case the sound intensity in the cell will be greatest in the spectral region where the maximum radiation of the source occurs. If the absorption coefficient of the plate is low and the absorption bands are intense and occur at a spectral region far from the maximum of the radiation

source, we can neglect the superimposition of the Bell effect on the acoustic effect of the gas under study in the region of its absorption band.

If we assume that the phase shift corresponding to the Bell effect changes with concentration according to a law close to that which determines the change in the temporal instrumental shift, then we can supplement the usual measurements made at wavelengths corresponding to the absorption bands of the gas under study by measurements of the phase shift in the region of the maximum of the source radiation (around 1.4μ for example); this enables us to obtain a reference point by which we can judge the degree to which the instrumental phase shift changes in going from higher concentrations to lower.

Figure 5 shows the results of these measurements on mixtures of carbon dioxide with nitrogen at a frequency of 1100 cps. The graph in Fig. 5a represents the variation of micrometer reading with carbon dioxide concentration for two cases: curve 1 for the wavelength region corresponding to the 4.3μ absorption band, and curve 2 for the region around 1.4μ. Figure 5a shows that at low concentrations the phase shift in the 4.3μ band is greater than that in the 1.4μ region, and at high concentrations it is less. The phase shift in the 1.4μ region does not change with change in concentration and φ_0 remains constant. Figure 5b shows values of $\tau_{4.3\mu}$ calculated from the data of the graph of Fig. 5a by the equation $\tau_{4.3\mu} = (1/\omega)$ arctan kωl. The value of l is measured off from the ordinate l = 68 mm, that is, it is assumed that for 100% CO_2 the time $\tau_{4.3\mu}$ is almost zero. In this way, a measurement of the phase shift of the signal arising from the Bell effect can also be used to find the absolute values of τ.

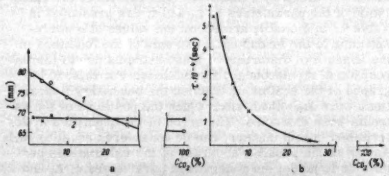

Fig. 5. Eliminating the temporal instrumental phase shift by using the Bell effect (modulation frequency 1100 cps). a—variation of micrometer reading with CO_2 concentration in the mixture with N_2 (curve 1—4.3μ CO_2 band; curve 2—spectral region around 1.4μ); b—variation of $\tau_{4.3\mu}$ with CO_2 concentration in in the mixture with N_2.

(C) ELIMINATING φ_0 BY MODULATING THE RADIATION AT TWO FREQUENCIES[3]

This method is based on measuring the difference in the phase shifts corresponding to any two absorption bands at two different frequencies of chopping the radiation. The phase shift difference $\Delta\psi = \varphi_{\lambda_1} - \varphi_{\lambda_2}$ measured for two absorption bands λ_1 and λ_2 at arbitrary modulation frequency can be used to eliminate φ_0 at this frequency. If we repeat the measurement of the difference at a frequency different from the preceding one, we obtain a new value $\Delta\psi' = \varphi'_{\lambda_1} - \varphi'_{\lambda_2}$, in which the instrumental phase shift φ_0 is eliminated again. Knowing the ratio of the modulation frequencies and measuring the values $\Delta\psi$ and $\Delta\psi'$, we can determine τ_{λ_1} and τ_{λ_2} for each concentration under investigation. The accuracy of the method is reduced if τ_{λ_1} and τ_{λ_2} are close in value or if their values are small by comparison with the modulation period, which may not be greatly reduced since the receiver sensitivity falls with increasing frequency. The two frequency method was used to determine $\tau_{4.3\mu}$ and $\tau_{2.7\mu}$ in mixtures of carbon dioxide with nitrogen in the concentration range 0.5 to 10% CO_2 (see reference 3).

(D) ELIMINATING φ_0 BY USING THE NEGATIVE OPTICAL-ACOUSTIC EFFECT[4]

In addition to the methods presented above, we may mention another way of determining the temporal instrumental phase shift, based on observing the optical-acoustic effect under the action of long wavelength infrared radiation, corresponding to rotational absorption lines, using, for example, the negative optical-acoustic effect. We can expect that the lifetime of the excited rotational states will be very small, and therefore the measured phase shifts should be equal to φ_0.

COMPARISON OF RESULTS

It is interesting to intercompare the results obtained by the methods described for the 4.3μ carbon dioxide band (Fig. 6). For convenience of comparison, we have plotted on the y-axis the reciprocal of the relaxation time, the probability $p = 1/\tau$. The figure shows that a series of values obtained by the first three methods lie on a good straight line. The slope of this line tells us that at 100% concentration the relaxation time is 1.2×10^{-5} sec. The points corresponding to data obtained by the two frequencies method lie a little above the straight line. These measurements were apparently made on moister mixtures.

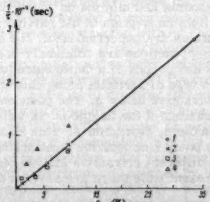

Fig. 6. Variation of the probability $p_{4.3\mu} = 1/\tau_{4.3\mu}$ with CO_2 concentration in the mixture with N_2. Method of eliminating the temporal instrumental phase shift: 1—moistening the mixture; 2—comparison with measurements at 100% concentration according to reference 1; 3—using the Bell effect; 4—using the two frequency method (according to reference 3).

Finally, we should note that when the gas has several absorption bands and the difference of the phase shifts corresponding to them can be measured accurately enough, the two frequency method is the best. The other two methods, which can also be applied when the gas under investigation has only one absorption band, are evidently less accurate: in the method based on moistening the mixture doubts arise as to whether the relaxation time in the presence of water vapor is actually less than the measurement error, and using the Bell effect doubts arise as to whether the phase shift corresponding to it changes with concentration according to the same law as φ_0. However, the agreement between the results obtained

with the different methods shows that the assumptions on which they are based are valid and that each of them can be used for finding the absolute values of the relaxation time.

REFERENCES

1. P. V. Slobodskaya and E. S. Gasilevich. Opt. i Spektr. 7, 97 (1959), Optics and Spectroscopy 7, 58 (1959).
2. P. V. Slobodskaya. Izvest. Akad. Nauk SSSR, Ser. Fiz. 12, 656 (1948);
P. V. Slobodskaya and B. I. Stepanov. Trudy Gosudarst. Opt. Inst., Leningrad 23, No. 133 (1951).
3. P. V. Slobodskaya. Doklady Akad. Nauk SSSR 120, 1238 (1958).
4. M. L. Veingerov, Ya. I. Gerlovin, and N. A. Pankratov. Opt. i Spektr. 1, 1023 (1956);
B. I. Stepanov and A. S. Rubanov. Inzh-Fiz. Zhur. 2, 52 (1959).

A COMPARISON OF LIGHT SCATTERING FUNCTIONS OF SPHERICAL PARTICLES

Yu. V. Mal'tsev

Received 16 March 1959

The accuracy and limits of application of different generalized parameters are examined for that graphical representation of the scattering function in which the positions of the respective fundamental extrema of the different functions coincide. A new generalized parameter is proposed, the application of which for the calculation of the positions of the extrema in the normal construction of the functions does not require any information about its functions. The scattering functions, depending on the new parameter, have a form convenient for comparison.

The light flux scattered by a spherical particle is characterized by the ratio of the light flux scattered by the particle in all directions to the flux incident on its cross section in the form of a parallel beam. The dependence of this ratio on the parameter α, equal to the length of the particle circumference divided by the wavelength of the scattered light, is called the light scattering function of the spherical particle. The scattering functions are calculated by theoretical formulas and have fundamental maxima and minima on which, in the absence of significant light absorption of the particle, weak secondary fluctuations are superimposed. The calculations of the scattering functions are commonly presented in the form of tables and graphs of a dependence on the parameter α for each type of particle, being characterized by the relative refractive index n. The positions of the fundamental maxima of the functions, as well as the distances between them, depend on n. This makes it difficult to use the study functions for light scattering by particles with different refractive indices, especially since at the present time there are several tens of such functions.

For a more convenient comparison of graphs of the scattering functions generalized parameters, depending on α and n, are introduced. Thus, in the book by Shifrin[1] the generalized parameter is

$$k = (n-1)\alpha. \tag{1}$$

In the work of Boll, Gumprecht, and Sliepcevich[2] another generalized parameter was used

$$L = \frac{n^2-1}{n^2+2}\alpha. \tag{2}$$

From our short communication[3] we introduce a third generalized parameter

$$k = \frac{n^2-1}{4}(\alpha-1). \tag{3}$$

We will determine these parameters for the first five fundamental extrema of the scattering functions, calculated in detail by Penndorff.[4] The results of the calculation of the parameters δ, L, and k are presented in Table 1. In the table are shown the values of α corresponding to the fundamental extrema of the functions in the absence of distortion of these extrema due to the imposition of the secondary fluctuations. For this, in the graphs of the scattering function the secondary fluctuations were smoothed, after which the positions of the extrema were extracted. The error of the quantities α, determined in this manner, can be considered equal to ± 0.1. As far as the possible accuracy of the calculations permits us to judge, the generalized parameters δ, L, and k, corresponding to the extrema of the different scattering functions, do not change systematically with increase of n; and the magnitudes of each separate parameter differ from one another within 8% limits. Accordingly, it is possible to assign average values for the five functions to the generalized parameters, corresponding to a given extremum. The average values of the generalized parameters k are equal to the ordinal numbers of the extrema to an accuracy of 4%. The corresponding magnitudes of the parameters δ and L appear as fractions. The intervals between adjacent extrema for each generalized parameter are essentially constant, since their average values for 5 maxima are $\Delta k = 1.01$, $\Delta L = 0.98$, and $\Delta\delta = 1.65$.

Table 1. The Generalized Parameters Corresponding to the First Five Extrema of the Light Scattering Function of Spherical Particles

Refractive index, n	The parameter α and generalized parameters k, L, and δ corresponding to the extrema with the following ordinal numbers																			
	1				2				3				4				5			
	α	k	L	δ	α	k	L	δ	α	k	L	δ	α	k	L	δ	α	k	L	δ
1.33	6.2	1.00	1.26	2.04	11.5	2.02	2.34	3.80	16.3	2.95	3.32	5.38	21.3	3.92	4.35	7.03	26.0	5.00	5.30	8.59
1.40	5.2	1.01	1.28	2.06	9.7	2.08	2.34	3.88	13.5	3.00	3.27	5.40	17.8	4.03	4.31	7.11	22.0	5.04	5.32	8.80
1.44	4.8	1.02	1.27	2.11	9.0	2.16	2.38	3.96	12.3	3.05	3.24	5.41	16.0	4.05	4.22	7.05	19.5	5.00	5.15	8.58
1.486	4.4	1.03	1.26	2.14	8.0	2.11	2.38	3.89	11.2	3.08	3.20	5.45	14.5	4.08	4.15	7.04	18.0	5.13	5.15	8.75
1.50	4.3	1.03	1.26	2.15	7.5	2.03	2.21	3.75	11.0	3.13	3.24	5.50	14.0	4.06	4.11	7.00	17.5	5.16	5.14	8.76
Average . . .		1.02	1.26	2.09		2.08	2.36	3.86		3.04	3.26	5.43		4.03	4.20	7.07		5.07	5.20	8.69
	Average intervals between extrema:					$\Delta k = 1.01$				$\Delta L = 0.98$				$\Delta\delta = 1.65$						

Table 2. Comparison of the Parameters α Obtained from the Graphs of the Scattering Function, with the Calculated Values $\alpha(k)$, $\alpha(L)$, and $\alpha(\delta)$ using the Generalized Parameters k, L, and δ

Refractive index, n	The parameters α, $\alpha(k)$, $\alpha(L)$, and $\alpha(\delta)$, corresponding to the extrema with the following ordinal numbers																			
	1				2				3				4				5			
	α	$\alpha(k)$	$\alpha(L)$	$\alpha(\delta)$	α	$\alpha(k)$	$\alpha(L)$	$\alpha(\delta)$	α	$\alpha(k)$	$\alpha(L)$	$\alpha(\delta)$	α	$\alpha(k)$	$\alpha(L)$	$\alpha(\delta)$	α	$\alpha(k)$	$\alpha(L)$	$\alpha(\delta)$
0.8	10	12	9	10	20	23	17	19	30	34	24	27								
0.9	20	22	14	21	40	43	27	39	55	64	37	54	70	85	48	71				
0.93	30	31	20	30	55	60	38	55	80	90	52	78								
1.29	7.0	7.0	6.9	7.2	13.0	13.0	13.0	13.3	18.6	19.0	17.9	18.7								
1.33	6.2	6.2	6.2	6.3	11.5	11.4	11.6	11.7	16.3	16.6	16.0	16.5	21.3	21.8	20.8	21.4	27.0	27.0	26.0	26.4
1.40	5.2	5.2	5.2	5.2	9.7	9.3	9.6	9.6	13.5	13.5	13.4	13.6	17.8	16.7	17.3	17.7	22.0	21.8	21.4	21.8
1.44	4.8	4.7	4.8	4.8	9.0	8.5	8.9	8.8	12.3	12.2	12.3	12.3	16.0	16.0	15.9	16.1	19.5	19.7	19.7	19.8
1.486	4.4	4.3	4.4	4.3	8.0	7.7	8.2	7.9	11.2	11.0	11.3	11.2	14.5	14.4	14.6	14.5	18.0	17.7	18.1	17.9
1.50	4.3	4.2	4.3	4.2	7.5	7.4	8.0	7.7	11.0	10.6	11.2	10.8	14.0	13.8	14.3	14.1	17.5	17.0	17.6	17.4
1.55	3.6	3.9	4.0	3.8																
2.0	2.2	2.3	2.5	2.1	3.9	3.7	4.7	3.9	(5.5)	5.0	6.5	5.5	(7.1)	6.3	8.4	7.1	(8.8)	7.7	10.8	8.7
∞	2	1	1.3	0																

The distances between extrema of the scattering functions, constructed with a dependence on the generalized parameter k, are very close to unity.

The calculated generalized parameters for the extrema of the light scattering function of particles with other refractive indices differ somewhat from the average values for n within the limits 1.33 to 1.50. However, to draw conclusions from the calculations is premature, since there are not sufficiently accurate values of α corresponding to the extrema of the function for particles with other refractive indices. In addition, calculations of this king only permit a judgment of each generalized parameter separately; the intercomparison of them is difficult.

For an estimation of the possibility of using the generalized parameters we calculate, with the aid of expressions (1)-(3) and the average values of the generalized parameters, the quantities α corresponding to the first five extrema of the function, well known from references 2, 4-7. The results of the calculation are given in Table 2. The parameters α were taken from graphs of the scattering function with smoothed secondary fluctuations; only three values of α, included in Table 2 in brackets, were taken as separate points calculated by Penndorff.[7] In the determination of the parameters α for $n < 1$, all of the formulas for the generalized parameters give negative quantities; in Table 2 the absolute values of these quantities are indicated. In the determination of α with the generalized parameter k, the average magnitudes of this parameter were taken as the numbers of the respective extrema. This insignificantly decreases the calculated values of $\alpha(k)$, but simplifies the application of formula (3). Table 2 permits us to draw the following conclusions. For particles with refractive indices from 1.29 to 1.55 no one of the generalized parameters takes preference. The values of $\alpha(\delta)$, $\alpha(L)$, and $\alpha(k)$, calculated with their aid, coincide with the parameter α completely, or differ from α by a few percent. The calculation of the positions of the extrema of the functions for particles with $n < 1$ using the parameter δ gives very good results; using the parameter k gives high results, and using L gives significantly lower results than α taken from the curves. For $n = 2.0$ the parameters δ and k give $\alpha(\delta)$ and $\alpha(k)$ coinciding with α for two extrema, and L gives high results; the coincidence of α and $\alpha(\delta)$ for the other extrema shows only that Penndorff's calculations[7] can be repeated with the aid of the parameter δ. The calculations of the position of the first maximum for a completely reflecting particle $n = \infty$ are contradictory: $\alpha(k) = 1$, $\alpha(L) = 1.3$, and $\alpha(\delta) = 0$, and α approximately equals 2. The maximum cannot be located at $\alpha = 0$, the other two calculated values differ significantly from $\alpha = 2$.

It is possible to apply the generalized parameters for light scattering functions of absorbing particles; for this it is sufficient to substitute for the refractive index n in the respective formulas the absolute magnitudes of the complex refractive index $|m| = \sqrt{n^2(1 + x^2)}$, where x is the index of absorption. The calculated positions of the first maxima and minima of the light scattering functions of absorbing particles are given in Table 3. These quantities α also correspond to maxima and minima of the scattering curve constructed without consideration of the secondary fluctuations, if such fluctuations occur. For particles with a refractive index between 1.14 and 1.42 and an index of absorption $x < 1$ the calculated positions $\alpha(\delta)$, $\alpha(L)$, and $\alpha(k)$ of the first two extrema of the scattering functions coincide with α with an error of less than 7%. For particles with a larger absorption, the generalized parameter δ is inapplicable to the calculation of the positions of the extrema. The parameters L and k give results differing from one another by less than 30%, with $\alpha(L)$ always larger than $\alpha(k)$. The accuracy of the quantity α for functions with indices of absorption $x > 1$ is insufficient to make a choice between the parameters k and L.

As has been seen, the generalized parameters can be applied to a graphical representation of the scattering functions. Then the corresponding maxima and minima of the functions, constructed with a dependence on a generalized parameter, lie one over the other for particles with different refractive indexes. An example of the use

Table 3. Position of the Maximum and Minimum of the Scattering Function of Absorbing Spherical Particles

Refractive index	Index of absorption	The parameters α, $\alpha(k)$, $\alpha(L)$, and $\alpha(\delta)$ corresponding to the first maximum and minimum								Refractive index	Index of absorption	The parameters α, $\alpha(k)$, $\alpha(L)$, and $\alpha(\delta)$ corresponding to the first maximum and minimum							
		Maximum				Minimum						Maximum				Minimum			
n	x	α	$\alpha(k)$	$\alpha(L)$	$\alpha(\delta)$	α	$\alpha(k)$	$\alpha(L)$	$\alpha(\delta)$	n	x	α	$\alpha(k)$	$\alpha(L)$	$\alpha(\delta)$	α	$\alpha(k)$	$\alpha(L)$	$\alpha(\delta)$
1.14	0.10	13.4	13.7	13.3	14.4					1.29	1.73	0.8	1.7	1.9	1.3				
1.17	0.18	10.8	10.6	10.4	11.0					1.29	2.00	1.2	1.5	1.8	1.1				
1.22	0.05	8.9	9.2	9.0	9.5					1.29	2.25	1.2	1.5	1.7	1.0				
1.28	0.04	7.2	7.2	7.2	7.5	14.0	13.5	13.4	13.8	1.29	4.00	1.2	1.2	1.4	0.5				
1.28	0.23	5.5	6.5	6.4	6.7					1.29	100	1.2	1.0	1.3	0				
1.29	0.05	6.6	7.0	6.9	7.2	13.0	13.0	13.0	13.0	1.29	∞	1.5	1.0	1.3	0				
1.29	0.10	6.8	6.8	6.8	7.0					1.33	0.01	6.2	6.2	6.2	6.3	11.5	11.5	11.6	11.7
1.29	0.25	6.6	6.2	6.2	6.3					1.33	0.03	6.1	6.2	6.2	6.3	11.8	11.4	11.6	11.7
1.29	0.50	4.0	4.7	4.8	4.7					1.33	0.30	5.0	5.3	5.3	5.3				
1.29	1.00	1.5	2.7	2.9	2.5					1.42	0.01	4.9	4.9	5.0	5.0	9.3	8.8	9.3	9.2

of the parameter δ is given in Kondrat'ev's book[9] in Fig. 36, in which are shown graphs of the scattering functions for n equal to 1.00, 1.33, and 1.50. In reference 2 the parameter L was applied to a comparison of the scattering functions with n equal to 0.8, 0.9, and 0.93. And there, in another figure, is given the form of the function for $n > 1$, $n = \infty$, and $n < 1$. As an example, we give the construction of the scattering functions with dependence on k in Figs. 1 and 2 (in Fig. 2 the function for x = 0 was constructed from the data of Houghton and Chalker[8] without the secondary fluctuations). In the scattering function constructed with dependence on a generalized parameter, the respective fundamental maxima and minima satisfactorily lie opposite whole values of k, and the interval

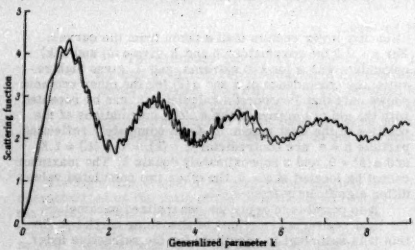

Fig. 1. Light scattering function of transparent particles with different refractive indices. Dotted curve—n = 1.40; solid curve—n = 1.50.

between adjacent fundamental extrema is approximately constant and equal to $\Delta k = 1$. A deficiency of the graphical functions using the parameter k is the presence of a negative branch of the curve, corresponding to the interval $0 \leq \alpha < 1$. However, it is not possible to consider this a substantial deficiency: in this part of the scattering function there are no characteristic features requiring comparison. In addition, in the portion of low α's the scattering functions are calculated without difficulty by simplified formulas; therefore, a study of the scattering functions in the portion $0 \leq \alpha < 1$ with the help of some generalized parameters is completely superfluous.

The construction of scattering functions with the aid of generalized parameters is convenient for a comparative study of the features of these functions. The coincidence of the positions of the fundamental extrema creates the conditions for a comparison of the magnitudes of the fundamental maxima and minima. For transparent particles, the magnitudes of the first maxima increase with an increase of the refractive index from n = 0.8 to n = 2.0.

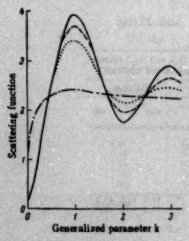

Fig. 2. Light scattering function of absorbing particles with n = 1.33 and different indices of absorption. Solid curve—x = 0; dotted curve—x = 0.03; dashed curve—x = 0.01; dashed dotted curve—x = 0.30.

The magnitudes of the other fundamental extrema of the light scattering function by particles with n in the range 1.33-1.50 differ from one another by an insignificant amount.

For the light scattering function of absorbing particles there develops with an increase of the index of absorption x a damping of the fundamental vibrations, as a result of which the curve becomes one with a single maximum. From the calculations given in reference 5 for the function with n = 1.29, on further increase of x from 0.5 to 2.25 the maximum of the curve grows approximately to the magnitude of the first maximum of the curve in the absence of absorption and then begins to fall again. For x = 100 the curve approximately coincides with the curve of a completely reflecting particle, $n = \infty$.

The coincidence of the fundamental maxima is convenient for the study of the secondary fluctuations. The secondary fluctuations of the light scattering functions of transparent particles, calculated by Penndorff, are similar for the different functions in the portion from the beginning of the curves to the first minimum, as for example in Fig. 1.

CONCLUSIONS

With the help of the generalized parameters δ, L, and k it is possible to calculate the parameters α, corresponding to the fundamental extrema of the light scattering functions of spherical particles. In the application of the parameter k it is sufficient to consider that it is equal to the ordinal number of the corresponding extremum. In the use of the generalized parameters δ and L, it is necessary to know the parameters α for the extrema of at least one scattering function. The error of the calculation of α with generalized parameters does not exceed 7% for particles with indices of absorption x from 0 to 0.5 and refractive indices n from 0.8-1.5 with the calculation using the parameter δ, and from 1.14 to 1.50 using the parameters L and k.

For such particles it is possible to present graphically the dependence of the scattering functions on the generalized parameters. Then the extrema of the different functions fall one under the other, and the distance between adjacent extrema is constant. In the functions constructed with a dependence on the generalized parameter k, the extrema satisfactorily lie opposite whole numbers with the interval between adjacent extrema equal to unity.

The use of generalized parameters is convenient not only for a comparative study of the features of the scattering functions, but can also be useful for approximate calculations of light scattering by different spherical particles.

REFERENCES

1. K. S. Shifrin. "Rasseyanie sveta v mutnoi srede." (Light Scattering in a Turbid Medium) Izd. Tekh-Teoret., 1951.
2. R. H. Boll, R. O. Gumprecht, and C. M. Sliepcevich. J. Opt. Soc. Am. 44, 18 (1954).
3. Yu. V. Mal'tsev. Opt. i Spektr. 7, 124 (1959), Optics and Spectroscopy 7, 76 (1959).
4. R. B. Penndorff. J. Opt. Soc. Am. 47, 1010 (1957).
5. J. C. Johnson and J. R. Terrell. J. Opt. Soc. Am. 45, 451 (1955).
6. D. Sinclair. J. Opt. Soc. Am. 37, 475 (1947).
7. R. B. Penndorff. J. Opt. Soc. Am. 46, 1001 (1956).
8. H. C. Houghton and W. R. Chalker. J. Opt. Soc. Am. 39, 995 (1949).
9. K. Ya. Kondrat'ev. "Luchistaya Energiya Solntsa." (Radiant Energy of the Sun) Gidrometeoizdat, 1954.

STUDY OF ABERRATIONS OF A CONCAVE GRATING UNDER DEFOCUSING CONDITIONS

A. I. Kozlenkov

Received 3 August 1959

A theoretical study of the aberrations of a concave diffraction grating and their relations to its ultimate resolving power is undertaken. We study the geometrical form of the focus near the Rowland circle, establish the dependence of particular focus characteristics on adjustment errors, obtain expressions for the aberrations in the presence of such errors, and give simple methods of evaluating the resolving power.

The theoretical limit for the resolving power of a concave diffraction grating is determined by aberrations. The latter depend not only on the size of the illuminated surface of the grating, but also on the precision of the alignment of grating, entrance slit, and film (or slit and counter) on Rowland's circle. In view of this it appears necessary to calculate the magnitude of the aberrations taking account of possible adjustment errors and, having found the aberration for a given case, to determine the resolving power.

Existing theory of resolving power was worked out for cases of ideal adjustment, by which in what follows we shall understand the following: (1) the entrance slit, the center of the grating, and the slit of the counter are accurately positioned on the Rowland circle; (2) a tangent drawn through the center of the grating coincides with the tangent to the "instrumental circle," i.e., the circle on which the slit and center of the grating are located.

For this ideal case, Mack, Stehn, and Edlen[1] found the distribution of intensity on the Rowland circle. Their method was based on graphical evaluation of the diffraction integrals in the complex plane. However, when errors in the positioning of slit and grating are taken into account the integrals become more complicated and their form depends on the particular errors under consideration.

A simpler method of evaluating the resolving power involves calculating aberrations in the focus using the approximation of geometric optics. Beutler,[2] starting from the characteristic Hamiltonian function[3] and Fermat's principle, constructed a geometrical theory of representation and obtained, in particular, expressions for the optimum width of the grating $W_{opt.}$, practically coinciding with the formula obtained previously in reference 1. In the work of Namioka[4] a series of errors introduced by Beutler was corrected and a detailed analysis of the so-called Eagle mounting was carried out. However, Beutler and Namioka both limit their analysis to aberration on Rowland's circle. This does not permit them to determine the correct value for $W_{opt.}$, since Rowland's circle is not the optimum location of the focus for minimizing aberration, and also does not permit the establishment of the dependence of resolving power on the adjustment error, since the aberration and resolution are found only for the ideal case.

Bowen,[5] for the first time, established that aberration in the focal region can be partially compensated if the entrance slit and the film (or counter slit) are displaced from the Rowland circle by specific distances calculated by him. When the special conditions are fulfilled the resolution is increased by $\sqrt{2}$ times compared with the value on Rowland's circle.

The purpose of the present work is to use Beutler's method as a basis for studying the geometrical form of the focus near Rowland's circle, to establish the dependence of certain characteristics of the focus on the adjustment error, to obtain expressions for aberration in the presence of these errors, and to give a simple method of evaluating the resolving power. The formulas obtained in this paper may be used to establish accuracy requirements for one or another adjustment of devices having a diffraction grating as analyzer and to determine whether they attain the accuracy of resolution needed in a given experiment.

As will be shown, all errors occurring in practice lead, in the final analysis, to displacement of the entrance slit towards the center of the grating and to displacement of the film (or counter slit) along the central diffraction ray. Therefore, in what follows, we limit ourselves to the examination of only these two aspects of the error. Moreover, we shall study the focal region only in the plane of Rowland's circle, presuming that the vertical length Z of the entrance slit is so small that it does not influence the magnitude of the aberration in the plane of Rowland's circle.

1. Let us start with the derivation of the caustic equation. In Fig. 1 we show the relative positions of the entrance slit S, assumed to be a point source of monochromatic light, the grating W, and the instrument circle, on which are disposed the entrance slit, the center of the grating, and the film (or slit in front of a counter or photomultiplier adjustable along this circle). The instrument circle coincides with the Rowland circle only if the grating is tangent to the instrument circle at its center. In the approximation of geometrical optics those rays which are diffracted by a small element $\Delta\omega$ of the grating, distant from the center by ω, are focused at B, located on the central ray, at a distance $\Delta r'$ from the point of intersection of the central ray and Rowland's circle. In general $\Delta r'$ is a function of both the coordinate ω and the displacement of the entrance slit along the ray incident upon the center of the grating, that is, Δr. The dependence on ω indicates that the grating possesses aberration which for $\Delta r \neq 0$ is asymmetrical with respect to the central ray.

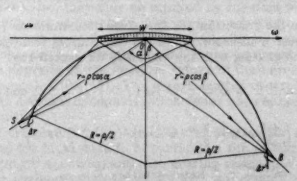

Fig. 1

As an initial expression for the caustic equation, with $\Delta r \neq 0$, the formula derived by Bowen[5] relating the quantities $\Delta r'$, ω, and Δr may be used:

$$\Delta r' = A\frac{\omega^2}{\rho^2} + B_0\Delta r\cdot\frac{\omega}{\rho} + C, \qquad (1)$$

where

$$A = \frac{r}{2}(\sin\alpha\cdot\tan\alpha + \sin\beta\cdot\tan\beta);$$

$$B_0 = -\frac{3}{2}(\tan\alpha - \tan\beta),\ (\beta < 0)$$

and

$$C = -\Delta r + \frac{(\Delta r)^2}{\rho}\left(\frac{1}{\cos\alpha} + \frac{1}{\cos\beta}\right) \approx -\Delta r.$$

The notation is clear from Fig. 1 (Δr and $\Delta r'$ are taken as positive for displacements outside of Rowland's circle).

Bowen's formula may be obtained by Beutler's method. We give the derivation here, since a series of intermediate expressions in it will be utilized later in the calculation of optimum grating size. The characteristic Hamiltonian function has the form

$$F = AP + PB + \frac{m\omega\lambda}{\sigma},$$

where P(ω) is an arbitrary point of the grating and σ is the distance between adjacent grating lines. Point B is the focus of rays diffracted from a small part of the grating $\Delta\omega$ with coordinate ω, if $\partial F/\partial\omega = 0$ at the point ω. The equation for F becomes explicitly

$$\begin{aligned} F = {} & r - \omega\sin\alpha + r' - \omega\sin\beta + \frac{m\omega\lambda}{\sigma} + \frac{\omega^2}{2}\left(\frac{\cos^2\alpha}{r} - \frac{\cos\alpha}{\rho}\right) \\ & + \frac{\omega^3}{2r}\sin\alpha\left(\frac{\cos^2\alpha}{r} - \frac{\cos\alpha}{\rho}\right) + \frac{\omega^4}{2}\frac{\sin^2\alpha}{r^2}\left(\frac{\cos^2\alpha}{r} - \frac{\cos\alpha}{\rho}\right) \\ & + \frac{\omega^2}{2}\left(\frac{\cos^2\beta}{r'} - \frac{\cos\beta}{\rho}\right) + \frac{\omega^3}{2r'}\sin\beta\left(\frac{\cos^2\beta}{r'} - \frac{\cos\beta}{\rho}\right) \\ & + \frac{\omega^4}{2r^2}\sin^2\beta\left(\frac{\cos^2\beta}{r'} - \frac{\cos\beta}{\rho}\right) + \frac{\omega^4}{8\rho^2}\left(\frac{1}{r} - \frac{\cos\alpha}{\rho}\right) \\ & + \frac{\omega^4}{8\rho^2}\left(\frac{1}{r'} - \frac{\cos\beta}{\rho}\right) + 0\left(\frac{\omega^4}{\rho^2}\Delta r,\ \frac{\omega^4}{\rho^2}\Delta r'\right). \end{aligned} \qquad (2)$$

Here r and r' are distances along the centrally incident and diffracted rays. On Rowland's circle $r = \rho\cos\alpha$ and $r' = \rho\cos\beta$. In the general case, $r = \rho\cos\alpha + \Delta r$ and $r' = \rho\cos\beta + \Delta r'$, where the errors in the slit and film positions are small, i.e., $\Delta r \ll r$ and $\Delta r' \ll r'$.

Let us express F in terms of Δr and $\Delta r'$ and find the derivative $\partial F/\partial\omega$. Considering that $\sin\alpha + \sin\beta = m\lambda/\sigma$, we get

$$\frac{\partial F}{\partial\omega} = -(\Delta r + \Delta r')\frac{\omega}{\rho^2} - (\Delta r\cdot\tan\alpha + \Delta r'\tan\beta)\frac{3}{2}\frac{\omega^2}{\rho^2} + \frac{A\omega^3}{\rho^4}, \qquad (3)$$

where A is the same as in formula (1). In formula (3) we neglect $(\Delta r)^2/\rho\cos\alpha$ and $(\Delta r')^2/\rho\cos\beta$ compared with Δr and $\Delta r'$.

From the condition $\partial F/\partial\omega = 0$ we determine $\Delta r'$, that is, the point of intersection of the ray coming from point P(ω) of the grating with the centrally diffracted ray.

$$\begin{aligned} \Delta r' &= \left[\frac{A\omega^2}{\rho^2} - \Delta r - \frac{3}{2}\Delta r\tan\alpha\cdot\frac{\omega}{\rho}\right]:\left(1 + \frac{3}{2}\frac{\omega}{\rho}\tan\beta\right) \\ &\approx \left(\frac{A\omega^2}{\rho^2} - \Delta r - \frac{3}{2}\frac{\omega}{\rho}\Delta r\tan\alpha\right)\cdot\left(1 - \frac{3}{2}\frac{\omega}{\rho}\tan\beta\right) \\ &\approx \frac{A\omega^2}{\rho^2} - \frac{3}{2}(\tan\alpha - \tan\beta)\Delta r\cdot\frac{\omega}{\rho} - \Delta r, \end{aligned}$$

which coincides with the result given in reference 1.

In this expression we have omitted terms containing $(\omega/\rho)^3$ and $(\omega/\rho)^2\Delta r$, since $\omega \leq \frac{1}{2}W_{opt.}$ ($W_{opt.} \approx 20$–40 mm) and the ratio ω/ρ for ordinarily used gratings of radius 1 or 2 meters does not exceed 0.02–0.01.

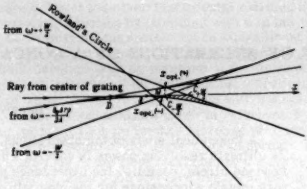

Fig 2.

To derive the caustic equation for the case $\Delta r \neq 0$ and $\Delta r' \neq 0$, we also take into account the fact that the angle at which the ray diffracted at point ω of the grating intersects the central one is $\varphi \approx \omega/\rho$.

In Fig. 2 we show the focal region in the case $\Delta r \neq 0$. Rays from the center of the grating $\omega = 0$ are focused at the point $\Delta r' \approx -\Delta r$. We take this point as the origin of coordinates, with the x-axis to the right along the central ray of the grating, and the y-axis in the plane of Rowland's circle, with $y > 0$ in the half-plane where $\omega > 0$. Thus we obtain the equation for the family of rays in the form

$$y = y'\left(x - A\frac{\omega^2}{\rho^2} - B_0\Delta r\cdot\frac{\omega}{\rho}\right) \qquad (4)$$

or, since $y' = -\omega/\rho$,

$$y = xy' - Ay'^2 + B_0\Delta r\cdot y'^2. \qquad (4a)$$

The equation of the caustic envelope is defined by the solution of the system

$$\left.\begin{aligned} y &= xp - Ap^2 - B_0\Delta r p^2, \\ x &- 3Ap - 2B_0\Delta r p = 0 \end{aligned}\right\} \qquad (5)$$

and has the form

$$\begin{aligned} y = {} & x\left[\frac{B}{3A} \pm \left(\frac{B^2}{9A^2} + \frac{x}{3A}\right)^{\frac{1}{2}}\right] - A\left[\frac{B}{3A} \pm \left(\frac{B^2}{9A^2} + \frac{x}{3A}\right)^{\frac{1}{2}}\right]^2 \\ & + B\left[\frac{B}{3A} \pm \left(\frac{B^2}{9A^2} + \frac{x}{3A}\right)^{\frac{1}{2}}\right]^2. \end{aligned} \qquad (6)$$

Here $B = B_0\Delta r$, and the sign (+) refers to the negative half-plane.

$$-\frac{W}{2\rho} < \left[\frac{B}{3A} \pm \left(\frac{B^2}{9A^2} + \frac{x}{3A}\right)^{\frac{1}{2}}\right] < +\frac{W}{2\rho}.$$

In the particular case $\Delta r = 0$ the caustic equation has the form

$$y = \pm\frac{2}{3}\left(\frac{1}{3A}\right)^{\frac{1}{2}}x^{\frac{3}{2}}. \qquad (7)$$

From Eq. (6), and also the equations of the extremal rays of the grating (4a), where in place of y' we substitute $y' = -(1/\rho) \pm (W/2)$, the form of the focus was investigated and some focal characteristics were determined.

The ray trajectories at the focus are shown in Fig. 2. As seen from the figure, Rowland's circle intersects the centrally diffracted ray at point M. At point B rays from the center of the grating ($\omega = 0$) are focused. At points C$_{+W/2}$ and C$_{-W/2}$ are found the foci of the extremal rays. Nearest to the grating (at point D) rays from the portion of the grating with the coordinate $\omega = -B_0\Delta r\rho/2A$ are focused. In Fig. 2 are also shown the caustic envelopes of both half-planes. The narrowest focal region does

not occur on Rowland's circle. There are two optimal points, denoted $x_{opt.}(+)$ and $x_{opt.}(-)$, which coincide only in the case $\Delta r = 0$.

We next give formulas defining the locations of the characteristic points and the focal width at these points. Rays from the central section of the grating are focused at the point

$$\Delta r'_{\omega=0} = -\Delta r. \tag{8}$$

The distances of the optimum points from Rowland's circle are

$$s_{opt.}(\pm) = \frac{3}{16} A \frac{W^2}{\rho^2} \pm B_0 \Delta r \frac{W}{4A} - \Delta r. \tag{9}$$

The narrowest portion of the focus lies between points $x_{opt.}(+)$ and $x_{opt.}(-)$, where the interval $\Delta x_{opt.}$ is equal to

$$x_{opt.}(+) - x_{opt.}(-) = \frac{B_0 \Delta r W}{2\rho}. \tag{10}$$

Extremal rays from the grating are focused at distances

$$C_{\pm\frac{W}{2}} = \frac{AW^2}{4\rho^2} \pm \frac{B_0 \Delta r W}{2\rho} \tag{11}$$

from Rowland's circle.

The cross section width of the focus in the optimum region is given by

$$S_{opt.} = \frac{AW}{4\rho}\left(\frac{W^2}{4\rho^2} + \frac{B_0^2(\Delta r)^2}{A^2}\right). \tag{12}$$

The width on Rowland's circle in the event that both optimum points lie beyond it, is equal to

$$S_{Rowl.} = \frac{AW^3}{4\rho^3} - \Delta r \frac{W}{\rho}. \tag{13}$$

Comparing (12) and (13) we see that for $\Delta r \leq 0$ the width on Rowland's circle is larger than at the optimum points.

To find the widths along the focal circle, $S_{opt.}$ and $S_{Rowl.}$, defined by formulas (12) and (13), they must be multiplied by $1/\cos\beta_0$.

The depth of focus, i.e., the distance between the focal point nearest to the center of the grating and that furthest removed from it, is given by

$$\Delta f = \frac{A}{4}\left(\frac{W}{\rho} - \frac{B_0 \Delta r}{A}\right)^2. \tag{14}$$

for

$$\frac{W}{2} > -\frac{B_0 \Delta r \rho}{2A}$$

and

$$\Delta f = -\frac{B_0 \Delta r W}{\rho}$$

for

$$\frac{W}{2} < -\frac{B_0 \Delta r \rho}{2A}. \tag{15}$$

In particular, for $\Delta r = 0$

$$\Delta f = \frac{AW^2}{4\rho^2}.$$

For $\Delta r = 0$, instead of (9), (11), (12), and (13) we have

$$s_{opt.} = \frac{3}{16} A \frac{W^2}{\rho^2}, \tag{9a}$$

$$C_{\frac{W}{2}} = \frac{AW^2}{4\rho^2}, \tag{11a}$$

$$S_{opt.} = \frac{AW^3}{16\rho^3},$$

$$S_{Rowl.} = \frac{AW^3}{4\rho^3}.$$

These last formulas coincide with the corresponding equations derived in reference 5.

We shall make a series of comments relative to the shape of the focus and its dependence on the value of the error Δr.

a. For the nondisplaced source ($\Delta r = 0$) the narrowest region of focus lies beyond Rowland's circle. The magnitude of the aberration in this region is less than on the Rowland circle, and the optimum size of the grating $W_{opt.}$, i.e., the size corresponding to a limit of maximum wave aberration of magnitude $\lambda/4$, is larger than the optimum size calculated for the Rowland circle. Therefore, if the film is located in the indicated optimum region a gain in resolution can be obtained in comparison to Rowland's circle, if, correspondingly, the grating is enlarged to the new value $W_{opt.}$.

b. If $\Delta r > 0$, the optimum focal region is displaced towards Rowland's circle and at some value of Δr falls on the circle. However, in this case, as seen in Fig. 2, the focal region is asymmetrical relative to the central ray (i.e., x-axis). The asymmetry occurs as a consequence of the presence in Bowen's formula of a term containing an odd power of ω/ρ. This complicates the conditions for compensating the aberration. Bowen showed that by special choice of the displacements Δr and $\Delta r'$ the coefficient of the odd term in the expression for wave aberration can be reduced to zero and at the same time the aberration on Rowland's circle can be partially compensated. Constructionally this method is more complex, and the increase in resolution compared with the ideal case is just the same as can be obtained by displacement of the film beyond Rowland's circle for $\Delta r = 0$ (this will be shown below).

For a still greater increase of Δr the optimum region is displaced inside Rowland's circle and the resolution on the circle diminishes. For $\Delta r < 0$ the focal width on the circle increases. Thus, the shift of the entrance slit inside Rowland's circle degrades the resolution.

We have studied here only the error due to a shift Δr of the entrance slit along the ray incident upon the center of the grating. This is explained by the fact that practically all mistakes of adjustment occurring in practice lead to this type of error. Let us suppose that we have only an angular mistake $\Delta\alpha$ (with r = const.). In the preceding results this will manifest itself in two ways: first, the angles $\alpha + \Delta\alpha$ and $\beta + \Delta\beta$ will now be substituted into the expressions for the angular functions A and B_0; secondly, the source is now displaced from the circle by $\Delta r_{eff.}$, dependent on $\Delta\alpha$. Functions A and B_0 change slowly with the angles, so that even for relatively large mistakes, $\Delta\alpha$, they may be counted as constant for the spectral line under study, and we may substitute into the formula values of A and B_0 corresponding to $\Delta\alpha = 0$. It is necessary to determine only the displacement $\Delta r_{eff.}$, which depends on the specific nature of the error, and use formulas (8)-(15). The determination of $\Delta r_{eff.}$ from simple geometric considerations does not represent a difficulty.

Formulas (8), (9), and (11) may be used for determining the focal points. In particular, for an ultrashort wavelength spectrograph with grating radius $\rho = 2000$ mm, for an angle of incidence of $\alpha = 85°$, wavelength $\lambda = 100$ A, and grating size optimum for 100 A ($W_{opt.} = 20$ mm), we get A = 18,400. If $\Delta r = 0$ the best focusing takes place 0.4-0.5 mm, measured along r', beyond the Rowland cir-

cle. For wavelengths of 60, 100, and 200 A the distances are equal to 0.49, 0.46, and 0.40 mm, respectively. Consequently, for all regions from 60 to 400 A one may either record all spectra at a mean distance of 0.45 mm beyond Rowland's circle, or carry out a more exact adjustment for each wavelength zone.

If in the spectrograph a radiation counter or photomultiplier is used as a receiver, the slit in front of it will have to be displaced not along the Rowland circle of radius R, but along a circle of radius R + ΔR. Since ΔR amounts to 50–100 μ, for an equivalent displacement along r′ from Rowland's circle of 0.4–0.5 mm, the carriage bearing the receiver slit must be provided with an adjustment device allowing smooth displacement of the slit along the ray (along r′). This control is most important for achieving the maximum resolving power of the apparatus.

2. Now we examine how the correct formulas for resolving power can be obtained on the basis of geometrical optics. Geometrical optics does not yield expressions for the distribution of intensity in the focal region, so that the focal width determined by Eqs. (12) or (13) is not directly a measure of resolution. Exact calculation of resolving power is possible only on the basis of physical optics[3], i.e., through computation of the diffraction integrals. However, the optimum grating width and the optimum resolving power may be found from the condition that the wave aberration defined by the integral

$$\int_A^B \frac{\partial F}{\partial \omega}\, d\omega,$$

is limited to λ/4, corresponding to the Rayleigh criterion. The limits of integration correspond to the center and end points of the wave front.

When Δr = 0, the optimum grating width for points on Rowland's circle is found from the condition

$$\int_0^{\frac{W}{2}} \frac{\partial F}{\partial \omega}\, d\omega = \frac{\lambda}{4}.$$

in which the quantity ∂F/∂ω is defined by Eq. (3), with Δr = Δr′ = 0. The center of the wave front corresponds to rays coming from the center of the grating (ω = 0). For Δr = 0 the aberration is symmetrical relative to the central ray, so that

$$\int_0^{-\frac{W}{2}} \frac{\partial F}{\partial \omega}\, d\omega$$

satisfies Rayleigh's criterion, if only

$$\int_0^{+\frac{W}{2}} \frac{\partial F}{\partial \omega}\, d\omega = \frac{\lambda}{4}.$$

Calculating the integral leads to the following equation:

$$W = W_{\text{opt.(Rowl.)}} = 2\rho\left(\frac{\lambda}{A}\right)^{\frac{1}{4}}, \qquad (16)$$

obtained by Beutler[2] and practically coincident with the formula of Mack, Stehn, and Edlen.[4]

Let us now find the wave aberration and $W_{opt.}$ for point C of the focal region, distant from B by Δr′, studying as before the special case Δr = 0. Point C is the focus of the rays diffracted by an element Δω of the grating surface, a distance ω_1 from its center, where $\omega_1 = \rho(\Delta r'/A)^{1/2}$, according to (1). We first calculate the integral

$$I_1 = \int_0^{\omega_1} \left.\frac{\partial F}{\partial \omega}\right|_{r'} d\omega.$$

Substituting the quantity ∂F/∂ω from formula (3), we get

$$I_1 = -\frac{\omega_1^2}{2\rho^2}\Delta r' - \Delta r' \frac{\tan\beta \cdot \omega_1^3}{2\rho^3} + \frac{A\omega_1^4}{4\rho^4}.$$

The first two terms depend on Δr′, and the second is ω tan β/ρ times smaller than the first. The ratio ω/ρ is usually smaller than 0.01, and the value of tan β even for grazing angles does not exceed 10.

For example, at α = 85° in the ultrashort wavelength spectrograph SP-24[6] the registering wavelength region lies between 40 and 500 A. For λ = 40 A the angle β ≈ 82.5° and tan β ≈ 7.6. Therefore (ω/ρ) tan β < 0.1, where for smaller angles the inequality is stronger. On the basis of these estimates, in what follows we shall neglect the second term in comparison to the first. In that case

$$I_1 = -\frac{\omega_1^2 \Delta r'}{2\rho^2} + \frac{A\omega_1^4}{4\rho^4}$$

or, since

$$\omega_1 = \rho\left(\frac{\Delta r'}{A}\right)^{\frac{1}{2}}, \qquad I_1 = -\frac{(\Delta r')^2}{4A}. \qquad (17)$$

Calculation of the integral

$$I_2 = \int_{\omega_1}^{\frac{W}{2}} \frac{\partial F}{\partial \omega}\, d\omega$$

in the same approximation gives

$$I_2 = \frac{1}{4A}\left[\frac{AW^2}{4\rho^2} - \Delta r'\right]^2.$$

In the integrals I_1 and I_2 corresponding to the above-given approximation only even powers of ω/ρ appear. Consequently the aberration is symmetrical in ω, and it is sufficient to consider I_1 and I_2 for one half-plane (e.g., for ω > 0).

From the condition $I_2 = \lambda/4$ we get

$$W_{\text{opt.}} = 2\rho\left(\frac{1}{A}\right)^{\frac{1}{2}}\left[(\lambda A)^{\frac{1}{2}} + \Delta r'\right]^{\frac{1}{2}}. \qquad (19)$$

It is clear that here I_1 must not exceed λ/4 either, according to Rayleigh's criterion. The maximum value of $W_{opt.}$ is obtained at point C, where $I_1 = (\Delta r')^2/4A = -\lambda/4$, that is, $\Delta r'_{opt.} = (\lambda A)^{1/2}$.

In this case

$$W_{\text{opt. (max)}} = 2\sqrt{2}\,\rho\left(\frac{\lambda}{A}\right)^{\frac{1}{4}}$$

instead of

$$W_{\text{opt. (Rowl.)}} = 2\rho\left(\frac{\lambda}{4}\right)^{\frac{1}{4}}$$

for Rowland's circle. Thus, at point C determined by the condition $\Delta r' = (\lambda A)^{1/2}$, with the corresponding grating opening a gain in resolution of $\sqrt{2}$ times compared with the maximum resolution on Rowland's circle may be obtained. The quantity $\Delta r'_{opt.}$ may be expressed also in terms of $W_{opt.(Rowl.)}$

$$\Delta r'_{opt.} = \frac{AW^2_{opt.(Rowl.)}}{4\rho^2}.$$

For $\Delta r' > (\lambda A)^{1/2}$ the resolution diminishes, since I_1 becomes larger than $\lambda/4$. For those points for which $\Delta r' < 0$ the resolution is also worse than on the Rowland circle.

We have thus determined the maximum possible resolution at points of the focal region. The actual resolution may be worse if the grating dimension W is not equal to the optimum $W'_{opt.}$ for a given point. If $W < W'_{opt.}$ the resolution is below optimum by a factor of $W/W'_{opt.}$, since for $W < W_{opt.}$ the resolution varies practically linearly with W, which follows, for example, from the results of reference 1. For $W > W'_{opt.}$ the resolving power is also below optimum for a given point, but its value is at least as large as the asymptotic value mentioned in reference 1.

Accurate calculation of wave aberration in the case $\Delta r \neq 0$ is considerably more complicated, because in addition to the displacement of focal points in this case, asymmetry relative to the central ray occurs. Here however we simplify the investigation by considering the term $(\Delta r \tan\alpha + \Delta r' \tan\beta)\omega^3/2\rho^3$ small by comparison with $c - (\Delta r + \Delta r')\omega^2/2\rho^2$ in the expressions under the integral sign.

In this approximation a change of source position by Δr displaces the focal region, preserving its symmetry relative to the centrally diffracted ray. In particular, the focus of rays from the center of the grating is displaced by $\Delta r' \approx -\Delta r$. The corresponding integrals are

$$I_1 = \int_0^{\omega_1} \frac{\partial F}{\partial \omega}\, d\omega = -(\Delta r + \Delta r')\frac{\omega_1^2}{2\rho^2} + \frac{A\omega_1^4}{4\rho^4} = -\frac{(\Delta r + \Delta r')^2}{4A},$$

$$I_2 = \int_{\omega_1}^{\frac{W}{2}} \frac{\partial F}{\partial \omega}\, d\omega = \frac{1}{4A}\left[\frac{AW^2}{4\rho^2} - (\Delta r + \Delta r')\right]^2.$$

From the condition $I_2 = \lambda/4$ we find

$$W_{opt.} = 2\rho\left(\frac{1}{A}\right)^{\frac{1}{2}}\left[(\lambda A)^{\frac{1}{2}} + (\Delta r + \Delta r')\right]^{\frac{1}{2}}. \qquad (21)$$

At point C, for which $I_2 = -\lambda/4$, $\Delta r' = (\lambda A)^{1/2} - \Delta r$ and

$$W_{opt.} = W_{opt.\,(max)} = 2\sqrt{2}\,\rho\left(\frac{\lambda}{A}\right)^{\frac{1}{4}}.$$

The resolution on Rowland's circle is

$$W_{opt.(Rowl.)} = 2\rho\left(\frac{1}{A}\right)^{\frac{1}{2}}\left[(\lambda A)^{\frac{1}{2}} + \Delta r\right]^{\frac{1}{2}}.$$

All the results obtained above are based on the utilization of Beutler's method. It is necessary to note that Namoika discovered in Beutler's paper a series of mistakes after critically analyzing the derivations and the results. The fundamental error shown by Namioka is the incorrect use of the characteristic Hamiltonian function. In the calculations this mistake appears in the fact that Beutler introduces an incorrect connection between the angle $\Delta\beta$ and the derivative $\partial F/\partial\omega$. Let us clarify the meaning of these quantities. For $\Delta r = 0$ the derivative is calculated at point B, the intersection of the central ray with Rowland's circle. Here

$$\left.\frac{\partial F}{\partial \omega}\right|_B \neq 0$$

at all points of the grating surface for which $\omega \neq 0$. This implies that point B is the focus of only those rays which are diffracted at the center of the grating. Rays diffracted at point ω_1 of the grating are focused at a point B', for which the angle between the directions of the beams from ω_1 to B and from ω_1 to B' is $\Delta\beta$. The actual connection between this angle and the derivative $\partial F/\partial\omega$, taken at point B, is given by the formula

$$\Delta\beta(\omega_1) = \frac{1}{\cos\beta}\left.\frac{\partial F}{\partial \omega}\right|_{\omega = \omega_1},$$

whereas Beutler mistakenly assumes

$$\Delta\beta(\omega_1) = \left.\frac{\partial F}{\partial \omega}\right|_{\omega = \omega_1}.$$

The transverse focal width on Rowland's circle (for $r' = \rho\cos\beta$) is given by

$$S = 2r'\Delta\beta = \frac{2\rho\cos\beta}{\cos\beta}\left.\frac{\partial F}{\partial \omega}\right|_{\omega = \frac{W}{2}} = 2\rho\left.\frac{\partial F}{\partial \omega}\right|_{\omega = \frac{W}{2}}.$$

It is easy to show that calculation from this formula leads to the magnitude of S which is determined by Eq. (13a). Consequently, all the above-mentioned results are based on correct use of the Hamiltonian function.

The trajectory of rays diffracted at point ω of the grating can be found by two methods: by determining the angle $\Delta\beta(\omega)$, after first finding the derivative $\partial F/\partial\omega$ on Rowland's circle (i.e.

$$\left.\frac{\partial F}{\partial \omega}\right|_B),$$

or from the condition

$$\left.\frac{\partial F}{\partial \omega}\right|_{B'} = 0,$$

under which point B' is the focus of rays from the point ω ($\Delta r'(\omega)$ is determined, i.e., the position of B' is found from the condition

$$\left.\frac{\partial F}{\partial \omega}\right|_{B', \omega} = 0$$

The second method is thus connected with Bowen's formula. It does not require the determination of $\Delta\beta(\omega)$ and is convenient for studying the influence of defocusing.

In estimating the magnitude of the aberration, we have not examined a number of other factors: the influence of the vertical length of the ruling l and the effects connected with the finite width of the entrance slit S_{1a}. In the case of a point source the grating may be regarded with good approximation as one-dimensional, i.e., the aberration may be calculated only as a function of the dimension W. This follows from the fact that the extent of a Fresnel zone in the l direction is considerably less than in the horizontal direction. It was precisely this situation which gave Namioka a basis for using the usual equation for $W_{opt.}$ (independent of l) in estimating the resolution on Rowland's circle by comparing results from geometric and physical optics.

The resolution on Rowland's circle depends also on the width of the entrance slit S_{1a}. However for slit widths from 0.6 to 1.5 μ[7] the width of the aberration considerably exceeds the width of the geometrical image of the slit $S_{1a}/\cos\beta$. Besides, since the width of the geometrical image is practically independent of the angular and radial errors in the arrangement of the entrance slit, the applicability of the expressions obtained above seems justified to us.

In conclusion, the author expresses his appreciation to I. B. Borovskii for suggesting the problem and for his valuable comments and to Yu A. Boshko for his help with the work.

REFERENCES

1. J. E. Mack, J. R. Stehn, and B. Edlen. J. Opt. Soc. Am. 22, 245 (1932).

2. H. G. Beutler. J. Opt. Soc. Am. 35, 311 (1945).
3. W. R. Hamilton. "Geometrical Optics. Mathematical Papers," Vol. 1, p. 17. Cambridge Univ. Press, London, 1931.
4. T. Namioka. J. Opt. Soc. Am. 49, 446 (1959).
5. J. S. Bowen. J. Opt. Soc. Am. 23, 313 (1933).
6. A. I. Efremov and A. M. Tyutikov. Izvest. Akad. Nauk SSSR, Ser. Fiz. 20, 792 (1956).
7. T. Magnusson. Nova Acta Regiae Soc. Sci. Upsaliensis 11, No. 3 (1938).

COMPARISON OF THE RAYLEIGH AND JAMIN TYPES OF INTERFEROMETERS

Yu. V. Kolomiitsov

Received 5 August 1959

It is shown that when the width and location of the diaphragms which limit the interfering light beams in Jamin type interferometers are changed, these interferometers become similar to Rayleigh type interferometers. A general formula for the dependence of the contrast of fringes on the width of the light source and on other factors is obtained for both types of interferometers. It is shown that conclusions that may be drawn from this formula make it possible to define more accurately several points in the theory of Rayleigh type interferometers, and to substantiate the requirements for the adjustment of Jamin type interferometers.

QUALITATIVE COMPARISON OF THE RAYLEIGH AND JAMIN SYSTEMS

It is well known that in interferometers of the Rayleigh type the interference pattern may be observed only in the diffraction image of a narrow light source, whereas in Jamin type interferometers the fringes of equal inclination, which are also observed in the image of the source, are found to be clearly contrasted even in a wide field. In connection with this it is usually assumed that diffraction effects play a decisive role in the formation of the fringes in a Rayleigh interferometer, whereas in the theory of the Jamin interferometer these phenomena are usually not considered. However, as was shown by Zakhar'evskii,[1] the presence of additional diaphragms can convert Jamin type interferometers into Rayleigh type interferometers. Below, the conditions are examined that are necessary to bring about this conversion and it is shown that the dependence of the contrast of the fringes on the dimensions of the source is subject to one and the same law for interferometers of both types. It is assumed here that two diffraction images of each point of the source coincide exactly with one another.

Figure 1 shows the layout of an interferometer which is similar to Michelson's stellar interferometer. A diaphragm containing a slit is placed in the focal plane of the objective O_1 with the slit perpendicular to the plane of the figure. The light source, which is not shown in the figure, is projected onto the slit. The angular width of the slit is 2ε. Rays originating from the central point S_0 of the slit, after passing through the objective O_1, are parallel to its axis. Mirrors M_1 and M_2 isolate two narrow beams of light. These light beams, after reflection by the mirrors M_3 and M_4, fall onto the objective O_2 which forms two coincident images S_0' of the point S_0 in the plane F. A diaphragm with two slits of width a is placed in front of the objective O_2. The separation between the two midpoints A_1 and A_2 of the two slits is c_2. The rays q_1 and q_2 which pass through the points A_1 and A_2 are at a distance c_1 from one another when leaving the objective O_1. It is easy to see that the above arrangement is transformed into the usual Rayleigh interferometer system when $c_1 = c_2$, which can take place in the absence of mirrors M_1-M_4.

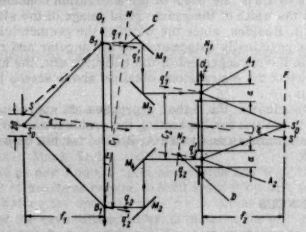

Fig. 1

After having passed through the slits A_1 and A_2, each of the light beams forms diffraction fringes in the plane F. It is well known that the angular separation β between the midpoint S_0' of the central maximum and the center of the next minimum is equal to

$$\beta = \frac{\lambda}{a}, \qquad (1)$$

the vertex of the angle β being at the center of the objective O_2 and λ being the wavelength of the light. When two diffraction maxima are superimposed on one another, a system of interference fringes is obtained whose angular separation is equal to

$$\varphi = \frac{\lambda}{c_2}. \qquad (2)$$

In the arrangement of Fig. 1, $c_2 \geq a$ and $\varphi \leq \beta$, which means that on a diffraction maximum there are not less than two interference fringes. The location of the fringes is determined by the magnitude of the original path difference Δ_0 which can be changed, for instance, by shifting one of the mirrors M_1 or M_4. If $\Delta_0 = 0$, then the center of the zero order fringe will coincide with S_0'.

Rays originating from the end point of the source, which is at an angular distance ε from S_0, form a plane wave N after passing through the objective O_1. The part of the wave N_1 is a distance $\Delta' = B_1C$ ahead of the part N_2. From a consideration of the figure it is seen that

$$\Delta' = \varepsilon c_1. \qquad (3)$$

The midpoints of the central diffraction maxima formed by the waves N_1 and N_2 are at the point S' which is the geometric image of the point S. As a result of interference there appears a second system of fringes which is displaced with respect to the first system. Anal-

ogous systems of fringes originate from all other points of the source. The relative displacement of the various fringe systems is proportional to the magnitude of Δ', that is, to the separation c_1 between the principal rays entering the interferometer. As a result of the superimposition of the systems of fringes a decrease of the contrast of the final interference pattern takes place, making it impossible to observe the pattern on the image of a wide light source. However, using a semitransparent mirror one can vary the magnitude of c_1 over a wide range. The case when $c_1 = 0$ is shown in Fig. 2. Here M_1 is a semitransparent mirror which divides the axial ray q that falls onto it into two rays q_1 and q_2. The mirrors M_1 to M_4 are located in such a way that the paths of the rays q_1 and q_2 from the objective O_1 to the points A_1 and A_2 are equal. It is easy to show that at an arbitrary point in the plane F all pairs of waves (originating from different points of the source) give the same result of interference; this makes it possible to observe a clearly contrasted pattern in the presence of a wide source.

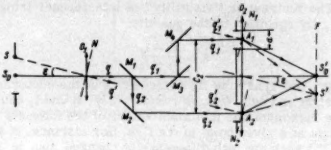

Fig. 2

The arrangement in Fig. 2 does not differ in principle from the systems of Jamin type interferometers, and particularly from the Mach-Zehnder interferometer system shown in Fig 3. Here M_1 and M_4 are semitransparent and M_2 and M_3 are opaque mirrors. The mirror M_3 is parallel to M_1 and the mirror M_4 is parallel to M_2. Here, as in the arrangement of Fig 2, the central rays of the beams q_1 and q_2 falling onto the objective O_2 are homologous, that is, they are derived from the same original ray q ($c_1 = 0$). The separation c_2 between homologous rays in the general case is not equal to the separation c_3 between the central rays of the beams (in Figs. 2 and 3, $c_3 = c_2$). The separation c_2 depends on the angle between the mirrors M_1 and M_2, and also on the separation between the mirrors of the interferometer. By shifting the mirror M_4 one can arrange for the path difference of the interfering beams to be zero at the point S'_0.

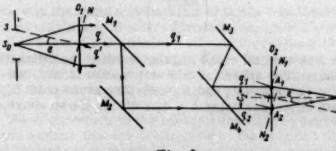

Fig. 3

The systems shown in Figs. 2 and 3 can easily be transformed into systems of the Rayleigh type. Thus, to do this, in the arrangement of Fig. 2 it is sufficient to shift the slit A_1 or A_2 through a distance $c_1 > a$ in the direction perpendicular to the axis of the objective O_2. Then, just as in the system of Fig. 1, none of the rays that pass through the slit A_1 will have homologous rays in the beam passing through the slit A_2 and this leads to the disappearance of fringes when a wide source is used.

In Figs. 4 and 5 are shown two methods of transforming a Mach-Zahnder interferometer into an interferometer of the Rayleigh type. The first method (Fig. 4) consists of setting up diaphragms R_1 and R_2 which separate two narrow beams of width a from the wide beam of light entering the interferometer. The diaphragm

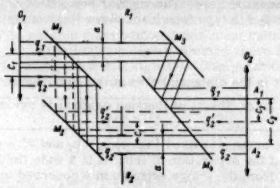

Fig. 4

R_2 is set up in such a way that the central ray q_2 of the beam passing through it is at a distance c_1 from the ray q'_2, the latter being the homologous ray of q_1. If $c_1 > a$, there are no pairs of homologous rays in the light beams falling onto the objective O_2 and the system changes into a Rayleigh system. The same result can be obtained by using one slit-shaped diaphragm R before the objective O_2 (Fig. 5), provided the slit width $a < c_3$.

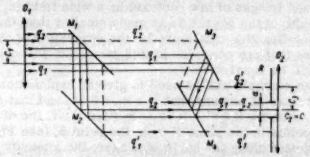

Fig. 5

Systems that are intermediate between the Rayleigh and the Jamin systems are of special interest. Such systems can be obtained, for instance, from the arrangements shown in Figs. 4 and 5, if $a > c_1$. The increase of the width a of the slits (for a fixed c_1) leads to a reduction of the width of the diffraction maxima in the imaging of points of the source, and because of this, to a smaller superposition of these maxima and to an increase in contrast of the interference pattern. The quantitative examination of this problem will be carried out later; here we shall formulate the following general law: the contrast of fringes observed in a wide field is determined by the ratio c_1/a, that is, by the number of pairs of homologous rays contained in the interfering beams of light. Maximum contrast is obtained when $c_1 = 0$ (the case of Jamin type interferometers without limiting diaphragms), and is equal to zero when $c_1 > a$ (the case of Rayleigh type interferometers). When

$$0 < \frac{c_1}{a} < 1$$

the contrast may have some intermediate value. Thus an incorrect location of the diaphragms may lead to a considerable reduction of the visibility of fringes in Jamin type interferometers, a fact that must be borne in mind during their adjustment.

It is well known[2, 3] that the contrast of fringes of equal inclination is small when the interfering light beams falling onto the telescope objective are not parallel, and that one can increase the contrast by placing a diaphragm

in front of the objective. However, the above considerations show that a lowering, instead of an increasing of contrast of the fringes can occur as a result of such diaphragming.

There is no obvious answer to the question of what fringe separation should be observed in a wide field when c_1 is not equal to zero. The angular separation φ' of the fringes in Jamin type interferometers is given by

$$\varphi' = \frac{\lambda}{c_3}, \qquad (4)$$

where c_3* is the distance between the homologous rays.

*Editor's note: The c_2 in Russian original is evidently a misprint.

In the arrangement of Fig 3, $c_3 = c_2$ and $\varphi' = \varphi$; this means that the separation of fringes in a wide field does not differ from the fringe separation φ observed in the diffraction maximum from a narrow source. In the general case, $c_2 = c_3 - c_1$. Hence, when the diaphragms R_1 and R_2 are introduced in the system of Fig. 4 (and when the width of the source is reduced), the fringe separation φ can be larger or smaller than the separation φ' of the fringes that are observed in a wide field prior to the introduction of the diaphragms. Experiment shows that when the quantity c_1 is changed from 0 to a by shifting the diaphragm R_2, the contrast of the fringes gradually decreases to zero, and their separation, which is given by expression (4), remains constant. If, however, having obtained fringes of low contrast in a wide field ($c_1 < a$) the width of the source 2ε is made smaller than the width of the diffraction maximum 2β, the separation of the fringes that are observed in this maximum will change and will be equal to φ.

An example will be used to give an explanation of this effect. Let us assume that $c_1 = c_2 = 0.5c_3$ and that $a = 1.5c_1$, then $\varphi = 0.5\varphi' = 0.75\beta$. In Figs. 6a-f, the distances x of points in the plane F from the point S_0' (see Fig. 1) are plotted along the horizontal axes; the intensity of the diffraction maxima from different points of the source (broken lines) and the intensity of interference fringes on these maxima (full lines) are plotted along the vertical axes. Diffraction maxima are shown, whose centers are at the points x = 0, -0.5φ, $+0.5\varphi$, φ, 1.5φ and 2φ. For the relative values of c_1 and c_2 chosen, the centers of the zero order fringes in Figs. 6b-f are at distances -0.25φ, $+0.25\varphi$, 0.5φ, 0.75φ, and φ away from the point x = 0. Thus, in Fig. 6f the midpoint of the first order fringe coincides with the center of the diffraction maximum. The final interference pattern can be obtained by the addition of the intensities produced at a given point of the field by light from all points of the source (Fig. 6g). The maxima of the final interference pattern occur at the points x = 0 and x = 2φ, and the minimum occurs at the point x = φ; this explains why in a wide field fringes with a separation $\varphi' = 2\varphi$ are obtained. If the source is limited in such a way that its angular width is equal to $\pm 0.5\,\varphi$, then the final curve (obtained by the addition of the solid curves of Figs. 6a-e) will have maxima separated from one another by a distance $\varphi = 0.5\varphi'$.

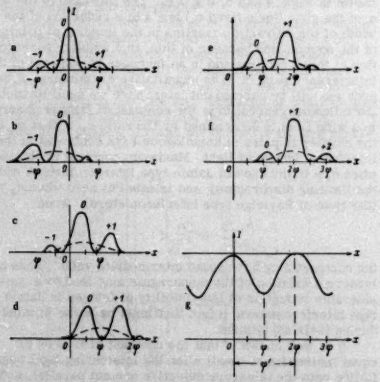

Fig. 6

THE DERIVATION AND EXAMINATION OF A FORMULA FOR THE CONTRAST OF INTERFERENCE FRINGES

The contrast or "visibility" of interference fringes is usually specified by the quantity

$$K = \frac{I_1 - I_2}{I_1 + I_2}, \qquad (5)$$

where I_1 and I_2 are the light intensities at the center of the bright and dark fringes respectively. I_1 and I_2 can also be the maximum and minimum values of the intensity of the light at a given point in the field (for instance, at the point S_0') when the path difference is changed, that is, when the fringes are moved across the field. If the two diffraction maxima, produced by the interfering waves, coincide exactly with one another, both concepts of the contrast will yield the same value of K, but when the second concept is used, the derivation of the formulas is simpler.

In Fig. 7, as in the previous figures, O_1 is the objective of the collimator and O_2 is the objective of the telescope. The interferometer is located between O_1 and O_2 and is represented schematically by a rectangle. The light source is a rectangular slit of angular width 2ε. The central point S_0 of the source produces a plane wave N_0, and the point P, at an angular distance α away from S_0, produces a wave N. The interferometer divides this wave into two waves N_1 and N_2; these waves form two coincident diffraction maxima with centers at the point P′ in the plane F. It is well known that the intensity of each maximum at the point S_0', at an angular distance α from P′, is proportional to the ratio

$$\left(\frac{\sin\frac{\pi\alpha}{\beta}}{\frac{\pi\alpha}{\beta}}\right)^2, \qquad (6)$$

where β is one half of the angular width of the diffraction maximum. The spherical diffraction wave fronts, centered on the points A_1 and A_2, interfere at the point S_0', the path difference being $\Delta = \Delta_0 + \Delta'$. As shown above,

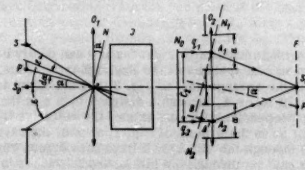

Fig. 7

$\Delta' = \alpha c_1$, where c_1 is the separation between the principal rays from which the rays q_1 and q_2 are derived. A narrow strip of the source of width $d\alpha$ produces a resultant intensity dI at the point S_0'. To obtain the total intensity at the point S_0' due to the whole source, it is necessary to integrate dI with respect to α between the limits $-\varepsilon$ and $+\varepsilon$.

$$I = C\int_{-\varepsilon}^{+\varepsilon}\left(\frac{\sin\frac{\pi\alpha}{\beta}}{\frac{\pi\alpha}{\beta}}\right)^2\left[1+\cos\frac{2\pi}{\lambda}(\Delta_0+\alpha c_1)\right]d\alpha, \qquad (7)$$

where C is a proportionality constant.

The evaluation of the integral (7) is made considerably simpler by making the assumption that is usually made in the theory of Rayleigh type interferometers, namely that $\beta \gg \alpha$, and hence that the expression (6) is equal to 1. The physical meaning of this assumption is that the widths of the slits A_1 and A_2 are small, and that the broad diffraction maxima produced by all the points of the source have the same intensity at the point S_0'. When this is so,

$$I = 2\varepsilon C\left[1+\cos\frac{2\pi\Delta_0}{\lambda}\,\frac{\sin\frac{2\pi\varepsilon c_1}{\lambda}}{\frac{2\pi\varepsilon c_1}{\lambda}}\right]. \qquad (8)$$

The quantity (8) has maximum values I_1 when $\Delta_0 = 0, \lambda, 2\lambda, \ldots$, and minimum values I_2 when $\Delta_0 = \lambda/2, 3\lambda/2, \ldots$. The corresponding values I_1 and I_2 are equal to

$$I_1 = 2\varepsilon C\left[1+\frac{\sin\frac{2\pi\varepsilon c_1}{\lambda}}{\frac{2\pi\varepsilon c_1}{\lambda}}\right],$$

$$I_2 = 2\varepsilon C\left[1-\frac{\sin\frac{2\pi\varepsilon c_1}{\lambda}}{\frac{2\pi\varepsilon c_1}{\lambda}}\right].$$

Hence we obtain the following formula, previously derived by Michelson,[4] for the contrast K at the point S_0'

$$K = \frac{\sin\frac{2\pi\varepsilon c_1}{\lambda}}{\frac{2\pi\varepsilon c_1}{\lambda}}. \qquad (9)$$

If we put $c_1 = nc_2$, formula (9) will take the form

$$K = \frac{\sin\frac{2\pi\varepsilon n}{\varphi}}{\frac{2\pi\varepsilon n}{\varphi}}, \qquad (9')$$

where φ is the angular separation of fringes on the diffraction maximum. It follows from (9) that $K = 1$ when $c_1 = 0$ and that $K = 0$ when $\Delta' = \varepsilon c_1 = \lambda/2$. Formula (9′) shows that $K = 0$ when $2\varepsilon = \varphi/n$. Thus, for instance, in the Rayleigh interferometer $n = 1$, and the fringes disappear if the source width 2ε is equal to the fringe separation φ.

We shall return to the examination of the integral (7) and assume that the dimensions of the source are not small compared to the width of the diffration maximum. We shall introduce the symbols

$$z = \frac{\pi\alpha}{\beta}, \quad z_1 = \frac{\pi\varepsilon}{\beta}, \qquad (10)$$

$$Q = \frac{2c_1\beta}{\lambda} = \frac{2c_1}{a}. \qquad (11)$$

Then we get

$$I = C'\int_{-z_1}^{+z_1}\left(\frac{\sin z}{z}\right)^2\left[1+\cos\left(\frac{2\pi\Delta_0}{\lambda}+Qz\right)\right]dz, \qquad (12)$$

where the constant $C' = \beta C/\pi$. In the general case ($z \neq 0$) when z is reduced, the contrast K tends to the value given by expression (9). If a continuous transition is to exist, it is necessary that the magnitude of I given by (12) should assume maximum and minimum values at the same Δ_0 as in the limiting case examined above (for $z = 0$), that is, at $\Delta_0 = 0$ and at $\Delta_0 = \lambda/2$. The substitution of these values in (12) yields

$$I_1 = C'\int_{-z_1}^{+z_1}\left(\frac{\sin z}{z}\right)^2\left[1+\cos Qz\right]dz,$$

$$I_2 = C'\int_{-z_1}^{+z_1}\left(\frac{\sin z}{z}\right)^2\left[1-\cos Qz\right]dz.$$

Considering the definition of the functions under the integral signs, we obtain the final expression for the contrast of the interference pattern at the point S_0'

$$K = \frac{\int_0^{z_1}\left(\frac{\sin z}{z}\right)^2\cos Qz\,dz}{\int_0^{z_1}\left(\frac{\sin z}{z}\right)^2 dz}. \qquad (13)$$

It is interesting to find K for the case of an infinitely wide source, that is, for $z_1 = \infty$. Integrating expression (13) by parts and using tabulated values of some integrals,[5] one can show that

$$K_\infty = 1-\frac{Q}{2} = 1-\frac{c_1}{a} \quad \text{for} \quad c_1 \leqslant a,$$
$$K_\infty = 0 \quad \text{for} \quad c_1 \geqslant a. \qquad (14)$$

In a Rayleigh type interferometer system (Fig. 1) $c_1 > a$ and $K_\infty = 0$, a result that is well known. In a Mach-Zehnder interferometer (Fig. 4) equipped with diaphragms R_1 and R_2, the quantity c_1 can assume arbitrary values, and this makes it possible to vary K_∞ between the limits 1 and 0. One can assume that the contrast of an interference pattern is good when $K = 0.75$, that is, when $c_1 = 0.25a$. Thus, a displacement of the diaphragms which limit the width a of the interfering light beams from the calculated location for which $c_1 = 0$ is permissible during the setting-up and adjustment of the interferometer, but the magnitude of this displacement should not exceed $0.25a$. One can calculate K_∞ in an analogous way for the case of one diaphragm R, placed before the objective of the telescope (Fig. 5).*

*Where the width of the slits $a > D - c_2$ (where D is the width of the light beams emerging from the interferometer) it is necessary to take into account the magnitude of D during the evaluation of K. This problem is not considered in this work.

In the general case of a source with finite dimensions ($z_1 \neq \infty$), it is necessary to resort to graphical integration for the evaluation of K from formula (13); the family of curves in Fig. 8 shows the results of this evaluation. The values of K are plotted along the ordinate axis and ε/β, the ratio of the source width to the width of the diffraction maximum, is plotted along the abscissa. Each curve corresponds to a given value of the ratio c_1/a. It follows from (11) that the magnitude of β depends on a. Thus, in order that the same scale along the abscissa should correspond to the different curves of Fig. 8, it is

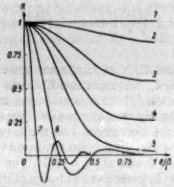

Fig. 8. Values of c_1: curve 1—0; curve 2—0.25a; curve 3—0.5a; curve 4—0.75a; curve 5—a; curve 6—2a; curve 7—5a.

necessary to consider constant magnitudes of a and β. When this is done, the curves immediately give the dependence of K on the width of the source 2ε and on the displacement c_1 of the principal rays. From an examination of Fig. 8 it is possible to draw the following conclusions.

1. For a given value of c_1 the contrast K falls when the dimensions of the source 2ε are increased, tending to the limiting value K_∞ given by expression (14). The decrease of K is more rapid the larger the value of c_1. In practice K does not depend on ε if $\varepsilon > \beta$. This can be explained by the fact that under these conditions the intensities of the interference patterns produced at the central point of the field by the points at the edge of the source are negligibly small.

2. For a source of given dimension 2ε the contrast K is higher the smaller the value of c_1. In the Rayleigh interferometer $c_1 > a$ and to obtain a satisfactory contrast (K = 0.75) it is necessary for the width of the source to be 5 to 20 times smaller (depending on the ratio of c_1 to a) than the width of the diffraction maximum. The permissible dimension of the source is then approximately inversely proportional to c_1. When $c_1 < a$ * which is the case in interferometers of the Jamin type, it is possible to observe fringes with $\varepsilon > \beta$, that is, in a wide field.

*Editor's note: $c_1 > a$ in Russian original is evidently a misprint.

3. If $c_1 > a$ the contrast K first decreases to zero and then assumes negative values when the source dimension is increased. This means that $I_2 > I_1$, that is, the intensity of the resultant wave at the point S_0' is higher for $\Delta_0 = \lambda/2$ than for $\Delta_0 = 0$. This effect can be easily proved experimentally with a Rayleigh interferometer whose collimator is provided with a smoothly adjustable slit.

It is interesting to investigate the dependence of K on the width of the beams a for different dimensions 2ε of the source and for a constant fringe separation φ, that is, for constant values of c_2 and c_1. For this purpose it is necessary to redraw the curves of Fig. 8 plotting the quantity $2n\varepsilon/\varphi$ along the abscissa in place of ε/β. From (1) and (2) it follows that

$$\beta = \frac{c_1\varphi}{an},$$

where $n = c_1/c_2$. Hence

$$\frac{2n\varepsilon}{\varphi} = \frac{2c_1}{a}\frac{\varepsilon}{\beta}.$$

Multiplying the abscissa of the curves in Fig. 8 by the factor $2c_1/a$ we obtain a new family of curves (Fig. 9). One can also obtain the dependence of K on the ratio a/c_1 for a constant source width 2ε. In Fig. 10 are shown such curves for the cases $2\varepsilon = 0.4\varphi/n$, $2\varepsilon = \varphi/n$, and $2\varepsilon = \infty$. An examination of the curves of Figs. 9 and 10 enables one to draw the following additional conclusions.

4. When $a \ll c_1$ (this case occurs in the stellar interferometer) the fringes disappear (K = 0) when $2\varepsilon = \varphi/n$; this agrees with the conclusion drawn from Michelson's formula (9'). When $a = c_1$ (the limiting case of Rayleigh type interferometers) the disappearance of fringes takes place only when $2\varepsilon \approx 2\varphi/n$.

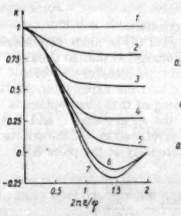

Fig. 9

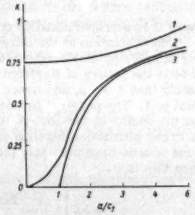

Fig. 10

Fig. 9. Values of a: curve 1—∞; curve 2—$4c_1$; curve 3—$2c_1$, curve 4—$1.33c_1$; curve 5—c_1; curve 6—$0.5c_1$; curve 7—$0.2c_1$.
Fig. 10. Values of 2ε: curve 1—0 $4\varphi/n$; curve 2—φ/n; curve 3—∞.

5. In Rayleigh type interferometers ($a < c_1$) a good fringe contrast (K = 0.75) is obtained when $2n\varepsilon/\varphi = 0.4$, that is, for $\varepsilon = 0.2\lambda/c_1$. In this case the value of K is practically independent of a, as can be seen from the uppermost curve of Fig. 10.

6. When the contrast of fringes in Rayleigh interferometers is small, its value depends on the width of the slit a. Thus, for instance, for $2\varepsilon = \varphi/n$ (which corresponds to the middle curve in Fig. 10), K = 0 when $a \ll c_1$, but for values of a close to c_1, K ≈ 0.17.

7. The contrast K rises rapidly with an increase in a in interferometers of the intermediate type for which $a > c_1$. The change of the width of the source 2ε from φ/n to ∞ in this case does not significantly influence the magnitude of K.

CONCLUSIONS

1. The contrast of fringes in interferometers of the Rayleigh and Jamin types (with diaphragms) can be expressed by the general formula (13).

2. Fringes of equal inclination with the largest contrast are obtained in Jamin type interferometers when for every ray in one of the interfering beams there exists a homologous ray in the other beam. For this reason during the adjustment of interferometers it is necessary to take care that the diaphragms which limit the light beams (for instance, the rims of cells containing liquids or gases) are symmetrically disposed with respect to the homologous rays. It is also necessary for the effective diameter of the telescope objective to be sufficiently large.

3. The contrast of annular fringes of equal inclination which occur with considerable path differences was not examined in this work, but from the above considerations it follows that the introduction of limiting diaphragms will first of all cause a fading of the annular fringes at the edge of the field of view.

REFERENCES

1. A. N. Zakhar'evskii. "Interferometry." (Interferometers). Oborongiz, 1952.
2. Yu. V. Kolomiitsov. Opt. i Spektr. 1, 937 (1956).
3. A. A. Zabelin. Optiko-Mekh. Prom. No. 1(?), 23 (1957).
4. A. A. Michelson. Phil. Mag. 30, 1 (1890).
5. I. M. Ryzhik. "Tablitsy integralov, summ, ryadov i proizvedenii." (Tables of Integrals, Sums, Series, and Products), Gosudarst. Izd. Tekh.-Teoret. Lit., 1943.

PASSAGE OF LIGHT THROUGH LIGHTGUIDES

A. R. Daich, Yu. A. Tsirlin, and L. E. Pargamanik

Received 18 September 1959

The passage of light through cylindrical lightguides with specular walls is investigated in the approximation of geometrical optics. Transmissivities for lightguides with total reflection and with reflecting coverings are calculated. Account is taken of absorption of light in the material of the lightguide. The dependence of the transmissivity on the dimensions of the lightguide and on the reflection conditions at the walls is explained. A comparison is made between various types of lightguides.

Interest in lightguides has arisen recently in connection with the requirements of scintillation counter technique and with the distortion-free transmission of images over a distance by means of fibers.[1-6]

Papers concerned with the passage of light through lightguides have appeared.[7-12] In these works certain empirical rules have been found without any attempt at theoretical analysis of them and without the establishment of general relationships. As a result of this, the conclusions of different authors are difficult to compare, are frequently contradictory, and have significance only under conditions approximating the experimental setup of a given author. This is explained by the fact that even a simple cylindrical lightguide is characterized by a considerable number of factors: the type of reflection at the lateral surfaces (specular or diffuse); the presence or absence of total internal reflection; the presence or absence of a boundary at the entrance and exit of the lightguide; the quality of polish of the specular surfaces (a bad polish on the sides leads to a change of reflection coefficient); the angular intensity distribution of light entering the lightguide; the presence or absence of a reflecting covering and the magnitude of the reflection coefficient r of the walls; the value of the absorption coefficient k_0 of the lightguide material; and the ratio $l = L/R$ of the length L to the radius R, and the magnitude of R itself.

In the present work we shall consider lightguides with specular side surfaces.*

*There exist data in the literature on the advantage of lightguides with diffusely reflecting side surfaces over those with specular sides[8] and also data of an opposite nature.[12] We plan to devote subsequent work to the investigation of lightguides with diffusely reflecting surfaces.

The following cases are considered: lightguides with isotropic sources lying on the axis of the guide and with sources whose light intensity is proportional to the cosine of the angle u with the axis of the guide; lightguides with and without total reflection from the side surfaces and also with total reflection and an additional reflecting covering. Solutions are obtained both with and without consideration of absorption in the lightguide material.

PRELIMINARY CONDITIONS

The source, which emits in the solid angle 2π a luminous flux equal to 1, is taken to be a point lying on the axis of the lightguide at the end of the cylinder. The dimensions of the lightguide are assumed to be sufficiently large for the application of geometrical optics. The reflection coefficient r for lightguides without total reflection is independent of the angle of incidence i. The walls are ideally smooth. Reflection on entrance and exit is not considered.

For lightguides with total internal reflection from the walls

$$\left.\begin{array}{ll} r = \text{const} < 1 & \text{for } i < i_k, \\ r = 1 & \text{for } i > i_k, \end{array}\right\} \quad (1)$$

where i_k is the critical angle. Fresnel reflection is not taken into account. The latter accounts for about 5% of the magnitude of the transmissivity for $l < 3$ and is completely negligible for larger l.

We shall calculate the luminous flux falling on the second end of the cylinder.

A. ISOTROPIC EMITTER

In accordance with reference 12 let us consider the luminous fluxes F_1, F_2, ... F_m, ... falling on the end of the cylinder after single, double, m-fold reflections and also F_0, which falls on the end directly from the source (Fig. 1).

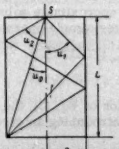

Fig. 1. Path of rays in lightguide: u_0—half-angle of cone of zero order; u_1, u_2—same for first and second orders.

The total flux falling on the end of the cylinder under the indicated conditions is equal to the transmissivity of the lightguide

$$\tau = \sum_{m=0}^{\infty} \tau_m, \quad (2)$$

where

$$\tau_m = r^m \int_{u_{m-1}}^{u_m} e^{-\frac{kL}{\cos u}} \sin u\,du, \tag{3}$$

$$\tan u_m = \frac{2m+1}{l}. \tag{4}$$

We shall consider special cases.

1. Nonabsorbing Medium ($k_0 = 0$)

a. Lightguide without total reflection ($r = \text{const} < 1$). For $k_0 = 0$ it follows Eqs. (2) and (3) that

$$\tau_0 = 1 - \cos u_0 \tag{5}$$

and

$$\tau_m = r^m (\cos u_{m-1} - \cos u_m) =$$

$$r^m \left[\frac{1}{\sqrt{1+\left(\frac{2m-1}{l}\right)^2}} - \frac{1}{\sqrt{1+\left(\frac{2m+1}{l}\right)^2}} \right]. \tag{6}$$

For small values of l the series for τ_m rapidly converges and numerical calculation presents no difficulties (results obtained by this accurate calculation are plotted as circles in Fig. 2).

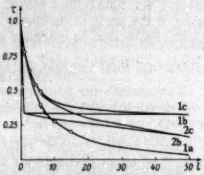

Fig. 2. Transmissivity τ for isotropic emitter as a function of the length l of the lightguide. Lightguide without absorption: curve 1a—with reflector, r = 0.85; curve 1b—with total reflection, n = 1.5, without covering; curve 1c—with total reflection, n = 1.5, and reflector, r = 0.85. Lightguide with absorption, $k_0 = 0.01\ \text{cm}^{-1}$, R = 1 cm: curve 2b—with total reflection, n = 1.5, without covering; curve 2c—with total reflection, n = 1.5, and reflector, r = 0.85.

When $l \gg 1$, an approximate solution is possible. For $2m \gg 1$, after simple operations we get

$$\tau_m \approx \frac{4ml r^m}{(l^2+4m^2)^{\frac{3}{2}}}, \tag{7}$$

where, in the expansion of Eq. (6), the quantity $(l^2 + 4m^2)^{-1}$ has been neglected, introducing an error no larger than 1%.

Assuming that (6) is correct beginning with m = 3, we may write

$$\tau = \tau_{02} + S, \tag{8}$$

where

$$\tau_{02} = \sum_{m=0}^{2} \tau_m, \tag{9}$$

$$S = \sum_{m=3}^{\infty} \frac{4ml r^m}{(l^2+4m^2)^{\frac{3}{2}}}. \tag{10}$$

Let us replace the sum S by the integral

$$S = \int_{\frac{5}{2}}^{\infty} \frac{4ml r^m dm}{(l^2+4m^2)^{\frac{3}{2}}}. \tag{11}$$

Defining

$$z = \frac{2m}{l}; \quad z_0 = \frac{5}{l}; \quad \alpha = \left|\ln r\right|; \quad c = \frac{\alpha l}{2},$$

we get

$$S = \int_{z_0}^{\infty} \frac{z e^{-cz}}{(1+z^2)^{\frac{3}{2}}}\, dz. \tag{12}$$

Calculation of S is presented in the appendix. For large l ($l \gg 2/\alpha$) the transmissivity τ may be expressed by the following approximate equation:

$$\tau = \frac{1}{l^2}\left[5\left(1 - r + \frac{5}{2}r^2\right) + \frac{4}{3^3}\right]. \tag{13}$$

The dependence of τ on l for r = 0.85 (reflection for polished aluminum), obtained with the use of (7) and (11), is presented in Fig. 2 (curve 1a; the dashed curve is an approximate calculation).

b. Lightguide with total internal reflection and without covering. This case can be characterized by values of the reflection coefficient in accordance with (1).

The transmissivity τ is expressed by the relations

$$\left.\begin{aligned} &\tau = 1 - \cos u_0 \quad \text{for } l < l_k, \\ &\tau = 1 - \cos u_k = \tau_k = \text{const} \quad \text{for } l > l_k, \end{aligned}\right\} \tag{14}$$

where

$$l_k = \operatorname{cotan} u_k.$$

The dependence of τ on l for n = 1.5 is presented in Fig. 2, curve 1b.

c. Lightguide with total internal reflection and reflecting walls. This case corresponds to a rod of transparent material with a polished metal casing which does not make optical contact with the lightguide.

For $l < l_k$, this case does not differ from case 1a.

For $l > l_k$, the solution has the form

$$\tau = \tau_k + H, \tag{15}$$

where

$$H = \int_{\xi}^{\infty} \frac{z e^{-cz}}{(1+z^2)^{\frac{3}{2}}}\, dz, \tag{16}$$

$$\xi = \frac{2m_k}{l}, \quad m_k = \frac{1}{2}(l \tan u_k - 1). \tag{17}$$

The calculation of (16) is analogous to the calculation of (13) (see Appendix). For sufficiently large l the transmissivity of the lightguide is expressed by the formula

$$\tau = 1 - \cos u_k + \frac{2}{\alpha l} \sin u_k \cos u_k e^{-\frac{1}{2}\alpha l \operatorname{sec} u_k}. \tag{18}$$

The dependence of τ on l for n = 1.5, r = 0.85 is presented in Fig. 2, curve 1c.

2. Medium with Absorption ($k_0 \neq 0$)

The only solution of interest is for $l \gg 1$.

a. Lightguide without total internal reflection. The solution is determined by Eqs. (2) and (3). For this case a solution in closed form could not be found.*

*It should be noted that each term (3) of the series (2) leads to tabulated functions (integral exponential functions) and does not require numerical integration, as is used in the solution of the analogous problem in reference 12.

b. Lightguide with total internal reflection and without covering. The solution is expressed by the equation

$$\tau_k = \int_0^{u_k} \sin u e^{-\frac{k_0 L}{\cos u}} du. \tag{19}$$

Introducing the definitions $k_0 R = k$, $kl = k_0 L = \beta$, and taking cos u as the new variable, we get the solution in the form

$$\tau = e^{-\beta} - \frac{1}{n} e^{-n\beta} + \beta [E_i(-\beta) - E_i(-n\beta)], \tag{20}$$

where $E_1(x)$ is the integral exponential function, tabulated, for example, in reference 13.

The dependence of τ on l for $k_0 = 0.01$ is presented in Fig. 2, curve 2b.

c. Lightguide with total internal reflection and reflecting walls. For angles u in the limits from 0 to u_k the solution coincides with that presented in Section A,1b. The total luminous flux equals

$$\tau = \tau_k + D, \tag{21}$$

where

$$D = \int_{m_k}^{\infty} \frac{4ml r^m e^{-\frac{ml}{\cos u}}}{\left[1 + \left(\frac{2m}{l}\right)^2\right]^{\frac{3}{2}}} dm = \int_{l}^{\infty} \frac{2z e^{-xz} e^{-k l \sqrt{1+z^2}}}{(1+z^2)^{\frac{3}{2}}} dz.$$

For calculation of D see Appendix. For n = 1.5 we have approximately

$$D = e^{-0.5\beta} \int_{l}^{\infty} \frac{2z e^{-(c+0.8\beta)z}}{(1+z^2)^{\frac{3}{2}}} dz, \tag{23}$$

i.e., the problem leads to the case of Section A,1a for a lightguide with reflection coefficient r_1:

$$a_1 = |\ln r_1| = \frac{2}{l}(c + 0.9\beta) = a + 1.8k \tag{24}$$

with the additional factor $e^{-0.5\beta}$.

The dependence of τ on l for r = 0.85, $k_0 = 0.01$, is presented in Fig. 2, curve 2c.

For large l the dependence (22) can be presented in the form

$$D = \frac{\sin u_k \cos^2 u_k e^{-l \sec u_k \left(\frac{a}{2} \sin u_k + k\right)}}{l\left(k \sin u_k + \frac{a}{2}\right)}. \tag{25}$$

B. COSINUSOIDAL EMITTER

Let us assume a source whose intensity is subject to the law

$$j = \frac{dF}{d\omega} = \frac{1}{\pi} \cos u. \tag{26}$$

By analogy with (3) we can write

$$\tau'_m = 2r^m \int_{u_{m-1}}^{u_m} \cos u \sin u e^{-\frac{k_0 L}{\cos u}} du. \tag{27}$$

1. Nonabsorbing Medium

a. Lightguide without total reflection. For $k_0 = 0$, from (22) we get

$$\tau_0 = 1 - \cos^2 u_0 = \sin^2 u_0, \tag{28}$$

$$\tau'_m = r^m (\cos^2 u_{m-1} - \cos^2 u_m)$$

$$= r^m \frac{\left(\frac{2m+1}{l}\right)^2 - \left(\frac{2m-1}{l}\right)^2}{\left[1 + \left(\frac{2m-1}{l}\right)^2\right]\left[1 + \left(\frac{2m+1}{l}\right)^2\right]}. \tag{29}$$

The total luminous flux is determined by a sum analogous to (2), where for small l (less than six), the value of τ is determined by a direct summation of the series.

For $2m \gg 1$, (29) can be presented in the form

$$\tau'_m = \frac{4r^m}{l} \frac{\frac{2m}{l}}{\left[1 + \left(\frac{2m}{l}\right)^2\right]^2}. \tag{30}$$

Equations (10) and (12) give the following expression for the luminous flux leaving the lightguide:

$$\tau = \sum_{m=0}^{k} \tau'_m + S', \tag{31}$$

where

$$S' = 2 \int_{k}^{\infty} \frac{z e^{-cz}}{(1+z^2)^2} dz. \tag{32}$$

Calculation of S' is given in the Appendix. For large l the transmissivity τ can be expressed by the following approximate formula:

$$\tau = \frac{1}{l^2}\left[1 + 8c + 16c^2 + 8c^3\left(\frac{3}{a} + \frac{1}{a^2} - 9\right)\right]. \tag{33}$$

The dependence of τ on l, calculated with the aid of (31) and (32) for r = 0.85, is shown in Fig. 3, curve 1a.

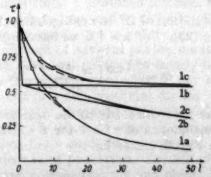

Fig. 3. Transmissivity τ for a cosinusoidal emitter as a function of the length l of the lightguide. Designations are same as in Fig. 2.

b. Lightguide with total internal reflection and without covering. The transmissivity is expressed by the relationships

$$\left.\begin{aligned} \tau &= \sin^2 u_0 \text{ for } l < l_k, \\ \tau &= \sin^2 u_k \text{ for } l > l_k. \end{aligned}\right\} \tag{34}$$

The dependence of τ on l for n = 1.5 is presented in Fig. 3, curve 1b.

c. Lightguide with total internal reflection and absorbing walls. By analogy with 1c we get

$$\tau = \tau'_a + G, \tag{35}$$

where

$$G = 2 \int_{l}^{\infty} \frac{z e^{-cz}}{(1+z^2)^2} dz. \tag{36}$$

Calculation of (36) is analogous to the calculation of (32). The dependence of τ on l for r = 0.85, n = 1.5 is

presented in Fig. 3, curve 1c.

For large l Eq. (36) can be written in the form

$$G = \frac{2\sin u_k \cos^3 u_k e^{-l\sec u_k\left(\frac{\alpha}{2}\sin u_k + k\right)}}{l\left(k\sin u_k + \frac{\alpha}{2}\right)}. \quad (37)$$

2. Medium with Absorption

a. Lightguide without total internal reflection. For this case a solution in finite form could not be found.

b. Lightguide with total internal reflection and without covering. The solution is expressed by the formula

$$\tau_2 = 2\int_0^{u_k} \sin u \cos e^{\frac{-k_0 l}{\cos u}} du. \quad (38)$$

By a method analogous to that given in Section A,2b, we get

$$\tau_2 = \left\{e^{-\beta}\left(1-\beta\right) - \frac{e^{-n\beta}}{n}\left(\frac{1}{n}-\beta\right) + \beta^2\left[E_i\left(-n\beta\right) - E_i\left(-\beta\right)\right]\right\}. \quad (39)$$

The dependence of τ on l is presented in Fig. 3, curve 2b.

c. Lightguide with total internal reflection and reflecting walls. For angles u in the limits from 0 to u_k the solution is Eq. (39) given in Section B,2b. The total luminous flux equals

$$\tau = \tau_2 + D', \quad (40)$$

where

$$D' = \int_{m_2}^{\infty} \frac{2m}{l} \frac{e^{m_2} e^{-\frac{kl}{\cos u}}}{\left[1+\left(\frac{2m}{l}\right)^2\right]^2} dm = 2\int_{\xi}^{\infty} \frac{z e^{-cz} e^{-kl\sqrt{1+z^2}}}{(1+z^2)^2} dz. \quad (41)$$

The calculation of D′ is analogous to that of D in Eqs. (21) and (23). For n = 1.5 we have approximately

$$D' = 2e^{-0.5\xi}\int_{\xi}^{\infty} \frac{z e^{-(c+0.9\beta)z}}{(1+z^2)^2} dz. \quad (42)$$

Thus, the problem leads to the case given in Section B,1a. The dependence of τ on l for r = 0.85, k_0 = 0.01 is presented in Fig. 3, curve 2c.

CONCLUSIONS

From the above calculations (cf. Figs. 2 and 3) it follows that lightguides with additional reflecting side surfaces which do not make optical contact with the material of the guide have better transmission than those without any covering and that this advantage is particularly strong for short lengths. For small l (l < 10-15) lightguides with coverings which make optical contact possess a greater transmissivity than those with no covering; for large lengths they yield in favor of the other two types. In the absence of absorption in the material of the lightguide the transmissivity is determined by the ratio L/R = 1 and not by the absolute dimensions; therefore, geometrically similar lightguides transmit light identically. When absorption is present, the transmissivity depends on two dimensionless parameters (for example, l and k).

Comparison of these results with various experimental data (e.g., reference 12) shows that for carefully polished lightguides the experimental conditions were such as to deviate only slightly from those which we assumed, but that the deviations from our assumed conditions were considerable in the case of insufficiently smooth surfaces (see reference 14).

A separate report will be devoted to the results of experimental testing of the data obtained in this article.

APPENDIX

1. The integral (12) does not lead to elementary functions. Integration by parts leads to the expression

$$S = T - c(P - M), \quad (43)$$

where

$$T = \frac{e^{-cz_0}}{\sqrt{1+z_0^2}}; \quad P = \int_0^{\infty} \frac{e^{-cz}dz}{\sqrt{1+z^2}}; \quad M = \int_0^{z_0} \frac{e^{-cz}dz}{\sqrt{1+z^2}}. \quad (44)$$

The integral M can be evaluated by a series expansion considering the smallness of c or by a linearization of the function $(1 + z^2)^{-1/2}$ in the interval in question.

The integral P can be written in the form

$$P = \frac{\pi}{2}\left[\Omega_0(c) - N_0(c)\right], \quad (45)$$

where Ω_0 and N_0 are tabulated functions, namely: $\Omega_0(c)$ is the Lommel-Weber function; $N_0(c)$ is the Bessel function of the second kind (see, for example, reference 13).

2. For the approximate calculation of (22) (for n = 1.5) let us take $\xi = 1.12 - 0.5/l \approx 1.1$ in conformity with (17).

Since the major contribution to the magnitude of D is for not very large values of z, in the evaluation by Eq. (22) we can take

$$\sqrt{1+z^2} = 0.5 + 0.9z \quad (1 < z < 4), \quad (46)$$

which transforms (22) into (23).

3. Integration of (32) by parts leads to the expression

$$S' = B - c(R - Q), \quad (47)$$

where

$$B = \frac{e^{-cz_0}}{1+z_0^2}; \quad R = \int_0^{\infty} \frac{e^{-cz}dz}{1+z^2}; \quad Q = \int_0^{z_0} \frac{e^{-cz}dz}{1+z^2}. \quad (48)$$

The integral R can be written in the form

$$R = \mathrm{Ci}(c)\sin c + \cos c\left[\frac{\pi}{2} - \mathrm{Si}(c)\right], \quad (49)$$

where Ci(c) and Si(c) are the tabulated sine and cosine integrals (see reference 13).

The integral Q can be evaluated analogously to the integral M.

REFERENCES

1. A. C. S. van Heel. Nature 173, 39 (1954).
2. R. E. Hopkins and N. S. Kapany. Nature 173, 39 (1954).
3. N. S. Kapany. J. Opt. Soc. Am. 47, 413 (1957).
4. N. S. Kapany, J. A. Eyer, and R. E. Keim. J. Opt. Soc. Am. 47, 423 (1957).
5. N. S. Kapany and R. E. Hopkins. J. Opt. Soc. Am. 47, 594 (1957).
6. N. S. Kapany and J. N. Pike. J. Opt. Soc. Am. 47, 1109 (1957).
7. A. Timmerhaus, V. Giller, R. C. Duffield, and J. W. Drickamer. Nucleonics 6, No. 6, 37 (1950).
8. J. Koechlin. J. phys. radium 16, 849 (1955).
9. C. C. Harris and P. R. Bell. IRE Trans. on Nuclear Sci. NS-3, No. 4, 87 (1956).
10. P. A. Tove. Rev. Sci. Instr. 27, No. 3, 143 (1956).

11. R. Ettinger. Rev. Sci. Instr. 26, No. 8, 763 (1955).
12. A. Coche and G. Laustriat. J. phys. radium 19, No. 6, (1958).
13. E. Jahnke and F. Emde. "Tables of Functions." (Russian translation), Gosudarst. Izd. Tekh.-Teoret. Lit., Moscow-Leningrad, 1948.
14. R. M. Weinstein and H. V. Bradt. Rev. Sci. Instr. 30, No. 3, 206 (1959).

SHORT COMMUNICATIONS

PRESSED SAMPLES FOR INFRARED SPECTROMETRY

V. S. Akselrod

Received 14 September 1959

Pfund,[1] and later Barnes et al.[2] had shown that the decrease in the intensity of infrared radiation passing through powdered samples is due to the true (resonance) absorption of energy in the substance, if the linear dimensions of the grains d are significantly smaller than the wavelength λ. If the condition $d \ll \lambda$ is not satisfied, the refraction in the microcrystals causes increased scattering with subsequent lowering in intensity of the beam passing through the sample, even in the absence of true absorption by the substance. In general, the decrease in intensity of the radiant energy in the sample is determined by absorption and dispersion. The frequently observed nonsymmetric distortions of the absorption bands may be caused not only by the fact that the condition $d \ll \lambda$ is not satisfied, but also by a very large difference between the index of refraction of the grains and that of the medium.[3]

With a suitable choice of immersion the experimental curve may approximate the true absorption curve of the sample. A coincidence in the refraction indices of the sample and the medium gives rise to an absorption band which is symmetric with respect to the resonance frequency. In the absence of such coincidence the absorption maximum is shifted away from its true position. The degree of distortion of the absorption band is determined by the magnitude $R(n - 1)$, where R is radius of the particles and n is a complex relative index of refraction of the dispersed substance and the immersion medium.[3] These distortions are especially dangerous in the low wavelength region of the spectrum ($\lambda < 6\mu$ with $R \sim 1\mu$).

As well as possessing the required index of refraction, the substances which are used as immersions must have other characteristics such as being transparent over large spectral intervals, chemically inert, stable, and hydrophobic. An extensive use is being made of alkali halides as immersions (principally potassium bromide), which are pressed together with substances under investigation.[4] Such samples (in what follows, referred to as pellets) are characterized by transparency over wide spectral regions and by homogeneous distribution of the powdered substance. The latter quality results in a linear relationship between the optical density and the concentration of the substance. The main disadvantage of the pellets consists of the possibility of interaction between the alkali halide medium with some substances (usually containing hydroxyls).

In the present communication a method developed by us is described which allows one to obtain pellets of high quality for infrared spectroscopy.

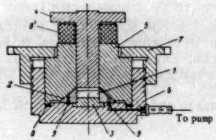

CONSTRUCTION OF THE DIE

The vacuum die, shown in the diagram, possesses good technical qualities. It provides for high quality of the samples, is easy to use, and is durable. Its design is analogous to the one published in reference 5. The matrix of the die is composed of several parts: massive steel cylinder, 5, with a conical cavity fits snugly onto the conical ring, 2. The latter, according to our observations, should be made out of a soft material (brass, duralumin-num). The bottom part of the working channel is formed by a small plunger, 3, which is made of tempered steel. Its surface, facing the sample to be pressed, 1, is polished to the desired degree of precision. The big plunger is also tempered and polished on the end plane. The sample chamber, 1, is connected to the vacuum pump by means of grooves and channels, 9, in the ring and the body, 6, of the die.

The hermetic tightness of the working channel is provided by a large size rubber vacuum gasket, 8′, and a thin ring, 8. The separate parts of the die are assembled together by means of the nut, 7, with the help of a wrench. The small plunger, 3, in our model lies freely in the cavity at the bottom of the body, 6, and is lifted up together with the ring. To separate these parts one has to turn them one with respect to the other with any standard wrench; for this reason parallel notches are provided both on the ring, 2, and on the plunger, 3. The instrumental steel U-10A* is recommended for the construction of the die.

*Editor's note: we are not sure of this symbol or trade name.

The effect of the conditions of pressing on the quality of samples is described in several papers (cf., for example, references 4 and 6). The magnitudes of pressure and of the time of applying and releasing the pressure chosen by us provide satisfactory and stable pellets.

These magnitudes are: pressure P = 7-8 · 10^3 kg/cm², the time of evacuation prior to pressing of the powder, 3 to 5 min (a vacuum of several tenths of mm Hg), the time of pressure development to the full load, 2 to 3 min. After some time of full load application, the pressure is released gradually (for 3-5 min), while evacuation is discontinued prior to the removal of the load. It must be noted that a poor vacuum results in the immediate or gradual clouding of the samples.*

*In contradiction with the opinion expressed in reference 7.

This clouding may be also traced to the poor fit between the conical ring and the matrix, which results in deformation of the ring in the die. After the ring is removed from the die the deformation gradually disappears, causing the formation of microscopic fissures in the sample. If, on the other hand, the fit between the conical ring and the matrix is satisfactory, the construction guarantees the transmission of the tension to which the ring is subjected under the load to the massive steel matrix. This provides for negligible deformation of the ring, compared to the deformation that would have resulted if a ring of the cylindrical type were used.

PREPARATION OF THE SAMPLES BEFORE PRESSING

The alkali halides which are used as immersions must be thoroughly purified. Thus potassium bromide should be of the highest purity (from the mechanical residues in prism manufacturing). The pulverization of potassium bromide was conducted manually in our experiments (in an agate mortar), as well as with the help of a vibratory grinder. This operation was carried out in a dry box.

The author wishes to express his gratitude to Y. I. Riskin for guidance in this work.

REFERENCES

1. A. H. Pfund. J. Opt. Soc. Am. **23**, 375 (1933).
2. O. Barnes, R. Rowling, O. Brattain, R. Robert, and R. Firestone. Phys. Rev. **47**, 792 (1935).
3. H. Primas and Hs. H. Gunthard. Helv. Chim. Acta **37**, 360 (1954).
4. M. M. Stimson and M. T. O'Donnell. J. Am. Chem. Soc. **74**, 1805 (1952).
5. F. Burchard. Z. Naturforsch. **9**, 276 (1954).
6. D. N. Ingebrighton and A. L. Smith. Anal. Chem. **26**, 1765 (1954).
7. N. Clauson-Kaas and P. Nedenskev. Acta Chem. Scand. **8**, 1088 (1954).

SIMPLE FORMULAS FOR THE EVALUATION OF ABERRATIONS OF A MIRROR OBJECTIVE

K. I. Tarasov

Received 21 September 1959

In the research laboratory it is often necessary to set up a model of a spectrograph, monochromator, or some other optical instrument. Spherical reflecting elements are thereby commonly used. In addition to being readily available, they are achromatic and have a good image quality. To estimate the expected image quality of such a system it is not necessary to trace exactly the passage of the rays through the system. It is sufficient to evaluate the third order aberrations using relatively simple formulas. In effect, the third order approximation formulas give a better insight into the performance of the system than the exact tracing.

Maksutov[1] derived formulas for the spherical aberration, coma, astigmatism, and the field curvature of a spherical mirror which coincides with the position of the aperture stop of the optical system (i.e., the element that limits the diameter of the light beam that passes through the system). In the praxis this condition occurs only very rarely. However, Maksutov's formulas can be readily rewritten for the general case, i.e., for an arbitrary position of the aperture stop within the optical system.

Let A be the relative aperture of the mirror, i.e., the ratio of the mirror diameter D to its focal length f′, and let ω be the field angle, i.e., the angle of the beam with the axis of the system. For the case considered by Maksutov the third order aberrations are given by the following expressions.

The radius of the circle of confusion of the lateral spherical aberration in the Gaussian image plane is given by

$$\rho_1 = -\frac{1}{64} A^3 f'. \qquad (1)$$

The radial length of the comatic tail is $3\rho_2$ and its largest width is $2\rho_2$, where

$$\rho_2 = -\frac{1}{16} A^2 \omega f'. \qquad (2)$$

Astigmatism and curvature of field are manifested by the fact that in the Gaussian image plane the image of a point is elongated into a line section of length

$$2a = -A\omega^2 f', \qquad (3)$$

which lies in the meridional cross section of the beam.

This astigmatic focus is formed by the rays lying in the sagittal plane of the mirror (normal to the plane of Fig. 1). In the sagittal cross section of the beam, closer to the mirror, lies a second astigmatic focal line of the same length. This focal line is perpendicular to the first one and is formed by the rays lying in the meridional plane of the mirror (that is, the plane of Fig. 1). The distance l_m, between the two focal lines (the astigmatic dis-

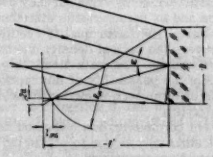

Fig. 1

tance, or astigmatism) is given by

$$l_{ms} = \frac{2a}{A} = -\omega^2 f'. \tag{4}$$

The second focal line lies on a surface which can be closely approximated by a spherical surface having its center between the focal surface and the mirror and having a radius of curvature equal to

$$R_m = -\frac{1}{2} f'. \tag{5}$$

For $\omega = 0$ (that is, on the axis of the mirror) this sphere is tangent to the Gaussian image plane.

To rewrite Eqs. (1) to (5) into a general form we will transform the position of the effective aperture stop onto a corresponding position on the mirror, for each field angle ω of the incident collimated light beam. Such a transfer in the position of the aperture stop which does not affect the path of the rays will naturally not cause any changes in the aberrations of the beam. It does, however, permit the use of Eqs. (1) to (5) for the general case if we only replace the field angle ω by a new field angle ω'. This new field angle depends on the actual field angle ω and on the actual position of the aperture stop. In deriving the new expressions we will assume that all angles are small so that they can be replaced by their tangents and vice versa.

The position of the aperture stop is determined by the distances H and t_0 of its center from the optic axis and from the vertex of the mirror respectively. From Fig. 2 it is seen that for small angles ω

$$\omega' = \omega + \Delta\omega,$$

where

$$\Delta\omega = \frac{H + \omega t_0}{-2f'}, \tag{6}$$

from which it follows that

$$\omega' = \omega - \frac{1}{2f'}(H + \omega t_0) = -\frac{\omega t_c + H}{2f'}, \tag{7}$$

where

$$t_c = -2f' + t_0$$

is the distance of the aperture stop from the center of curvature of the mirror.

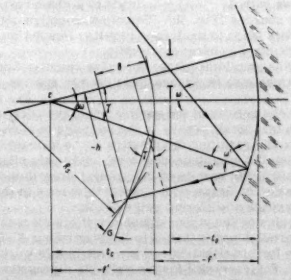

Fig. 2

Substituting in place of ω the expression for ω', as given by Eq. (7), into the Eqs. (1) to (5) we obtain the following results.

The spherical aberration is independent of the field angle ω and is therefore given, as before, by Eq. (1).

The coma is given by

$$p_2 = \frac{1}{32} A^2 (\omega t_c + H). \tag{8}$$

The length of the astigmatic focal line is

$$2a = \frac{-A}{4f'} (\omega t_c + H)^2. \tag{9}$$

The astigmatic difference is

$$l_{ms} = -\frac{1}{4f'} (\omega t_c + H)^2. \tag{10}$$

From the last equation it is seen that $l_{m,s} = 0$ when $\omega = -H/t_c$, that is, the two focal lines have a common point when the principal ray passes through the center of curvature of the mirror.

We will now determine the curvature of field. The sagittal focal line lies in a plane which is tangent to a sphere of radius $-f'$ with a center coinciding with the center of curvature of the mirror. The centers of the sagittal focal lines lie on a sphere. From symmetry considerations it can be seen that the center of curvature of this sphere must lie on the straight line joining the center of curvature of the mirror with the center of the aperture stop. We will now find the radius R_s of this sphere.

On the basis of simple geometrical considerations we find from Fig. 2 that

$$R_s = \frac{h^2}{2b}, \tag{11}$$

$$h = -\gamma f' - \omega' f', \tag{12}$$

$$\gamma = -\omega' \frac{t_0}{t_c}, \tag{13}$$

$$b = -\frac{(\gamma f')^2}{2f'} - \gamma\omega' f'. \tag{14}$$

Substituting Eqs. (12), (13), (14), and (7) into Eq. (11) we obtain

$$R_s = -\frac{4f'^3}{4f'^2 - t_c^2}. \tag{15}$$

The sagittal focal line intersects the tangent to this sphere at an angle

$$\sigma = \frac{-h}{R_s} - \gamma = -\frac{t_0}{4f'^2}(\omega t_c + H). \tag{16}$$

The meridional focal line lies on a sphere of radius

$$R_m = \frac{h^2}{2(b - l_{ms})} = -\frac{4f'^3}{4f'^2 - 3t_c^2}. \tag{17}$$

Equations (15) and (17) show that the astigmatic focal surfaces can be planes:

1. $R_s = \infty$ when $t_c = -2f'$, $t_0 = 0$ (starting case, when the position of the aperture stop coincides with the spherical mirror), and when $t_c = 2f'$, $t_0 = 4f'$.

2. $R_m = \infty$ when $t_c = \pm(2/\sqrt{3})f' = \pm 1.15f'$, that is, when $t_0 = 0.85f'$ and $t_0 = 3.15f'$.

The interesting case is when $R_s = R_m$. This occurs when $t_0 = 0$. Then,

$$p_2 = \frac{1}{32} A^2 H, \quad 2a = -\frac{AH^2}{4f'}, \quad l_{ms} = -\frac{H^2}{4f'}, \quad R_s = R_m = -f'$$

and the aberrations are independent of the field angle ω, that is, they are the same over the entire field of view. The sagittal and meridional focal surfaces have the same curvature except that their centers are displaced by $-H^2/4f'$. They coincide only when the center of the aperture stop coincides with the center of curvature of the mirror.

Equations (1), (8), (9), and (10) give the aberrations

of a single spherical mirror for an arbitrary position of the aperture stop. The dimensions of the image of a point are determined by the sum of the individual aberrations calculated for the given image plane.

REFERENCE

1. D. D. Maksutov. "Astronomicheskaya optika." (Astronomical Optics) Moscow, Leningrad, 1945.

ON THE POSSIBILITY OF USING AMPLITUDE-PHASE OBJECTIVES TO RESOLVE TWO NONMONOCHROMATIC LIGHT SOURCES

A. N. Ryazanov

Received 12 October 1959

A preceding work[1] considered the problem of increasing the resolving power of optical systems to resolve two light sources of the same order of intensity. Our theoretically calculated and constructed amplitude-phase objectives (more precisely, diaphragms) were a system of three or four pairs of slits arranged with a common axis of symmetry. Of these some pairs had a phase shift of π obtained by covering the corresponding slit with a layer of dielectric of the necessary thickness.

The stated phase shift had the given value only for the particular wavelength λ = 5461 A. It is therefore certainly not evident that the properties of the amplitude-phase objectives remain unchanged in the presence of nonmonochromatic light sources. Thus, it is of definite interest to investigate the intensity distribution in the focal plane of such objectives in the presence of a source of white light, and to determine the possibility of resolving two such sources unresolved by a single objective. The present paper carries out these aims.

A calculation of the intensity distribution in the focal plane of these objectives for λ = 6500 A and λ = 4500 A reveals that here the width of the zero maximum changes insignificantly. With respect to their intensities, for example, for an objective of three pairs of slits with relative transmission intensities $A_1^2 : A_2^2 : A_3^2 = 1 : 2.98 : 1.84$, for λ = 6500 A the intensity is equal to ~4.49 and for λ = 4500 A it is equal to ~8.56. This increase in intensity and also the moderate broadening of the zero maximum is accompanied by a decrease in the intensity of the nearest bright maxima. For λ = 5461 A the intensity of the zero maximum is assumed to equal 1. This explains the fact that upon visual observation of diffraction patterns from the amplitude phase objectives in white light the zero maximum has a blue tint. The shift of the nearest of the intense side maxima relative to one another for the given wavelengths is comparatively small, so that there is a real possibility for the practical use of these objectives in white light. For the plan of the apparatus see reference 1, Fig. 3. The light filter C is absent The same objectives were used as were used in the earlier work.[1]

In Fig 1 is presented a microphotogram of the zero maximum from a single slit objective. It is somewhat broader in comparison with the case of a monochromatic source (cf. reference 1, Fig. 4a). In Fig. 2, as an example, is presented the intensity distribution in the focal plane of an amplitude-phase objective, which for λ = 5461 A

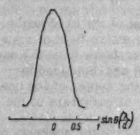

Fig. 1

Fig. 2

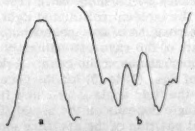

Fig. 3

satisfies the conditions $A_1 = -A_2 = A_3$. The scales under Figs. 1 and 2 give the values of $\sin\theta$ in units of λ/d (θ is the angle of diffraction); 2d = 4mm is the full width of the objective; λ = 5461 A. The curve in Fig. 2 is analogous to the corresponding curve in the earlier work[1] (cf. Fig. 5c). The intensity distribution in the focal plane of the amplitude-phase objectives with half-wave plates (for λ = 5461 A) on the corresponding slits, with three pairs of slits of relative transmission intensity $A_1^2 : A_2^2 : A_3^2 = 1 : 2.60 : 1.65$ and four pairs of slits with the relations $A_1^2 : A_2^2 : A_3^2 : A_4^2 = 1 : 5.1 : 4.2 : 1$, is also analogous to the corresponding curve in the earlier work[1] (cf. Figs. 5a and 5b). The smallest indices A_i correspond to the innermost pair of slits.

The central maxima, as is to be expected, are slightly broadened. The nearest intense side maxima are displaced a little farther than in Fig. 5[1] and apparently they correspond chiefly to red light. The photography was done with "panchrome" film. In Fig. 3a is presented a microphotogram of two sources of white light unresolved by a single objective. Replacement of the single objective by an objective with $A_1 = -A_2 = A_3$ leads to a clear resolution of the sources (Fig. 3b). Use of an objective with four pairs of slits leads to analogous results. Resolution of the sources can be observed visually.

Thus the amplitude-phase objective calculated for λ = 5461 A can also be successfully used to resolve white sources.

From the results of the earlier work[1] the conclusion was drawn that small errors in the intensity of each pair will change the resulting distribution in the diffraction pattern from the amplitude-phase objective only slightly. On the basis of the results of the present work this same conclusion can be drawn with respect to errors in the phase difference of different pairs of slits.

In conclusion the author considers it his pleasant duty to express sincere thanks to his supervisor K. D. Sinel'nikov for his attention and interest in this work, and to I. N. Shklyarevskii for his valuable discussions and constant attention.

REFERENCE

1. K. D. Sinel'nikov and A. N. Ryazanov. Opt. i Spektr. 5, 184 (1958).

THE RELATION OF ELECTRON TRANSITIONS IN IMPURITY MOLECULES TO LATTICE VIBRATIONS OF THE CRYSTALLINE SOLVENT

V. N. Vatulev

Received 16 October 1959

The low temperature absorption and luminescence spectra of many aromatic compounds that have been introduced into crystalline solvents as impurities consist of narrow bands of lines, wherein both the pure electronic transition and its combination with the molecular vibrations usually occur as groups of lines with different intensities, rather than single lines. The spectra of anthracene impurities in crystals of 9, 10-dihydroanthracene[1] are an example. The complexity of spectra of this kind is in part associated with the fact that different types of centers with several discrete transition energies can develop when a single impurity is introduced into the crystal. There are some rather conclusive experimental data[2] that verify this point. A second cause of the fine structure is the presence in the spectra of "lattice" lines. Their appearance is explained by the interaction of intramolecular transitions in the impurity molecules with lattice vibrations. An experimental proof of this statement for the case of 9, 10-dihydroanthracene with an anthracene impurity is put forth in this paper.

The spectra of a solid solution of anthracene in 9, 10-dihydroanthracene at 20°K are described in reference 1. A Hilger E_1 spectrograph was used to study the spectra. The changes that occur in the spectra when the impurity concentration is increased are also covered. In the spectra several series of lines are distinguished which can be related to different impurity centers. Here we show a photograph in which a group of satellites of a line corresponding to a pure electronic transition is seen in the absorption and luminescence spectra of the same crystal with low impurity concentration, and when for practical purposes there is present in the crystal only one type of center out of the number that can be successfully distinguished on the basis of concentration studies.[1] The photograph was taken with a DFS-3 spectrograph having a diffraction grating with 600 lines/mm. In view of the fact that the weakest satellites in the photograph are difficult to separate, a diagram of these portions of the spectrum is presented along with them.

In the figure the distances are shown (in cm^{-1}) from a pure electronic transition line to those satellite lines that are visible in these two photographs. Since the satellites are weak and situated in a high background, the precision with which their positions are resolved is significantly lower than for the location of the fundamental series lines. Nevertheless it is clearly seen from the figure that there is a mirrorlike similarity between these portions of the absorption and luminescence spectra. In the absorption spectrum more than ten satellites can be distinguished and all of them correspond to lines in the luminescence spectrum. It is also seen from the figure that some peculiarities in distribution of intensities that are observed in the absorption spectrum recur in the luminescence spectrum. On these grounds it can be asserted that in this case the mirror symmetry is not a result of a chance matching of the intervals between bands. The fact that this mirror symmetry of the satellites with respect to the pure electronic transition bands is present confirms the hypothesis that these lines are associated with one and the same absorption center (more accurately, to one type of center), but inasmuch as we are dealing with

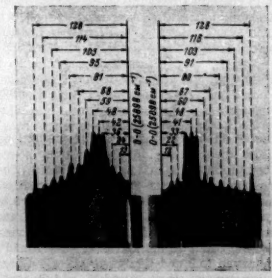

the low frequencies of the "gross" band, it is impossible to associate them with intramolecular vibrations. Proceeding from this, one can consider it experimentally verified that the appearance of some of the satellites in the impurity spectra depends on the interaction of intramolecular transitions with solvent lattice vibrations. In addition it should be noted that such an interaction can take place both with phonons and with local vibrations that have been reported[3] as arising when impurity molecules are introduced into the crystal lattice.

The fact that mirror symmetry of some of the satellites is not observed in other impurity spectra can be associated with two circumstances in particular. In the first place there are the reasons previously mentioned, i.e., the accuracy with which the positions of many satellites are resolved is not sufficient; in general some of them can remain unnoticed. In the second place along with the "lattice" satellites there often are lines related to other kinds of impurity centers, and these lines disrupt the mirror similarity of parts of the spectrum.

It was shown in the paper by Davydov and Rashba[4] that for interaction with phonons the spacing of "lattice"-associated satellites from lines due to the nonphonon transition must not correspond to the limiting frequency of the crystal branches, but to some intermediate frequency value.* For this reason it turns out to be impossible to distinguish the lattice lines by direct comparison of the distances between components of the fine structure with lattice vibration frequencies obtained from infrared spectra and Raman scattering spectra. From the example considered in this work it is clear that the phenomenon of mirror symmetry of satellites can in some cases be used as a spectral criterion for distinguishing "lattice" lines in impurity spectra.

*Reference 4 does not deal with impure crystals. However, it is pointed out that this conclusion carries over completely to the case of impurity absorption.

In conclusion I consider it my pleasant obligation to express my profound gratitude to A. F. Prikhot'ko for his scientific guidance, interest in the work, and helpful discussions, and also to E. I. Rashba for discussion of the results.

REFERENCES

1. V. N. Vatulev. Ukrain. Fiz. Zhur. 5, 40 (1960).
2. V. L. Broude, A. F. Prikhot'ko, and E. I. Rashba. Uspekhi Fiz. Nauk 67, 99 (1959).
3. I. M. Lifshits. Zhur. Eksptl. i Teoret. Fiz. 17, 1076 (1947);
A. F. Lubchenko. Ukrain. Fiz. Zhur. 1, 281 (1956).
4. A. S. Davydov and E. I. Rashba. Ukrain. Fiz. Zhur. 2, 220 (1957);
E. I. Rashba. Kand. diss., Inst. Fiz. Akad. Nauk Ukr. SSR Kiev, 1955.

INVESTIGATION OF N- AND O-COLOR CENTERS IN THE KCl:Tl CRYSTALLINE PHOSPHOR

P. A. Khellenurme

Received 5 November 1959

A series of absorption bands in the visible, infrared, and ultraviolet spectral regions, which arise at excitation, have been found in alkali halide crystals. To these bands correspond electronic-vibrational transitions in electron and hole color centers. In recent years the nature of the simplest electron color centers (F- and M-centers) has been studied from many points of view.[1-4] Weak absorption bands in the infrared were found[5] during a study of x-rayed KCl and KBr crystals. The corresponding color centers were called N- and O-centers. It is commonly considered that the N- and O-centers are constituted by electrons localized at lattice defects consisting of several negative and positive vacancies. The structure of these centers has not been ascertained in detail.

We have shown earlier the following result for thallium activated alkali halide crystals: stimulation after x-ray or ultraviolet excitation will result in an optical flash of Tl^+ ions not only in the F- and M-bands (cf. references 4 and 6) but also in the region of N- and O-absorption bands.[7-9]

Here we give certain results of an investigation of N- and O-centers in the crystalline KCl:Tl phosphor. The phosphors were excited in the short wavelength activator absorption band (196 mμ) by means of a spark with aluminum electrodes. The optical flash was recorded by means of the usual photoelectric apparatus, which we described earlier.[7]

Figure 1a contains the spectra of the stimulated optical flash of the KCl:Tl phosphor. The excitation of Tl^+ ion luminescence in F-, M-, N-, and O-absorption bands is clearly shown.

N- and O-bands are caused by electron color centers. This assertion is supported by the following experimental fact: after the N- and O-bands have been discolored, they can be easily re-established by irradiating the phosphor in the electronic F-band of absorption.

The finding of the optical flash of Tl^+ activator ions for excitation in the electronic N- and O-absorption bands indicates that the optical flash is a recombination luminescence. The electrons are stored on N- and O-capture levels of the host substance, while the act of radiation occurs within activator luminescence centers.[7]

The optical flash stimulated in the N- and O-bands can be completely frozen when the temperature of the excited crystal is lowered. Hence, as in the case of F- and M-centers,[4, 10, 11] we are dealing with a two-stage photothermal ionization of N- and O-centers. The N- and O-bands correspond to optical excitation, not to the optical ionization of the centers.

If the simplest associations of vacancies correspond to the N- and O-centers, then these centers must be anisotropic. Their anisotropy can be found from the appearance of dichroism in the region of the N- and O-bands after illumination of the crystal by polarized light. A direct investigation of N- and O- centers by means of absorption is made difficult by the need to deal with a very small concentration of centers and hence with small absorption. (This is particularly true for our method of exciting the crystal.)

The luminescence methods for dichroism investigation have great sensitivity (cf., for example, reference 10). Following Lushchik's suggestion we used the phenomenon of optical flash for a study of dichroism. For low absorption and quasi-monomolecular kinetics of the relaxation processes, the brightness of the optical flash is proportional to the absorption coefficient. Due to the great sensitivity of the method it becomes possible to study exceptionally weakly colored samples.

Figure 1a contains the results obtained in studying the KCl:Tl phosphors. The phosphor was excited and investigated at 180°K. The excited phosphor was illumi-

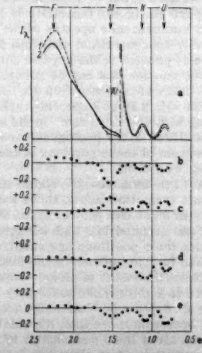

Fig. 1. Spectrum of the stimulated optical flash in the KCl:Tl phosphor after irradiation with linearly polarized light ([011]) with λ = 825 mμ. a—Curves 1 and 2 correspond to the orientation of the electric vector of the stimulating light along the directions [011] and [011] respectively. The "dichroism spectra" measured for the KCl:Tl phosphor after irradiation with linearly polarized light ([011]) are shown at b—λ = 825 mμ; c—λ = 560 mμ; d—λ = 1120 mμ; and e—γ = 1530 mμ.

nated through a UM-2 monochromator and a Nicol prism by a linearly polarized light beam with λ = 825 mμ (M-band) at normal incidence to the (100) plane. The electric vector was oriented in the [011] direction. After sufficiently prolonged irradiation, a measurement was made of the spectrum of optical flash stimulation of the luminescence of Tl^+ ions in the 305 mμ radiation band. The flash was stimulated by polarized light. Two measurements were made for each frequency of the stimulating light. In one case the electric vector was oriented in the [0$\bar{1}$1] direction (curve 2), in the other in the [011] direction (curve 1). The failure of curves 1 and 2 to overlap indicates the appearance of dichroism. Figure 1b gives the degree of dichroism

$$d = \frac{I_{\parallel} - I_{\perp}}{I_{\parallel} + I_{\perp}}$$

as a function of the stimulating light frequency. It represents a "dichroism" spectrum.

We see that the illumination of an excited KCl:Tl phosphor in the M-band causes the appearance of dichroism in the M-band. This effect is natural, since in a series of papers (cf., for example, reference 11) the M-centers have been shown to be anisotropic formations. Figure 1b shows, however, that simultaneously with the appearance of dichroism in the region of the M-band, there appears also dichroism of the same sign in the N- and O-bands* and dichroism of opposite sign in the F-band. (The latter effect was already observed earlier in absorption experiments.[12])

*In the region ~1.25 ev a minimum is observed in the dichroism spectrum. (Usually the degree of dichroism is constant within the boundaries of the elementary absorption band.) The overlap of the M- and N-absorption bands with the stable F-absorption band (extremely broad at 180°K) may possibly play a role here.

Figures 1c, d, and e show the "dichroism spectra" obtained by the method described above. These were measured for the KCl:Tl phosphor after illumination with polarized light ([011]) with λ = 560 mμ (F-band), 1120 mμ (N-band), and 1530 mμ (O-band, respectively. In all three cases we observed the appearance of dichroism not only in the absorption band in which the preliminary illumination by polarized light was carried out but in all the remaining bands as well.

If the KCl:Tl phosphor is subjected after excitation to additional heating which causes all color centers except the F-centers to disappear, then its irradiation by polarization light in the F-band does not result in the appearance of dichroism. (See also reference 12.) Presumably we are dealing with an induced dichroism of F-centers caused by the nearness of M-centers.

The nature of the dichroism of N- and O-centers, which we have found, is as yet not clear. We are probably dealing with induced dichroism in this case as well. We think that an important factor in this phenomenon is the migration of energy between closely lying F-, M-, N-, and O-centers. We found this effect in studying the "optical de-excitation spectra" of color centers in the KCl:Tl phosphor.* It was also found in reference 13 in a study of the spectra of excitation of infrared radiation of color centers in KCl. The polarization effects observed during the migration of energy between centers have not been explained so far and present a great deal of interest for the theory of energy migration.

*Our data were confirmed in reference 14.

In conclusion I wish to express my deep gratitude to Ch. B. Lushchik for his interest in this work and for his extremely helpful comments during its discussion. The author is also sincerely grateful to O. A. Shmit for helpful advice and comments.

REFERENCES

1. F. Seitz. Revs. Modern Phys. **26**, 7 (1954).
2. S. I. Pekar. "Issledovanie po elektronnoi teorii kristallov." (Investigation Concerning the Electronic Theory of Crystals), Moscow, 1951.
3. Ch. B. Lushchik. Trudy Inst. Fiz. i Astron., Akad. Nauk Eston.SSR No. 3, 3 (1955).
4. Ch. B. Lushchik, F. N. Zaitov, V. I. Kark, L. A. Teiss, and V. I. Yaek. "Mater. V Soveshch. po lyuminestsentsii. Kristallofosfory." (Proceedings of the Fifth Conference on Luminescence. Crystalline Phosphors), Tartu, 1957.
5. S. Petroff. Z. Physik **127**, 443 (1950); E. Burstein and J. Oberly. Phys. Rev. **76**, 1254 (1949); Ibid **86**, 799 (1952).
6. I. A. Parfianovich. Izvest. Akad. Nauk SSSR, Ser. Fiz. **15**, 669 (1951).
7. P. A. Khellenurme. Trudy Inst. Fiz. i Astron., Akad. Nauk Eston.SSR, No. 6, 132 (1957).
8. P. A. Khellenurme. Trudy Inst. Fiz. i Astron., Akad. Nauk Eston.SSR, No. 7, 340 (1958).
9. P. A. Khellenurme. Dokl. na VII Soveshch. po lyuminestsentsii (Report at the Seventh Conference on Luminescence), Moscow, 1958.
10. P. P. Feofilov. Zhur. Eksptl. i Teoret. Fiz. **12**, 328 (1942); Doklady Akad. Nauk SSSR **92**, 743 (1953); Ibid. **92**, 545 (1953).
11. M. Ueta. J. Phys. Soc. Japan **7**, 107 (1952).
12. O. A. Shmit. Izvest. Akad. Nauk SSSR, Ser. Fiz. **20**, 492 (1956); Opt. i Spektr. **2**, 755 (1957); C. Doorn and Y. Haven. Phys. Rev. **100**, 753 (1955); H. Kanzaki. Phys. Rev. **110**, 1063 (1958).
13. J. Lambe and W. Compton. Phys. Rev. **106**, 684 (1957).
14. W. Compton and C. Klick. Phys. Rev. **112**, 1620 (1958).

CALCULATION OF THE CHAMBER OF A BARO-OPTICAL SOURCE OF RADIATION

A. O. Sall'

Received 15 December 1959

In a previous work[1] a selective gaseous source of modulated radiation was described which was based on the emission from a gas whose temperature changed periodically when it was alternately compressed and expanded.

We shall carry out an approximate calculation of the depth of the chamber of such a source of radiation. For this purpose we shall first of all obtain the formula for the amplitude of the fluctuation of the average volume temperature of the gas and then the expression for the amplitude of the modulated radiation flux. In the first approximation we shall assume that the transfer of heat from the gas to the body of the chamber is accomplished principally through thermal conduction.[2, 4] Utilizing the relationships (2.1), (2.6), and (2.7) from reference 2 (which are correct also in the present case when the gas in the chamber is not exposed to a modulated light flux, i.e., when q = 0), we obtain

$$c_p \frac{\partial \vartheta}{\partial t} = \lambda \Delta \vartheta + \frac{\partial p}{\partial t} = \lambda \Delta \vartheta + \frac{P \vartheta}{V \vartheta t} \left[\frac{\int \vartheta dV}{T} - v \right], \qquad (1)$$

where c_p is the specific heat of unit volume of the gas, λ is the thermal conductivity of the gas, ϑ is the amplitude of fluctuation of the temperature of the gas, p is the acoustic pressure, P is the atmospheric pressure, T is the absolute temperature, V is the volume of the chamber, and v is the change in volume of the chamber taking place during the compression and expansion of the gas.

Considering a time dependence of the form $e^{i\omega t}$ we get

$$\Delta \vartheta - \frac{i\omega c_p}{\lambda} \vartheta + \frac{i\omega P \int \vartheta dV}{\lambda T V} - \frac{i\omega P v}{\lambda V} = 0. \qquad (2)$$

In the case of a harmonic time variation of the volume of the chamber we may write for the amplitude of the fluctuation of the average volume temperature

$$\left(\bar{\vartheta} = \frac{1}{V} \int \vartheta dV \right)$$

the following relationship

$$G \bar{\vartheta} + i\omega C \bar{\vartheta} + i\omega P v = 0. \qquad (3)$$

The material coefficients G and C, which depend on ω, we shall call respectively the heat conduction and heat capacity. For a sufficiently high frequency the heat capacity C is approximately equal to the heat capacity of the gas within the chamber (product of the specific heat at constant volume c_v and the magnitude of the volume V). Actually, if we integrate the above expression (2) term by term with respect to the volume, we find that for a sufficiently high frequency the result of the integration of the first term is considerably smaller than the integrals of the remaining terms. Taking this into account, we obtain the approximation

$$-c_v V \bar{\vartheta} = Pv.$$

The expression (3) takes the form $C\bar{\vartheta} = Pv$ for sufficiently large values of ω. Equating the last two expressions we obtain:

$$C \simeq c_v V.$$

We shall now derive an expression for the heat conduction G that is correct for a sufficiently low modulation frequency. For this case Eq. (2) takes the form

$$\Delta \vartheta + \frac{q}{\lambda} = 0, \qquad (4)$$

where

$$q = -\frac{i\omega P v}{V}.$$

Expression (4) agrees with Eq. (1) in reference 3, which allowed calculation of the temperature during the liberation of heat in the volume of a solid body or of a gas. Hence for the calculation of ϑ one may use formulas for G that are valid for the selective optical-acoustic radiation detector.[3-5] In these formulas $Q = qV = -i\omega Pv$. For instance, for a cylindrical chamber[4] we have

$$G \simeq 8\pi\lambda l + \frac{12\pi\lambda r^2}{l}, \qquad (5)$$

where r is the radius of the chamber window and l is the depth of the chamber.

In an approximate calculation of $|\bar{\vartheta}|$ from formula (3), one may, as in the case of the optical-acoustic radiation detector,[3] regard G to be the heat conduction corresponding to such a low frequency that the depth of penetration of the temperature vibrations[2] is significantly larger than the chamber dimensions, and regard C to be the heat capacity of the gas occupying the chamber.

If one considers the heat exchange by radiation between the gas in the chamber and its surroundings, then the expression (3) will take the form

$$(G + G_{rad.}) \bar{\vartheta} + i\omega C \bar{\vartheta} + i\omega P v = 0, \qquad (6)$$

where $G_{rad.}$ is the coefficient representing the heat exchange by radiation between the gas filling the chamber of the radiation source and its environment.

The amplitude of the modulated radiation flux is given by

$$|I| = |G_{rad.} \bar{\vartheta}| = \left| \frac{i\omega P v G_{rad.}}{G + G_{rad.} + i\omega C} \right| \simeq \frac{\omega P v G_{rad.}}{\sqrt{G^2 + (\omega C)^2}}. \qquad (7)$$

since usually $G_{rad.} \ll G$.

The conduction by radiation $G_{rad.}$ depends on the volule concentration of that component of the gaseous mixture filling the chamber which emits the radiation. For small values of the concentration the quantity of the emitting gas in the chamber is small, and hence there is little heat exchange by radiation. However, an excessive increase in the concentration of the emitting gas causes the radiation emitted from the central part of the chamber to be absorbed to a large extent in the inactive layer of gas close to the chamber window whose temperature is lower than that of the gas at the center of the chamber. Thus there exists a definite value of the concentration of the emitting component which corresponds to the maximum value of $G_{rad.}$.

One might mention, that for the optical-acoustic radiation detector there also exists a definite value of the concentration in the chamber of the radiation absorbing component, corresponding to the maximum sensitivity of the detector.[3, 5, 6]

For each given value of l the concentration of the emitting component can be chosen so that maximum emission from the gas is obtained. When this is so, $G_{rad.}$ will be considerably less dependent on l than will G and C. Therefore, we can show that to the first approximation the depth of the chamber must be such that the quantity $\sqrt{G^2 + (\omega C)^2}$ is a minimum.

Taking into account that $C = \pi r^2 l c_v$, calling the frequency of modulation f, and employing Eq. (5), we obtain for the optimum depth of the chamber

$$l_0 \simeq 1.2r\left[1 + \left(\frac{\pi c_v \delta f}{4\lambda}\right)^2\right]^{-0.25}. \qquad (8)$$

This expression fully agrees with the formula for the optimum depth of the light-receiving cylinder of the selective optical-acoustic radiation detector.[4] The derived formula is approximately correct also in the case of such large values of $\bar{\delta}$ that the heat exchange by radiation is not proportional to $\bar{\delta}$ but is given by a more complicated relationship.

It should be mentioned that the spectral width of the part of the spectrum in which the emission of the gas occurs depends on the depth of the chamber. In those cases where the calculated value of the depth of the chamber obtained from formula (8) does not provide the necessary spectral width, the depth of the chamber must be increased in an analogous way to that used in the case of the optical-acoustic radiation detector.[7]

If previously greatly expanded gas is compressed in such a way that the volume of the chamber is reduced several times, we can obtain a considerable rise in temperature of the emitting gas. This can be attained without an appreciable rise in temperature of the body of the chamber.

REFERENCES

1. A. O. Sall'. Opt. i Spektr. 7, 576 (1959); Optics and Spectroscopy 7, 355 (1959).
2. A. O. Sall'. Zhur. Tekh. Fiz. 25, 157 (1956).
3. A. O. Sall'. Zhur. Tekh. Fiz. 29, 324 (1959).
4. A. O. Sall'. Opt. i Spektr. 6, 219 (1959); Optics and Spectroscopy 6, 139 (1959).
5. A. O. Sall'. Opt. i Spektr. 6, 556 (1959); Optics and Spectroscopy 6, 355 (1959).
6. A. O. Sall'. Zhur. Tekh. Fiz. 29, 330 (1959).
7. A. O. Sall'. Opt. i Spektr. 7, 432 (1959); Optics and Spectroscopy 7, 278 (1959).

OPTICAL-ACOUSTIC EFFECT IN MERCURY VAPOR

P. I. Bresler and B. N. Ruzin

In references 1 and 2 observations of the optical-acoustic effect in the ultraviolet and visible regions of the spectrum were reported. The experiments were conducted with oxygen, nitrogen, acetylene, chlorine, and nitrogen dioxide. In reference 2 it was shown that in this case the mechanism of the optical-acoustic effect is complicated in comparison with that in the infrared region, because photodissociation of the molecule may play a definite role. It is also interesting to consider the possibility of optical-acoustic effects occurring in monatomic substances. For this purpose it is satisfactory to use mercury vapor, because its resonant absorption line lies in the near ultraviolet region (2536.7 A). In addition, mercury atoms, excited by ultraviolet radiation, become photochemically active, as a consequence of which the optical-acoustic effect (if it occurs) may appear in conjunction with photochemical reactions between the mercury vapor and the gases with which it is mixed.

In this connection we have conducted observations of the optical-acoustic effect in mercury vapor with the aid of the arrangement used in reference 2, with the difference that the absorption cell and the comparison cell were removed, and the optical-acoustic chamber was equipped with three connecting branches. To one of these branches was joined a glass vessel containing a small quantity of liquid mercury, and two others were used to fill the chamber with one gas or another which did not absorb ultraviolet radiation in the spectral region of the radiation source. The gas in the optical-acoustic chamber was maintained at atmospheric pressure. To create the necessary mercury vapor pressure in the chamber the whole arrangement was placed in a temperature bath and heated. The temperature used ranged from 18 to 36 C. A mercury-quartz lamp of the type PRK-4, fed from a high frequency generator, was used. With this method of supplying the lamp most of its radiation occurs at 2537 A, which practically excludes the phenomenon of self-reversal. We also note that the intensity of radiation from the lamp under this condition does not change with time.

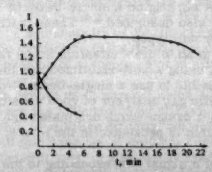

Measurements made with the above-described arrangement showed that as the chamber is filled with air or argon the optical-acoustic effect gradually diminishes from the start of the exposure and practically vanishes in the course of approximately 4-5 min. Cutting off the exposure (with the aid of a shield in front of the optical-acoustic chamber) during the time necessary for diffusion of the mercury vapor into the light-receiving chamber, led to the restoration of the original magnitude of the optical-acoustic effect, and the whole process was repeated. It should be noted that this phenomenon took place even when drops of mercury were present in the light receiver itself. This latter circumstance apparently may be explained by the fact that evaporation and diffusion of mercury appear to be quite slow processes.

In the case when the chamber was filled with hydrogen, the reverse phenomenon took place: the optical-acoustic effect gradually increased, reached a stationary state (approximately one and a half times the effect in air) and started to decrease slowly only 20 min after the beginning of exposure. The dependence of the magnitude of the optical-acoustic effect I (in arbitrary units) from the time of filling the optical-acoustic chamber with air (lower curve)

and with hydrogen (upper curve) is presented in the figure. We note that in raising the temperature in the thermostat to 36°C, i.e., increasing the mercury vapor pressure in the optical-acoustic chamber approximately four times, the generated signal increases by a factor of about two.*

*A very strong effect was observed when the lamp was excited from the line. However, as a consequence of the self-reversal of the line at 2537 A and weakening of radiation in this region as the lamp heated up, the magnitude of the effect rapidly decreased, starting from the time the lamp was turned on. Hence accurate observations were impossible with this setup.

Interpretation of the results requires additional investigation; however, it is already clear that even a preliminary qualitative explanation requires examination of the photochemical reactions that may take place under the experimental conditions. In particular, the decrease with time of the optical-acoustic effect in air may be explained by the oxidation of mercury vapor during the half-period of exposure occurring considerably faster than the restoration of vapor pressure by diffusion into the light-receiving chamber. The analogous situation upon filling the optical-acoustic chamber with argon may be explained in the same way, since for the oxidation reaction only an insignificant amount of oxygen impurity in the argon is required. The fact that the optical-acoustic effect is larger in hydrogen and that its magnitude decreases considerably more slowly with time, may be explained by a photochemical reaction of mercury vapor with hydrogen, leading to dissociation of the hydrogen molecule, as well as by a sensitization of the mercury vapor by the exothermic reaction between the hydrogen and the oxygen present in it as an impurity. Both of the indicated reactions may lead to an increase of optical-acoustic effect as well as an increase in the time interval during which the effect can be observed, in view of the fact that in these reactions the mercury atoms do not enter into stable compounds with the corresponding gases.

REFERENCES

1. Ya. I. Gerlovin. Opt. i Spektr. 7, 571 (1959); Optics and Spectroscopy 7, 352 (1959).
2. P. I. Bresler and B. N. Ruzin. Opt. i Spektr. (in press).

A SINGLE-BEAM OPTICAL-ACOUSTIC GAS ANALYZER

M. L. Veingerov and A. A. Sivkov

Received 12 January 1960

The current widespread optical-acoustic gas analyzers are based on the double-beam principle. Recently, gas analyzers working on a single-beam two-channel scheme were also described.[1,2] These instruments are differential or null types.

Here we wish to draw attention to the fact that at the present time, using a well-stabilized and linear amplifier, it is possible to use a single-beam single-channel optical-acoustic gas analyzer of good sensitivity and accuracy, using a design which originated more than 20 years ago, which is presented in the figure, taken from reference 3.

Instead of a signal corresponding to the second comparison channel of normal gas analyzers, we used a voltage from the auxiliary stabilized source, applied to a constant current measuring instrument (the amplifier is provided with a rectifier).

Schematic of the Optical-Acoustic Analyzer. 1—source of the radiation, 2—chopper, 3—gas cell, 4—optical-acoustic detector, 5—window, transparent for infrared radiation, 6—microphone, 7—amplifier, 8—constant-current-measuring instrument.

This voltage is equal and opposite in sign to the voltage from the output of the amplifier, when there is no gas under examination in the absorption cell. The readings of the apparatus correspond then to a difference between the compensating signal and the signal produced with gas in the cell, and the calibration curve has the usual form.

Such a construction eliminates difficulties with the realization of sufficiently complete compensation of the optical-acoustic signals or with the changes of current or voltage, produced by the microphones, corresponding to them.

REFERENCES

1. M. L. Veingerov, A. A. Sivkov, and A. S. Baryshnikova. Opt. i Spektr. 1, 1024 (1956).
2. M. D. Liston, A. J. Andreatch, and C. Beebe. ISA Journal 4, 118 (1957).
3. M. L. Veingerov. Doklady Akad. Nauk SSSR 51, 191 (1946); M. L. Veingerov. Comp. Rend Acad. Sci. URSS 51, 195 (1946).

A MONOCHROMATOR WITH AN AMMONIUM DIHYDROGEN PHOSPHATE PRISM

A MONOCHROMATOR WITH AN AMMONIUM DIHYDROGEN PHOSPHATE PRISM

V. N. Vishnevskii and N. A. Romanyuk

Received 10 November 1959

Among the materials suitable for the manufacture of optical components, the optically inactive ammonium dihydrogen phosphate (ADP) crystal is interesting. In the visible region of the spectrum it has an ordinary ray refractive index slightly inferior to that of crystalline quartz, and it has also considerable birefrigence.[1-6] Use of the crystal is recommended for the manufacture of polarizers for the visible spectrum,[3] certain components for infrared devices,[7, 8] and also for crystalline light filters.[9] In the present paper we show the possibility of using it for manufacturing dispersing prisms for inexpensive spectral apparatus to be used in the ultraviolet region.

The refractive indices n for the ordinary and extraordinary rays in the range 3500-8000 A are given in the literature. We have made careful measurements of n for the ordinary ray, extending the range of measurements into the ultraviolet. The measurements were carried out in the range 2500-6700 A by the diffraction method.[10] We used an ISP-22 spectrograph; in the ultraviolet region our light source was a hydrogen lamp, in the visible it was a powerful incandescent lamp.

The refractive index n of a crystal at a given wavelength λ was determined from readings taken on the spectrograms by using the relation

$$d(n - n_B) = m\lambda, \qquad (1)$$

where n_B is the refractive index for air for wavelength λ, d is the thickness of the plate being investigated and m is the order of the interference fringe on the spectrogram.

In the plates investigated the optic axis of the crystal coincided with the normal to the surface of the plate, which was placed exactly perpendicular to the incident beam. This normal incidence was obtained by autocollimation. The thickness of the polished plates d and the order of the interference fringe m were determined spectrographically by using the data given in the literature for n in the visible region of the spectrum.[4, 5]

Figure 1 gives the curve $n = n(\lambda)$ (solid line) constructed from the data of measurements on four ammonium dihydrogen phosphate crystals grown in different laboratories from solution by the planetary method. The thickness of the plates investigated varied from 0.1162 to 0.2331 mm. The curve was constructed on the basis of more than nine hundred experimental points. We determined the precision of an individual measurement in the ultraviolet range to be 1-2 units in the fourth place after the decimal point. The figure shows the values of n taken from the literature; the solid dots indicate results taken from reference 2, the open circles, from reference 3. The cross gives a result taken from 4. The curve obtained supports the view that the values of n given in references 2-4 are only reliable in the range $\lambda > 4000$ A. Indeed, the only measured value of n known to us in the ultraviolet region for $\lambda = 3500$ A[3] is clearly too low. On the same figure the broken curve shows the variation of the refractive index for a similarly oriented quartz crystal.[5, 6]

The curve for ammonium dihydrogen phosphate is approximated well by the dispersion equation:

$$n^2 = 1 + \frac{B\lambda^2}{\lambda^2 - a^2} + \frac{D\lambda^2}{\lambda^2 - b^2} \qquad (2)$$

where B = 1.298, D = 0.179, a = 9.9×10^{-6} cm and b = 2.5×10^{-4} cm.

Figure 2 shows the results of measuring the absorption of the crystal. The absorption coefficient k was determined from the relationship $I = I_0 \exp(-kd)$ where I_0 and I are the intensities of a beam of monochromatic radiation before and after passing through the crystal of thickness d in the direction of its optic axis. The curve shown was obtained for a crystal of thickness 4 cm with a photoelectric spectrophotometer built up from a KSA-1 spectrograph and a UM-2 monochromator. The light sources were the same as for the measurements of refractive index.

It follows from Figs. 1 and 2 that, in the spectral region investigated, an ammonium dihydrogen phosphate crystal has a considerable refractive index and a high transmission for rays in the direction of the optic axis. In addition, Fig. 1 and analysis of Eq. (2) show that the dispersion of the refractive index $dn/d\lambda$ for the crystal exceeds the dispersion of a specimen of similarly oriented crystalline quartz.

These facts permit us to suggest using ADP crystals in some cases for manufacturing ultraviolet optics.

To verify this possibility directly, we made 60° prisms with a 40 mm base out of uniform crystals. The prisms were placed in turn in a specially made Wadsworth type monochromator with mirror objectives, F = 325 mm. To avoid the damaging effect of atmospheric moisture on the polished surfaces of the prisms, the whole of the apparatus, including both slits, was enclosed in a hermetically sealed box with two UViol windows placed in front of the input and output slits. The region within the box was dried.

The angular and linear dispersions were calculated and measured experimentally for this apparatus in the spectral range 2500-6700 A.

In Fig. 3 the solid dots and the open circles show the experimentally determined spectral variation of angular

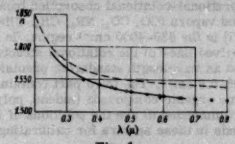

Fig. 1

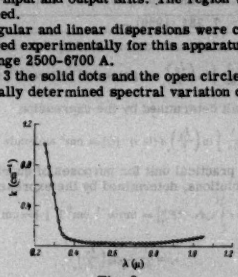

Fig. 2

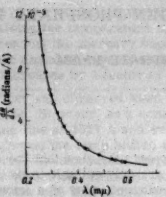

Fig. 3

dispersion for two of the prisms studied. The curve shows the calculated variation of the dispersion. In both cases calculation and experiment apply to prisms in which the bisector of the angle of refraction is perpendicular to the optic axis of the crystal.

The apparatus that we made has been in use for more than two years during which no deterioration of the polished prism surfaces has been observed.

Figure 4 shows spectrograms of the radiation of a PRK-4 mercury lamp obtained with an ISP-22 spectrograph, a—with a quartz prism, b—with a prism of the crystal studied. The spectra were brought into coincidence at λ = 3600 A. Spectrogram b was taken with the photographic plate 14 cm closer to the camera lens than for spectrogram a.

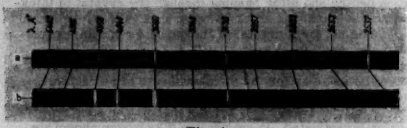

Fig. 4

Comparing the data of Figs. 3 and 4 with the calculated data of the same characteristics for similar apparatus with a crystalline quartz prism, we see that for certain cases where dispersing prisms have to be manufactured for inexpensive spectral equipment intended for the near ultraviolet, the use of ammonium dihydrogen phosphate crystals instead of expensive crystalline quartz is completely possible.

In conclusion the authors thank F. M. Alemalkin, who placed several ammonium dihydrogen phosphate crystals at their disposition.

Student V. M. Smetana took part in this work.

REFERENCES

1. M. H. Senarmont. An. Chem. et Phys. ser. 3, 33, 391 (1851).
2. H. Topsoe and C. Christiansen. Ann. Phys. Chem. Ergaenzungsband 6, 499 (1874).
3. I. Solc. Czechoslov. J. Phys. 5, 230 (1955).
4. B. H. Billings. J. Opt. Soc. Am. 42, 14 (1952).
5. Landolt-Börnstein. "Physik-chem. Tabellen," 5 Aufl., Vol. 2, pp. 915, 927, 1923.
6. International Critical Tables, New York, Vol. 6, p. 342, 1929; Vol. 7, p. 19, 1930.
7. V. A. Osipov. Optiko-Mekh. Prom. No. 1(?), 10 (1956).
8. S. S. Ballard and K. A. McCarthy. Nuovo Cimento, Suppl. 2, Ser. 10, No. 3, 648 (1955).
9. I. Solc. Czechoslov. J. Phys. 9, 237 (1959).
10. I. V. Obreimov. "O prilozhenii frenelovoi difraktsii dlya fizicheskikh i tekhnicheskikh izmerenii." (The Application of Fresnel Diffraction to Physical and Engineering Measurements), Izd. Akad. Nauk SSSR, Moscow, Leningrad, 1945.

EVENTS

DECISIONS OF THE INTERNATIONAL COMMISSION FOR MOLECULAR SPECTROSCOPY

On August 27-28 in Munich (West Germany) and on September 7 and 9, 1959, in Bologna (Italy), successive official meetings of the Commission for Molecular Spectroscopy of the International Union of Pure and Applied Chemistry (IUPAC) were held, at which decisions were made on the following questions:

1. Units for intensity measurements in infrared spectra

The following symbols were recommended for the units of integrated intensity previously introduced:*

*Opt. i Spektr. 7, 281 (1959).

A—the absolute unit, determined by the expression

$$A = \frac{1}{bn}\int \ln\left(\frac{I_0}{I}\right)_\nu d\nu, \quad [A] = \text{cm}^2\ \text{molecule}^{-1}\ \text{sec}^{-1}.$$

Q—the unit determined by the expression

$$Q = \frac{1}{bn}\int \ln\left(\frac{I_0}{I}\right)_\nu d\,(\ln\nu), \quad [Q] = \text{cm}^2\ \text{molecule}^{-1}.$$

$E^{\nu_2}_{\nu_1}$—the practical unit for purposes of quantitative analysis of solutions, determined by the expression

$$E^{\nu_2}_{\nu_1} = \int_{\nu_1}^{\nu_2} \varepsilon_\nu d\nu, \quad \left[E^{\nu_2}_{\nu_1}\right] = \text{mole}^{-1}\ \text{cm}^2\ \text{l}, \quad [\nu] = \text{cm}^{-1},$$

$$\varepsilon_\nu = \frac{1}{bc}\log_{10}\left(\frac{I_0}{I}\right)_\nu;$$

It was recommended that the limits of integration ν_1 and ν_2 be attached to the symbol E in every case.

2. Wavelength standards for the infrared region

The Commission recommended for publication, as a guide, the report of the Subcommission for Wavelength Standards. The report was composed by a North American group, the basic work being carried out by R. C. Lord, E. K. Plyler, R. N. Jones, and R. Brattain with the cooperation of the following organizations: National Bureau of Standards, National Research Council of Canada, Massachusetts Institute of Technology, U. S. National Science Foundation, and Shell Development Co. The report consists of four parts. The first part contains wavelength standards for the calibration of high-resolution spectral apparatus in the 6600-45000 A region, with a precision of 10^{-7}. The emission spectra of Ne, Ar, Kr, Xe, Cd, and Hg^{198} are used as standards. The second part represents an atlas of vibrational-rotational absorption bands of some gases and vapors (CO, CO_2, NH_3, CH_4, CH≡CH, H_2O, HBr, HCl) in the 630-4000 cm^{-1} region. In this case, individual resolved lines of the rotational structure of the bands are used as wavelength standards; precision 10^{-3}, resolution 0.06-0.9 cm^{-1}. The third part contains standard spectra of some organic compounds (indene, polystyrene, etc.); it is recommended to use the positions of individual absorption bands in these spectra for calibrating prism

spectrometers of medium and low dispersion. The fourth part includes standards for the far infrared region (below 600 cm^{-1}). It is planned to publish Parts I and II in final form in 1960, and Parts III and IV somewhat later.

3. Unification of terminology and units

A report by J. Lecomte (France) containing a list of corresponding English, French, and German terms used in molecular spectroscopy was considered. The Commission proposed to extend the list, adding to it the corresponding Japanese and Russian terminology.

The Commission also discussed the problems of unification of terminology and methods of intensity measurement in infrared spectra, optical activity, nuclear magnetic resonance, measurements in the vacuum ultraviolet region, etc. The preparation of corresponding recommendations during the current year is contemplated.

V. Nikitin

ABBREVIATIONS FOR JOURNALS, PLACES, ETC. OFTEN REFERRED TO IN "OPTICS AND SPECTROSCOPY"**

Doklady Akad. Nauk SSSR - Proceedings of the Academy of Sciences of the USSR

Izvest. Akad. Nauk SSSR - Bulletin of the Academy of Sciences of the USSR
Ser. Fiz. - Physical Series
Ser. Mat. - Mathematical Series
Otdel Khim. Nauk - Chemical Sciences Section

Uspekhi Fiz. Nauk - Advances in Physical Sciences

Uspekhi Khim. - Advances in Chemistry

Zhur. Eksptl. i Teoret. Fiz. - Journal of Experimental and Theoretical Physics

Zhur. Tekh. Fiz. - Journal of Technical Physics

Zhur. Obshchei Khim. - Journal of General Chemistry

Zhur. Priklad. Khim. - Journal of Applied Chemistry

Zhur. Russ. Fiz.-Khim. Obshchestva - Journal of the Russian Physical-Chemical Society

Zhur. Fiz. Khim. - Journal of Physical Society

Trudy Fiz. Inst., Akad. Nauk SSSR, Fiz. Inst. im. P.N. Lebedev - Transactions of the Institute of Physics, Academy of Sciences of the USSR, named for P.N. Lebedev

Trudy Fiz.-Tekh. Inst., Akad. Nauk Uzbek. SSR - Transactions of the Physico-Technical Institute, Academy of Sciences of the Uzbek SSR

Trudy Inst. Krist., Akad. Nauk SSSR - Transactions of the Institute of Crystallography, Academy of Sciences of the USSR

Trudy Inst. Nefti, Akad. Nauk SSSR - Transactions of the Petroleum Institute, Academy of Sciences of the USSR

Trudy Gosudarst. Opt. Inst., Leningrad - Transactions of the Optical Institute in Leningrad

Trudy Inst. Fiz. i Astron., Akad. Nauk Eston. SSR - Transactions of the Institute of Physics and Astronomy, Academy of Sciences of the Estonian SSR

Trudy Inst. Fiz., Akad. Nauk Ukr. SSR - Transactions of the Institute of Physics, Academy of Sciences of the Ukrainian SSR

Trudy Vsesoyuz. Nauch.-Issledovatel. Inst. Metrol. - Transactions of the All-Union Scientific Research Institute of Meteorology

Vestnik Leningrad. Univ. - Bulletin of the Leningrad University
Ser. Fiz. i Khim. - Series on Physics and Chemistry

Vestnik Moskov. Univ. - Bulletin of Moscow University
Ser. Fiz.-Mat. i Estestven. Nauk - Series of Physical-Mathematical and Natural Sciences

Uchenye Zapiski Leningrad. Gosudarst. Univ. im. A. A. Zhdanov - Scientific Reports of the Leningrad State University named for A. A. Zhdanov
Ser. Fiz. Nauk - Series on the Physical Sciences
Ser. Khim. Nauk - Series on the Chemical Sciences

Uchenye Zapiski, Moskov. Gosudarst. Univ. im. M. V. Lomonosova - Scientific Reports, M.V. Lomonosov Moscow State University

Uchenye Zapiski Tomsk. Gosudarst. Univ. in. V. V. Kuibysheva - Scientific Reports of the Tomsk State University named for V. V. Kuibyshev

Opt. i Spektr. - Optics and Spectroscopy

Pribory i Tekh. Eksp. - Instruments and Technique of Experiment

Astron. Zhur. - Astronomical Journal

Fiz. Metal. i Metalloved., Akad. Nauk SSSR, Ural. Filial - Physics of Metal and Metallography, Academy of Sciences of the USSR, Ural Branch

Priborostroenie - Instrument Manufacturing

Zavodskaya Lab. - Factory Laboratory

Radiotekhnika - Radio Engineering

Radiotekh. i Elektron. - Radio Engineering and Electronics

Inzhener.-Fiz. Zhur., Akad. Nauk Belorus. SSR - Engineering-Physics Journal, Academy of Sciences of White Russian SSR

Ukrain. Fiz. Zhur. - Ukrainian Physics Journal

Automat. i Telemekh. - Automatics and Telemechanics

Nauch.-Issledovatel. Fiz.-Tekh. Inst., Leningrad. Univ. - Scientific Research Institute of Physics and Technology, Leningrad University

Nauch.-Issledovatel. Radio-fiz. Inst., Gor'kii Univ. - Scientific Research Institute of Radiophysics, Gorki University

Gorkov. Issledovatel. Fiz. Tekh. Inst. - Gorki Research Institute of Physics and Technology

Gosudarst. Izd. Tekh.-Teoret. Lit. - State Publishers of Technical-Theoretical Literature

Gosudarst. Izd. Fiz.-Mat. Lit.- State Publishers of Physical-Mathematical Literature

**These abbreviations must be used by OiS translators in their translations. This list will be added to from time to time.

(FILLER MATERIAL - NOT IN RUSSIAN ORIGINAL)

Gosudarst. Opt. Inst. - State Optical Institute

Moskov. Fiz.-Tekh. Inst. - Moscow Physico-Technical Institute

Izd. Inostrannoi Lit. - Publishers of Foreign Literature

Izd. Akad. Nauk SSSR - Academy of Sciences Press

Inst. Fiz., Akad. Nauk Ukr. SSR, Kiev - Institute of Physics, Academy of Sciences of the Ukrainian SSR, Kiev

Inst. Fiz. i Astron., Akad. Nauk Eston. SSR, Tartu - Institute of Physics and Astronomy, Academy of Sciences of the Estonian SSR, Tartu

THE OPTICAL SOCIETY OF AMERICA

Why should you join OSA?

There is no other association of opticists in existence to promote and disseminate knowledge in this field. The Optical Society of America was organized in 1916 "to increase and diffuse the knowledge of optics in all its branches pure and applied, to promote the mutual interests of investigators of optical problems, of designers, manufacturers and users of optical instruments and apparatus of all kinds, and to encourage co-operation among them".

What about the advantages of membership?

You receive three monthly publications:

THE JOURNAL OF THE OPTICAL SOCIETY OF AMERICA: *This is the official publication of OSA*

OPTICS AND SPECTROSCOPY: *an English translation of the leading scientific journal of the USSR Academy of Sciences in this field*

PHYSICS TODAY: *as OSA is a member society of the American Institute of Physics, OSA members receive this publication**

From JOSA and OPTICS AND SPECTROSCOPY you will not only learn what your American colleagues are doing, but also discover what the Russians are working on in your field. Together these two journals publish the work of American and Russian scientists in all branches of optics and spectroscopy, including X-ray, ultraviolet, visible, infrared and microwave, filters, lens design, thin layer optics, geometric optics, electron optics, diffraction gratings, electroluminescence, wave mechanics, thermal radiation backgrounds, detectors, infrared polarizers, and their many applications in science and industry.

You will also receive announcements and programmes of all meetings (OSA holds at least two a year) and, even if you cannot attend many of these, you will know what is going on in your area. And you can submit a paper and have it given by proxy.

Who can join?

OSA invites to membership all who are interested in any branch of optics, either in research, in teaching, in optical applications, in the manufacture and distribution of optical equipment of all kinds, or in physiological and medical optics.

What are the membership dues? $13.00 per annum.

How can you join?

Write Dr. Mary E. Warga, Executive Secretary, Optical Society of America, 1155 16th Street, N. W., Washington 6, D. C., for an application form.

*OSA members may also subscribe to other AIP publications at a reduced rate.

OPTICAL SOCIETY *of* AMERICA

1155 SIXTEENTH STREET, N. W. WASHINGTON 6, D. C.

TRANSLITERATION OF CYRILLIC CHARACTERS

used by the Optical Society of America

А	а	a	Р	р	r
Б	б	b	С	с	s
В	в	v	Т	т	t
Г	г	g	У	у	u
Д	д	d	Ф	ф	f
Е	е	e	Х	х	kh
Ж	ж	zh	Ц	ц	ts
З	з	z	Ч	ч	ch
И	и	i	Ш	ш	sh
Й	й	i	Щ	щ	shch
К	к	k	Ъ	ъ	"
Л	л	l	Ы	ы	y
М	м	m	Ь	ь	'
Н	н	n	Э	э	e
О	о	o	Ю	ю	yu
П	п	p	Я	я	ya

(FILLER MATERIAL - NOT IN RUSSIAN ORIGINAL)

EDITOR'S NOTE

Comments on the scientific content of the translated Russian articles published in OPTICS AND SPECTROSCOPY are invited. They should be addressed as a Letter to the Editor of the Journal of the Optical Society of America and forwarded to the Editor of that journal, Dr. W. R. Brode, National Bureau of Standards, Washington 25, D.C.

VOL. VIII, NO. 5 OPTICS AND SPECTROSCOPY MAY 1960

CONTENTS

Spectroscopic Investigation of the State of the Gas Behind a Shock Wave. II ... F. S. Faizullov, N. N. Sobolev, and E. M. Kudryavtsev 311
Theory of the Infrared Spectral Intensities of Deuteroethylenes. VII ... L. M. Sverdlov 316
Spectroscopic Investigation of the Hydrogen Bond in Acid Silicates and Phosphates ... Ya. I. Ryskin and G. P. Stavitskaya 320
Vibrational Spectra of Alkoxysilanes and Siloxanes III. Vibrations of Silicon-Oxygen Chains in the Spectra of Polyalkoxysiloxanes ... A. N. Lazarev and M. G. Voronkov 325
The Temperature Dependence of the Dispersion and Absorption of Light in Molecular Crystals I. Theory ... V. L. Strizhevskii 329
Absorption Spectra of Benzene Homologues IV. Peculiarities of Crystal Spectra ... V. L. Broude and M. I. Onoprienko 332
Spectroscopic Study of the Processes of Vibrational Energy Transformation of Complex Molecules in Collisions I. On the Determination of the Amount of Energy Transferred and the Efficiency of Collisions ... B. S. Neporent and S. O. Mirumyants 336
On the Theory of Luminescence Quenching in Liquid Solutions ... Yu. A. Kurskii and A. S. Selivanenko 340
On the Concentration Depolarization of the Phosphorescence of Organoluminophors ... P. I. Kudryashov and B. Ya. Sveshnikov 344
Peculiarities of the Luminescence of Ortho-Disubstituted Aromatic Hydrocarbons III. The Fluorescence and Absorption Spectra of Some Carboxylic Acids ... Yu. V. Naboikin, B. A. Zadorozhny, and E. N. Pavlova 347
Thermoluminescence and the Localized Levels of ZnS:Mn Phosphors ... V. L. Levshin and V. F. Tunitskaya 350
Luminescence of Unactivated CsI Crystals. II ... Z. L. Morgenshtern 355
Development of a Method for Determining Relaxation Time using a Spectrophone. II. Eliminating the Instrumental Phase Shifts ... P. V. Slobodskaya and E. S. Gasilevich 358
A Comparison of Light Scattering Functions of Spherical Particles ... Yu. V. Mal'tsev 362
Study of Aberrations of a Concave Grating under Defocusing Conditions ... A. I. Kozlenkov 365
Comparison of the Rayleigh and Jamin Types of Interferometers ... Yu. V. Kolomiitsov 370
Passage of Light Through Lightguides ... A. R. Daich, Yu. A. Tsirlin, and L. E. Pargamanik 375

SHORT COMMUNICATIONS

Pressed Samples for Infrared Spectrometry ... V. S. Akselrod 379
Simple Formulas for the Evaluation of Aberrations of a Mirror Objective ... K. I. Tarasov 380
On the Possibility of using Amplitude-Phase Objectives to Resolve Two Nonmonochromatic Light Sources ... A. N. Ryazanov 382
The Relation of Electron Transitions in Impurity Molecules to Lattice Vibrations of the Crystalline Solvent ... V. N. Vatulev 383
Investigation of N- and O-Color Centers in the KCl:Tl Crystalline Phosphor ... P. A. Khellenurme 384
Calculation of the Chamber of a Baro-Optical Source of Radiation ... A. O. Sall' 386
Optical-Acoustic Effect in Mercury Vapor ... P. I. Bresler and B. N. Ruzin 387
A Single-Beam Optical-Acoustic Gas Analyzer ... M. L. Veingerov and A. A. Sivkov 388
A Monochromator with an Ammonium Dihydrogen Phosphate Prism ... V. N. Vishnevskii and N. A. Romanyuk 389

EVENTS

Decisions of the International Commission for Molecular Spectroscopy ... V. Nikitin 389